Design and synthesis of novel biobased polyamines for non- isocyanate polyurethanes (NIPUs)

Zur Erlangung des akademischen Grades einer

DOKTORIN DER NATURWISSENSCHAFTEN

(Dr. rer.nat.)

von der KIT-Fakultät für Chemie und Biowissenschaften

des Karlsruher Instituts für Technologie (KIT)

genehmigte

DISSERTATION

von

M.Sc. Francesca Chiara Destaso

1. Referent: Prof. Dr. Michael A.R. Meier
2. Referent: Prof. Dr. Henri Cramail

Tag der mündlichen Prüfung: 25/02/2025

THÈSE PRÉSENTÉE EN VUE DE L'OBTENTION DU GRADE DE

DOCTEUR DE

L'UNIVERSITÉ DE BORDEAUX

ÉCOLE DOCTORALE DES SCIENCE CHIMIQUES

Spécialité : Polymères

ET

DOCTEUR DE

KARLSRUHE INSTITUTE OF TECHNOLOGY

ÉCOLE DOCTORALE DE CHIMIE

Par **Francesca Chiara DESTASO**

Design and synthesis of novel biobased polyamines for non- isocyanate polyurethanes (NIPUs)

Conception et synthèse de nouvelles polyamines biosourcées pour les polyuréthanes sans isocyanate (NIPUs)

Entwicklung und Synthese neuartiger biobasierter Polyamine für Nicht-Isocyanat-Polyurethane (NIPUs)

Direction de thèse : Prof. Dr. Henri Cramail (Université de Bordeaux)
Codirecteur de thèse : Prof. Dr. Michael A.R. Meier (Karlsruhe Institute of Technology)

Soutenue le 25/02/2025 à Bordeaux

Membres du jury :

Mme Sophie Guillame	CNRS Research Director, University of Rennes-	Président du jury, Rapporteur
M. Sylvain Caillol	CNRS Research Director, University of Montpellier	Rapporteur
M. Laurent Plasseraud	CNRS Researcher, Université de Bourgogne-Dijon	Examinateur
Mme Hatice Mutlu	Junior Professor¸ Université Haute de Alsace	Examinateur
M. Stefan Bräse	Full Professor, Karlsruhe Institute of Technology	Examinateur
M. Etienne Grau	Assistant Professor, Université de Bordeaux	Examinateur
M. Henri Cramail	Full Professor, Université de Bordeaux	Directeur de thèse
M. Michael A.R. Meier	Full Professor, Karlsruhe Institute of Technology	Codirecteur de thèse

To Francesco

Design and synthesis of novel bio-based polyamines for non-isocyanate polyurethanes (NIPUs)

ABSTRACT

Nowadays, the depletion of petroleum deposits along with the human and environmental costs associated to the fossil-derivatives manufacturing chain are far-reaching issues. In this context, this research work focused on the investigation of *more* sustainable monomers and polymers. This work was developed in the frame of the NIPU-EJD European project, aiming on progressing the field *of non- isocyanate polyurethanes,* NIPUs. The first part of the research focused on the design of less hazardous and efficient synthetic strategies to achieve novel biobased polyamines and cyclic carbonates as monomers. All the pathways were required to follow the principles of *Green Chemistry* to the highest possible extend. Subsequently, the synthesized polyamines were employed in the development of vinylogous urethane (VUs) polymers, epoxy resins and poly(hydroxy urethane)s (PHUs) achieving partially and fully bio-based materials. The resulting polymers were characterized and their chemical and physical properties were tested and compared.

Key words: polyamines, bio-based, non-isocyanate polyurethanes (NIPUs), polyurethane, isocyanate-free.

RESUME

Actuellement, l'épuisement des gisements de pétrole ainsi que les coûts humains et environnementaux associés à la chaîne de fabrication des dérivés fossiles sont des problématiques majeures. Dans ce contexte, ce travail de recherche s'est concentré sur l'étude de monomères et de polymères plus durables. Cette étude s'inscrit dans le cadre du projet européen NIPU-EJD, qui porte sur les polyuréthanes sans isocyanates, les NIPUs. La première partie de la recherche s'est concentrée sur la synthèse de monomères biosourcés nécessaires à la synthèse des NIPUs: les polyamines et les carbonates cycliques, au travers de synthèses moins dangereuses, plus efficaces et respectant les principes de la chimie verte. Toutes les voies suivies devaient respecter les principes de la chimie verte dans la mesure du possible. Par la suite, les polyamines synthétisées ont été utilisées pour la synthèse de polymères d´uréthanes vinylogues (VUs), de résines époxy et de poly(hydroxyuréthane)s (PHUs), aboutissant à des matériaux partiellement ou entièrement biosourcés. Les polymères obtenus ont été caractérisés et leurs propriétés chimiques et physiques ont été évaluées et comparées.

Mots-clés: polyamines, biosourcé, polyuréthanes non-isocyanates (NIPUs), polyuréthane, sans isocyanate.

ZUSAMMENFASSUNG

Die Erschöpfung der Erdölvorkommen sowie die erheblichen menschlichen und ökologischen Kosten, die mit der Herstellung fossiler Derivate verbunden sind, stellen heutzutage große Herausforderungen dar. In diesem Zusammenhang konzentrierte sich diese Forschungsarbeit auf die Untersuchung nachhaltigerer Monomere und Polymere. Sie wurde im Rahmen des europäischen Projekts NIPU-EJD durchgeführt, das darauf abzielt, die Entwicklung von nicht-isocyanat Polyurethanen (NIPUs) voranzutreiben. Der erste Teil der Arbeit konzentrierte sich auf die Entwicklung effizienter und weniger gefährlicher Synthesestrategien zur Herstellung neuartiger biobasierter Polyamine und zyklischer Carbonate als Monomere. Dabei wurde besonderes Augenmerk daraufgelegt, die Prinzipien der Grünen Chemie so weit wie möglich einzuhalten. Im Anschluss kamen die synthetisierten Polyamine in der Entwicklung von vinylogischen Urethanen (VUs), Epoxidharzen und Poly(hydroxyurethane)s (PHUs) zum Einsatz, mit dem Ziel, sowohl teilweise als auch vollständig biobasierte Materialien zu schaffen. Die resultierenden Polymere wurden umfassend charakterisiert, wobei ihre chemischen und physikalischen Eigenschaften analysiert und miteinander verglichen wurden.

Schlüsselwörter: Polyamine, biobasiert, nicht-isocyanat Polyurethane (NIPUs), Polyurethan, isocyanatfrei.

ACKNOWLEDGMENTS

After 3.5 years of working on my doctoral research in three different laboratories and two Countries, I would like to express my gratitude.

Firstly, I would like to thank my supervisors, Prof. Dr. Michael A.R. Meier and Prof. Dr. Henri Cramail, for their constant support and availability during both prosperous and challenging times. Their scientific knowledge, wise advice and exemplary leadership, management, and guidance have been invaluable. I have learned so much from them and words will never suffice to express my gratitude.

I extend my thanks to Dr. Etienne Grau, Dr. Thomas Vidil, and Dr. Audrey Llevot for their warm welcome and scientific support during my stay at LCPO.

To the members of the NIPU-EJD European project: Our connection exceeded all my expectations. I found in you the most valuable colleagues I could have imagined. We supported each other on scientific topics, PhD-life challenges, and during the hardest moments of our doctoral program. We always understood and uplifted one another. I thoroughly enjoyed working with you, both for your professionalism and for the wonderful individuals I had the pleasure of getting to know. I am grateful to have shared my academic journey with you. Special thanks to the colleagues with whom I shared my secondment in France: Nichollas, Florent, and Christy. You made me feel at home in a foreign country and provided wonderful cooperation during that time. To Christy, thank you for becoming my dearest friend. To Luca and Federico, who quickly became my friends, for the privilege of sharing both the hardest and most joyful times together, for cheering each other up in the darkest and most stressful moments - here's to our brotherhood.

To Anne, our project manager: Thank you for your remarkable work, even in difficult situations. Your constant presence, support, and proactive approach have been greatly appreciated.

To the AK Meier research group: the first international team I worked with and where my PhD journey began. Being part of this group was a profoundly formative experience - not only professionally but also as part of a community. The spirit of collaboration, eagerness to discuss scientific topics, hardworking attitude and willingness to support others are defining characteristics of this group. I am grateful to have met such a diverse and wonderful group of people, all of whom I will cherish in my memories. Special thanks to Clara, the kindest person I have ever met - it was a pleasure to collaborate with you; to Celeste, with whom it was exciting to conduct research; to Philipp, who ensured the days were never boring; to Qian Yu the most clever and amusing lady ever met, your company is gold! To Catylin, for sharing Chinese culture, traditions and food!

To the IOC team: it was a pleasure to spend my final PhD year with you in the lab. The environment was unique and enjoyable. Thank you for the great time and the team experience. Special thanks to Timo, for being great company during my first PhD year; to Andre, one of the nicest people I have met; to Peter and Luis, for sharing your passion and knowledge of chemistry alongside your music tastes! To Ms. Pinar Sancar: thank you for your invaluable administrative assistance and patience over these years. Your help has been truly appreciated. To all members of the AK Meier group (it's almost impossible to mention everyone!): a heartfelt thank-you.

A special thank-you to Arjun, an incredibly energetic chemist who became a great friend in addition to being a valuable colleague. It was amazing to work with you on our project and during the PhD journey at KIT. I am deeply grateful to have met you.

I would also like to thank Ing. Birgit Huber for the kindness and support given for TGA analyses.

To the LCPO research group: thank you for making my research journey extraordinary. The atmosphere at LCPO is unparalleled - an incredible place where I found kind and passionate professionals willing to share their experiences and foster a strong team spirit. Special thanks to the engineers: Frédérique Ham-Pichavant, Sylvain Brousseau, Léna Alembik, Cédric Le Coz and Paul Marque for sharing their expertise with diverse analytical devices and helping me during my research. I am immensely grateful to you. To Ms. Severine Saint-Drenant and Ms. Emilie Lalande: thank you for your administrative support during my time at LCPO.

To all Team 2: thank you for the scientific discussions and the time shared together! To Quentine and Manon, my amazing office colleagues: thank you for the pleasant times we shared together. To Clement, for being a fantastic office and lab mate. To Arthur, the most amusing colleague I had the pleasure to meet. To Yelin, Dongxu, Yupei, Sifan and Guanfei: thank you for your company during this time in France, for sharing lunch breaks, Chinese dinners and anecdotes about your culture.

To the Henkel industrial partner - Adhesive and Technology department: thank you, Dr. Olaf Hartmann, Mr. Jordan Diaz and Dr. Christian Holtgrewe, for the insightful guidance and working experience in your teams. To Dr. Brian Spiegelberg, for enriching discussions and support. To Ms. Juliana Kutter and Mr. Patrick Seggewiss: thank you for welcoming me into your research team and laboratory.

To the NIPU-EJD MSCA European funding (this project has received funding from the European Union's Horizon 2020 research and innovation programme under the Marie Skłodowska-Curie grant agreement No 955700): without it, this research would not have been possible. Thanks to the Karlsruhe Institute of Technology and LCPO, University of Bordeaux, for hosting me during these 3.5 years.

To my dearest friends Elena, Grazia, Sma, Mapi and Silvia: your support and friendship mean the world to me. No matter the time, distance, or number of messages, you all hold a special place in my heart.

To my old and dear friend Dario: thank you for continually being critical and encouraging me at the

same time.

To Alessandro: thank you for always being able to make me smile.

To Elia: thank you for always finding time to listen, offering advice, and being the rational voice I needed in the hardest times. You are a diamond in my life.

To my family: thank you for your unwavering presence and support, no matter the distance.

Finally, to Francesco: my greatest supporter over the last three years. Without you, this research would not have been completed. Thank you for guiding me in becoming the woman I am today.

P.S. I'm deeply sorry if I forgot anyone. Throughout this journey, I met so many people that I fear I may have missed mentioning some! Thank you, even if I didn't mention you.

TABLE OF CONTENTS

Abbreviations (alphabetic order)

CAHC: Cysteamine hydrochloride

CC: cyclic carbonates

$CDCl_3$: deturated chloroform

$CHCl_3$: chloroform

CO: castor oil

COTA: castor oil triamine

CyHex: cyclohexane

DCM: dichlormetane

DMSO-d6: deuterated diethyl sulfoxide

DMSO: dimethyl sulfoxide

Et_2O: diethyl ether

EtOAc: ethylacetate

EtOH: ethanol

FA: fatty acid

GC: glycerol carbonate

HOSO: high oleic sunflower oil

iPrOH: isopropanol

LO: linseed oil

MeOH: methanol

MO: methyl oleate

NIPU: non-isocyanate polyurethane

PA: polyamine

PHU: poly (hydroxy urethane)

RO: ring opening

TRG: triglyceride

UBC: urethane bis-cyclic carbonate

Conception et synthèse de nouvelles polyamines d'origine biologique pour les polyuréthanes sans isocyanate (NIPUs)

RESUME DE LA THESE

Chapitre 0 : La chimie verte

L'épuisement des gisements de pétrole prévu dans un avenir proche et la crise environnementale actuelle sont des enjeux urgents pour l'humanité. Il est ainsi primordial d'explorer des molécules précurseurs dérivées de ressources naturelles abondantes ou de déchets. Par la suite, en tirant partie de ces nouveaux composés, de nouveaux matériaux polymères doivent être développés afin de remplacer ceux existants qui ne respectent pas les principes de durabilité. L'idée est d'établir une chimie plus durable pour s'inscrire dans une société plus respectueuse de l'Homme et de l'environnement et promouvoir un modèle d'économie circulaire (Figure 1).

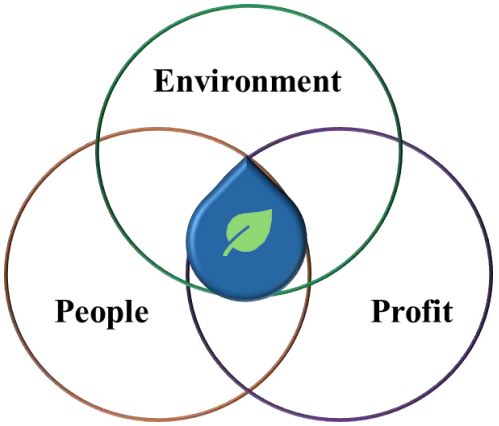

Figure 1. Équilibre Environnement-Population-Profit.

Chapitre 1 : Contexte théorique et état de l'art

Dans ce contexte, cette thèse vise à contribuer à la science et à la société dans le cadre d'une chimie organique et des polymères plus durables et responsables. En particulier, ce travail de recherche se concentre sur la conception et la synthèse de nouveaux monomères biosourcés, synthétisés selon les principes de la chimie verte autant que possible, dans le but de développer des matériaux analogues aux polyuréthanes. Plus précisément, la conception et la synthèse de nouvelles polyamines biosourcées ont été étudiées. De plus, des carbonates bicycliques biosourcés et des polyacétoacétates ont également été synthétisés. Enfin, à partir de ces blocs de construction, de nouveaux matériaux ont été développés comme alternatives possibles aux polymères issus du pétrole et testés pour diverses applications.

Notamment, l'objectif a été de développer des polymères pouvant remplacer les polyuréthanes par des alternatives sans isocyanates.

Chapitre 2 : Polyamines issues d'huiles végétales et de terpènes

Des voies synthétiques variées ont été conçues pour obtenir des polyamines. Deux classes naturelles de composés ont été sélectionnées pour atteindre les monomères ciblés : les huiles végétales (triglycérides, TRG) et les terpènes (et terpénoïdes). Tout d'abord, un protocole en deux étapes a été élaboré pour obtenir des triamines TRG à partir de l'huile de tournesol riche en acide oléique (HOSO). Cette voie consiste en une oxydation initiale de l'insaturation du composé HOSO, suivie d'une amination réductrice catalytique (Figure 1A).

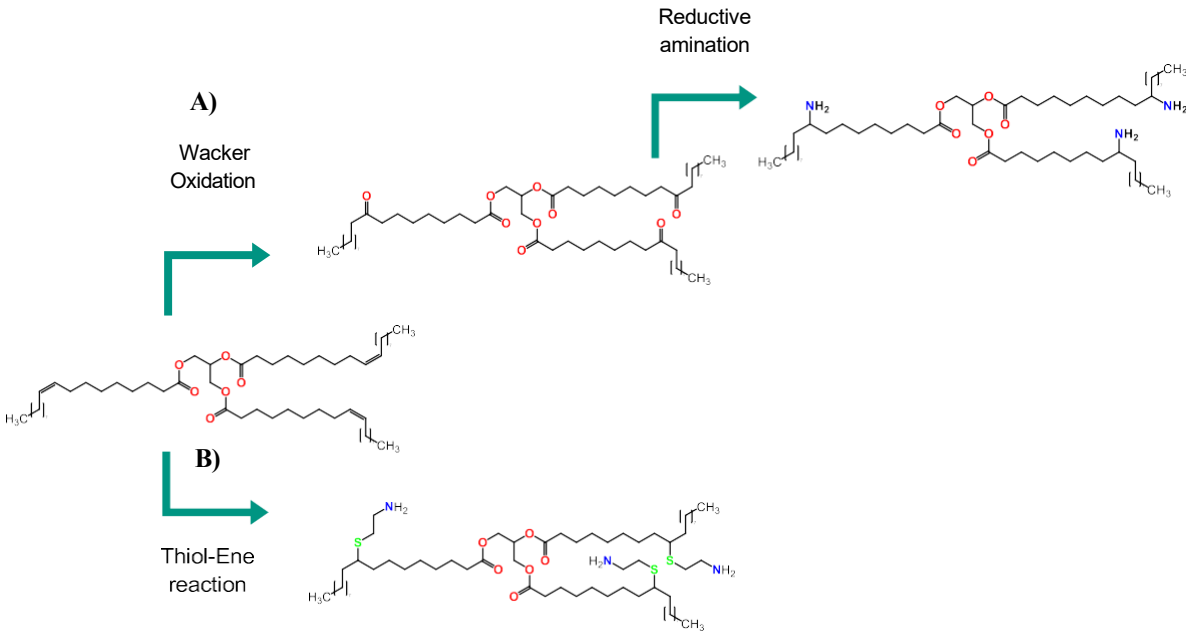

Figure 2. Voies possibles pour obtenir des polyamines à partir d'huiles végétales. A) Oxydation de Wacker + aminométhylation réductrice. B) Réaction de clic thiol-ène.

L'oxydation de l'HOSO a été étudiée de manière plus écologique via la réaction d'oxydation de Wacker. Dans un premier temps, un système catalytique en milieu homogène a été testé dans diverses conditions de réaction en utilisant l'oxygène comme seul oxydant. Le criblage des paramètres tels que le temps, la température et la charge catalytique a été effectué. La meilleure conversion obtenue est de 60 %, avec une charge catalytique de 25 % mol de $PdCl_2$ après 24 heures à 70 °C. En raison de la quantité de catalyseur requise, de son coût élevé et de la rareté du palladium, il a été jugé déraisonnable de tester des charges catalytiques plus élevées en raison de l'inapplicabilité pratique de cette stratégie synthétique et de sa faible durabilité. En alternative, une stratégie par catalyse hétérogène a été étudiée en utilisant un catalyseur de phosphure de palladium supporté sur silice (Pd_3P/SiO_2). Cette stratégie a été développée

en collaboration avec le groupe de recherche en chimie inorganique de l'Institut de Technologie de Karlsruhe, dirigé par le Prof. Hanf. Le catalyseur a été produit par le doctorant Arjun Neyyathala, qui l'avait précédemment testé pour l'oxydation du styrène en acétophénone dans les conditions classiques de l'oxydation de Wacker-Tsuji. L'objectif de cette collaboration a été de développer une stratégie plus écologique pour l'oxydation des acides gras et des huiles à l'aide de Pd_3P/SiO_2. Initialement, l'oléate de méthyle a été utilisé comme composé modèle de départ. Les principaux paramètres influençant les résultats de la réaction ont été étudiés, notamment le temps, la température, le solvant, la charge catalytique et sa densité sur le support. Par la suite, l'oxydation de l'HOSO a également été réalisée dans les meilleures conditions identifiées. La meilleure conversion obtenue est également de 60 %, comme dans l'approche par catalyse homogène. Cependant, une charge de palladium bien plus faible est nécessaire dans ce cas. En effet, 25 % mol de $PdCl_2$ (Pd 59 %) ont été utilisés, contre Pd_3P 7,5 % mol catalyst de 1 % en poids de Pd sur silice.

Les TRG partiellement oxydés (polycétones) ont été soumis à diverses conditions catalytiques réductrices avec le catalyseur de Raney-Nickel®. Malheureusement, les différents essais testés se sont révélés inefficaces, contrairement aux résultats précédemment rapportés avec les acides gras. Cela pourrait être attribué à l'encombrement dû à la grande taille des molécules de TRG et à leur topologie, qui peut limiter l'accès aux sites actifs du catalyseur.

Avec le même HOSO de départ, un autre monomère polyamine a été envisagé après éthérification de l'HOSO. Un système catalytique utilisant le bromure de gallium comme catalyseur et le triméthylsilane comme agent réducteur a été utilisé dans des conditions inertes. Le produit final a été obtenu avec succès en un temps de réaction court. Une conversion complète des fonctions ester a été obtenue en 30 minutes, avec une trace de sur-oxydation (7 % de formation d'alcool détectée par RMN). En outre, des efforts ont été réalisés pour optimiser le processus de purification afin d'utiliser des solvants plus durables et de réduire la quantité de déchets. La meilleure stratégie a été obtenue avec l'utilisation de l'anisole comme solvant. Néanmoins, le problème de la présence résiduelle de polysiloxane (formé par polymérisation de l'agent réducteur) dans le produit final a persisté.

La réaction d'addition thiol-ène a ensuite été testée sur le dérivé HOSO éthérifié. Malgré la variation de différentes conditions expérimentales, les résultats s'avèrent insatisfaisants. En outre, une réaction thiol-ène amorcée thermiquement avec l'AIBN a également été testée mais n'a pas conduit aux résultats escomptés. Au final, la fonctionnalisation maximale atteinte est d'une fonction amino primaire par molécule de TRG. En raison de ce résultat, il n'a pas été possible d'utiliser ce précurseur pour l'élaboration de PHU.

Une méthode plus simple a été développée en appliquant la réaction thiol-ène sur des TRG insaturés, des terpènes et des terpénoïdes (Figure 1B). De cette manière, le produit souhaité peut être obtenu en une seule étape synthétique. La synthèse des polyamines de TRG a été étudiée et optimisée aux plans du processus et de la durabilité. L'amorçage photochimique a été choisi en raison de la sensibilité des

TRG à la chaleur, ce qui pourrait entraîner une oxydation indésirable. Les paramètres cruciaux sont le solvant, la source de lumière et la longueur d'onde, l'efficacité de l'irradiation et le temps de réaction. Tous ces paramètres ont été soigneusement étudiés. Au final, une conversion totale a été obtenue en 7 heures dans un mélange isopropanol/éthanol avec une LED UV de 2 W permettant d'obtenir une polyamine renouvelable en grande quantité (2 g huile végétale composé de départ). Grâce à une approche thiol-ène photo-amorcée, des diamines dérivées des terpènes ont également été obtenues à partir des isomères du linalol et du géraniol, et un mélange de di- et tri-amine a été obtenu à partir du myrcène. D'autres études pourraient être menées pour obtenir la conversion totale des insaturations. De plus, ces dérivés pourraient être utilisés comme monomères pour la synthèse de différents polymères tels que les époxydes, les NIPUs ou les polyurées.

Dans l'optique d'améliorer l'efficacité de la réaction, un système de chimie en flux a été expérimenté. Dans le cadre d'un système en flux continu, il a été observé qu'en augmentant le débit (de 0,5 mL/min à 9 mL/min), la conversion augmentait. Enfin, il a été possible de passer à une échelle de 2 g d'huile, de réduire le temps de réaction à 6 heures en utilisant un solvant plus sûr, atteignant une conversion supérieure à 99 %. De plus, la LED UV utilisée est une source de lumière à faible puissance (16 W, 365 nm), ce qui est un aspect favorable pour une faible consommation d'énergie. Il est envisageable que la réaction puisse être mise en œuvre en utilisant un débit plus rapide ou une concentration plus faible du mélange réactionnel de départ.

Chapitre 3 : Carbonates biscycliques d'uréthane sans isocyanates (UBC)

La synthèse de carbonates cycliques a également été étudiée. En collaboration avec le Dr. Federico Mundo, un collègue du projet européen NIPU, deux nouveaux monomères biscarbamates et porteurs de fonctions carbonate cyclique (UBC) ont été synthétisés via une voie sans isocyanate selon un processus plus durable (Figure 3).

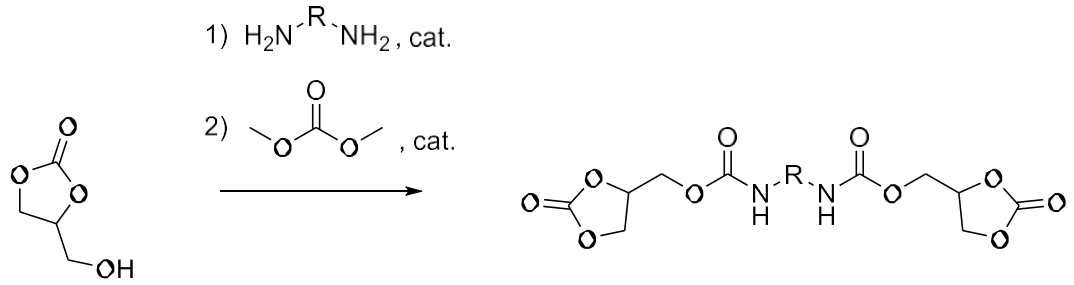

Figure 3. Synthèse de bis-CC sans isocyanate.

A titre de comparaison, la synthèse de ces monomères par la voie isocyanate a également été réalisée. La comparaison entre les deux voies a montré un impact environnemental (facteur E) plus faible pour la voie isocyanate (en considérant l'amine comme point de départ dans les deux cas). Ainsi, le processus

développé dans cette thèse s'avère une alternative plus sûre et ouvre la voie à la synthèse de monomères UBC à partir d'amines biosourcées présentant différentes structures chimiques. Malgré la faible masse molaire atteinte par polymérisation des monomères UBC avec différentes diamines, les PHUs obtenus ont montré de bonnes propriétés adhésives (colles à bois) lors des tests de cisaillement en traction. Ensuite, une investigation visant l'obtention de PHU de haute masse molaire à partir des UBC synthétisés a été réalisée. Par ailleurs, le développement d'une bibliothèque de nouveaux monomères UBC via une voie sans isocyanate est une perspective pour les études futures. Par ailleurs, l'utilisation d'amines et polyamines biosourcées serait également souhaitable pour améliorer la durabilité du processus.

Chapitre 4 : Nouveaux uréthanes vinyloges (UV) biosourcés

Trois acétoacétates dérivés de l'huile de ricin, du 1,4-butanediol et du glycérol (c'est-à-dire CoAcAc, BuAcAc et GlyAcAc, respectivement) ont été synthétisés et combinés avec des polyamines commerciales dérivées du pétrole ainsi que biosourcées pour obtenir des polymères uréthanes vinylogues (polyVUs).

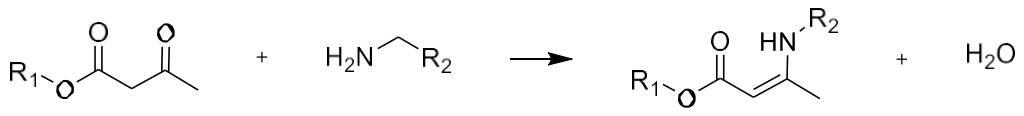

Figure 4. Schéma général de réaction pour la synthèse d'uréthanes vinylogiques.

Les polyamines sélectionnées sont l'isophorone diamine (IPDA), les *Jeffamine D230® et T403®, la Priamine 1071®* et la limonène diamine (LDA, synthétisée via thiol-ène photoamorcée). Les différences dans la structure chimique des monomères et la variété des combinaisons possibles ont permis l'élaboration de polyuréthanes vinylogues (polyVUs) thermodurcissables présentant différentes propriétés physiques, chimiques et mécaniques. En raison de la nature dynamique de cette classe de thermodurcissables, les polyVUs appartenant à la classe des CANs (Covalent Adaptable Network materials). Ces matériaux sont potentiellement recyclables, par rapport aux thermodurcissables conventionnels. Des tests de remise en forme des polyVUs produits ont été réalisés. Le processus de remise en forme plus facile pour les matériaux ayant des valeurs de Tg plus faibles. Les différences dans les propriétés adhésives étaient liées à la structure chimique et à la densité des groupes OH libres présents dans le réseau des polyVUs. En perspective, des tests de biodégradabilité et de biocompatibilité pourraient donner une vision plus large sur l'applicabilité des matériaux développés.

Chapitre 5 : Poly(hydroxyuréthane) biosourcés (PHU)

Les polyamines biosourcées mentionnées ci-dessus et obtenues via la réaction thiol-ène, HOSO-PA (polyamine d'huile de tournesol hautement oléique) et la polyamine d'huile de lin (LO-PA) ont permis de développer de nouveaux poly(hydroxyuréthane)s (PHUs). Deux différents carbonates cycliques biosourcés (CCs) ont été testés en tant que co-monomères, tels que le biscarbonate d'érythritol (EBC) et le bis(cyclocarbonate) de 1,6-hexanediol (HCC). Il a été observé que la fonctionnalité en fonctions amine plus élevée dans le cas de LO-PA permettait d'atteindre un taux de réticulation plus élevé, bien

que les taux de gel (64-75%) restent insuffisants pour des matériaux thermodurcissables. Afin d'obtenir de meilleurs taux de gel et des valeurs de Tg plus élevées, un troisième composant a été ajouté à la formulation pour améliorer la densité de réticulation. Des dérivés de lignine porteurs de fonctions carbonate cyclique (CCFL) ont été ajoutés au système HOSO-PA et érythritol biscarbonate cyclique (EBC), permettant l'élaboration de de réseaux PHU thermodurcissables. Ce travail a été réalisé dans le cadre d'un projet collaboratif avec la Doctorante Celeste Libretti du groupe de recherche du Prof. Meier de l'Institut de Technologie de Karlsruhe (KIT). Quatre réseaux thermodurcissables différents contenant différents taux de lignine ont été développés (T1 =26%, T2 =38%, T3 =57%, T4 =63%). Parmi les différentes formulations, T2 s'est avéré être le meilleur compromis en termes de rigidité, faible fragilité, densité de réticulation (taux de gel =87%) et Tg (97°C). En perspective, des tests de biocompatibilité et de biodégradabilité seraient intéressants à investiguer. De plus, des tests mécaniques, tels que des tests de cisaillement en traction et de traction, pourraient aider à établir des applications possibles de ces nouveaux matériaux thermodurcissables entièrement biosourcés.

Chapter 6: Fully and partially bio-based epoxy resins

Enfin, des résines époxy entièrement et partiellement biosourcées à partir de l'éther diglycidyle de bisphénol A (DGEBA) d'origine pétrolière et de l'éther diglycidyle d'isosorbide (DGEISO) ont été produites et comparées.

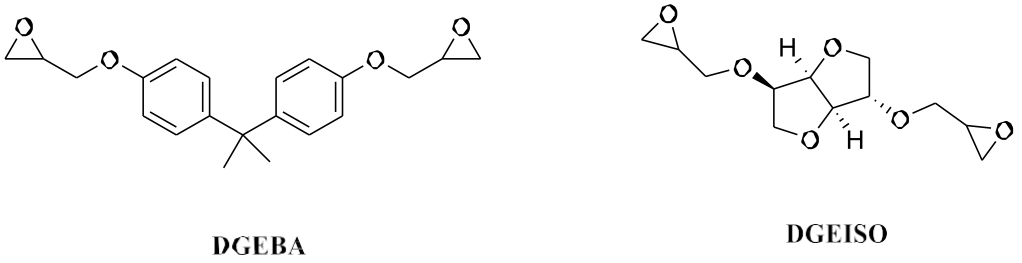

Figure 5. Structure chimique de l'éther diglycidyle provenant du bisphénol A (DGEBA) et de l'isosorbide (DGEISO).

Les réseaux obtenus à partir de DGEISO présentent des *Tg* au-dessus de la température ambiante mais restent inférieures à celle obtenue avec la DGEBA. La structure aromatique de la DGEBA est le principal facteur jouant un rôle dans la différence des propriétés des matériaux finaux. De façon logique,

il a été également observé que la nature chimique du durcisseur amine contribue fortement aux propriétés finales du polymère. Tous les réseaux ont montré un taux de gel élevé (86-95) et une bonne résistance à la dégradation à haute température (*Td,5%* de 200°C à >300°C). Les meilleures propriétés adhésives ont été enregistrées sur un substrat de bois avec le réseau époxy entièrement biosourcé composé de DGEISO et d'IPDA, surpassant celles du réseau époxy issu de DGEBA et IPDA. En général, toutes les formulations dérivées du DGEISO ont montré de meilleures performances de résistance Shore sur des substrats en bois par rapport à celles issues de la DGEBA.

0 CHAPTER 0: GREEN CHEMISTRY

INTRODUCTION

Since the beginning of the '80 of the 20th century, it was known to petrol companies that the continuous and growing release of CO_2 into the atmosphere from anthropological activities would lead to nefarious consequences on our planet.[1] Forty years later, we are experiencing drastic climate changes and environmental crises caused by the thoughtless human exploitation of natural resources and their processing and use.[2] For this reason, and the diverse accidents in the history of chemical industries, the field of chemistry has often had (and still has) a negative consideration in the public opinion. With the aim of slowing and blocking the negative effects of harmful human actions, a new branch of chemistry was born at the end of the last century.[3,4] In 1998, Paul Anastas and John Charles Warner articulated and published the pillar of a chemistry revolution: *the 12 principles of Green Chemistry*.[5] These statements were set as a guide to developing a more responsible way of thinking and conducting chemistry research and production. The 12 principles are listed as follows:

Table 1. The 12 Principles of Green Chemistry and their definitions.[5]

1. Prevention	Preventing wastes is more desirable than treating the wastes created along the process.
2. Atom Economy	Synthetic processes should be designed to maximize the incorporation of all starting atoms into the final product.
3. Less hazardous chemical syntheses	Wherever practicable, synthetic methods should be designed to use and generate substances that possess little or no toxicity to human health and the environment.
4. Designing safer chemicals	Chemical products should be designed to perform their desired function while minimizing their toxicity.
5. Safer solvents and auxiliaries	If auxiliary substances are employed (e.g., solvents, separation agents, etc.) their use should be reduced, eliminate or substitute with safer substances wherever possible.
6. Design for energy efficiency	Energy requirements of chemical processes should be recognized for their environmental and economic impacts and consequently minimized when possible. If possible, it is preferable to perform synthetic processes at ambient temperature and pressure.
7. Use of renewable feedstocks	A raw material or feedstock should be desirably renewable rather than depleting whenever technically and economically practicable.

8. Reduce derivatives	If feasible, unnecessary derivatization (use of blocking groups, protection/ deprotection, temporary modification of physical/chemical processes) should be minimized or avoided.
9. Catalysis	Catalytic reagents (as selective as possible) are more desirable than stoichiometric reagents.
10. Design for degradation	Chemical products should be designed so that at the end of their function they break down into innocuous degradation products and do not persist in the environment.
11. Real-time analysis for pollution prevention	Analytical methodologies need to be further developed to allow for real-time, in-process monitoring and control prior to the formation of hazardous substances.
12. Inherently safer chemistry for accident prevention	Substances and the form of a substance used in a chemical process should be chosen to minimize the potential for chemical accidents.

Following this example, in the following years, similar principles were established in different scientific subfields, such as green polymer chemistry and green engineering.[6,7]

The 12 principles of green chemistry are an effective and useful guideline; however, numerical parameters were needed to effectively estimate sustainability. Consequently, green chemistry metrics were introduced as practical tools. Overall, these parameters are concerned with evaluating the amount of chemicals used, product obtained, waste produced, energy efficiency, and environmental impact.[8] The attention to these aspects occurs in a larger scenario aiming at the transition from a linear to a circular economy model.[9] In fact, it is also important to consider the balance of the three macro groups, which should collimate in the sustainability core intersection between environment, people and profit (Figure 6).

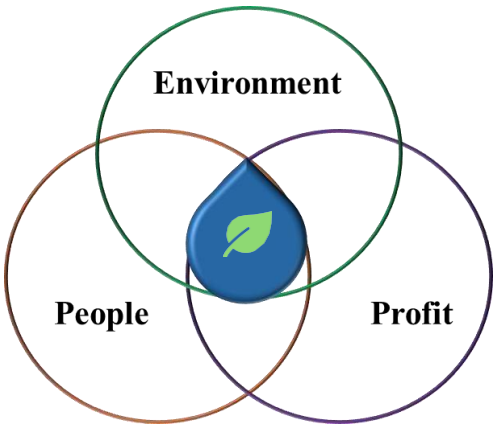

Figure 6. Environment-People-Profit balance.

In accordance with this, the United Nations drafted the sustainable development goals, which are summarized by 17 principles (Figure 7).[10]

Figure 7. 17 sustainability developments goals drafted by the United Nations.[10]

AIM OF THE WORK

In this scenario, this thesis aims at contributing to science and society in the frame of a more sustainable and responsible organic and polymer chemistry. In particular, this research work focuses on the design and synthesis of novel biobased monomers synthesized following the green chemistry principles to the greatest extent possible. Specifically, the design and synthesis of novel biobased polyamines were investigated. Principally, two synthetic strategies were studied: 1) homogenous and heterogenous catalyzed oxidation of double bonds, followed by catalytic reductive amination; 2) one-step functionalization of unsaturations through photoinitiated thiol-ene reaction to achieve primary polyamines. Moreover, bioderived bicyclic carbonates and polyacetoacetates were also synthesized. Furthermore, starting from these building blocks, new materials were developed as possible alternatives to the current petroleum-based polymers and tested for possible applications. Notably, the targets were polymers that could replace polyurethanes with non-isocyanate polyurethane alternatives.

1 CHAPTER 1: THEORETICAL BACKGROUND AND STATE OF THE ART

1.1 RENEWABLE RESOURCES FOR POLYMERS

Polymers that are typically classified as more sustainable can be divided into naturally occurring polymers (i.e. cellulose, lignin, natural rubber…) and polymers derived from renewable feedstock. The latter can result from natural resources, waste or recycled materials and ideally are recyclable, reusable or biodegradable.[11] Overall, a material is *more* sustainable than another if its environmental impact is lower. To evaluate this factor, the green chemistry metrics can be applied.[3]

Three major phases to the development of sustainable polymers can be listed as:1) the production of (biobased) building blocks; 2) the polymerization process; 3) post-processing, which includes reuse, recycling or biodegradation.[12]

Defining the sustainability of a polymer is a complex topic, insofar as many aspects have to be taken into account. If a polymer is bio-derived, the natural source should be preferably not food-competing and the health and security of landfills must be taken into consideration.[13] As such, the use of wastes (industrial or agricultural) as building blocks is the ideal option.[14,15] Another efficient synthetic sustainable strategy involves the action of microorganisms. One example of polymers produced in this manner are polyhydroxyalkanoate polyesters (PHAs), which are obtained *via* fermentation and are biodegradable and biocompatible.[16] At present, an often investigated waste is CO_2, as its use drives a double advantage in reducing its emission and helping climate change downturn.[17] This positive effect is even more enhanced if the technology of CO_2 removal from the environment is employed.[18] The *natural capital* has to be considered in order to build a real sustainable system.[19] *Natural capital* is defined as "*The "capital" part of natural capital refers to the notion that there are some resources (or capital) in nature that we need to use to survive and that enables the production of more resources".*[20] The use of renewable feedstocks promotes the switch from a fossil-dependent economy to a bioeconomy. Together with the *green* revolution, a new economic model has been formulated. The progression to a circular economy from the linear *"cradle to grave"* economy is a crucial point for a sustainable transition (Figure 8).

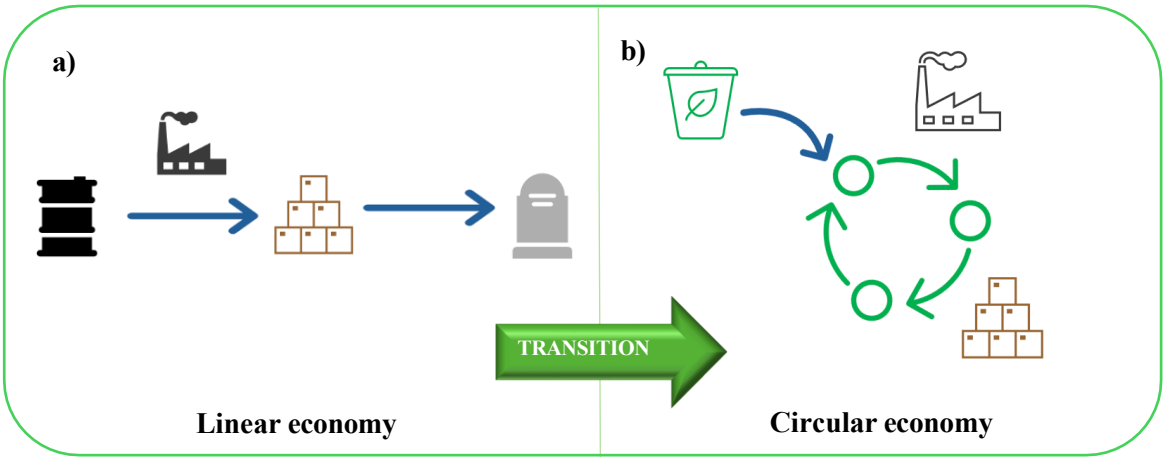

Figure 8. a) Linear economy model: the initial sources are converted to the product which is then used and at its end of life displaced. b) Circular economy model: renewable feedstocks are processed, used and, at the end of life, re-processed and re-used.

The circular economy implies the preservation of resources (preferably achieved from sustainable resources) in a continuous cycle from the initial source to a novel use of the product at its end of life. The recovery of the resource can be either directed to the same function as the initial scope or can be converted and redirected to a different application. The important point of this model is to limit the use of novel additional starting resources and to avoid the creation of waste.

An important note is that biobased does not mean biodegradable and biodegradable is not always the most desirable solution.[21] Moreover, the bio-assimilation in the environment of biodegradable polymers and its effects on the environment must be studied.[22–24] Alternatively, of great relevance is the research on the depolymerization process, which can be mechanical or chemical.[25] Energy consumption must be monitored, and energy production must be achieved from renewable energy sources (wind, sun, water…).[26] Water use and waste must be considered, as water is a precious resource for life. A useful tool to understand the impact of a product from its starting point to its use and post-use is the Life Cycle Assessment (LCA) (Figure 9).[27] With the help of this methodology, it is possible to have a numerical value, which can give an idea of the impact of the material production. It is relevant to mention that this tool uses approximations, which can be different in dependency on the model used. Further, the data collected are often not sufficient to have a reliable final evaluation.[28]

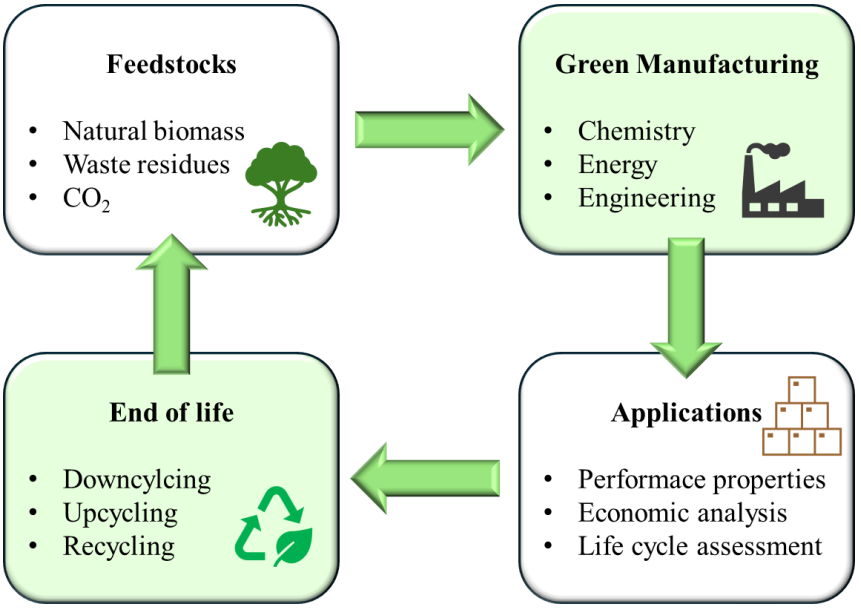

Figure 9. Life cycle assessment (LCA) of sustainable polymers.[29]

The United Nations Environment Programme (UNEP) is the authority of the United Nations which publishes reports and analyses related to current situations and challenges concerning the environmental crisis, which has an impact on the planet and human lives.[29] By now, many documents were released about plastic pollution status and prevention.[30] The use of renewable feedstocks is a central and fundamental point for the European Bioplastics organization.[30] This approach is reasonably applied if four statement are respected: i) resources being cultivated on (at least) annual basis; ii) full valorisation of biomass according to a cascade use; iii) reduction of the carbon footprint and greenhouse emissions; iv) saving and substituting fossil resources step by step".[31] Furthermore, standardization is of high relevance. The European Committee for standardization (CEN) drafted the definition of biopolymers and bioplastics, indicating polymers and plastics that are *bio-based* as **"**fully or partially made from biological resources, rather than fossil raw materials. They are not necessarily biodegradable or compostable" and *biodegradable* the ones which "biodegrade in certain conditions at their end of life. Compostable plastics - a subset of biodegradable ones – typically decompose in industrial composting facilities, and first need to be collected. Biodegradable and compostable plastics may be made from biological resources or fossil raw materials".[32] However, the use of these terms leads to misunderstanding, especially in commercial communication, leading to the phenomenon of *greenwashing*.[33] Moreover, definitions regarding the degradability of plastics were also introduced by the European Bioplastic organization.[17]

1.1.1 Vegetable oils

Vegetable oils are lipids extracted most commonly from the seeds of plants. 210 MMT (million metric tons) was the volume production of vegetable oils measured for the marketing year of 2023/2024 and the annual production is continuously growing.[34,35] Triglycerides are non-polar molecules consisting of three aliphatic fatty acid (FA) chains coupled *via* ester linkages to a glycerine unit (Figure 10). FA chains are classified by the number, position and configuration of the unsaturation along the aliphatic chain (Table 2).

Table 2. Structural details of most common fatty acids and their principal sources.

Name	Chain length: n° unsaturations	Unsaturation position	Common source
Palmitic	16:0	-	Palm oil
Stearic	18:0	-	Cocoa butter
Oleic	18:1	C9	Sunflower oil
Linoleic	18:2	C9, C11	Linseed oil
Linolenic	18:3	C9, C11, C13	Canola oil
Ricinolein	18:1	C9, C11 + alcohol	Castor oil
Vernolic	18:1	C9, C11 + epoxy	Vernonia oil
Arachidic	20:0	-	Peanut oil

Saturated fats are commonly solid at room temperature; oppositely unsaturated ones are viscous liquids. Typically, FA chains of vegetable oils consist of a number of unsaturation from 0 to 3 per chain. A higher unsaturation degree is present in fish and algae oils.[36]

Due to the presence of unsaturation, triglycerides are usually prone to oxidation in the presence of air and heat. Oxidation of oils involves the formation of allylic hydroperoxide radicals, leading to the formation of short-chain molecules (aldehydes, alcohols, ketones and acids) and oligomers.[37] Additionally, the presence of moisture and an alkaline environment leads to hydrolysis.[22]

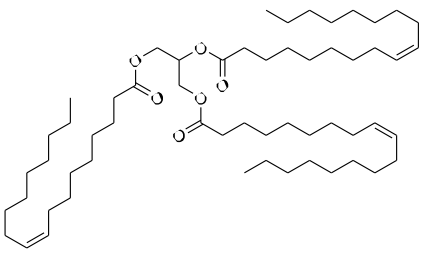

Figure 10. High oleic sunflower oil (HOSO) as model triglyceride.

Fatty acids were employed as monomers for producing polymeric materials.[38] The long chain aliphatic structure gives flexibility and softness characteristics to the final material.[39] Alternatively, triglycerides can be used as building blocks directly by adding desired functional groups. Most commonly, chemical modifications are made on unsaturated bonds. Direct polymerization of lipids *via* cationic polymerization has been studied. The electron-rich double bonds can undergo cationic or radical addition mechanisms.[40] Taking advantage of double bonds, thiol-ene chemistry can be used to produce polyfunctional molecules.[38] As an example, the synthesis of a library of polyols has been performed and applied in the field of polyurethanes and polyesters.[41–43] Less prolific, though of great interest, is the synthesis of the polyamines *via* thiol-ene radical reaction.[44,45]

Vernonia oil naturally contains epoxy groups, however, epoxidized oils (i.e. epoxidized soybean and linseed oil), are largely produced industrially *via* acid catalysis.[46] The ring opening (RO) of epoxides in the presence of an acid catalyst allows the production of polyols.[47] While the RO yields secondary alcohol groups, highly reactive primary groups can be obtained by hydroformylation of triglycerides. Different compounds can be obtained using the RO strategy, such as hydroxyalkylamides using amides or hydroxylamines while using secondary amines.[30]

A different approach *via* photoperoxidation reaction yields a hydroperoxide, which can be further transformed to Michael system introducing ketone moieties in alpha position to double bonds present on the chain.[48]

The more unsaturated bonds are present in a triglyceride, the higher is the number of new functionalities that can be introduced. This brings the possibility of using these monomers to produce crosslinked thermoset materials. Since the crosslinking takes place from a position along the chain, the remaining dangling chain often acts as a plasticizer. Vegetable oil-derived monomers are predominantly investigated to develop new bio-based thermosetting materials.[49] This interest is driven by the need to find alternatives to petrol-based commercially available materials, such as epoxy resins and polyurethane thermosets.[48]

1.1.2 Terpenes and Terpenoids

Essential oils often contain a mixture of volatile compounds among which terpenes and terpenoids. The name derives from turpentine and was given by Kekulé in 1880, when he discovered α- and β-pinene.[50] Terpene and terpenoid molecules are often secondary metabolites of plants. Their biosynthesis has different functions in nature, such as defence and signalling.[51] Essential oils are obtained by distillation or extraction of different components of plants. Terpenes are industrially relevant in the fragrance, medical, cosmetic and food sectors, with a registered annual market size of 0.692 $ billion in 2023, and it is estimated to reach 1.35 $ billion by 2032, considering a

compound annual growth rate (CAGR) of 7.69% during 2019-2022.[52] To answer the market demand, genetic engineering technologies have been studied.[53] Biotechnological strategies for the biosynthesis of basic building blocks for terpenes (isopentenyl diphosphate (IPP) and dimethylallyl diphosphate (DMAPP)) can be performed efficiently staring from simple carbon sources.[54] Terpenes consist of isoprene repeating units, leading to structural diversity and often presenting unsaturations (Figure 11). This feature makes them suitable for chemical modifications and use as monomers in the polymer field.[55] Terpenes are usually classified according to the number of repeating isoprene units as mono- (2 isoprene units, C10), sesqui- (3 isoprene units, C15), and di-terpenes (4 isoprene units, C20). Terpenes can also be distinguished as linear and cyclic. Moreover, they can be eventually differentiated for their biological function. A relevant characteristic is their chirality, which can affect the organoleptic properties of enantiomers.[56] Terpenoids are modified terpenes, presenting oxygen as an additional atom in the form of alcohol, aldehydes and ketone groups (Figure 11).

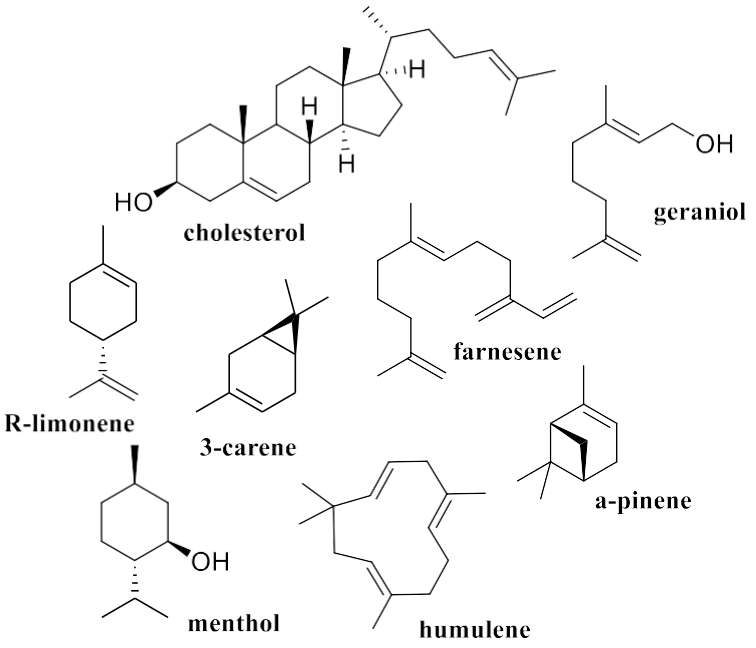

Figure 11. Structural diversity in terpenes and terpenoids.

Terpenes and terpenoids are ubiquitous, abundant molecules, which makes them appealing as building blocks for the development of new bio-based polymers. In the literature, different types of polymerization strategies have been applied to terpenes, such as radical, ionic and coordination pathways.[57] The most known terpene polymer existing in nature is *cis*-1,4-polyisoprene, which is commonly named *natural rubber*.[56]

Terpenes functionalization for creating novel monomers is of great interest.[58] In the last years, the groups of Winnacker and Rieger focused on investigating terpene monomers and their application in polymer synthesis.[59–61] Limonene is the most studied terpene derived from lemon and orange peel (*R* and *S* enantiomers, contained majorly in oranges and citrus, respectively). α- and β-pinene are the second most prominent terpenes in industry.[62] Pinenes are two versatile isomers due to the presence of endo or exo unsaturation, which is prone to different modifications.[63]

As another strategy to increase the availability of different terpene structures, catalytic isomerization routes have been developed. As an example, α-pinene can be isomerized to camphor. Due to the interest in this compound, this conversion has been investigated through different heterogeneous catalysis approaches.[64] Furthermore, α-pinene oxide can be isomerized to its respective aldehyde.[65] Many other catalytic synthetic routes can be applied to obtain different terpenes from more abundant terpene molecules such as hydroformylation, hydrogenation, oxidation, dehydrogenation, condensation and cyclization.[64]

1.1.3 Cellulosic derivatives

Wood is a source of a large number of bio(macro)molecules that can be valorized in a biorefinery concept.[66] Not only is it a renewable ubiquitous resource, it can also be recovered from wastes of the wood industry and further priced. Both natural polymers and small compounds can be obtained. Cellulose, hemicellulose and lignin are biopolymers found in wood.[67] Cellulose is the most prominent natural polymer present on earth.[68] It can be employed in different physical forms such as fibres or crystals and used in the field of biocomposites.[69] Generally, cellulose can be the source of many different molecules, such as different sugars and sugar-derived compounds. Cellulose is a polysaccharide consisting of hexose units, specifically glucose units connected by β-1,4 glycosidic linkages. This biopolymer can be depolymerized by diverse techniques[70] and new eco-friendly methods are being tested.[71] Likewise, *via* the triple dehydration of glucose, 5- hydroxymethylfurfurlaldheyde (5-HMF) can be obtained, the precursor of the respective diacid furan dicarboxylic acid (FDCA, Figure 12) .[72]

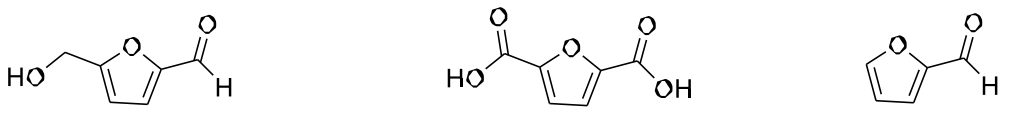

5-(Hydroxymethyl)furfural (5-HMF) **2,5-Furandicarboxylic acid (FDCA)** **Furfural (FF)**

Figure 12. Chemical structure of 5-HMF, FDCA and FF.

The latter is a very relevant aromatic building block, which presents structural similarity to terephthalic acid. FDCA allows the production of an important biobased alternative to polyethylene terephthalate (PET), named polyethylene furanoate (PEF). Parallelly, with an analogous process, furfural (FF, Figure 12) can be obtained from hemicellulose. Different furan-based monomers can be produced from 5-HMF and FF in specific catalytic conditions. Additionally, linear compounds such as levulinic acid (LevA) can also be obtained from the mentioned furans.[73]

Erythritol is a naturally occurring sugar found in numerous fruits and fermented foods and is also produced physiologically by humans (Figure 13).[74] However, the amount of erythritol in these natural sources is limited. For this reason, erythritol is produced by lactic acid bacteria from glucose or by the fermentation by fungi starting from more abundant natural sugars, such as glucose, fructose, xylose, and sucrose, which can be obtained from the depolymerization of lignocellulosic matrices.[75] In 2019, Meier *et al.* published a sustainable synthesis of erythritol-derived bicyclic carbonate,[76] which is a highly valuable monomer for polyhydroxyurethane (PHU) synthesis.[77]

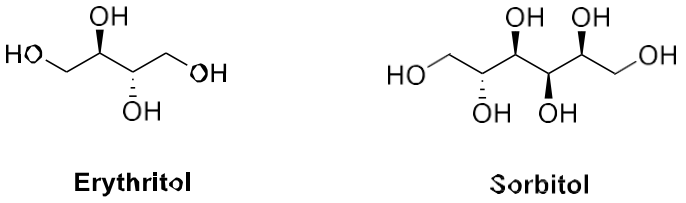

Figure 13. Chemical structures of erythritol and sorbitol.

Other sugar alcohols are also highly relevant, such as sorbitol. By the double dehydration of this compound, isosorbide can be synthesized. 1,4-Butanediol can be obtained through diverse pathways from succinic and fumaric acids, which are molecules both derivable from biomass.[48]

Lignin, unlike cellulose, has a more complex structure formed by different phenolic units, which provides its characteristic robustness. Reasonably, lignin is the main structural constituent of plants, which also acts as an antioxidant, explained by the presence of phenol groups. Together with cellulose and hemicellulose, the valorisation of lignin is under investigation.[78]

1.2 POLYURETHANES

Polyurethanes (PUs) represent 5.3% of total European polymer production.[73] These polymers are ubiquitous in human life and essential for complying with everyday human needs. PUs are employed in many diverse sectors such as medical, automotive, construction, packaging and others.[79] PUs are used in different forms, i.e. as elastomers, coatings, adhesives, plastics and foams (Figure 14).[80] The latter can be distinguished into soft and rigid, and their market share is leading over the other applications with about 50% of the total PUs production.[81]

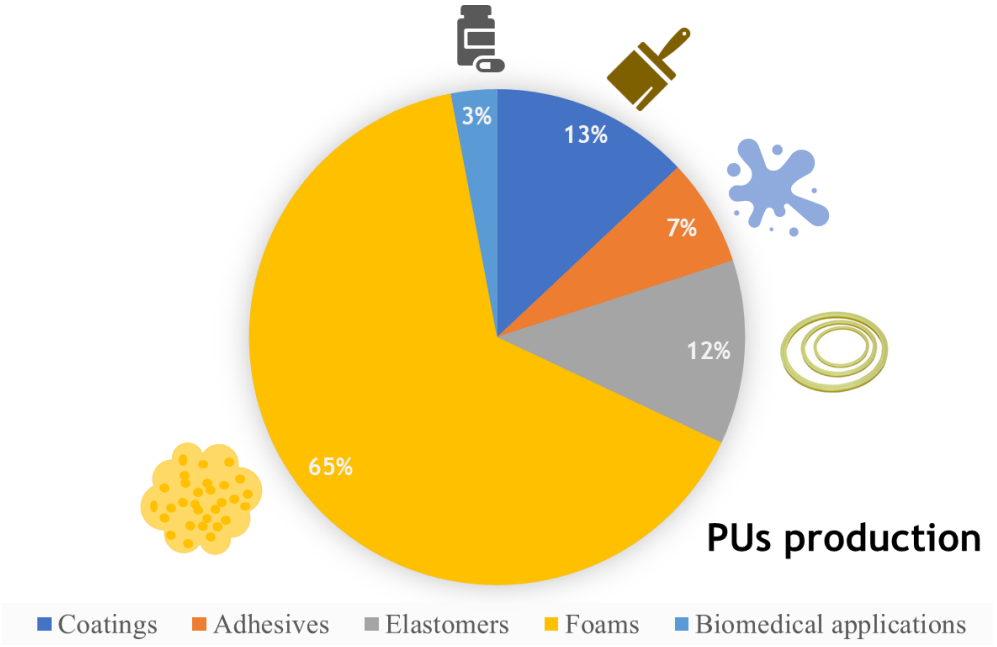

Figure 14. Polyurethane applications and their market volumes.[82]

The strategy to produce PUs was developed by Otto Bayer at the beginning of the 20th century.[83] The synthetic path typically consists of a step-growth polymerization reaction between diisocyanates and polyols (Figure 15).

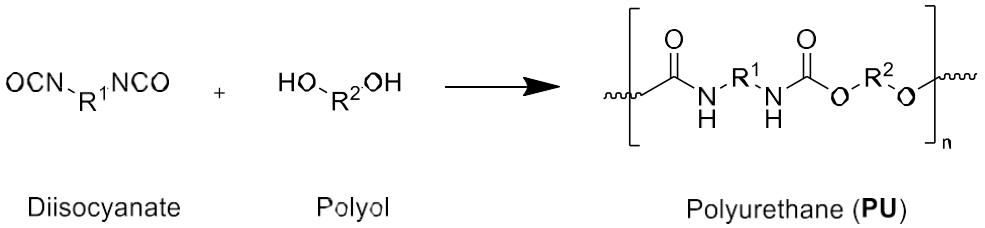

Figure 15. Reaction scheme for the synthesis of polyurethane from diisocyanates and polyols.

Many developments on polyurethane technologies have been achieved until present, achieving excellent physical and chemical properties for a plethora of applications.[84] Generally, PUs show chemical resistance and insensitivity to moisture and oxygen. Moreover, they possess high mechanical resistance, strength and flexibility.[85] In the field of medical applications, biocompatible PUs were developed.[86]

What makes PUs outstanding among other classes of polymers, is their great versatility of achievable properties. This is mainly related to the almost endless combination of different monomers, especially polyols, together with the presence of various types of additives. The chemical structure and size of the monomers selected are kye points for the successful design of the final polymer for a targeted application. Commonly, polyether polyols and polyester polyols are used as hydroxyl source. Generally, while the first are used to give flexibility to the final material, the latter provide more hardness. Usually, the molecular weight of the polyols is what influences the properties final polymer. Oppositely, the diisocyanates industrially used are short molecules. Methyldiphenyl diisocyanate (MDI) and toluene diisocyanate (TDI) are widely used examples. Their aromatic nature makes them very reactive monomers. After the polycondensation reaction between diisocyanates and polyols, the PU presents hard and soft segments domains (Figure 16).[85]

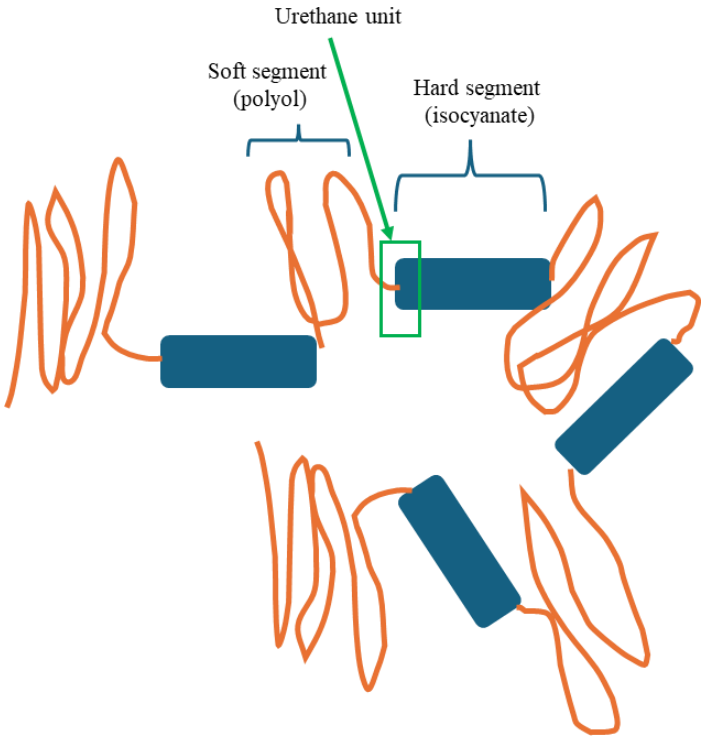

Figure 16. Schematic representation of hard and soft segments in polyurethanes.[85]

The first are related with the isocyanate structure and the hard segment content, while the seconds consist of polyether or polyester polyols longer chains. Consequently, selecting proper monomers, the ratio of hard and soft segments in the final polymer can be controlled. Despite all the positive aspects of these polymers, the process for the production of PU is under debate.[87] First concern is related to the origin of the monomers employed in their synthesis. Nowadays, the large majority of polymers are sourced from fossil resources. Nevertheless, the exploitation of oil by humans is resulting in nefarious consequences such as the rising level of CO_2 in the atmosphere, which results in unfavourable climate change.[88] Moreover, fossil deposits are finite resources.[89] For this reason, researchers are attempting to find alternative sources to produce novel building blocks applicable to polyurethane chemistry.[90] Indeed, the most common precursors of polyols are petroleum-based and derived from ethylene and propylene oxides, leading to polyether polyols by ring opening polymerization of the two mentioned monomers. On the other end, polyester polyols are made by a polycondensation reaction between diacids and dialcohols.

To overcome the source issue, many biobased alternatives were investigated starting from vegetable oils and lignocellulosic feedstock, generating a wide library of novel polyols.[91]

As an example, taking advantage of the unsaturations present in high oleic sunflower oil (HOSO), epoxy moieties can be obtained by a sequence of Shenk-Ene reaction, epoxidation and subsequent ring opening to achieve plant-oil based polyols.[91] Kessler *et al.* reported a series of vegetable oils-based polyols by epoxidizing the oil with formic acid and hydrogen peroxide and subsequently a ring-opening reaction was performed with castor oil fatty acid.[92] Commonly used petroleum-based diol chain extenders can be replaced to design polyester polyols, as such 1,4-butandiol (BDO), which can be bioderived from lignocellulosic feedstock. Alternatively, short chain biobased polyols derived from bio-derived carboxylic acids were employed to produce high-performance coatings.[93] Diverse thiols were employed to carry out thiol-ene reactions to functionalize the unsaturations present in the triglyceride structure and achieve different large-size polyols.[94,95] Following this scope, Jerahnno *et al.* published a comprehensive article about strategies for the upscaling of the production of biobased polyols from laboratory to market scale.[96]

Parallelly, the design of bioderived isocyanates has been developed by academia and industry.[97,98] Some examples of commercially available biobased isocyanates are shown in Figure 17:

- Vencorex Chemicals: Tolonate™ X FLO 100 (from palm oil 140±80 mPa s/25 °C).
- Covestro: Desmodur® eco N 7300 (viscosity= 9200 mPa s/25 °C).
- Mitsui Chemicals: STABIO™ D-310N (viscosity = 2 mPa s/25 °C).

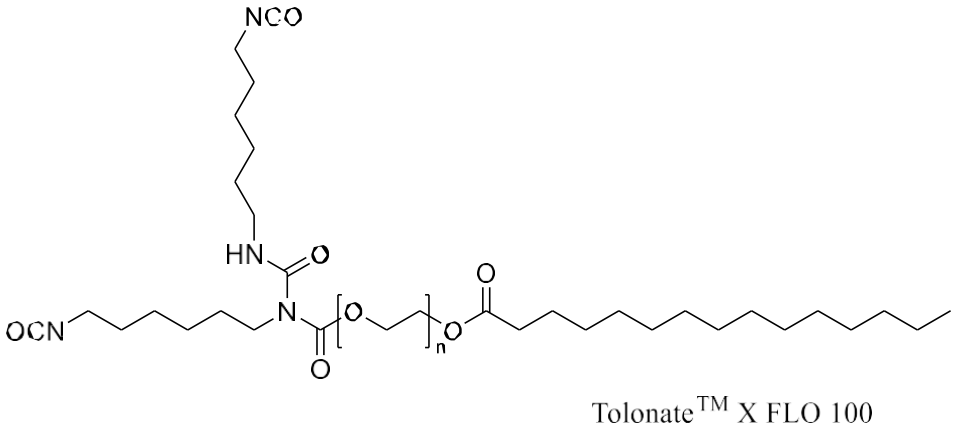

Tolonate™ X FLO 100

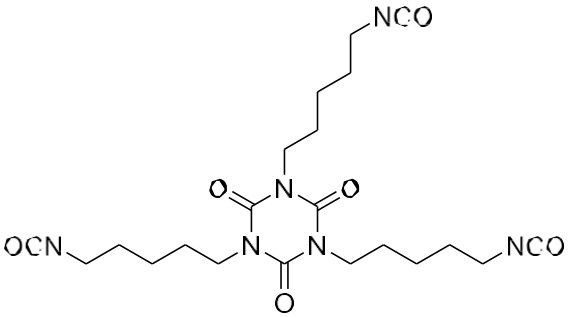

Desmodur® eco N 7300

STABIO™ D-370N

Figure 17. Chemical structures of Tolonate™ XFLO 100, Desmodour® eco 7300 and STABIO™ D-370N.[100]

It is important to consider that isocyanates are synthesized starting from phosgene, a highly toxic gas.[99] The inhalation of phosgene gas leads formation of HCl in the lungs and thus to damage to the respiratory system, internal lung bleeding and consequent death from asphyxia. Three synthetic pathways can be considered to overcome the use of phosgene, such as Curtius, Hoffman and Lossen rearrangements (Figure 18).

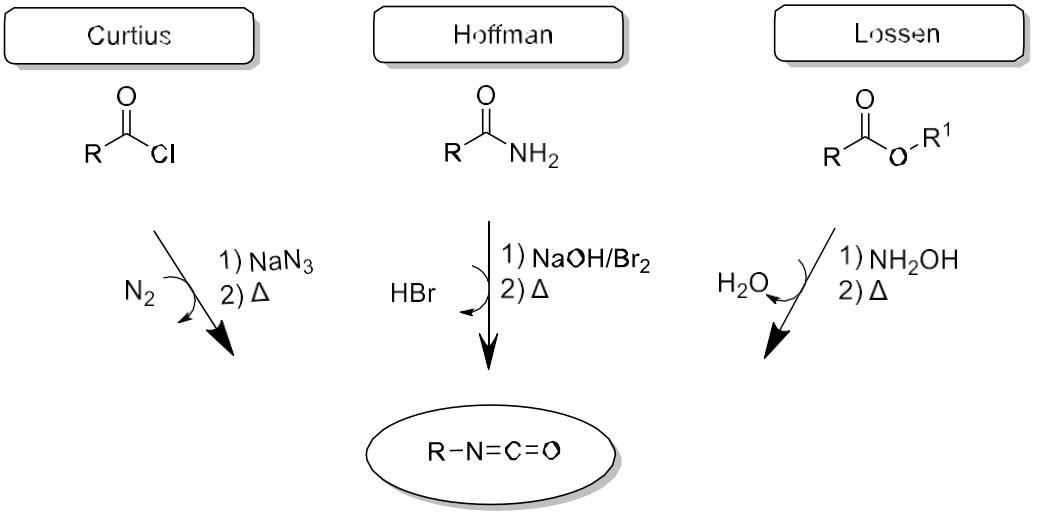

Figure 18. Curtius, Hoffman and Lossen rearrangments to achieve isocyanates.[100]

As an example, Hojabri *et al.*[101] prepared 1,7-heptamethylene diisocyanate (HPMDI) from oleic acid by the Curtius rearrangement. Caillol et al. reported the synthesis of bisguiacol diisocianate derived from lignin in a 4-step synthesis process.[97] Filippi and Meier reported a *in situ* formation of isocyanates *via* Lossen rearrangement without the need of isolating the isocyanate compounds.[98] In fact, besides the primary source for producing the monomers, an additional and relevant problem are the isocyanate compounds themselves. Isocyanates are proven to be hazardous chemicals for human health. These molecules are confirmed to be carcinogenic, sensitizing, and irritant.[102,103] Due to this, starting from the 24th of August 2023, restrictions on the use of diisocyanates were in force thanks to the proposal of 2020 from the European Commission and its approval of the REACH agency.[104] The newest precaution regulates a limit of < 0.1% diisocyanates by weight in commercial formulations.[105] Additionally, every employee handling these compounds must take mandatory training to ensure safety.[106,107] Because of the increasing restrictions and concerns, academia and industry both are investigating alternative monomers to produce analogous polymers to polyurethanes. To overcome all these problematics, a new class of macromolecules has been introduced in the last decades, reasonably called non-isocyanates polyurethanes (NIPUs).[108]

1.2.1 Non-isocyanate polyurethanes (NIPUs)

Alternative pathways have been studied to build PU-like polymers avoiding hazardous monomers. The innovators of the field were Dyer and Scott in 1957.[109] They reported the synthesis of cyclic urethanes and ureas reacting ethylene carbonateswithdifferent aminoalcohols anddiamines.

Different ways have been developed to produce alternative polymers to replace PU, as shown in Figure 19.[109] However, not all are considerably better alternatives to the polycondensation of isocyanate and polyols. Indeed, some alternative routes involve hazardous chemicals such the use acyl azides as monomers or the ring opening polymerization of cyclic carbamate or aziridines with supercritical CO_2 (Figure 19).[109]

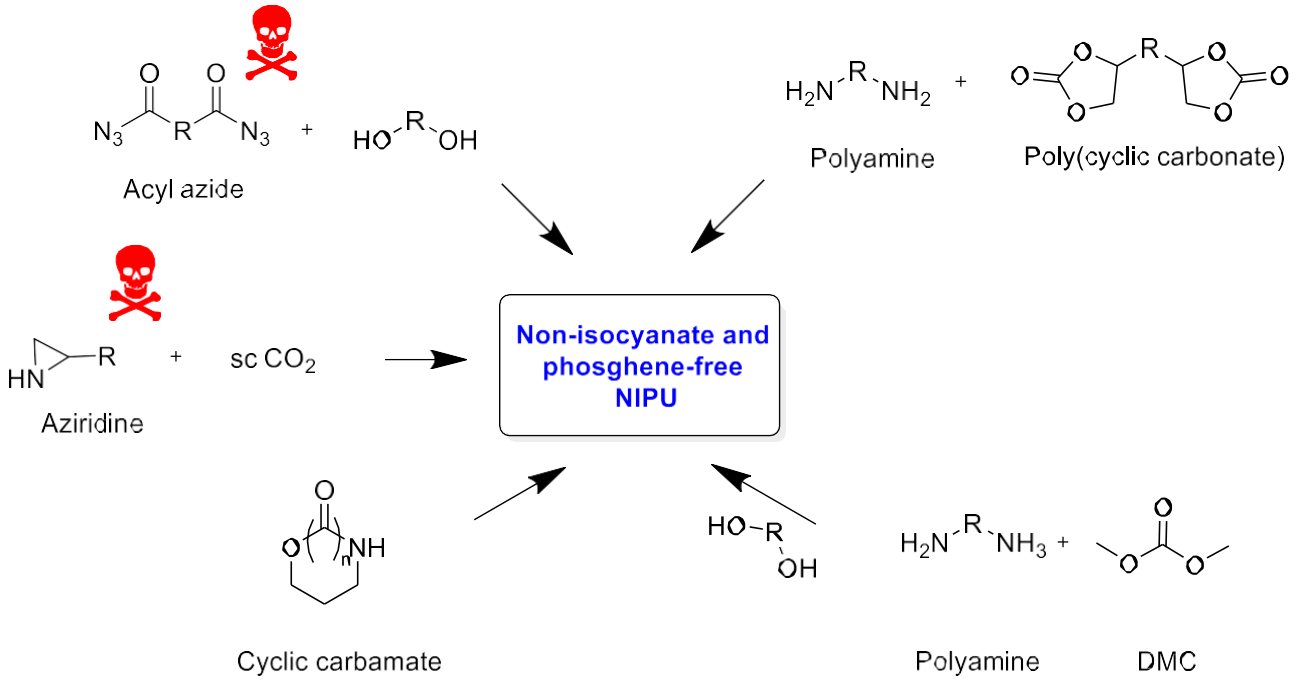

Figure 19. Non-isocyanates and phosgene-free routes to non-isocyanate polyurethanes.

Among all the reported routes, the most valuable and safer are:

- Polyaddition reaction between cyclic carbonates (CC) and amines (aminolysis).[110]
- Transurethanization reaction between carbamates and amines (Figure 20).[111]

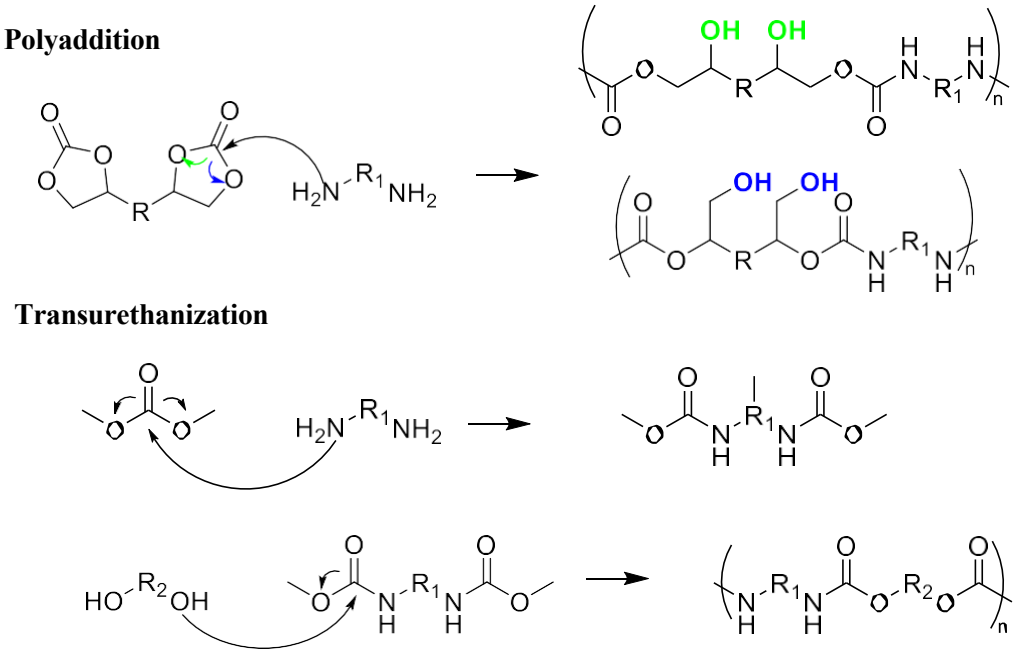

Figure 20. Aminolysis vs transurethanization reaction in the synthesis of NIPUs.

Currently, the polyaddition is the most studied pathway. This reaction yields polyhydroxyurethanes (PHUs), named after the presence of secondary and/or primary OH groups in β-position to the urethane groups as a consequence to the aminolysis RO reaction.

Despite the high desirability of NIPUs, weak points in their production are present. Indeed, the reaction between amino groups and CCs faces some limitation, such as the low molecular weight of the final polymers. First limiting factor is the low molecular weight of the starting monomers which leads to short polymer chains. Commonly, the high molecular weight of polyurethane is achieved due to the long chain polyols. Then, aminolysis reactions usually reach 80% conversion as maximum achievable threshold. Side reactions such as urea, CO_2, oxazolidinone formation and transcarbamoylation are the most common cause of this outcome. Additionally, it was hypothesized and studied that strong hydrogen bonds can lead to polymer gelation yielding limited M_w. This obstacle can be overcome screening different catalytic systems and monomer structures.[112]

Three catalytic activations can be considered, such as[113]:

1. increasing the electrophilicity of the carbonate centre (Figure 21a);
2. increasing the nucleophilicity of the amine (Figure 21b);
3. nucleophilic activation of the carbonate (Figure 21c).

Furthermore, strong bases, urea and thiourea and amine catalyst have been studied.

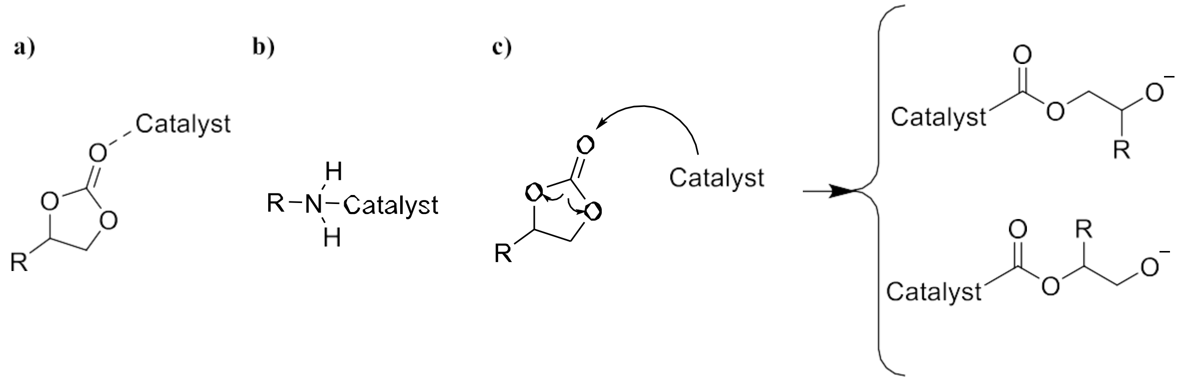

Figure 21. Types of catalytic activations in NIPU synthesis. a) increased electrophilicity of the carbonate centre; b) increased nucleophilicity of the amine; c) nucleophilic activation of the carbonate.[113]

Different types and sizes of CCs can be synthesized. However, 5-membered CC are the easiest to obtain, reacting an epoxy group with CO_2 (Figure 22).

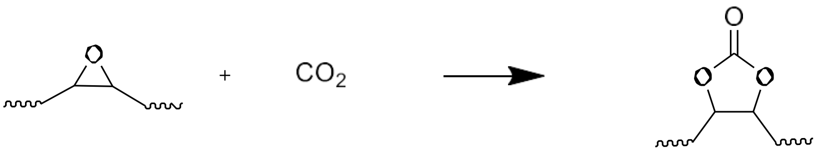

Figure 22. Reaction of epoxies and CO_2 r to produce 5-membered cyclic carbonates.

The reaction mechanism from epoxy to CC involves three steps. Firstly, the nucleophilic ring opening of the epoxy ring takes place, usually with the help of the coordination of the oxirane oxygen to a Lewis acid (LA). Subsequently, the insertion of CO_2 takes place followed by the cycloaddition, followed by ring closure and catalyst regeneration (Figure 23).[114]

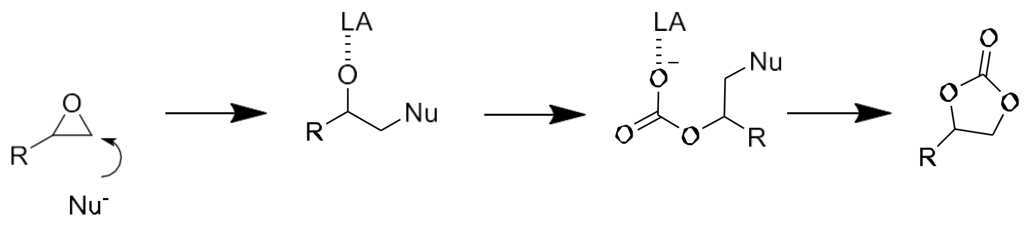

Figure 23. Mechanism from epoxy to cyclic carbonate with CO_2 through 1) ring opening 2) CO_2 insertion and 3) cyclization.

The convergence of CO_2 fixation, the use of renewable feedstocks and the isocyanate-free approach to the synthesis of NIPUs with sustainable processes is the aimed and best strategy for next-generation PU-like materials. The reactivity of the CC has been investigated, demonstrating that a proportional relationship between the monomer reactivity and its ring size exists.[115] Indeed, it has

been demonstrated that the larger the ring, the higher the reactivity of the CC in the aminolysis reaction. This evidence is commonly attributed to a larger ring strain (Figure 24).

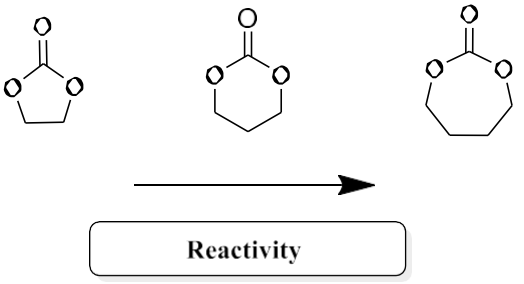

Figure 24. Cyclic carbonate reactivity by cycle size[115].

Moreover, this parameter can also be tuned with structure modifications leading to the so-called activated cyclic carbonate (ACC).[113] Commonly, these CCs present unsaturation or electron-rich groups in α or β position of the ring. Detrembleur *et al.* showed that reacting an ACC reacts with secondary amine, a PHU can be obtained. Moreover, it was also shown that ACC, specifically, bis(α--alkylidene cyclic carbonates), are highly reactive through aminolysis and tend to form poly(hydroxyoxazolidinone)s when reacting with primary amines (Figure 25).[116]

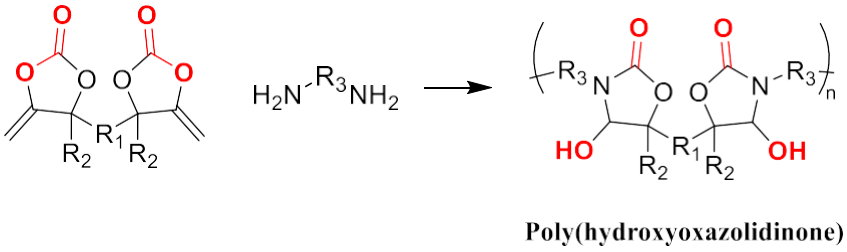

Figure 25. Poly(hydroxazolidinone) formation *via* polyaddition reaction of a bis(α-alkylidene cyclic carbonates) and a primary diamine.

Bio-based CCs have been synthesized from a wide number of molecules, among which epoxides. An effective way to introduce epoxy moieties is the nucleophilic addition of epichlorohydrin molecules to the chosen bioderived alcohol. On the other hand, a novel synthetic pathway to produce bio-based epichlorohydrin from glycerine has been developed by Solvay through the EPICEROL process.[117] Alternatively, epoxides can be formed *via* the oxidation reaction of unsaturated compounds using peroxides (i.e. meta-chloroperoxybenzoic acid, mCPBA)[118] or molecular oxygen.[119] Due to the high relevance of epoxides as intermediates, a large number of catalytic systems have been investigated to perform this reaction. This route is often applied, as epichlorohydrin can also be derived from glycerol, but it is a highly toxic chemical thus contradicting the principles of green chemistry.[120,121] The epoxidation of double bonds present in natural compounds, for instance triglycerides, is a preferred route.[113] Furthermore, the epoxies

obtained will react with CO_2 to get 5-membered CC units. With this approach, not only sustainable resources are employed, but CO_2 can be used as a building block. Caillol *et al*. generated different biobased CCs from cardanol and vanillin,[122,123] but the problematic epichlorohydrin was used (Figure 26).[124,125] Alternatively, the same group, achieved cardanol-based epoxy in an epichlorohydrin-free pathway, employing mCPBA (Figure 26).[126] However, allyl bromide was used. Similarly, another vanillin-based epoxy was achieved in a two-step synthesis from vanillic acid. Firstly, performing the allylation step and secondly employing an enzymatic lipase catalyst (Novozyme 435) to perform the final oxidation step. Nevertheless, allyl bromide, DMF and toluene were used in this procedure, making the process not in line with the green chemistry principles. [127]

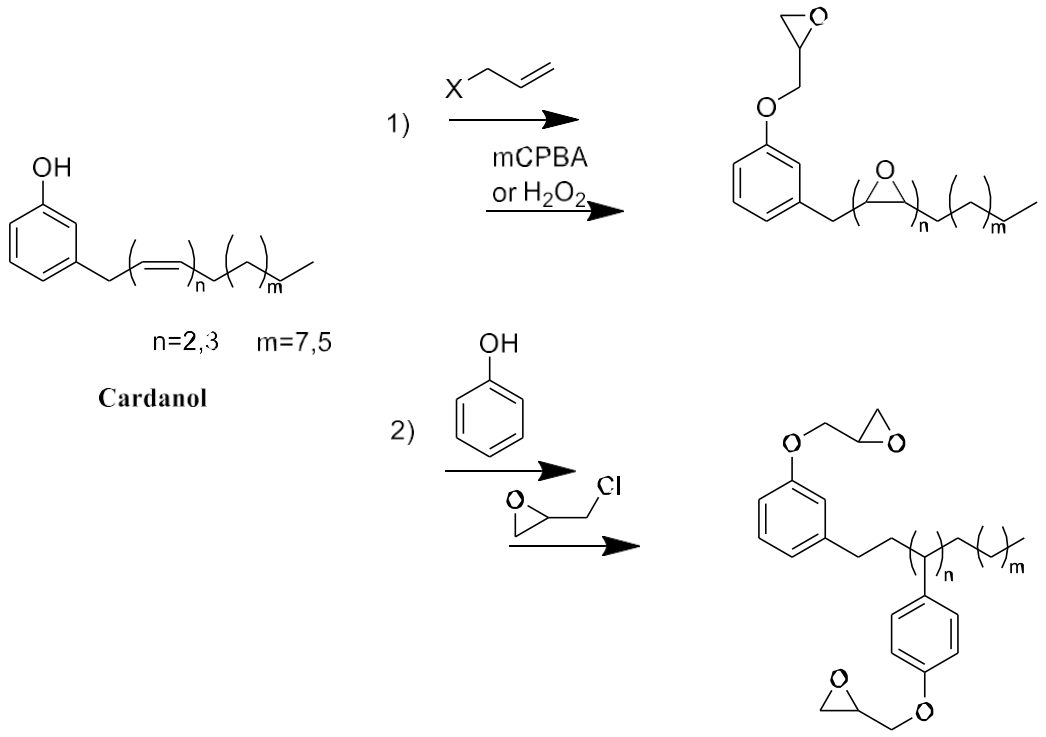

Figure 26. Possible synthetic strategies to achieve epoxy monomers from cardanol.

Diverse studies on vegetable-oil-based cyclic carbonates are available.[127-130] Commonly, the unsaturations present in the triglyceride structure are converted into epoxy groups *via* oxidative pathway employing mMPCA or H_2O_2, followed by the coupling with CO_2 (Figure 27).

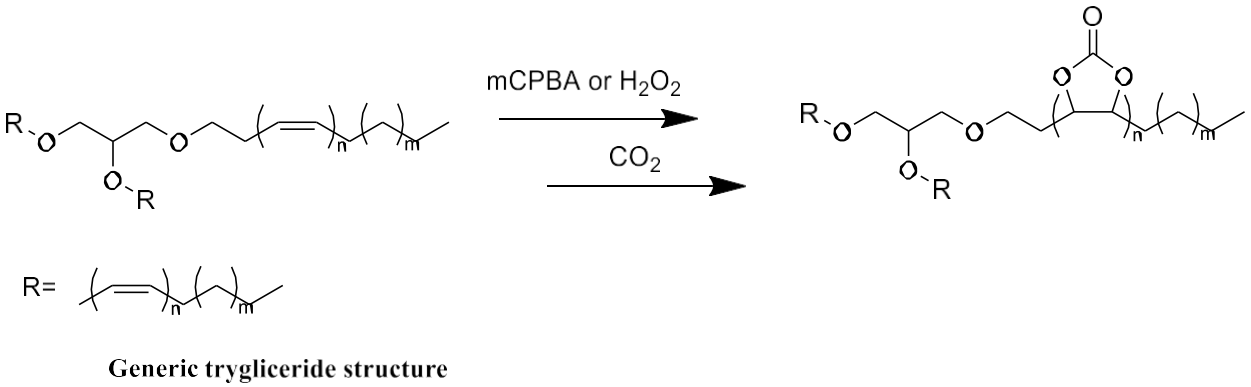

Figure 27. Direct epoxidation of vegetable oils.

0.1.1 Polyamines

Oppositely to the studies on CCs, much fewer articles can be found on the design of biobased polyfunctional amines.[131,132] At present, popular commercially available amines used for NIPUs synthesis are usually petroleum-based difunctional linear primary amines (i.e 1,6-hexamethylene diamine or *Jeffamines®)* or the cyclic isophorone diamine, which is potentially biobased (Figure 28). On the market, very limited options for trifunctional primary amines exist. One example is the amine T403 from the *Jeffamine*® series.

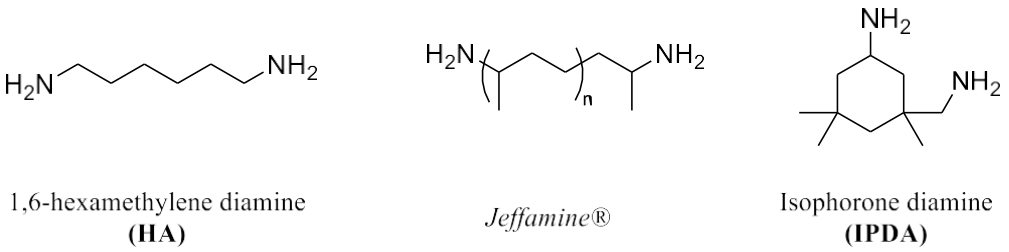

Figure 28. Chemical structures of 1,6-hexamethylene diamine, a general Jeffamine structure and isophorone diamine (IPDA).

As for CCs, the reactivity of different amines was examined. Diakoumakos and Kotzev evaluated the reactivity profiles of different amines with a 5-membered cyclic carbonate at room temperature.[133] They rationalized an increasing reactivity trend for aliphatic amines without α and β substituent. Concomitantly, in the same batch of high reactive polyamines, it was observed that the reactivity decreases with lowering the molecular weight (Figure 29).

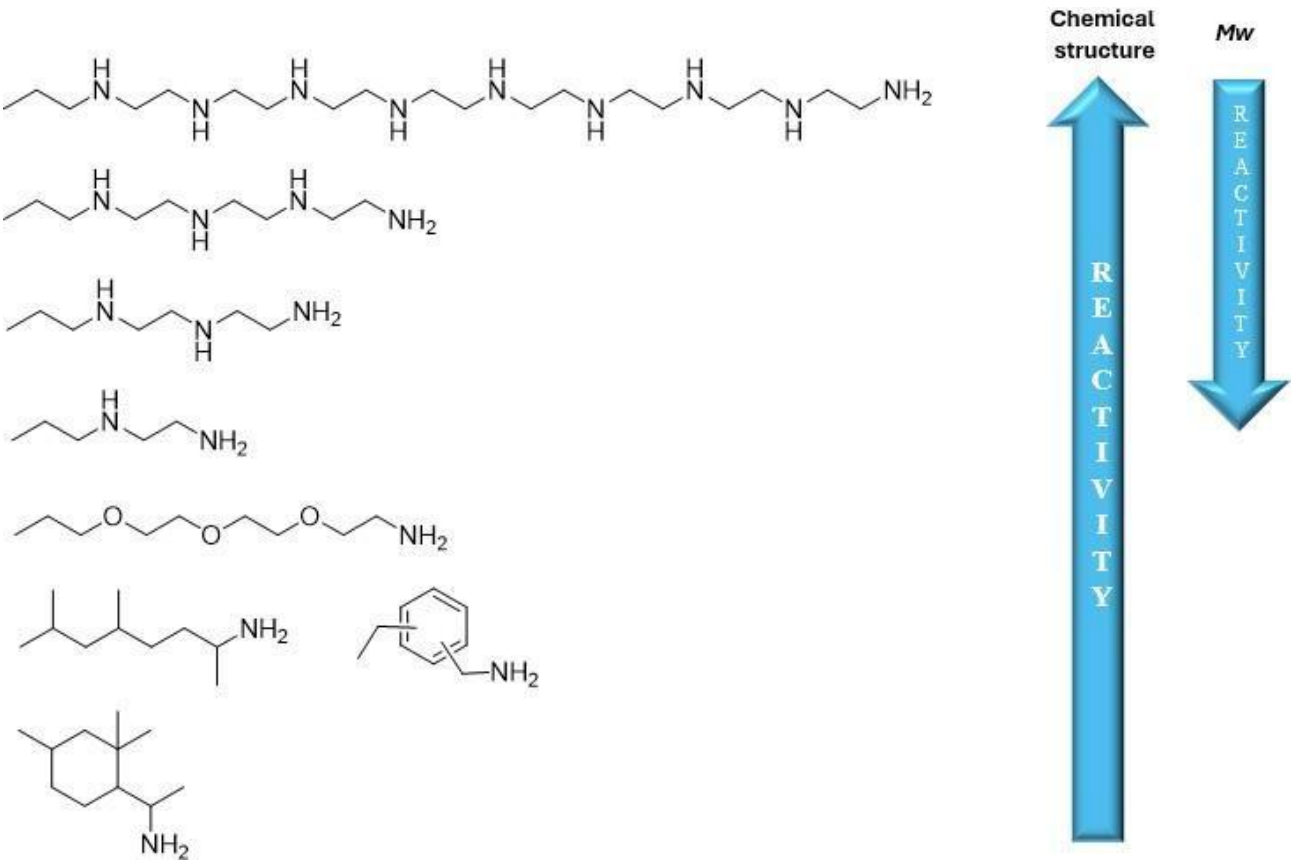

Figure 29. Reactivity of different amines with 5-CC at room temperature.[133]

In the study of Andrioletti *et al.*, it was shown that steric hindrance is a limiting factor for amine reactivity, while nucleophilicity favours aminolysis.[134] Moreover, it was demonstrated that β-hydroxy amines present an enhanced reactivity compared to the analogous aliphatic amines.[135] Main determining factors influencing the reactivity of amines are the combined effect of nucleophilicity and steric hindrance. It was reported that a primary amine on a secondary carbon (sec-butylamine) is less reactive than a primary amine on a primary carbon (n-butylamine).[136] Moreover, in the same study, primary amines on a tertiary carbon displayed no reactivity in the kinetic studies with propylene carbonate at 80°C. Furthermore, the inductive effect of heteroatoms in β-position to the amine nitrogen can lead to faster kinetics.[137] It is relevant to mention that, if the reaction with CCs is conducted in a solvent, this parameter can highly influence the reaction kinetics. The reaction rate is known to be highest in protic polar solvents due to the increased electrophilicity of the CC in this media (Figure 30).[117]

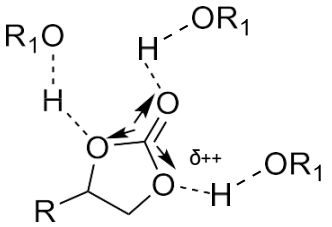

Figure 30. Effect of protic solvent on CC.[117]

0.1.2 Bio-based polyamines

Di- and tri-functional biobased primary amines are the most desirable monomers. A commercially well-established series of bioderived amines is the *Priamines*® from Cargill.[138] These amines are produced from fatty acid dimer obtained through isomerization and subsequent Diels-Alder cycloaddition and hydrogenation under harsh conditions. In the field of lignocellulosic-derived amines, it is possible to find a few examples. Aminated cellulose can be produced, however this synthesis was performed through a non-sustainable pathway.[139] A regioselective bromination on primary OH groups of cellulose followed by an amination using ethylene-1,2-diamine was performed. Recently, Avérous *et al*. published a strategy for the amination of lignin following the green chemistry principles.[140] The synthetic route consisted of an amidation reaction followed by hydrolysis using non-toxic chemicals (Figure 31).

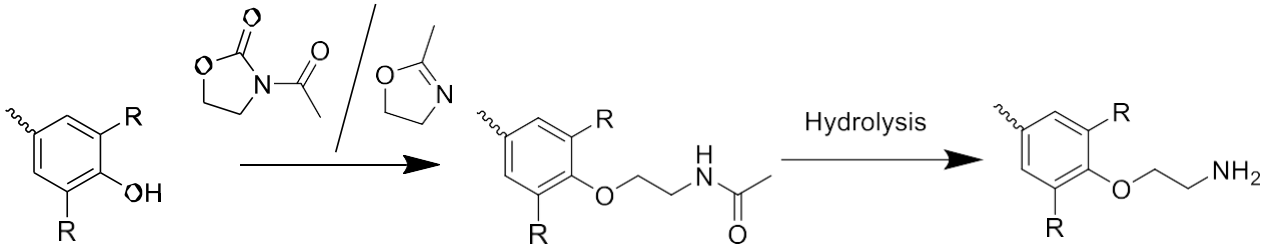

Figure 31. Two-step synthesis for lignin amination[140].

In 2023, Nam and coworkers showed a different pathway to achieve a lignin-based polyamine from Kraft lignin using diethylenetriamine (Figure 32).[141]

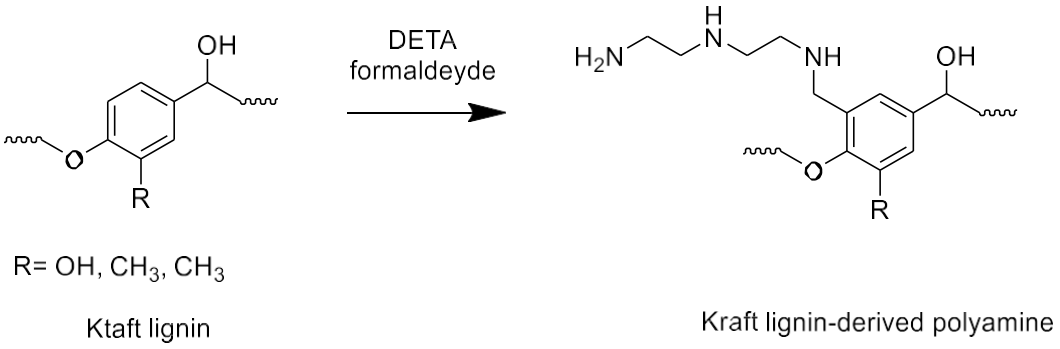

Figure 32. Amination process of Kraft lignin[141].

Two examples of furan-based amines have been reported. A dimer of furfural amine was obtained by an acid condensation reaction of the biobased furfuralamine.[143] Furan-based amine from 5-HMF *via* reductive amination was also synthesized. For this aim, different nickel-based heterogeneous catalysts were tested. (Figure 33). [144,145]

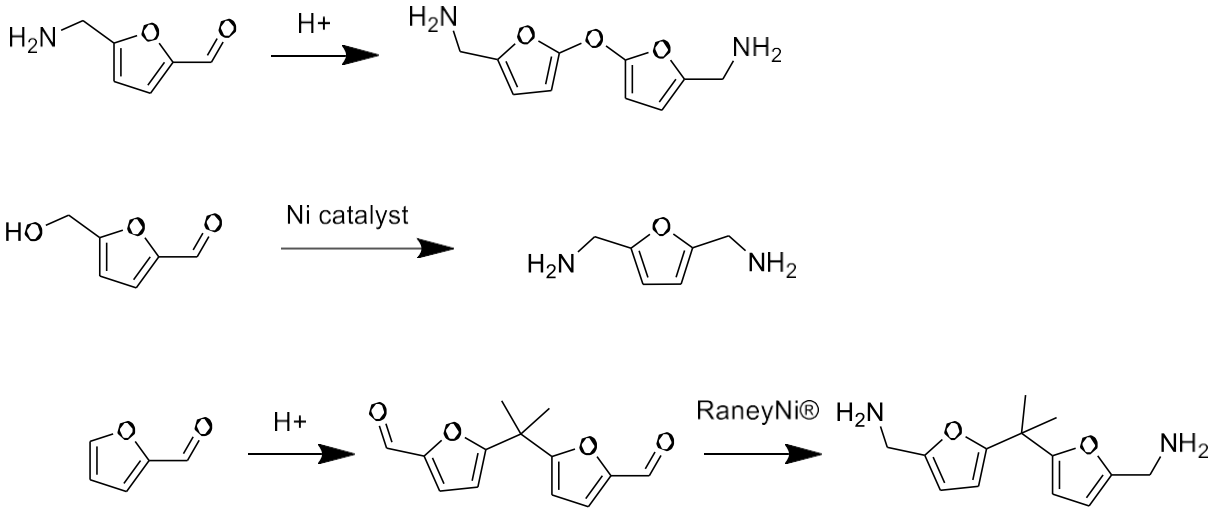

Figure 33. Synthesis and structures of furfural derived diamine.[144,145]

The dimerization of furfural was reported by Jerome and colleagues.[145] This aromatic dialdehyde can further allow the synthesis of the respective diamine *via* catalytic reduction with a nickel catalyst. Limonene diamine was synthesized by Meier *et al*.[146] *via* a thiol-ene photoinitiated reaction taking advantage of the naturally occurring unsaturation of the compound (Figure 34).

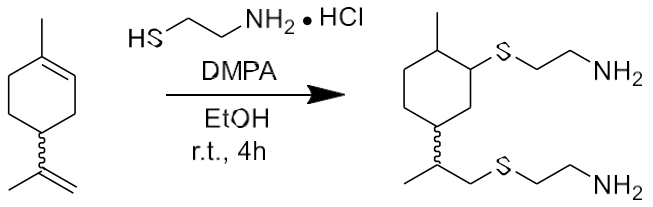

Figure 34. Thiol-ene reaction for the synthesis of limonene diamine.[146]

Rapeseed oil and canola oil-derived tri-functional amines were synthesized with thiol-ene analogous strategy (Figure 35).[147,148]

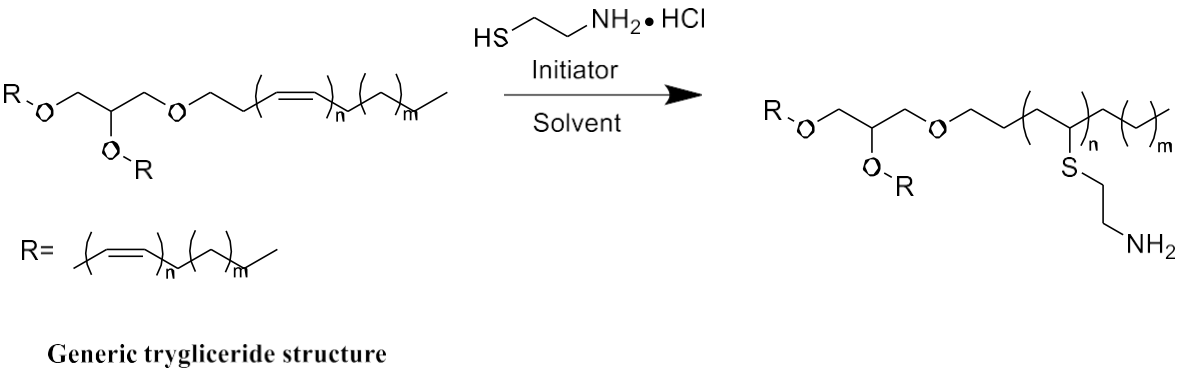

Figure 35. Thiol-ene reaction of vegetable oils.[147,148]

A three-step synthesis was reported to achieve a rigid aromatic diamine structure from the vanillin (Figure 36).[149] Also, a diamine from vanillin could be obtained after the synthesis of vanillin diepoxy compound, followed by a ring opening reaction (Figure 36). Moreover, an aromatic amine from cardanol, through the introduction of unsaturations *via* S_N2 reaction with a toxic allyl bromide and a subsequent thiol-ene reaction, was also described.[150]

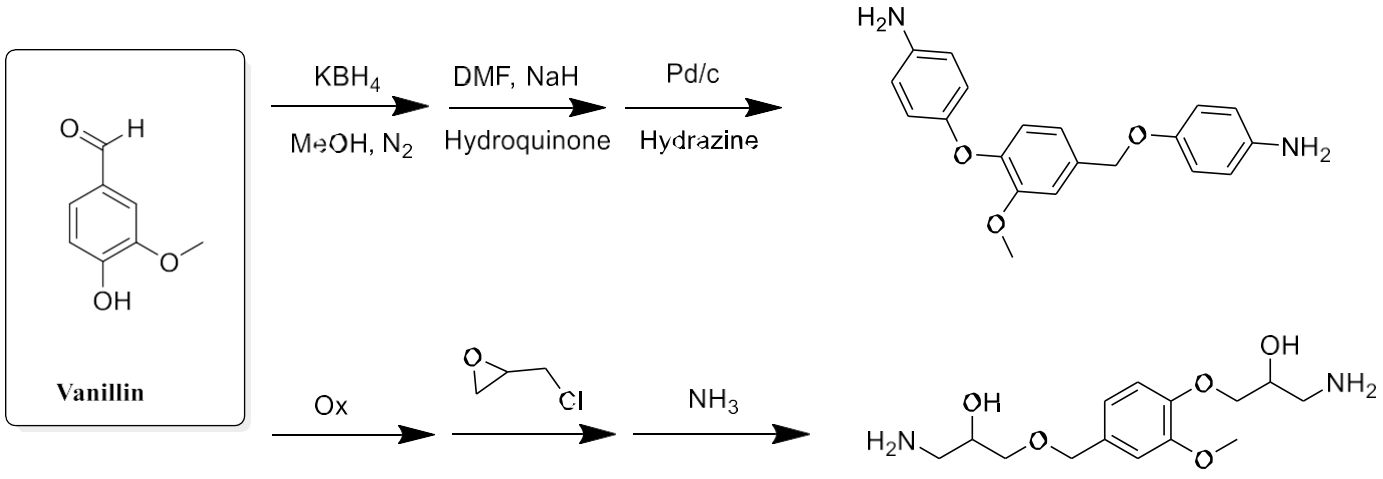

Figure 36. Possible strategies to synthesize a diamine compound from vanillin.[149,150]

Cramail and coworkers[151] designed two synthetic pathways to obtain diamines from vanillin dimer and methylated divanillic acid, achieving bis-benzylamine and bis-aniline moieties, respectively (Figure 37). The first synthetic route involved the alkylation of the hydroxy phenols, followed by oximation of the aldehyde functions to methylated divanillyloxime. Then, the oxime moieties were reduced to primary amines under 12 bar H_2 pressure and in presence of l RaneyNi® catalyst (Figure 37). The second route involved the conversion of the divanillin monomer to the respective diacid, followed a Curtius rearrangement to yield the diisocyanate product. Finally, the isocyanate groups were hydrolysed to amines (Figure 37).

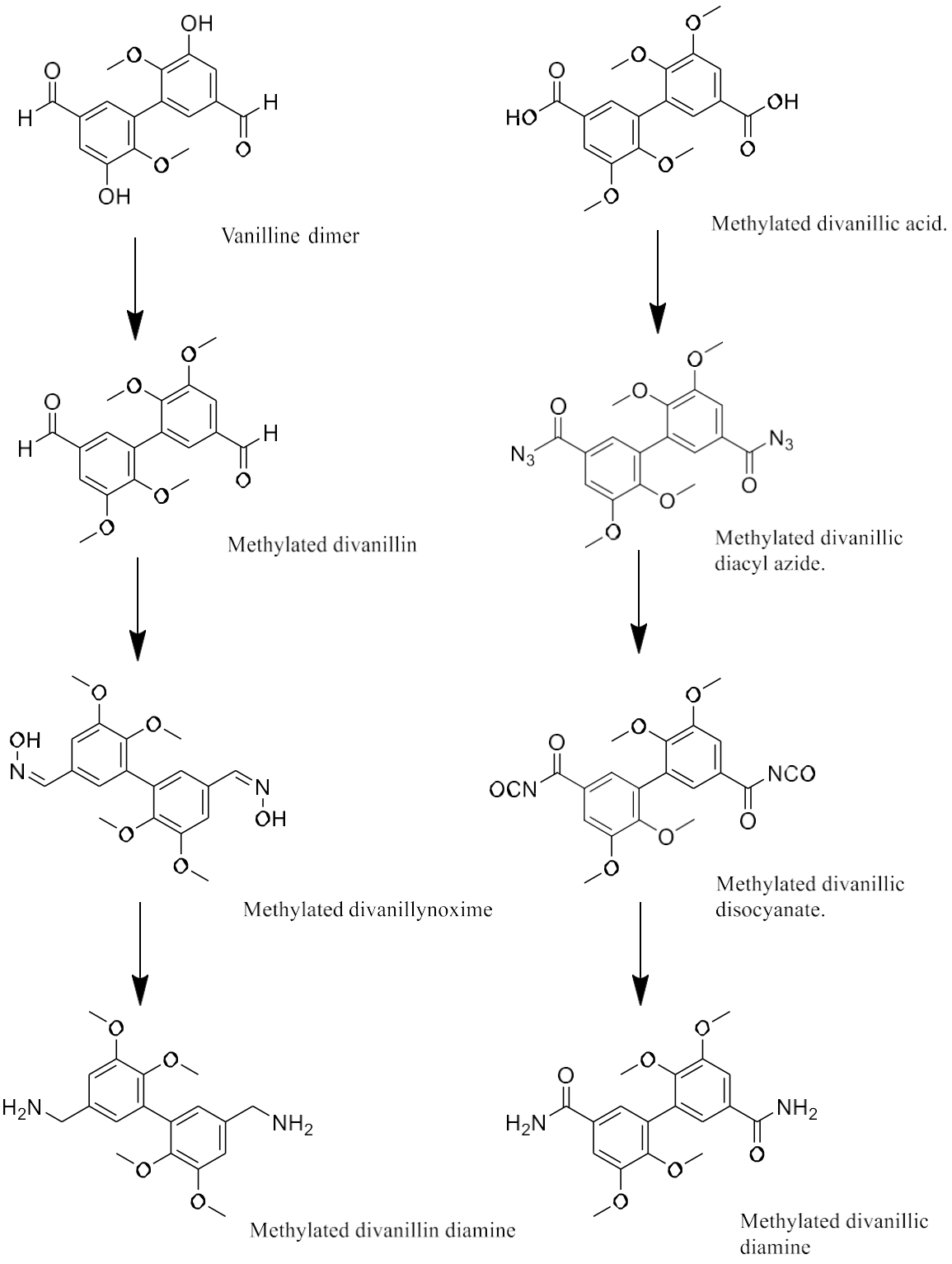

Figure 37. Synthetic pathways to achieve diamines from vanillin-derived dimers.[151]

The use of Raney Nikel® catalyst has also been reported to convert lignin-derived polyols to the respective amines in presence of aqueous ammonia.[152]

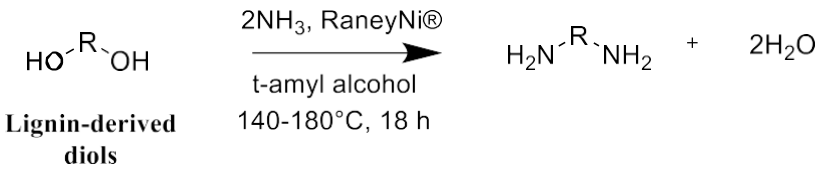

Figure 38. Catalytic route to lignin-derived diamine from lignin-derived diols.[152]

Knowing the current state of the art, this thesis focuses on finding strategies for the synthesis of novel bio-based polyamines and diverse monomers (cyclic carbonates and vinylogous urethanes) which can be useful for the production of more sustainable polyurethane-analogous materials. Indeed, the exploration of the latter have been also investigated. The purpose is to contribute to the bigger aim of a healthier maintenance of our planet and society. The practical goal is to support the transition from a linear economy to a circular model. In particular, the synthesis of novel biobased monomers synthesized following the green chemistry principles and the production of safer, bio-based, and useful polyurethane-analogous materials is aimed.

1 CHAPTER 2: POLYAMINES FROM VEGETABLE OILS AND TERPENES

1.1 FROM VEGETABLE OILS TO POLYAMINES

The synthesis of novel biobased monomers through more sustainable pathways is a relevant challenge. Bioderived polyamines are essential for developing greener materials, given that they are employed to produce diverse polymer materials such as polyamides,[153] NIPUs,[154] polyureas[155] and epoxy resins.[156] However, not many studies have been carried out on the topic.[157]

As discussed in Chapter 1, vegetable oils are an important renewable feedstock in the field of polymer chemistry.[40,158] Different research groups put efforts into studying fatty acid (FAs) and triglyceride (TRGs) modifications to enhance the value of such compounds. Great attention was given to the epoxidation of FAs due to their considerable applicability in the epoxy resin field or for further ring opening.[159] In the last decade, Meier *et al.* investigated the chemistry of FA and their modification.[160,161] Drawing on these studies, a synthetic pathway to yield polyfunctional amines in a two-step synthesis was designed through an oxidation reaction followed by reductive amination (Figure 39A).[162]

Few previous studies showed the possibility of achieving polyfunctional amines from vegetable oils. The chemical strategy applied is often *via* thiol-ene radical reaction (Figure 39B).[163,164] The photoinitiated pathway is preferred to the thermal initiated one because of the instability of TRGs when subjected to heat.[165] The first application of this strategy to achieve an amine-functionalized molecule was published by Meier *et al.*[45] using limonene as a starting building block in presence of cysteamine hydrochloride salt (CAHC) as thiol. Subsequently, these molecules were employed to produce epoxy and NIPU materials. Simultaneously, Rios *et al.* studied the amine functionalization of canola oil (or rapeseed oil) with the analogous approach.[166]

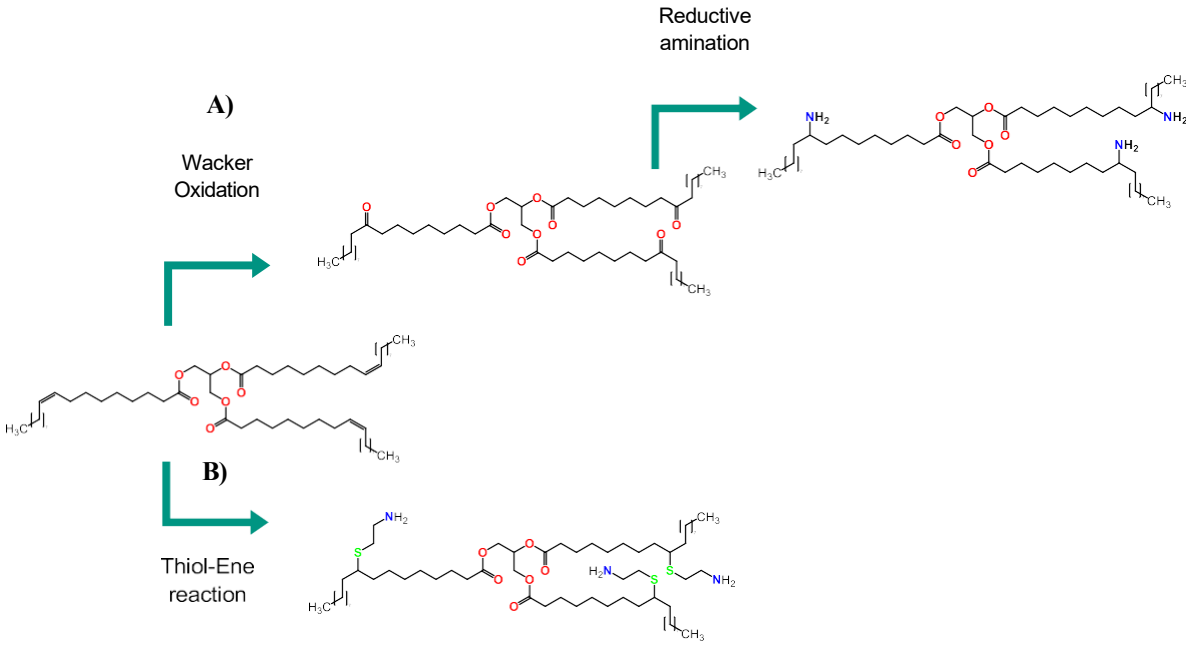

Figure 39. Possible pathways to achieve polyamines from vegetable oils. A) Wacker oxidation + reductive amination. B) thiol-ene click reaction.

1.1.1 Wacker oxidation

To investigate the oxidation of TRGs to polyketones in a sustainable fashion, the Wacker oxidation reaction was considered. The Wacker oxidation process was introduced in 1959 for the industrial conversion of ethene into acetaldehyde.[167] Besides its industrial importance, this catalytic reaction has been extensively studied for wider synthesis applications.[168–170] The industrial process was carried out in aqueous acidic media, while subsequently, Tsuji replaced it with a DMF/H_2O mixture as a solvent system for selective oxidation of terminal olefins.[171] Commonly, the laboratory scale reaction is referred to as Tsuji-Wacker oxidation. It is commonly defined as an aerobic reaction catalyzed by palladium(II) species in the presence of a copper co-catalyst (Figure 40).[172] Starting from a terminal olefin, ketones and aldehydes can be obtained as the anti-Markovnikov and Markovnikov products, respectively (Figure 41).[173]

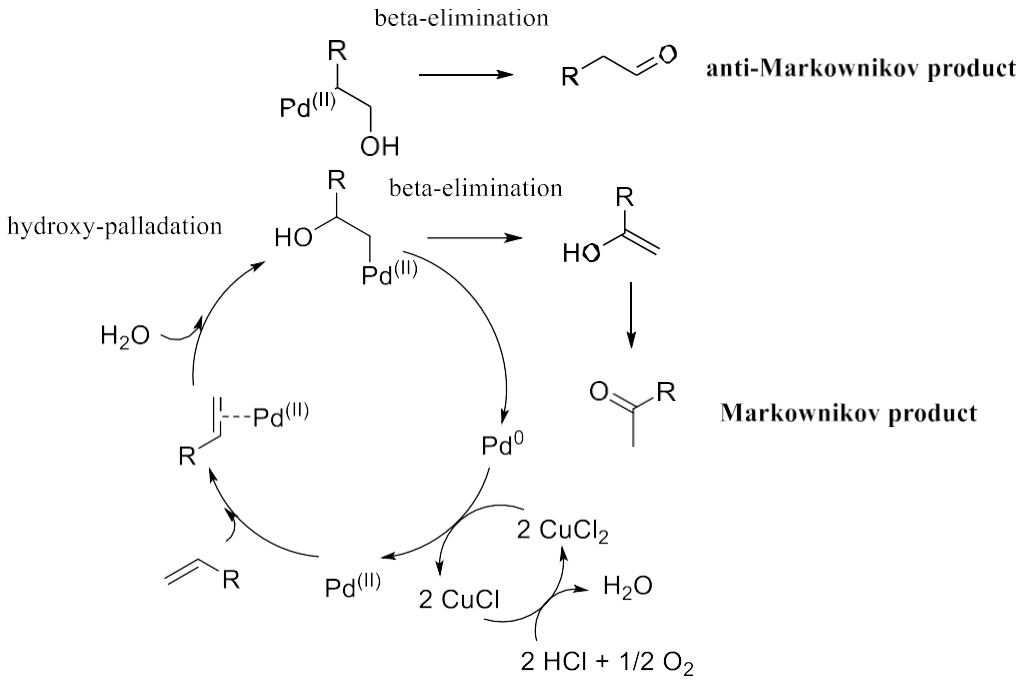

Figure 40. General mechanism of Wacker oxidation process.[173]

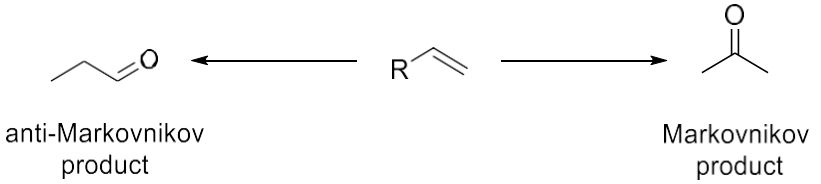

Figure 41. Markovnikov and anti-Markovnikov addiction on terminal olefin via Wacker oxidation.

The complex mechanism has been extensively studied;[176–179] however, unclear points remain. It is important to consider that in transition metal catalysis, factors such as pH, solvent, and ligands strongly affect the reaction mechanism and outcome.[177] In the frame of the Wacker oxidation, the most debated topic concerned the Pd(II) nucleophilic attack on the unsaturated system.[179] The *syn* or *anti* nature of the nucleophilic addition was discussed for a long time. Kinetic, stereochemical and theoretical investigations were performed to answer this question.[179] The resting state of $PdCl_2$ is its respective tetrachloropalladate $[PdCl_4]^{2-}$. The distinct reactions shaping the Wacker are the following (Figure 42).

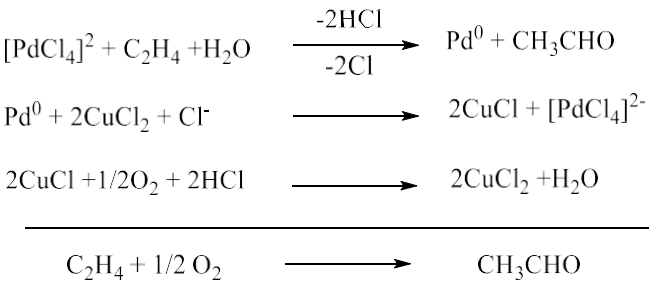

Figure 42. Individual reactions of the Wacker oxidation process[156].

As mentioned previously, the reaction conditions highly influence the reaction progress. As such, not every study can be considered valid for the final assumption. In their study, Lee and Henry[180] started studied the stereochemistry under non-Wacker oxidation condition. Starting from a mixture of isomers of 2-butene in presence of CO and other standard Wacker process conditions (methanol was used as solvent, however behaves similarly to water), 3-methoxy-2-methylbutanoate was selectively obtained (*anti* addition). Since CO can coordinate Pd, this prevents the methanol coordination, which is a requirement for *syn* addition. Therefore, the general assumption of an *anti* nucleophilic attack is not valid. Generally, if ligands are used to coordinate the Pd(II), steric hindrance might affect the *syn* addition.[177] Concentration of chlorides and co-catalyst have also an impact. Through deuterium labelling studies, it has been demonstrated that *anti* addition occurs at high concentrations (Cl^- > 3M; $CuCl_2$ >2.5 M) (Figure 43b). Oppositely, in case of Cl^- and $CuCl_2$ both < 1 M, an additional chlorinated product is obtained (Figure 43a).[177]

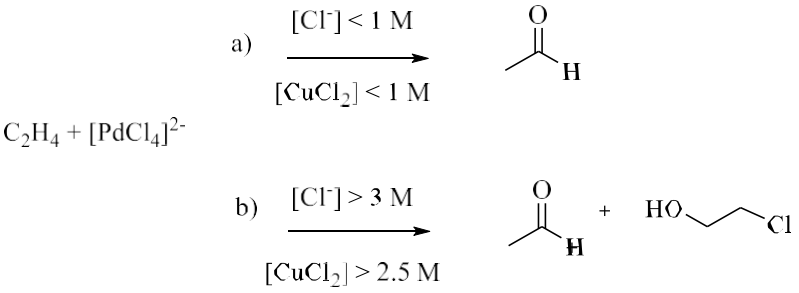

Figure 43. a) Wacker oxidation in low chlorine and co-catalyst concentration. b) Wacker oxidation in high concentration of chlorine and co-catalyst.[180]

Overall, it can be affirmed that the formation of the Markovnikov or anti-Markovnikov product depends on the hydroxypalladation stage. Regioselectivity studies to obtain preferentially one of the two products have been carried out.[176,181,182] It was shown that internal and terminal olefins bear different reactivity, with the second being more reactive.[183]

The high amount of $CuCl_2$ needed, the HCl corrosion problem, the production of hazardous wastes, the decomposition of palladium and the isomerization of olefins, drove the research on finding alternatives to design a more efficient and sustainable system.[172] Iron catalysts were proven to be effective as a cheaper and abundant metal option.[182] Moreover, alternatively to copper, other inorganics (hypervalent iodine,[184] CrO_3,[185] Oxone®,[186] H_2O_2 [187]) and organic oxidants (benzoquinone,[188] tBuONO,[189] tBuOOH[190]) were tested. A relevant example is the work of Grubbs *and coll*., which employed benzoquinone as a co-catalyst and an iron catalyst to internal olefins.[191] Moreover, the enzymatic pathway was screened.[192] Further, the substitution of the reaction media was experimented using ionic liquids[193] or supercritical CO_2.[194] Nickel-catalyzed Wacker oxidation was also tested.[195,196] One of the most significant modifications of this catalytic system was the use of oxygen (or air) as a sole oxidant in the absence of a co-catalyst.[183] Being a cheap and widely available resource, O_2 (or even better air) is generally considered the most sustainable oxidant. One first examples was published by Reddy *et al.* in 2016 employing 14 bar O_2 in DMAc/H_2O at 70°C. No co-catalyst was needed, but 50% mol. of $PdCl_2$ were used, achieving a 54% yield.[197] Kaneda *et al.* developed a more efficient system.[183] Initially, they investigated terminal olefins such as 1-decene, screening different solvents and Pd species. The best results were achieved by employing $PdCl_2$ as a catalyst in DMAc/H_2O in presence of molecular oxygen at 80 °C (81-96% yield) (Figure 44).

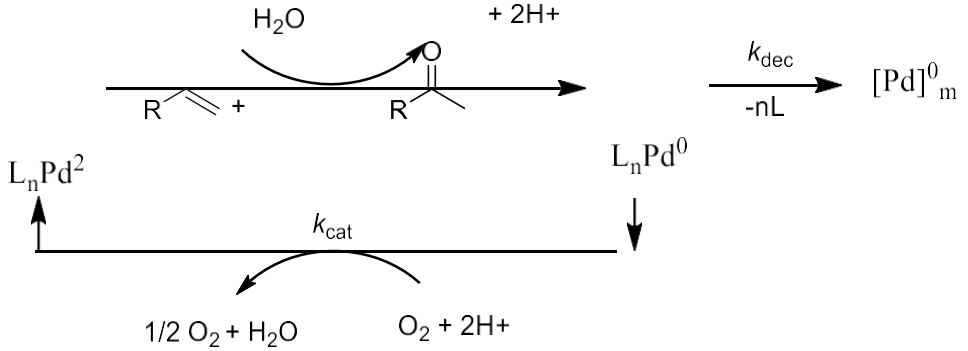

Figure 44. Proposed mechanism for co-catalyst free Wacker oxidation system.[183]

Four years later, the group showed the application to internal olefins.[198] In this case, the reaction was tested in the presence and absence of a copper co-catalyst. It was shown that there was a loss of activity in the oxidative pathway of internal unsaturation using copper. Further, the same approach was applied on different substrates (80-98% yield). In 2014, Meier *et al*. published a study on the oxyfunctionalization of methyl oleate and its further amination to produce biobased polyamides.[161] In general, a great advantage of this procedure is the recovery and reuse of the solvent-catalyst system without considerable loss of catalytic activity. Moreover, isomerization of olefins was not detected, which usually is a common drawback of the co-catalyzed system. It was observed that the increasing of the gas pressure resulted in a faster kinetic.[183]

1.1.2 Homogeneous catalysis for TRGs oxidation

Wacker oxidation, as described above, is a homogeneous catalyzed reaction. In this section, the study on the oxidation of a TRG (high oleic sunflower oil, HOSO) *via* Wacker oxidation using $PdCl_2$ as homogeneous catalysis is described. Related to the target molecule, a tri-functional ketone was previously obtained through a Schenk-Ene photoperoxidation reaction of high oleic sunflower oil.[49] In this study, the Wacker oxidation of HOSO was investigated using O_2 a sole oxidant. A commercial vegetable oil was used to demonstrate the applicability of the synthetic strategy on common unsaturated TRG substrates. HOSO takes its name from the high content of oleic acid. Other types of FA chains found in HOSO in a lower amount can generally be linoleic (two double bonds), linolenic (three double bonds) and saturated aliphatic chains. Therefore, the lipidic composition was analysed *via* proton NMR following the method developed by Salinero *and coll.*[199] (Figure 45). The integration of the proton signals relative to specific FA peaks were used in a system of equations (Equation 1). In this manner, the fraction of each FA chain form could be established.

$$\begin{cases} \int Vinylic\ H = 2A + 4B + 6C \\ \int Linoleic\ bisallylic\ H = 2B \\ \int Linolenic\ bysallylic\ H = 4C \\ A + B + C + D = 3 \end{cases} \quad \textbf{Eq 1.}$$

A = oleic chain (monounsaturated)

B = linoleic chain (diiunsaturated)

C = linolenic chain (triunsaturated)

D = saturated chain

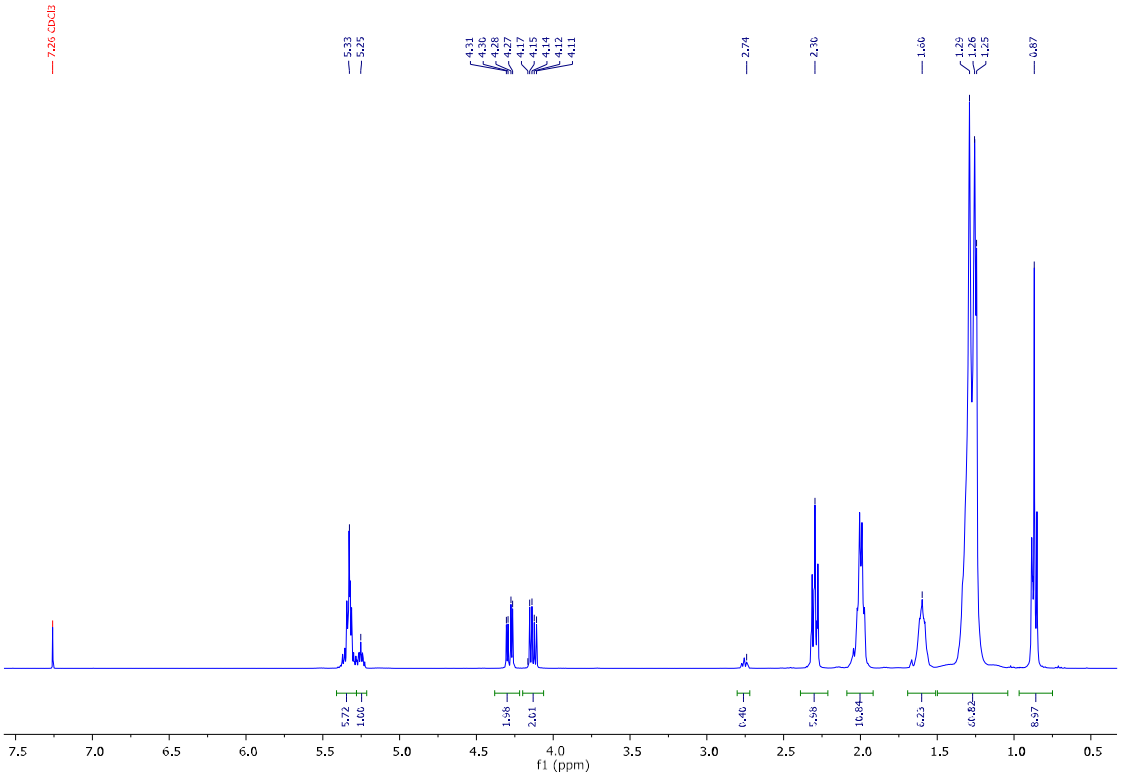

Figure 45.^{1}H–NMR (400 MHz) spectrum of HOSO in $CDCl_3$ (7.26 ppm) for the determination of its fatty acid composition.

After the normalization to the hydrogen linked to the glycerol carbon integral at 5.19 ppm to ∫= 1, the peaks of the glycerol -C**H**$_2$-CH-C**H**$_2$- unit (4.28 ppm), the integrals of the vinylic hydrogens (5.33 ppm), linoleic bisallylic hydrogens (2.74 ppm) and linolenic bisallylic hydrogen (~2.80 ppm) were evaluated according to the equation system showed above (Equation 1). In this oil, no linolenic chains were detected. (Figure 18).

$$5.72 = 2A + 4B + 6C$$
$$0.17 = 2B$$
$$0 = 4C$$
$$A + B + C + D = 3$$

This equation resulted in the fatty acid composition shown in Table 3 (A = 2.7, B = 0.085, C = 0, D = 0.215. TOT= 3).

Table 3. Percentage of different fatty acid chains calculated by proton NMR.

Peak	Percentage
A = oleic acid	90%
B = linoleic acid	2.8%
C = linolenic acid	0
D = saturated fatty acids	7.2%

The average amount of double bonds per TRG is the weighted average of double bonds per chain and equal to 0.96, which was approximated to 1 double bond per chain or approximately 3 per TRG for further experiments.

The experimental conditions were inspired by the work of Czapiewaki and Meier concerning the oxidation of fatty acid methyl esters (FAMEs).[160] $PdCl_2$ was used as a catalyst and DMAc/H_2O (9:1) as a solvent mixture. The reaction was carried out in a pressure reactor and O_2 (10 bar) was used as the sole oxidant, without the need for a co-catalyst. Initially, 5.6% mol of the catalyst were used and the reaction was carried out at 70 °C for 24 h. After purification *via* extraction, no conversion was detected by NMR. As a consequence, the amount of catalyst was increased to 15 % mol and 25 % mol of $PdCl_2$. The appearance of the triplet at 2.27 ppm corresponding to the carbonyl α-protons showed the successful formation of the product. As a result, the conversion to the desired product enhanced to 34% and 61% for 15% and 25% of catalyst loading, respectively. As mentioned above, the organic phase consisting of DMAc and the solid catalyst dispersed in it can be reused to carry the same reaction up to 3 times without significant loss of catalytic activity.[160] It is important to consider that, during the reaction, two possible regioisomers can be formed in position C9 or C10 of the oleic chain. However, no selectivity was detected in the formation of the ketone Halving the reaction time, the conversion decreased to 50% of the final product (**WO1**, Table 4). Keeping the conditions related to the best outcome (**WO0**, Table 4) constant, a screening of different reaction times was performed (Table 4). Reducing the time from 24 h to 8 h, the conversion was limited to only to 7% (**WO3,** Table 4). Similarly, a conversion of 12% was achieved after 12 h (**WO4,** Table 4). Further, the reaction time was investigated at 50 and 60°C. It was observed that 60°C for 24 h was leading to the same result recorded at 70°C after 12 h (50% conversion, **WO5** and **WO1,** Table 4).

Table 4. Screening of temperature and tie conditions for Wacker oxidation with O_2 as sole oxidant of high oleic sunflower oil (HOSO).

	Temperature (°C)	Time (h)	Conversion[b]
WO0[a]	70	24	62
WO1	70	12	50
WO2	50	24	14
WO3	60	8	7
WO4	60	12	12
WO5	60	24	50

For all the entries 25% mol catalyst was employed. [a] Best outcome conditions registered from the catalyst screening. [b] Measured by ^{1}H-NMR using triplet at 2.38 ppm (C**H**$_2$C=OC**H**$_2$) with reference integral of -CH_3 at 8.87 ppm (9H).

Compared to the classical Wacker oxidation process, several advantages can be found. Improvements in terms of green chemistry principles respected for this synthetic procedure are:

- Catalytic process
- Recyclability of the catalyst
- O_2 as sole oxidant (no need for a co-catalyst)
- Recyclability of the solvent media
- Simple work-up

As $PdCl_2$ is an expensive non-abundant metal, it was decided not to screen a higher catalytic load, as the advantageous aspects of catalysis and sustainability would have been missed.

1.1.3 Heterogenous catalysis for TRGs oxidation

As an alternative to homogeneous catalysis, heterogeneous catalytic systems were investigated for Wacker oxidation reactions.

Heterogeneous catalysis allows an easier catalyst recovery, which results in the possibility of its reuse and a simpler waste management. This often translates into cheaper and more sustainable processes. Additionally, heterogeneous catalysts possess better thermal stability. However, homogeneous catalysts typically show enhanced selectivity and activity (Table 5).[201]

Table 5. Generalized comparison between homogeneous and heterogeneous catalysis.[201]

	Homogeneous catalysis	**Heterogeneous catalysis**
Selectivity	excellent/good	good/poor
Thermal stability	poor	good
Catalyst recovery	difficult and expensive	easy and cheap

In the frame of Wacker oxidation, diverse strategies using a Pd/V_2O_5 catalysts supported on alumina,[202] titanium oxide,[203] silica[204,205] and carbon[206,207] can be found in the literature (Table 6). In these studies, a copper or vanadium co-catalyst was employed.

Table 6. Reaction conditions of different heterogeneous catalyst- systems and their selectivity in Wacker oxidation reactions.

Ref.	catalyst	support	T (°C)	Aldehyde	Ketone
Evnin et al.[182]	Pd/V_2O_5	α-Al_2O_3	140	~20%	trace
Peng et al.[186]	Pd^0	C	65	90%	nd
Barthos et al.[183]	Pd/V_2O_5	TiO_2	100	65%	nd
Barthos et al.[188]	Pd	VO_x nanotubes	150	95%	nd
Vafaeezadeh et al.[184]	Janus-type Pd	SiO_2	80	88%	9%
Wang et al.[187]	Co	N doped C particles	150	nd	95.8%
Hanf et al.[189]	Pd_3P	SiO_2	50	nd	100%

Barthos *et al*. prepared Pd particles supported on VO_x nanotubes.[208] A cobalt catalyst supported on charcoal was proposed by Wang and co-workers in 2020.[207] In this work, a single atom catalysis approach was adopted. The advantage of this approach, over classic heterogeneous catalysis, is the large availability of active catalytic sites. In fact, the absence of metal-metal bonds lead to an elevated surface area. This can be seen as equal to the activity of the sites present on the edge of a nanoparticle catalyst. Consequently, this characteristic enhances the reaction speed. In the work of Wang and colleagues,[207] the conversion of styrene to acetophenone was achieved using isopropanol as solvent and H donor, in an oxygen atmosphere at 150° C for 6 h. The best conversion to the desired product was 95.8%.

Recently, Hanf *et al.* developed a Pd-phosphide (Pd_3P) catalyst supported on silica and successfully tested its potential in the Wacker oxidation.[205] In this study, the effectiveness of Pd_3P/SiO_2 was tested on a model reaction converting styrene to acetophenone. Different reaction conditions were tested and the maximum selectivity was achieved at 50 °C in 6 h, reaching 70% conversion. Due to the great potential of Pd_3P/SiO_2, we decided to collaborate with the Prof. Hanf research group of the Inorganic Chemistry department of Karlsruhe Institute of Technology. The idea behind the investigation was to merge the previously mentioned O_2-sole oxidant methodology with heterogeneous catalysis. The preparation and characterization of this catalyst can be found in a recent paper, in which a metal-phosphide catalyst was used for Wacker oxidation.[205] For this work, the catalyst was kindly provided by MSc. PhD candidate Arjun Neyyathala from the Hanf research team.

The advantage of using phosphide catalysts relates to the large size of phosphorus atoms (1.23 Å atomic radius), which determine a significant interatomic spacing, leading to more accessible active metal sites. Indeed, it was demonstrated that the presence of P in Pd catalysts improved the catalyst performances.[210] Furthermore, the catalyst performances is influenced by the P/Pd ratio.[211] With the modification of this factor, the cluster size is decreasing following an inverse proportionality with the increase of P/Pd ratio. Therefore, the smaller the ratio, the bigger the cluster and the highest catalytic sites availability. Pd_3P is classified as metal-rich phosphorus species (nP < nM) and therefore contains M-M bonds (Figure 46).[73,212] It is needed to mention that in P-containing species Pd is mostly in the fundamental state, which helps the process.[212]

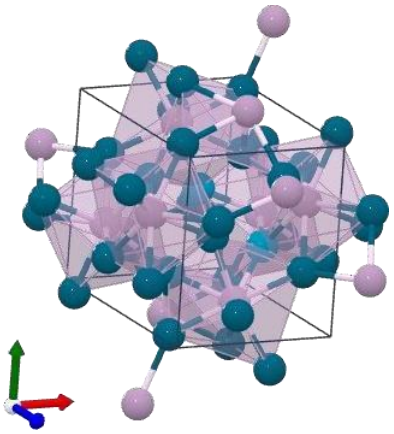

Figure 46. 3D structure of Pd_3P. mp ID for the Pd_3P is mp-19879 and data base version is same as below (data retrieved from the Materials Project for PPd_3 (mp-19879) from database version v2023.11.1.). Pd=blue, P= pink.

With the idea of applying this system of converting renewable feedstocks, methyl oleate was chosen as a fatty acid model compound. The aim of the study was the design of an efficient catalytic system in a *greener* fashion.

Pd_3P/SiO_2 with 10 wt.% palladium content was used for the initial experiments. As a comparison, also a pure supported palladium catalyst (Pd/SiO_2) was investigated. A previous study by Meier *et al.*[143] showed the achievement of 100% conversion of the double bond of methyl oleate fatty acid. The product was achieved within 24 h with 2.5 mol% $PdCl_2$ catalyst in the absence of a co-catalyst for methyl oleate in DMAc: H_2O at 70°C, in presence of 10 bar oxygen. The analogous conditions were used to test the catalytic activity of Pd_3P in this system. Moreover, with the aim of developing a more sustainable synthesis, a test in Me-THF/H_2O mixture as solvent media was carried out. In both cases, 2.5 mol% of catalyst were employed. Unfortunately, no conversion was detected in either test. Traces of epoxy isomers were formed (7% and 6%, respectively). A reaction trial was carried out with an increased catalyst loading (5 mol%) in both conditions.

In order to achieve better results, a Pd_3P/SiO_2 catalyst with 1% wt. metal loading was employed. The reduced density of the metal particles on the silica makes the active catalytic sites more accessible. As a consequence to the unsuccessful previous results, Pd_3P and MO were tested in the conventional Wacker oxidation condition under different conditions (Table 7).

Table 7. Reaction conditions tested for a conventional Wacker oxidation with Pd/SiO_2 and Pd_3P/SiO_2 catalysts on methyl oleate.

	Cat	Cat (mol%)	Co-cat (mol%)	Solvent	Conversion to ketone[a]%
P6	Pd_3P	2.5	5	THF:H_2O	56%
P7	Pd	2.5	5	THF:H_2O	60%
P8	Pd_3P	5	10	THF:H_2O	Trace
P9	Pd	5	10	THF:H_2O	-
P10	Pd_3P	2.5	5	Me-THF:H_2O	Trace
P11[b]	Pd_3P	5	10	THF:H_2O	-
P12[c]	Pd_3P	2.5	5	THF:H_2O	25
P13[d]	Pd_3P	7.5	15	THF:H_2O	56

Reaction conditions: catalysts Pd_3P/SiO_2 Pd 1 wt% supported on SiO_2 and $CuCl_2$ co-catalyst, 80°C, 24 h, O_2 10 bar. [a] Measured via GC-MS and ^{1}H-NMR. [b] Conducted under air at 1 atm. [c] Pd_3P/SiO_2 with Pd 5% wt. [d] High oleic sunflower oil as starting compound.

With the same catalytic loading and the presence of a $CuCl_2$ as a co-catalyst, the outcome improved. In fact, 60% and 56% conversion was reached in 24 h (80°C, in THF:H_2O, Table 7, **P6** and **P7**) with Pd and Pd_3P catalysts, respectively. A test in Me-THF was run with Pd_3P, to substitute the hazardous THF. However, a low conversion was achieved due to the unfavourable miscibility of the reactants in the solvent. To improve the result, a 5% mol catalyst was investigated in the same conditions with both catalysts (Table 7, **P8** and **P9**). From the GC-MS analysis, it was clear that the higher number of active catalytic sites present led to the formation of a mixture of side products, with significant production of those in the case of the pure Pd. A reaction, carried out in atmospheric condition led to no conversion (Table 7, **P11**). Further a Pd_3P catalyst with Pd 5%wt. was tested using the same conditions of the entry **P6 (P12)**. The aim was confirming the correlation between the Pd loading on the support and the reactivity of the catalyst. It was clear that this parameter was crucial to the product formation. This evidence can be explained by the higher availability of active catalyst sites and fewer M-M interactions. Indeed, while with Pd_3P - Pd 10% wt. MO conversion was not detected, with Pd_3P -Pd 5% wt. 25% conversion was achieved (**P12**) and an even higher value was obtained with Pd 1% wt. (56 %, Table 7-**P6**), considering same mol% conditions. This result can be explained

by the easier accessibility of metal active site on the supported catalyst when the Pd density is lower. Indeed, it was observed that higher conversion was achieved at lower Pd wt. % loading on the support. Nevertheless, when only metal Pd whit Pd 1% wt. loading supported catalyst was employed, multiple side products were detected. This points out the requirement on the active sites accessibility and their nature to maintain the selectivity on the final product. After testing the oxidation of MO, the heterogeneous catalyst was applied for the oxidation of HOSO. The conditions were adapted to the new compound, meaning that 2.5% mol of Pd_3P catalyst for double bond present in the triglyceride structure were used. An experiment in the best conditions achieved with MO (**WO0**-Table 6) led to 56% conversion to the polyketone (Table 7, **P13**). Comparing the homogeneous and heterogeneous approach, similar conversions were achieved for the best reaction outcomes (**WO0**-Table 6 and **P13**-Table 7). However, much less catalyst was required in the second case considering that in **WO0** 25% mol of $PdCl_2$ (Pd 59%) was employed and in **P13** 7.5% mol Pd_3P/SiO_2 (Pd 1% wt.). In conclusion, the heterogeneous approach demonstrated to be an effective pathway due to the reduced amount of palladium of about 20 times. Also, this factor has to be taken into account together with the possibility of easy recover and reuse of the supported catalyst.

1.1.4 Reductive amination of TRGs

Following the example of Czapiewaki and Meier, the amination of the oxidized HOSO was performed.[213] In their study, the reductive amination of oxidized fatty acid methyl esters (keto-FAMEs) was accomplished. A catalytic route with the use of Raney-Nickel® catalyst together with two ammonium salts as a source of nitrogen for the *in-situ* formation of ammonia was employed. The reaction was conducted in ethanol at room temperature with 30 bar H_2 pressure. In 24 h, high yields were obtained. The procedure was adapted to the triglyceride. The catalytic loading of Raney-Ni® was fixed to 20% mol After purification, the NMR analysis showed no conversion of the initial product. Considering the importance of the solvent in reductive amination, alternatives to ethanol were evaluated.[195] After literature research, isopropanol was considered as a solvent, which could have improved the reaction outcome. Isopropanol, as a secondary alcohol, has been reported to possibly enhance the activation of catalytic sites of the Raney-Ni® (Figure 47).[214]

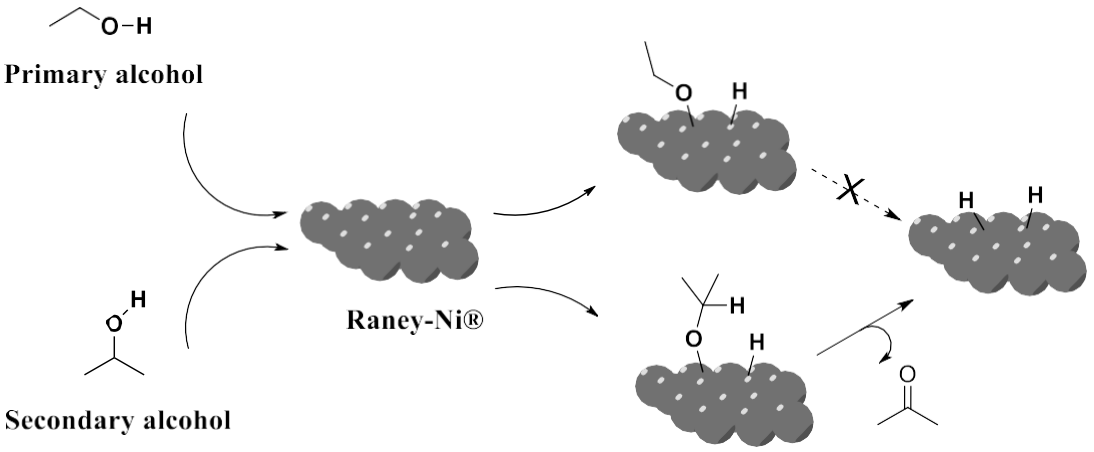

Figure 47. Primary and secondary alcohol interaction with Raney-Ni® catalyst.

Nevertheless, it was also underlined the role of isopropanol in the Wacker reaction as an effective hydrogen source in comparison to other solvent media.[214,215] It was displayed that the reaction proceeded more efficiently in isopropanol rather than in ethanol or methanol. Moreover, the results were worse in much sterically hindered solvents like *tert*-amyl alcohol. Repeating the experiment with the new solvent, no improvements were detected. Consequently, a different approach was undertaken. The catalyst was left unchanged, however a 2 N ammonia solution in methanol was employed instead of the ammonium salts. The reaction was carried out under 30 bar H_2 at room temperature for 24 h, as previously. Unfortunately, the result was unvaried. The reason might be attributed to the difficulty to the catalytic active sites to be in touch with ketone groups due to the large size of the molecule and the insufficient catalytic loading, which can be already considered quite high in the experimented trials. As a final point, the elevated catalyst percentage necessary for the Wacker oxidation and the incomplete conversion to the product made the oxidation process not viable in a sustainable perspective. Moreover, the additional ineffective reductive amination strategy led the direction of the research driving to more impactful synthetic pathways.

1.2 VEGETABLE OIL ETHERS *VIA* CATALYTIC REDUCTION

As previously mentioned, vegetable oils are highly valuable renewable feedstocks. Moreover, their performance in new materials can be improved by chemical modification of their structure. It is known that ester linkages can undergo hydrolysis and consequently, this leads to undesired polymer degradation if TRGs are used in polymeric materials. In order to avoid this issue, the reduction of the ester moieties in the TRG backbones can be considered an option. Additionally, the influence of ester and ethers analogous monomers can be evaluated in final polymers.

The first example of catalyzed reduction of esters with silanes was published by Tsurugi[216] using trichlorosilane as a reducing agent together with γ radiations. In 1995, the first metal-catalyzed reduction was shown using a Mg catalyst in the presence of $PhSiH_3$ as reducing agent.[217] Sakai and coll. studied esters reduction with different trivalent indium catalysts. Using $InBr_3$ (0.05 eq.) was proven to be a successful strategy at 60°C with 4 equivalents of Et_3SiH, obtaining moderate-low yield. They also displayed the inactivity of analogous halides, such as $InCl_3$.[218] The same indium catalyst was used on the analogous fatty acid molecule by Biermann.[219] Beller *et al.* reduced methyl oleate employing 0.1 eq $Fe_3(CO)_{12}$ as catalyst and 3 equivalents of TMDS as reducing agent. An example of lipid reduction was shown on the tristearin and trimyristin with $LiAlH_4$ in the presence of BF_3 etherate, resulting in major over-reduction and neglectable ether yields.[220] Better results (30% yield of ethers) were obtained by Müller *et al.* on glycerol with saturated alkyl bromides in presence of NaOH.[221]

In 2014, Biermann *et al.* extended the scope of the study to TRGs reducing high oleic sunflower oil.[222] The activity of two catalysts, $InBr_3$ and $GaBr_3$, was investigated. The vegetable oil triether was successfully synthesized with TMDS, with almost quantitative conversion and yield using the $GaBr_3$ catalyst. 93% was the best yield achieved, with 80% product and 20% polysiloxane. A critical point during the reaction is the control of the over-reduction of esters to alcohols. Lately, the effectiveness of this strategy has been demonstrated by the study on the reduction of different polyesters.[223,224] The mechanism of this reduction in not fully understood, but there are speculations about possibilities (Figure 48).

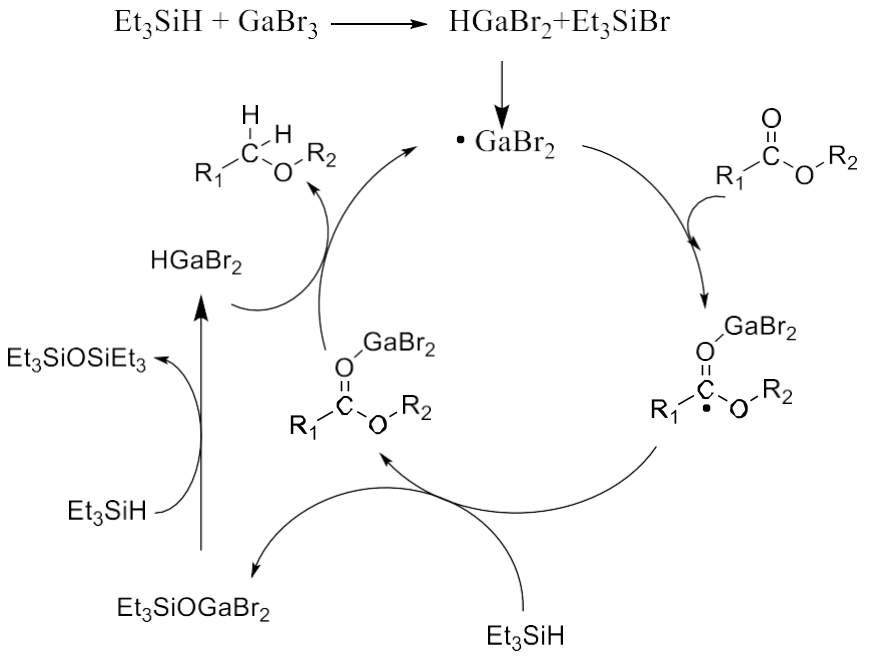

Figure 48. Proposed mechanism of catalytic reduction of esters by $GaBr_3$ catalyst and Et_3SiH reduction agent.[218]

Following the example of Biermann *et al.*, a study for the improvement of the reduction of high oleic sunflower oil was carried out. Principal aims were:

- Avoid the over-reduction to alcohols
- Improve the reaction conditions (i.e. lowering reaction time)
- Avoid using toxic chemicals (substitute toluene in the workup phase)
- Improve separation of the polysiloxane formed from the product.

A commercial vegetable oil was employed for this investigation. Generally, all tests were carried out at room temperature and in bulk conditions. The vegetable oil and the catalyst were stored in an argon atmosphere and similarly the reaction flasks. This was for two main reasons:

i) to avoid hydrolysis of the oil
ii) to avoid catalyst deactivation, which is sensitive to moisture.

Initially, the conditions of Biermann *et al.* were applied. Moreover, the injection flow of the TMDS was precisely set with a syringe pump at 2.6 mL/h. The overall amount of TMDS was added during 2h. After 2h, the reaction seemed completed, showing full conversion of the ester moieties. Additionally, in the IR spectrum, no -OH broad peak was detected, showing that over-reduction was at least not very pronounced. The results were confirmed by NMR (Figure 49).

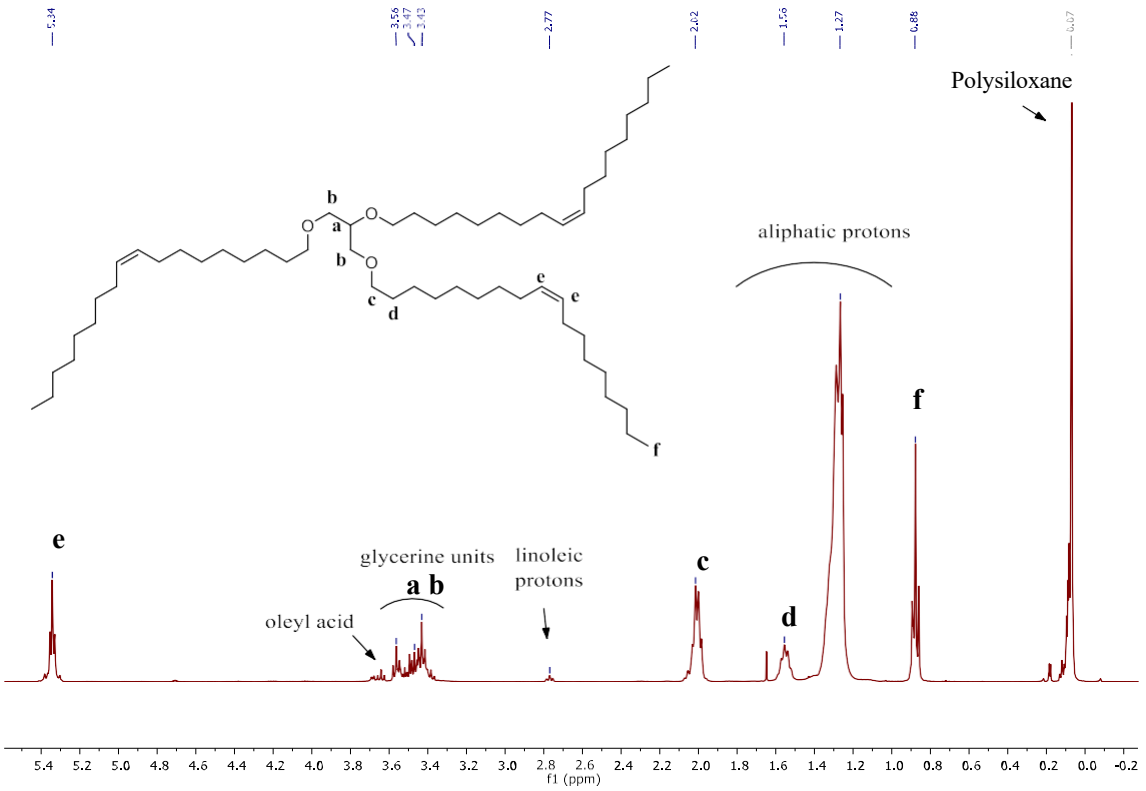

Figure 49. ETHOSO ^{1}H-NMR (400 MHz) proton spectrum in $CDCl_3$ (7.26 ppm).

In the spectrum, the characteristic H proton of the double bonds can be found at 5.34 ppm. A triplet at 2.27 ppm indicates the presence of the presence of allylic proton of the linoleic chains. It is possible to notice the disappearance of the CH of the glycerine unit (5.19 ppm) and its shift in the 3.60-3.30 ppm range where the glycerine unit protons are now located. The aliphatic protons of the fatty acid chains are invariably located at low ppm (1.60-1.0 ppm), with the methyl terminal group at 0.88 ppm. The peak at 0.73 ppm displaces the formation polysiloxane.

In the same reaction conditions, Et_3SiH (trimethylsilane, TES) was substituted as reducing agent. Since no improvements were registered, TMDS was kept for the following experiments. Subsequently, the reaction flow was increased to 2.6 mL/min. Consecutively, the reducing agent was fully injected after 3 min and the conversion was detected in shorter intervals through FT-IR. It was noticed that full conversion was achieved already after 30 minutes and no over-reduction occurred. The product structure was confirmed by NMR. Although no -OH band was found in FT-IR, the proton NMR showed the presence of a small peak at 3.64 ppm (Figure 10), attributed to the formation of oleyl alcohol (7% of the total).[225]

Further developments were needed for the purification steps in terms of yield and sustainability. The major issue of the reaction is the difficult separation and removal of polysiloxane (PS) formed from TMDS from the product due to similar solubility. Usually, toluene was reported as the solvent to remove the reducing agent and catalyst in the work-up procedure. It was demonstrated to be effective in removing PS partially. After this step, a separation *via* column chromatography with cyclohexane was performed, which was useful in reducing the PS amount, but the PS was not fully removed from the product. In order to substitute the harmful toluene, diethyl ether was used as solvent media in the work-up step. However, PS resulted in being fully soluble in this media and no separation occurred. As a *greener* alternative to toluene, anisole was tested. Within the scope of sustainability, the replacement of harmful and petrol-based solvents is a relevant topic. This aspect is far from being simple in reason of the different factors to consider. Certainly, the renewability of the source is of great importance, but also other aspects need to be evaluated.

Due to the complexity of the matter, the challenges of replacing classic organic solvents were defined by Jessop in 2010:

1) ensure green solvents may replace any nongreen solvent,
2) find and use methods of assessing the total environmental impact of solvents
3) find polar aprotic solvents that are easier to remove than existing solvents
4) eliminate energy-intensive distillations.

Walton *et al.* defined the parameters to define an ideal sustainable solvent:

a. having dual roles
b. leading to higher-quality products
c. reducing the number of synthetic steps
d. reducing by-product formation
e. improving product separation.

Moreover, researchers should also investigate the scalability of the process. Notably, disagreement can be present between researchers. As an example, Welton believes that the price of the final chemical product is strictly related to sustainability. Differently, Horváth and colleagues affirmed that sustainability is an intrinsic property of the molecule or process, therefore social and economic factors should be differentiated from this in order to develop sustainable processes instead of "suitable processes".

In recent years, different guides were drafted to help the choice and the transition to more sustainable solvents. The GSK evaluation (GlaxoSmithKline, pharmaceutical and biotechnology company) of the solvents employed in this study is reported in the following table (Table 8).

Table 8. GKS parameter scores of THF, diethyl ether and anisole.

	Mp °C	Bp °C	Waste	E impact	Health	Flammability /explosion	Reactivity /stability	LCS	EHS red flag
THF	-108	65	3	5	6	3	4	4	
Anisole	-38	154	6	6	7	7	6	5	
Diethyl Ether	-116	35	4	4	5	2	4	6	

E impact=environmental impact, LSC= Life Cycle Score (environmental impact of the production) EHS= properties related to environmental impact, health, and safety.

As displayed in the table, EHS and legislation have to be strongly taken into account.

Due to this boiling point, diethyl ether presents a higher risk of flaming in comparison to THF. Nevertheless, the low boiling point also allows a simple solvent removal and recycling of Et_2O, which leads to a more favourable waste factor (Table 8). Both solvents present an unfavourable EHS. A better evaluation is assigned to anisole, which is a bio-sourced solvent and doesn't present critical disadvantages. In fact, it possesses elevated scores in all the considered categories of examination (Table 8). Besides the costs, between the three, anisole is the most sustainable solvents in terms of safety, environmental impact and waste production.

In the case of ETHOSO, the use of anisole resulted in being a valuable strategy, achieving a similar result as the one obtained with the use in toluene. However, with anisole there is the advantage of using a safer, more sustainable solvent. Nevertheless, anisole could not be fully removed and traces of it remained in the final product. To quantify the amount of PS in the product, the factor Q was calculated (Equation 2, Table 9).

$$Q = \frac{\int PS}{\int terminal\ CH_3} \qquad \textbf{Eq. 2}$$

Table 9. ETHOSO purification methods in different solvents and respective Q factors.

	Purification method	**Solvent**	**Q**
ETHOSO1	filtration	toluene	3.7
ETHOSO1	filtration + column	toluene	2.2
ETHOSO2	filtration	diethyl ether	6.6
ETHOSO2	filtration + column	diethyl ether	4.0
ETHOSO3	filtration + distillation	anisole	3.0

Different purification methods were tested and Q was determined (Table 9). In both ETHOSO1 and 2, it can be noticed that the column filtration helped in decreasing the amount of PS by 40%. The lowest quantity of PS was obtained when toluene was employed. However, comparable results were gained when substituting toluene with anisole. Worse results were achieved with diethyl ether because of the highest solubility of PS in this media.

1.3 CONCLUSION

In this work, a catalytic oxidation, followed by reduction amination pathway was tested to achieve polyamines from vegetable oils.

The oxidation of vegetable oils was investigated in a *greener* fashion. In the first homogeneous catalyzed pathway of the Wacker oxidation, 60% conversion was achieved with 25% mol $PdCl_2$ catalytic load. Due to the latter factor combined with the expensiveness and rarity of palladium, it was unreasonable to test higher catalytic loading due to the practical applicability of the synthetic strategy and the loss in sustainability. Moreover, the reductive catalytic conditions experimented on the oxidate oil were ineffective, oppositely to the results previously on the FA species. The reason might be attributed to the hindrance owing to the large size of the TRG molecules and their aliphatic pending chain, which may limit access to the catalyst's active sites.

As tested for the first time, the heterogeneous Pd_3P/SiO_2 catalyst was tested on the simpler molecule FA methyl oleate instead of HOSO. After screening different reaction parameters, catalyst and loadings of immobilized catalyst, the best conversion achieved was equal to 60 %, likewise the homogeneous approach, but at much lower Palladium loading.

1.4 THIOL-ENE REACTION

At the start of this century, the concept of click chemistry was introduced to synthetic chemistry as a powerful tool. Introduced by Sharpless in 2001,[226] click chemistry was destinated to be not only an efficient synthetic strategy, but also a valid ally in the frame of Green Chemistry. In principle, click chemistry was born to facilitate the synthesis of complex drug molecules. Click chemistry was summarized by Sharpless in 9 points:

1. Modular
2. Stereospecific (not necessarily enantioselective)
3. No or safe by-products
4. High yields
5. Wide in substrate scope
6. Simple reaction conditions

7. Widley available starting materials
8. Simple to isolate (no chromatographic methods)
9. Benign solvent or less/no solvent

The key point to fulfil these requirements is the favourable thermodynamic driving force of the reaction, which is expected to be > 20 kcal/mol.[226] This enables to obtain robust heteroatom connections in the newly formed compound. As underlined in the abovementioned article, nature is driven in favour of carbon-heteroatoms bonds. Through this new approach, scientists can mimic nature to their formations. Pursuing this aim, thiol-ene click chemistry allows an effective and easy C-S bond formation. For this purpose, olefinic compounds and thiols are the necessary compounds.

Olefins are unsaturated compounds obtained for instance by the steam cracking of petrol. These small molecules are vital for the synthesis of industrially made organic compounds (90% by weight),[227] conforming their high relevance for our society. The first example of C-S coupling was reported by Posner in 1905[227] *via* hydrothiolation reaction, leading to the Markovnikov and anti-Markovnikov products, according to the chemical pathway. There are three possible options (Figure 50):

1. Nucleophilic
2. Radical
3. Electrophilic.

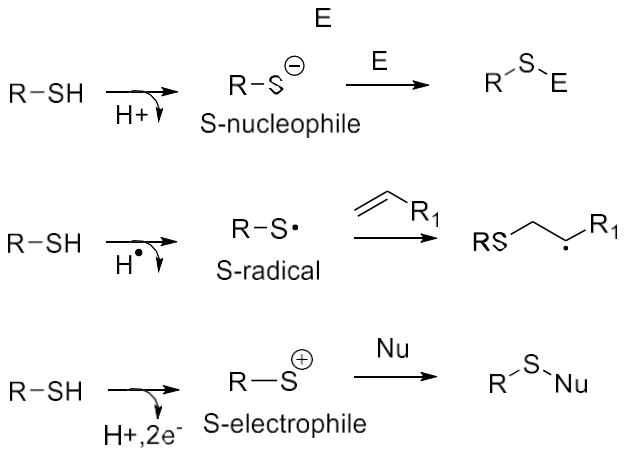

Figure 50. Thiols undergoing electrophilic, radical and nucleophilic reaction pathways.

The nucleophilic path (> 20 kcal/mol driving force)[226] is commonly referred as thia-Michael reaction which takes place in presence of weak Brønsted bases (i.e. triethylamine) or Lewis bases (i.e. phosphine).[229,230] This can be distinguished from the basic mechanism, which occurs with strong bases (DBU, TBD, DBN) (Figure 51).[231] In this case the thiolate anion is generated by acid-base reaction. This newly formed species can compete with the base to the hydrogen abstraction.

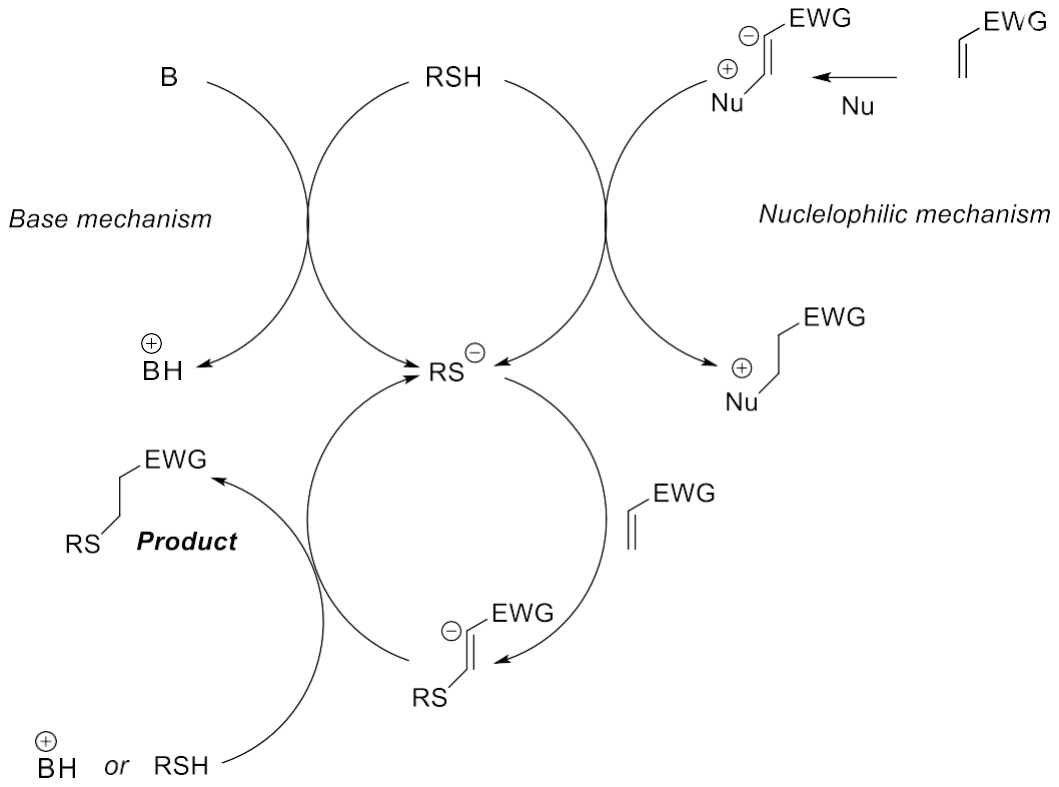

Figure 51. Nucleophile and base initiated mechanisms of the thia-Michael reaction.[232]

The middle (path 2) is pursued via a thermo- or photochemical reaction. The combination of heat or light and an initiator generate free radicals and consequently a thiyl radical, which is the species reacting with the unsaturation. In some cases, it was also shown that radicals were formed even in absence of initiators.[233] By evidence of cis and trans isomerization of olefins by a study of 1959,[234] it was demonstrated that the formation of the carbon radical is a reversible process. Once the carbon centred radical is formed, it extracts a thiol hydrogen, leading to the formation of a new thiyl radical and initiating the propagation step (Figure 52). In this case, the final compound has an anti-Markovnikov configuration.[234] As side reaction, dimerization, can also take place.

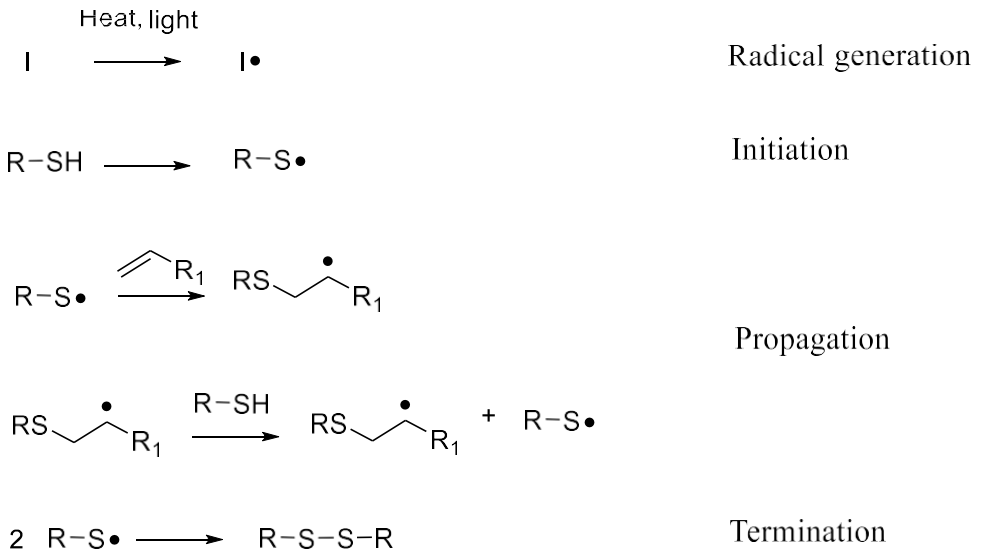

Figure 52. Radical thiol-ene reaction mechanism.

It is important to consider that structural characteristics of olefins involved in the reaction play a role. Three aspects are mainly relevant:[235, 236]

1. Stabilization of the carbon radical by resonance
2. The presence of electron withdrawing groups
3. Position of double bonds: terminal double bonds are more reactive than internal ones.

Hoyle and colleagues[237] established a reactivity scale of diverse olefins in the frame of thiol-ene reaction as follows:

Norbornene > Vinyl ether > Propenyl > Alkene ≈ Vinyl ester > N-Vinyl amides > Allyl ether~ Allyltriazine~ Allylisocyanurate > Acrylate > Unsaturated ester > N-substituted maleimide > Acrylonitrile~Methacrylate > Styrene > Conjugated dienes.

The structure of thiols is affecting the kinetic profile of the reaction. This was demonstrated by Chan *et al.*[236] through the evaluation of four compounds from different thiol classes. In order, the reactivity resulted to be: ethyl thioglycolate (thioglycolae ester) > 2-mecaptoproprionate (thiopropionate ester) > methyl 3-mecaptopropionate (thiopropionate ester) >> hexanethiol (alkylthiol). Moreover, the stoichiometry of thiol plays also a role. Most commonly, an excess of thiols in needed to reach full conversion.[238] Besides the reactants involved (alkene and thiol), the reaction conditions strongly influence the successful outcome. Crucial parameters are:

a) Temperature
b) Solvent/bulk condition
c) Solubility/miscibility of the components
d) Type of initiator

An appropriate temperature is essential to avoid side reactions, especially with thermally sensitive compounds. Moreover, in thermally initiated reactions, an inadequate temperature can lead to a low conversion due to limited formation of radicals.[238] The solubility in the solvent media or the miscibility of the reactants in bulk condition is a relevant factor for the formation of the desired product.[238]

In line to the reaction system, a proper initiator needs to be evaluated. In thermal reaction, 2,2′-azobis(isobutyronitrile) (AIBN) is the most used radical initiator.[220] With heating, cyanoisopropyl radicals are formed which consecutively generate sulfenyl radical.

Under photochemical conditions, two types of initiators are possible: type I and II photoinitiator.[238, 239] The first generate two radicals thought a unimolecular cleavage mechanism (Figure 53). Alternatively, type II initiators act *via* H-abstraction and form two species, such as sulfenyl and ketyl radicals, the second of which is unreactive against the double bond (Figure 54).

- **Type I photoinitiator**

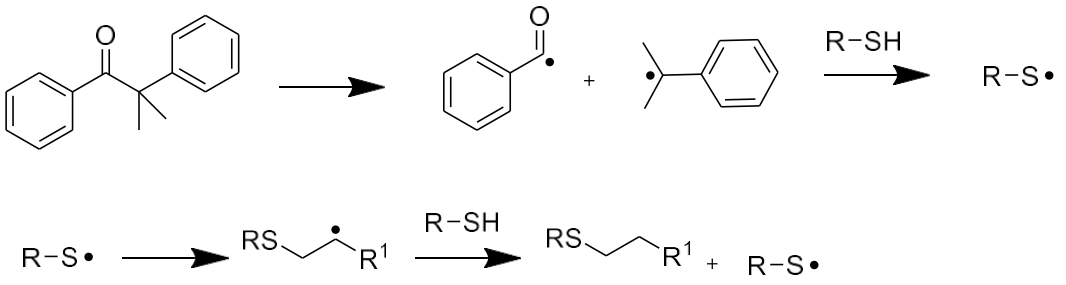

Figure 53. Thiol-ene reaction mechanism initiated by Type I photoinitiator

- **Type II photoinitiator**

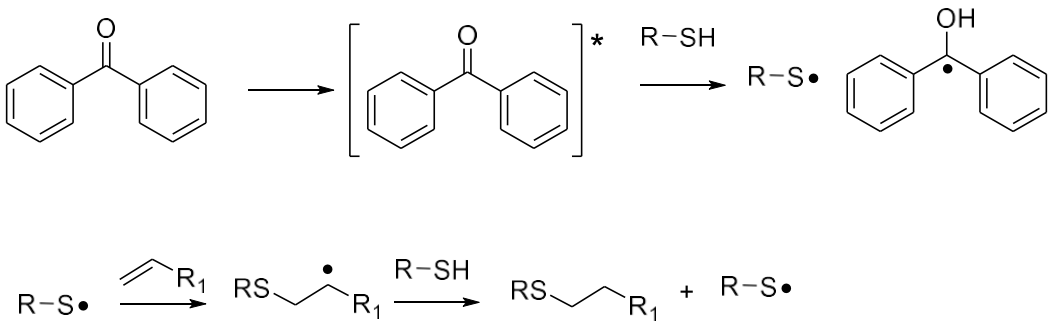

Figure 54. Thiol-ene reaction mechanism initiated by Type II photoinitiator.

It is relevant to mention that, in some cases, the presence of molecular oxygen can impact the reaction by the quenching of thiyl radicals, consecutively blocking or limiting the conversion.[240]

1.2.1 Thiol-ene reaction with TRGs

As discussed in the previous chapter (Chapter 1, 1.1.1 Vegetable oils), vegetable oils are important feedstocks in the field of polymer chemistry. In the frame of thiol-ene chemistry, the fist example applied on fatty acids (FA) and fatty acid methyl esters (FAME) was reported by Koenig in 1957[241] using thioacetic acid as sulfur source, generating diesters and diacids. Alternatively, difunctional compounds were obtained by addition of thioacetic acid with consecutive hydrolyzation and dimerization by oxidation in presence of iodine.[242] Hydrogen sulfide was employed to functionalize linseed oil and methyl oleate.[243] The kinetics of diverse thiol additions to FAs in photoactivated condition were evaluated. It was observed that *trans* isomers have faster reaction rates in comparison to *cis* analogous,[244] which is of advantage for plant oil, as they are present in nature only in cis configuration. In this context, in 1964, Testa[245] investigated the photosensitized cis-trans isomerization of methyl oleate in presence of benzophenone as sensitizer. The isomerization reaction is a reversible process; therefore, it was noticed that the equilibrium state between methyl oleate and methyl elaidate (*trans* form of methyl oleate) exists with 73% *trans* isomer.

Taking advantage of multiple unsaturations present along the aliphatic chain of vegetable oils, diverse polyfunctional monomers can be achieved. The functionalization strategies can be listed as (Figure 55):

1) Thiol-ene click reaction on mercaptanized oil
2) Direct thiol-ene addition on vegetable oil double bonds

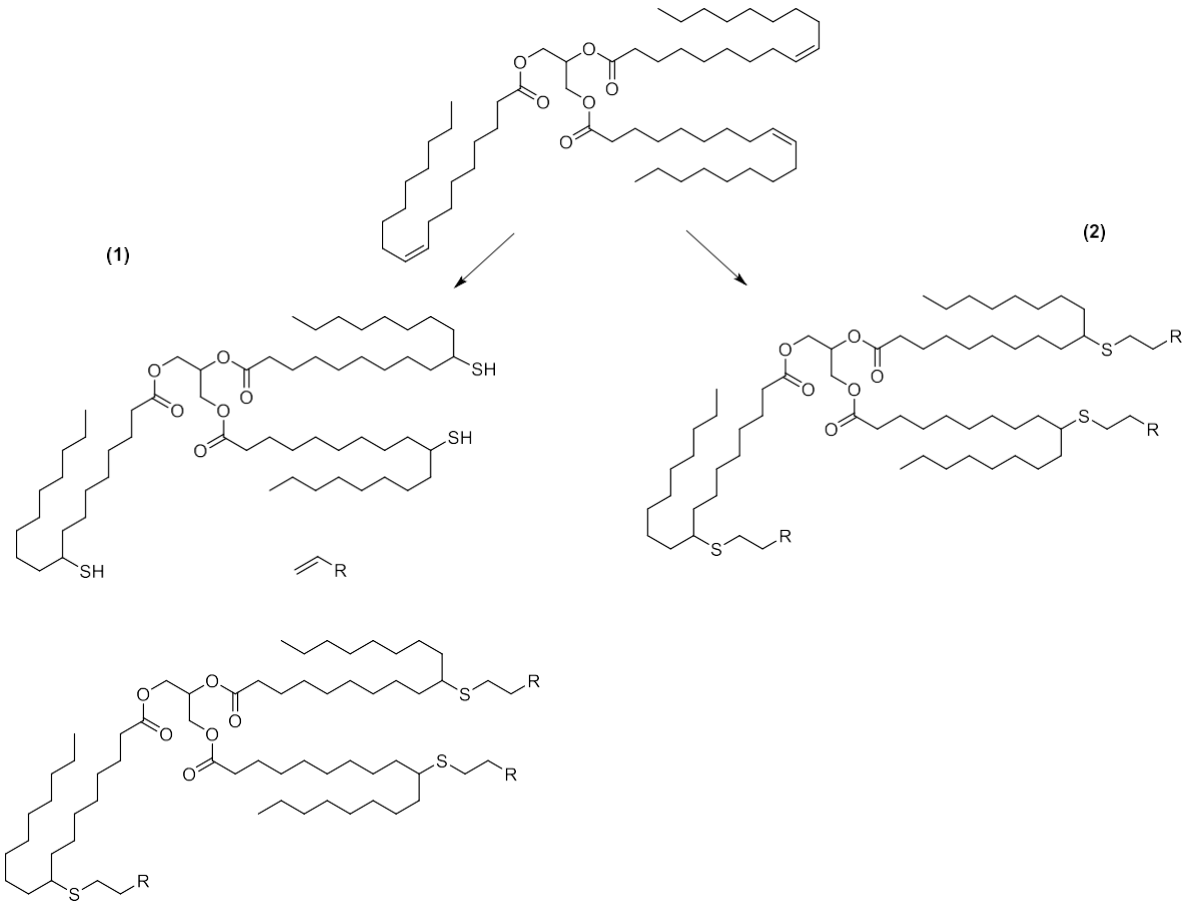

Figure 55. Representation of 1) thiol-ene on mercaptanized oil and 2) direct thiol-ene on vegetable oil.

The first approach implies the use of H_2S to previously synthesise the mercaptanized oil.[246] However, H_2S is a toxic and difficult to handle compound.[247] Evidently, the second strategy is more straightforward. As the R group changes (Figure 16), different functional groups can be attached to the TRG. In the field of polymer chemistry, numerous works report on the synthesis of vegetable oil-based polyols *via* thiol-ene reaction. This can be explained by the high demand of biobased polyol monomers, which are suitable for many applications in the polymer field such as polyether, polyesters and PU synthesis. Specifically, PUs gained large interest within the scope of the transition to bioderived materials.[248–250] Auvergne *et al*.[251] synthesized a polyol from rapeseed oil with mercaptoethanol and dodecanthiol. Waterborne polyurethane dispersions were obtained starting from diverse vegetable oil (canola, corn, grapeseed, rice bran, olive and linseed oil) obtained *via*

photochemical reaction.[252] With the same approach, Zhang and colleagues[253] created a platform of plant oil-based polyols (grapeseed, rice bran, olive and linseed oil) using 2-mercaptoethanol using UV light. These monomers were reacted with isophorone diamine (IPDA) with a 1:1.05 ratio. The thermomechanical property analyses of the final PUs showed that T_gs and tensile strength values were directly proportional to the amount of functionalization of the oil. Oppositely, thermal stability was decreasing with the increasing number of vegetable oil functionalizations. Nonetheless, all the samples displayed high thermal stability (>300°C). Furthermore, a Life Cycle Assessment (LCA) evaluation of vegetable oil-based polyols for PUs can be found.[254] The LCA of two different polyols derived from rapeseed oil via transesterification reaction with two different polyol amines was evaluated. After calculations, it was noticed that the primary impact on LCA was given by the oil and polyol amine productions. The main advantages in comparison with petrol-based polyols were estimated to be lower GHG (greenhouse gas) emission, water consumption and renewability of the energy employed. However, worse results were achieved in categories such as land use, marine eutrophication and ecotoxicity.

As the shift from conventional PUs to NIPUs is currently taking place, di- and polyamines are required monomers for the polyaddition reaction with bicyclic carbonates. Robin *et al.*[163] formulated a fully biobased epoxy resin using a rapeseed oil-derived polyamine. The thiol employed in this synthetic approach was an amino acid-derived compound, i.e. cysteamine hydrochloride (CAHC), the salt of the corresponding cysteamine, which is obtained from the decarboxylation of the amino acid cysteine.

Recently, Rios *et al.*[255] investigated in detail the synthesis of a similar polyamine. They implemented the system substituting the hazardous 1,4-dioxane solvent with the safer isopropanol and ethanol mixture.

In this work, the synthesis of commercially available High Oleic Sunflower Oil (HOSO) was investigated in different reaction system. Afterwards, the best approach was also applied to linseed oil and castor oil, as alternative renewable feedstocks. As mentioned above, solvent, concentration, light wavelength and penetration are crucial parameters, which were investigated. To start, the work of Meier and Firdaus[45] for the synthesis of limonene diamine was taken as a reference. As reported, 2,2-dimethoxy-2-phenyl-acetophenone (DMPA) was used as it is a well-known and extensively employed benzoin ether photoinitiator. Due to the immiscibility of the oil and the cysteamine hydrochloride salt (CAHC) and their different solubility, a solvent mixture of dichloromethane and ethanol was initially tested. It is needed to consider that, since CACH was used in excess (1:3 eq.), it was never fully solubilized in the media. The reaction mixture was irradiated with a UV lamp 365 nm (45 W) for 24 h. The initial HOSO concentration was equal to 0.04

g/mL (Table 10, entry 1). This first experiment led to only 40 % double bond conversion. Subsequently, a longer reaction time was applied together with the increase of equivalents of CACH and photoinitiator. However, only a slightly increased conversion was obtained in 48 h (55% conversion, Table 10, Entry 2). Taking as example the procedure reported by Stemmelen *et al.*[147] using grapeseed oil, the solvent mixture was changed to 1,4-dioxane: ethanol (7:3). Additionally, a LED irradiation system was chosen for the following experiments, in reason of lower energy consumption and the condition of not generating heat, which allows to reduce the distance between the sample and the light source. Heat is usually undesired because it can lead to side TRG oxidation.[256, 257] The set-up consisted of a metallic plate with LEDs installed on it. Two plates were used (custom built previously), one consisting of 365 nm LEDs (2W) and another of 405 nm LEDs (2W). Two identical reactions were irradiated by the two different wavelengths and run for 48 h **(**Table 10, Entry 4 and 5). In the above-mentioned work of Stemmelen and colleagues, 87 % conversion for grapeseed oil was obtained. In this case, 94 % and 100 % conversion of HOSO double bonds were achieved after 48 h under 365 nm and 405 nm irradiation, respectively (Table 10, Entry 3).

As pointed out, the concentration of the reaction mixture is a relevant parameter to evaluate. The cause is that high turbidity of the reaction mixture is an obstacle to the light penetration. An ineffective light action leads to low formation of radicals and consequential final low conversion. It was necessary to find a balance between a low amount of solvent, for sustainability reasons, and clearness of the reaction mixture. The concentration of the oil was increased until 0.28 g/mL. In this condition, already 89 % conversion was reached after 1 h and full conversion after 7 hours (Table 10, Entry 5).

Table 10. Comprehensive conditions tested for the synthesis of the HOSO-derived polyamine (PA) in batch *via* thiol-ene photoreaction. A UV lamp (45 W) and LED system (2W) were used. When DMPA was used as photoinitiator, 0.1 eq per double bond of the oil were used. TPO-L was used in 2wt% of the oil weight. For all entries, the scale of the reaction corresponds to 500 mg of oil.

	Photoinitiator	Solvent	Wavelength (nm)	Concentration (g/mL)	Conversion %	Time (h)
Entry 1	DMPA	DCM: EtOH (7:3)	365 lamp	0.04	40	24
Entry 2	DMPA	DCM: EtOH (7:3)	365 lamp	0.04	55	48
Entry 3	DMPA	Dioxane:EtOH (7:3)	365 LED	0.04	94	48
Entry 4	DMPA	Dioxane:EtOH (7:3)	405 LED	0.04	100	48
Entry 5	DMPA	Dioxane: EtOH	405 LED	0.28	100	7
Entry 6	TPO-L	Dioxane: EtOH	405 LED	0.28	100	7
Entry 7	DMPA	Isopropanol: EtOH	405 LED	0.42	100	7
Entry 8	TPO-L	Isopropanol: EtOH	405 LED	0.28	>99	7

To implement the system to comply with *the Green Chemistry Principles*, dioxane was substituted by isopropanol, as also reported by Rios *et al.*[164] (Table 10, Entry 7). Successfully, the reaction in this condition also reached full conversion within 7 hours.

In other to test a different photoinitiator, TPO-L (diphenyl(2,4,6-trimethylbenzoyl)-phosphine oxide) was evaluated in the same conditions. Having a wide absorption range (max absorption 272 nm, 382 nm), this initiator makes it suitable to be excited under 405 nm wavelength irradiation.[258] Using TPO-L, analogous result were acquired, resulting in quantitative conversions after 7 hours in each solvent media. (Table 10, Entries 6 and 8).

As all the previous experiments were run on a small scale (500 mg) a test on 2 g scale was carried out to obtain sufficient quantities of the HOSO-derived polyamine (PA) for further use as a monomer in NIPU synthesis. This was possible only with the employment of three UV lamps because of the bigger size of the system and therefore the need for more efficient irradiation. The solvent mixture iPrOH:EtOH was unchanged. The result was 95 % double bond conversion in 7 h. The integral of the double bond protons was monitored over time (5.37 ppm, Figure 34). In the best experiment, the disappearance of the peak was observed. Simultaneously, the presence of the CH_2 groups in α and β to the ammino group were detected in the 2.92 - 2.77 ppm region (Figure 34). The aliphatic protons of the chain are

invariably present in the 2.0 - 1.0 ppm range, as well as the protons related to the glycerine unit (CH at 5.25 ppm and $2CH_2$ between 4.08 - 4.34 ppm in $CDCl_3$). DOSY-135 experiment confirmed the amino cysteamine functionalization through the observation of the CH_2 in α and β to the amino group at 42 and 35 ppm and the CH linked to the sulfur atom resulted from the thiol-ene reaction at 46 ppm (Figure 56). The mass of the final product was detected by ESI-HRMS analysis equal to 1116.89.

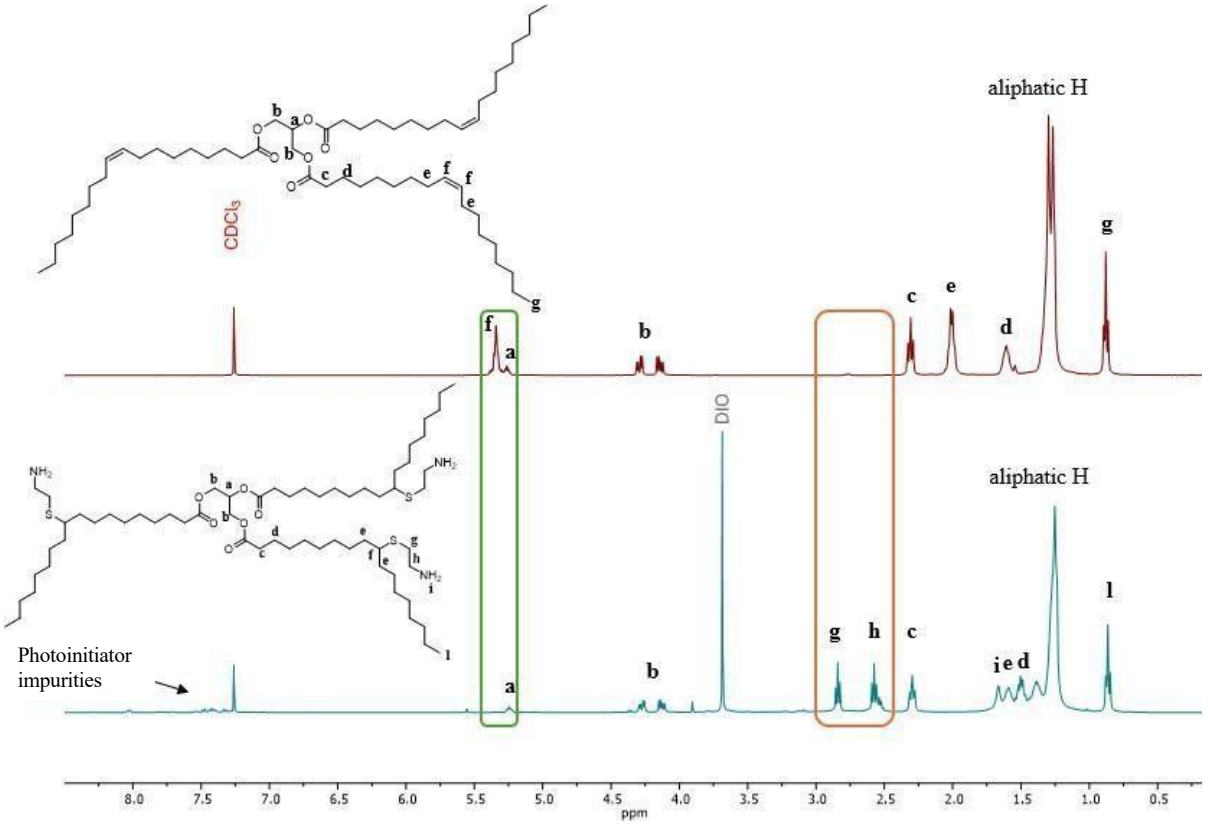

Figure 56. ^{1}H-NMR (400 MHz) proton spectrum in $CDCl_3$ (7.26 ppm) spectra of HOSO and HOSO-PA in comparison. In the top spectrum (HOSO- PA) It can be noticed the disappearance of the double bond peak at 5.37 ppm and the characteristic peaks of CH_2 of the cysteamine units at 2.77 and 2.99 ppm.

In the perspective of scaling up the processes, *flow* chemistry is an emerging and effective synthetic strategy. Through this approach it is possible to achieve high conversions in a short time. Moreover, in this way, chemical wastes and energy consumption can be reduced.

In the frame of a collaboration project with the PhD student Celeste Libretti (group of research of Prof. Dr. Meier) for the development of fully biobased NIPU thermosets, we investigated the *in flow* synthesis of HOSO-PA.

The strengths of *in flow* chemistry can be summarised as follow:

- Elevated conversions
- Short reaction times
- Room temperature reactions
- Low amount of solvent (and consequently waste)
- Energy efficiency

These factors can be attributed to high light penetration on a tiny section of the reaction mixture due to the proximity of the source of irradiation to the reaction mixture and the limited dimension of the tube diameter. Moreover, effective small-scale mixing is taking place. In fact, the flow along the tube can be seen as a series of small flasks placed consecutively.[259] In reason to those characteristics, a great potential can be perceived in combining the powerfulness of thiol-ene click reaction with an *in flow* system.

With the purpose of scaling up the process and make it more efficient, the thiol-ene reaction of HOSO was tested in a *continuous flow* system. In the first place, the reaction conditions were adapted for being suitable to the new set up. Primarily, taking as reference the best experimental parameters for the *in batch* model, isopropanol and ethanol were tested as solvents separately. It is needed to mention that the concentration was kept fixed as the same value of the *in batch* system (1g oil/ 7mL solvent). Between the two previously as suitable established solvents, isopropanol was selected. This choice was made given that in ethanol, the cysteamine salt (at the set concentration) exists in a disperse powder form. This would lead to possible unwanted clogging of the thin tube of the reactor system (1 mm diameter). Oppositely, isopropanol solubilized CAHC smoothly along the time. Thus, isopropanol was found to be effective for this system because the salt is solubilized regardless (even in slower rate) and preventing the reactor obstruction. In the following experiment, the addition of CAHC in aliquots was tested. The total amount of cysteamine salt needed was added in portion of ¼ every 2 hours. Eventually, this approach led to no benefits, therefore, in was not applied to the subsequent experiments. Considering the concept of *concentration* in the field of Flow Chemistry, the screening of different flow rates was investigated. The concentration of a product in an *in batch* system can be considered as an increasing value in *time*. Hence, the reaction rate is given by the derivate of the concentration of the reactant on time, displaying an exponential decrease along time (Equation 3).[259]

$$First\ order\ reaction\ rate = -\frac{d[A]}{dt} = k[A] \qquad \textbf{Eq 3.}$$

$$Second\ order\ reaction\ rate = -\frac{d[A]}{dt} = k[A][B] \quad or \quad k[A]^2$$

with [A] and [B] the concentration of the reactants (first or second order reaction) and k rate constant of the reaction. Moreover, taking into account an *in flow* system, the concentration is increasing with *distance.* In this system, the reaction time is defined as the residence time between the inlet and the position of the quenched inlet.[259] Overall, *time* in a *in batch* system is equal to *distance* in an *in flow* system (Figure 57).

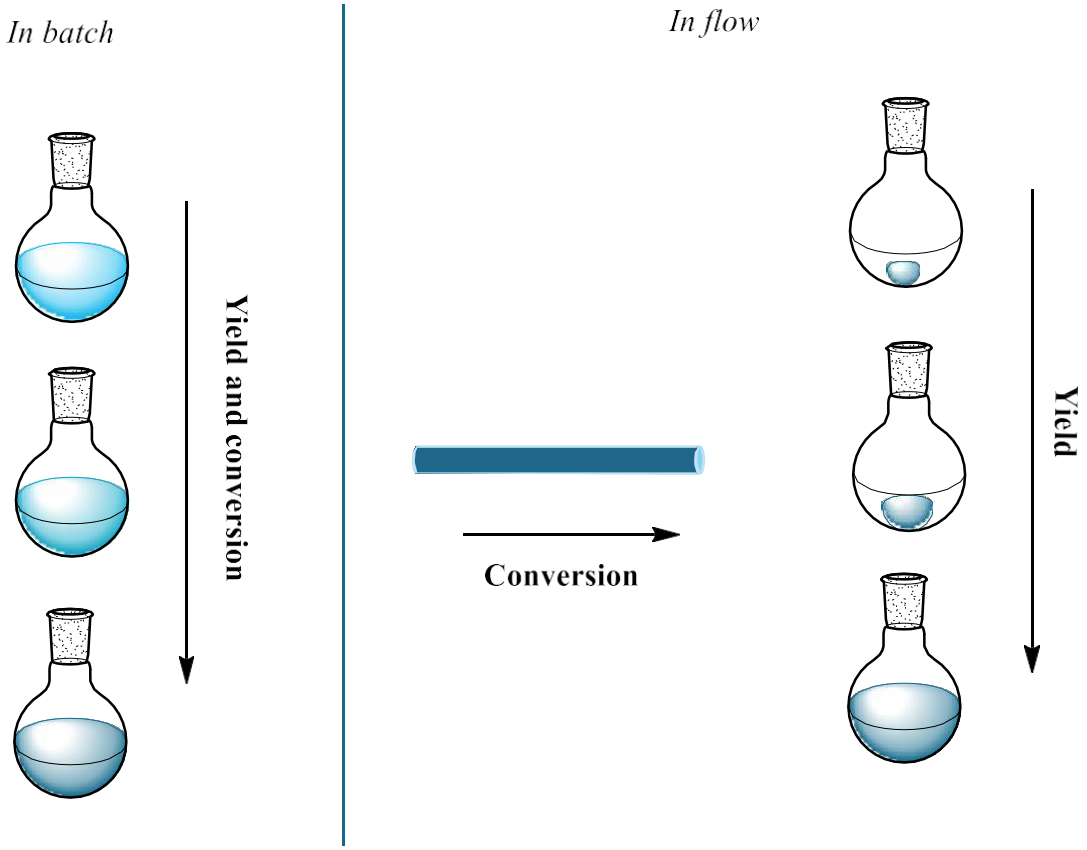

Figure 57. Visual representation of conversion and yield in *in batch* and *in flow* systems.[240]

Considering this definition, the faster the flow, the faster the formation of the product. It is needed to mention that, generally, in order to achieve a high conversion, it is important to consider a parameter called *residence time*. This is defined as the time in which the reaction mixture is exposed to light irradiation. The higher the residence time, the longer the time of light irradiation and consecutively the possibility of elevated conversion. Residence time and flow rate are inversely proportional. In this specific case, a very small flow rate could

lead to a clogging problem in the system. Nevertheless, the *continuous flow* method applied in those experiments is the key point to achieving high conversion with an elevated flow rate, overcoming the matter of clogging and the short residence time (Figure 58). Four different flow rates were tested: 500 µL/min, 1 mL/min, 2 mL/min and 9mL/min. As a result, for a fixed reaction time, the conversion increased proportionally with the flow. The conversion was determined by proton NMR.

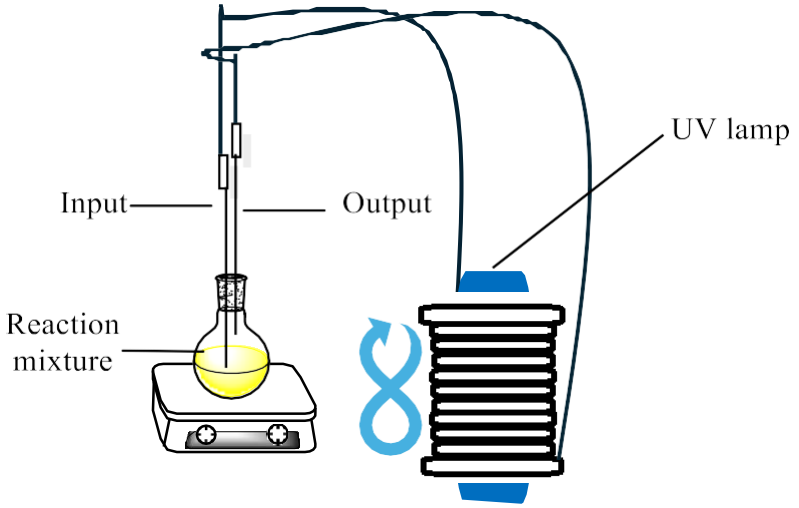

Figure 58. Schematic representation of a *continuous flow* system.

The best reaction condition *in flow* on a 2 g oil scale was achieved in 6 hours, in isopropanol, with UV irradiation of low power (16 W) reaching > 99% conversion.

To deepen the understanding of the system, *Reynolds numbers* (Re) for each flow rate were calculated. As previously mentioned, the small dimension of the tube allows an effective and homogeneous mixing of the reactants. In fluidic microreactors, two main mass transfer components can be distinguished, such as diffusion and convection. The first is passive transport determined by the concentration gradient, differently, convection is determined by the collective motion of the molecules in the fluid. Considering these parameters, two types can be differentiated. The first is laminar flow, among which diffusion is the main contribution to mass transfer. Laminar flow corresponds to Re < 100. For Re > 2500, turbulent flow is taking place. In this situation, convection is predominant. This ass transfer mode is influenced by the pumping energy on the fluid and structural deformation of the channels (helical or curved).[259] A flow state condition intermediate between the two mentioned ones, is called *transient* regime (100 < Re < 2500). Reynolds numbers are useful to identify the type of motions along the flow and therefore the specific flow regime. This value is given by the ratio of inertial and viscous forces. (Equation 4). Typically, viscous

forces are greater in laminal flow.

$$Re = \frac{inertial\ forces}{viscous\ forces} = \frac{\rho v L}{\mu} \qquad \textbf{Eq. 4}$$

where *v* is the velocity of the molecule relative to the fluid, L is the characteristic travelled length of the fluid, μ is the dynamic viscosity of the fluid, v is the kinematic viscosity and ρ is the density of the fluid (Table 11).

Table 11. Calculation of Reynolds numbers for different floe rates and the associate flow type.

m	ρ (kg/m^3)	μ (Pa*s)	v (m^2/s)	ml/min	m/s	Adimensional	
L	**tot density**	**tot dynamic viscosity**	**kinetic viscosity**	**Flow mL/min**	**Flow m/s**	**Re ρvL/μ= vL/v**	**Flow regime**
0.5	**807**	**0.025**	**0.0309**				
				0.5	0.005	**86**	Laminar
				1	0.011	**171**	Transient
				2	0.021	**343**	Transient
				9	0.096	**1542**	Transient

Besides the case of flow rate = 0.5 mL/min (laminar flow), all the other cases presented a transient flow regime. Therefore, is it possible to state that, in this experimental system, the mass transfer is controlled both by diffusion and convection factors.

As a summary, the main advantage of the flow system is the scalability of the process. This is related to efficient irradiation (radical formation efficiency) and mixing. *In batch* conditions these two factors cannot be maximised while working on large quantities, resulting in poor conversion. Moreover, the small section of the tube allows a high light-reaction mixture interaction and an effective mass transfer. Considering the reaction time, the flow needed 1 h less in comparison to the *in batch* synthesis. Possibly, with a higher flow rate, the time could be decreased even more.

As previously introduced, (2.2 Vegetable oil ethers *via* catalytic reduction**)** high oleic sunflower oil ether **(**HOSOET) was synthesized via catalytic ester reduction. Consecutively, the functionalization of the double bonds in HOSOET via thiol-ene reactions was explored. At first, the optimized conditions obtained for the trifunctional HOSO-PA were transferred to HOSOET by substituting the solvent mixture with diethyl ether:ethanol (1:1) due to the different nature of the starting material. Two tests were carried out with DMPA and TPO- L photoinitiator under 405 nm light irradiation. This led to 53% and 57% (ETPA1 and ETPA2, Table 12) conversion of the double bonds, respectively. Considering the CH_2 integral of the reacted cysteamine in ^{1}H-NMR, in average, only one

bond out of the three presents on the TRG was successfully converted (Figure 59). Due to these results, the solvent mixture ratio was changed to Et_2O:EtOH 7:3. In this situation, the conversion increased to 86% (ETPA3, Table 12), however the integrals of the CH_2 in alpha of the primary amine groups displayed lower integrals, showing an average functionalization of 0.8 (ETPA 3, Table 12). It is possible that some side oxidation and cleavage reactions occurred.

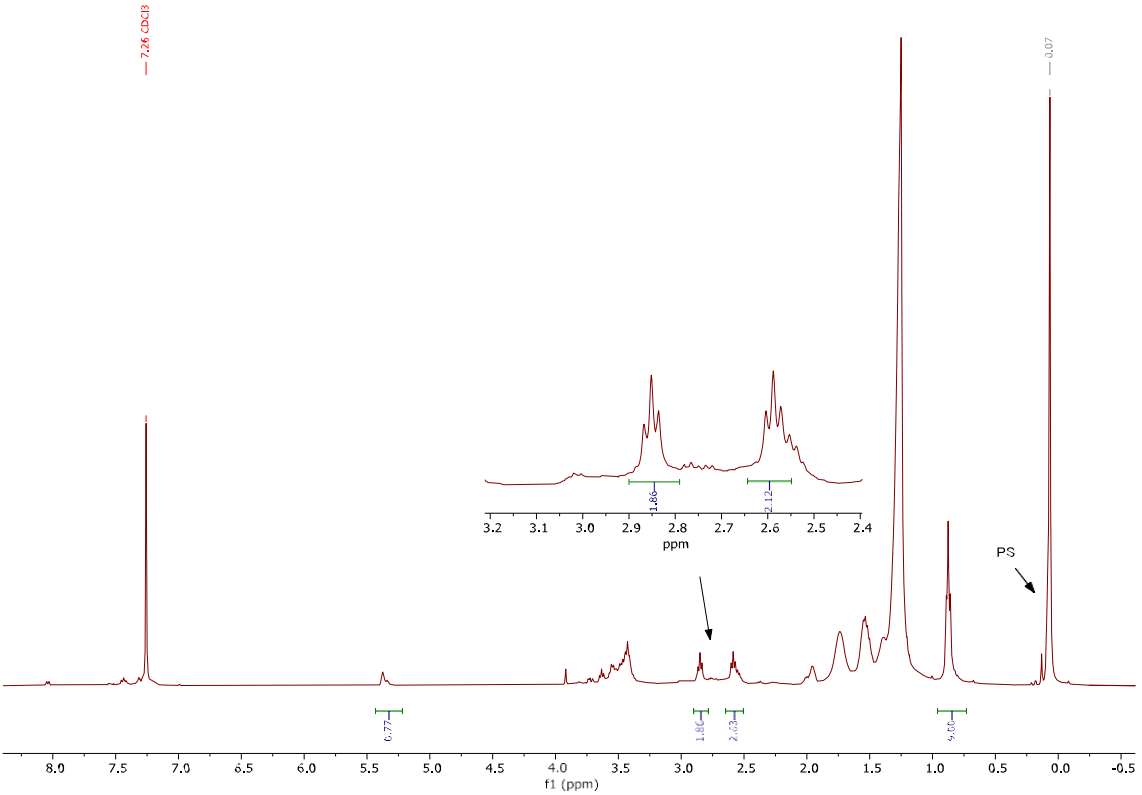

Figure 59. ^{1}H-NMR (400 MHz) proton spectrum in $CDCl_3$ (7.26 ppm). spectrum of **ETPA3** (Table 12). Detail of N-C**H**$_2$-C**H**$_2$-S proton signals. PS= polysiloxane.

Due to insufficient functionalization, an additional photoinitiator was used, namely Irgacure 2959, with the optimized solvent mixture and under 405 nm light. Nevertheless, a poorer result was achieved (14% conversion, ETPA 4, Table 12), showing the unsuitability of this initiator with the system. Alternatively, a thermal thiol-ene was also tested. Using AIBN in bulk condition at 80°C, which allowed the homogenization of the reagent mixture, only 11 % of the double bonds were derivatized.

Table 12. Conversion of the double bonds (db) in different thiol-ene reaction conditions on high oleic sunflower oil ether (HOSOET).

	Initiator	Solvent	Conversion db[a]	Amine functionality per TRG[b]
ETPA1	DMPA	Et_2O:EtOH (1:1)	53	Not measurable*
ETPA2	TPO-L	EtOAc	57	1.1
ETPA3	DMPA	Et_2O:EtOH (7:3)	86	0.8
ETPA4	Irgacure 2959	Et_2O:EtOH (7:3)	14	0.4
ETPA5	AIBN	-	11	0.08

[a]Measured via ^{1}H-NMR, considering terminal -CH_3 (0.88 ppm, 9H)[b] Measured via ^{1}H-NMR, by the N-C**H**$_2$ integral at 2.85 ppm.*Overlapping signals.

In summary, under all the tested conditions, the result was the thiol-ene addition only to one unsaturation of the HOSOET out of three. This showed an insufficient functionalization for future application of the compound as monomer. To implement the reaction outcome, further experiments can be performed by screening different concentrations or testing the reaction in flow, as was previously described for HOSO.

Besides TRGs, terpenes and terpenoids spark attention for structural modification *via* thiol-ene reactions as unsaturated linear and cyclic terpene derivatives occur in Nature. Although thiol-ene reaction is a straightforward strategy to achieve biobased amines, only two examples can be found in the scientific literature. The first difunctional terpene-derived amine was reported by Meier and Firdaus in 2012.[45] The two corresponding isomers were obtained from *R*-(+) and *S*-(-)-limonene in 84% and 81% yield, respectively. CAHC was used in excess (1:3) and DMPA was employed as photoinitiator, with 365 nm UV light (Figure 60). Consecutively, limonene diamine (LDA) was employed to synthesize polyamides.

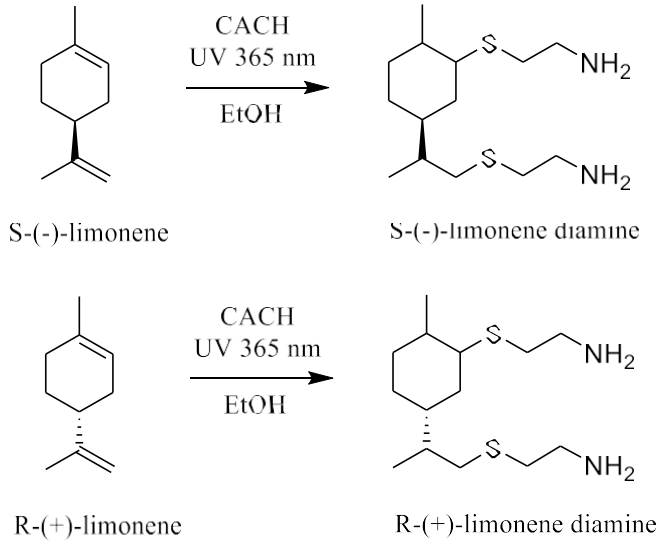

Figure 60. Limonene diamine obtained *via* photoinitiated thiol-ene reaction.

Through a thermoinitiated reaction, Alvès *et al*.[260] succeeded in the synthesis of the diamine derived from linalool. The reaction was carried out in THF at 80 °C, AIBN was used as thermal initiator in the presence of CAHC. Subsequently, three different formulations of NIPUs were produced. Inspired by these works, the investigation of photoinitiated thiol-ene reactions was carried on the geraniol and linalool isomers, as well as on myrcene (Figure 61).

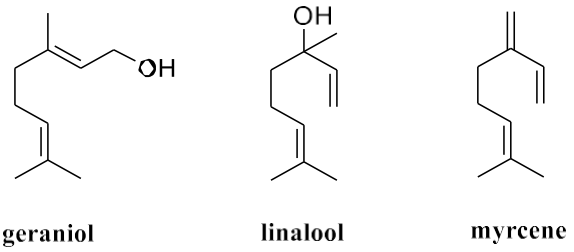

Figure 61. Chemical structure of geraniol, linalool and myrcene.

It is relevant to notice the different nature of the two unsaturations present in the two isomers. Indeed, linalool presents a terminal double bond, which is supposed to be much more reactive than the internal ones present in geraniol. Analogous to the synthesis starting from limonene, ethanol is a suitable renewable solvent for these compounds. EtOH was chosen as solvent, as terpenes and terpenoids are usually soluble in this media. Geraniol and linalool were tested in parallel with DMPA and TPO-L photoinitiators. Initially, myrcene was studied as a test compound. Taking as reference the study of Dove *et al*.,[242] TPO-L was used as photoinitiator (Table 13). Moreover, EtOH is a renewable and potentially biobased solvent. Due to the beneficial solubility of the overall system (CAHC is soluble in EtOH), two conditions were tested: diluted (0.04 g of terpene g /mL, Table 13 **T1**) and concentrated condition (0.285 g of terpene/mL, Table 13 **T2, T3, T4**).

Table 13. Thiol-ene reactions of terpenes in diluted and concentrated media.

	Terpene	**Concentration (terpene g/ mL)**	**Products**
T1	Myrcene	0.04	Monoamine
T2	Myrcene	0.285	Di-, triamine
T3	Linalool	0.285	Mono-, diamine
T4	Geraniol	0.285	Mono-, diamine

All the reactions were run with TPO-L photoinitiator, 405 nm UV-light LED (2W) for 6 h at room temperature.

In the first case, only the formation of monoamine was detected (214.018 m/z by ESI-MS, Figure 62-top). Alternatively, in the concentrated media, di- and triamines were formed, respectively (291.00 m/z and 384.19 m/z, Figure 62-bottom). The incomplete conversion of the double bounds can be attributed to their different substitution pattern.

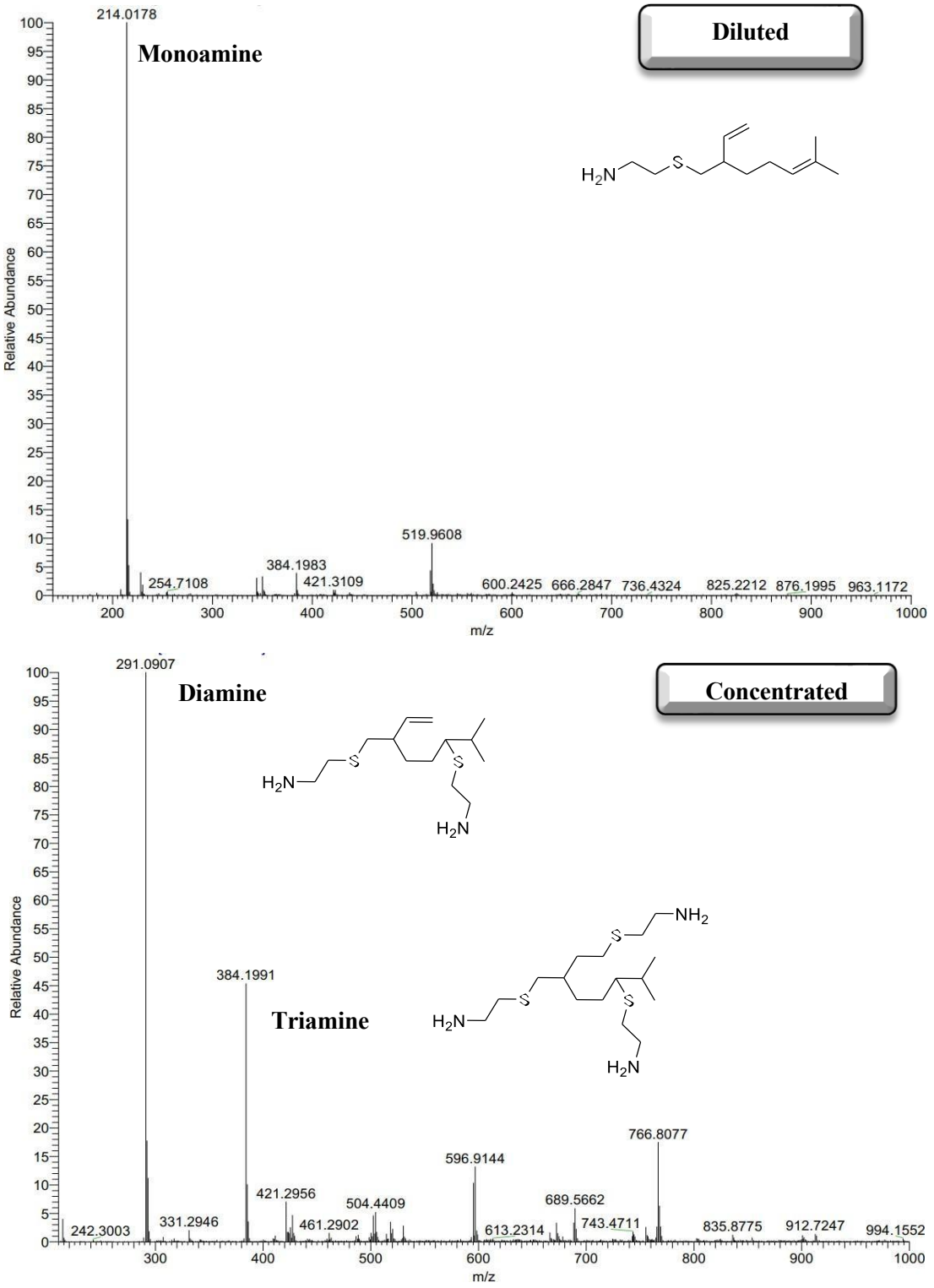

Figure 62. Top: thiol-ene reaction of myrcene in diluted condition (0.04 g/mL). Bottom: thiol-ene reaction of myrcene in concentrated conditions (0.285 g/mL).

In fact, terminal double bonds are known to be more reactive than internal ones in thiol-ene reactions, therefore the internal double bond present in myrcene is less prone to be functionalized by radicals. Owing to the successful conversion of myrcene to the di- and triamine, these reaction conditions were also applied with linalool and geraniol. As a result, a mixture of monoamine and diamine was obtained (Figure 63).

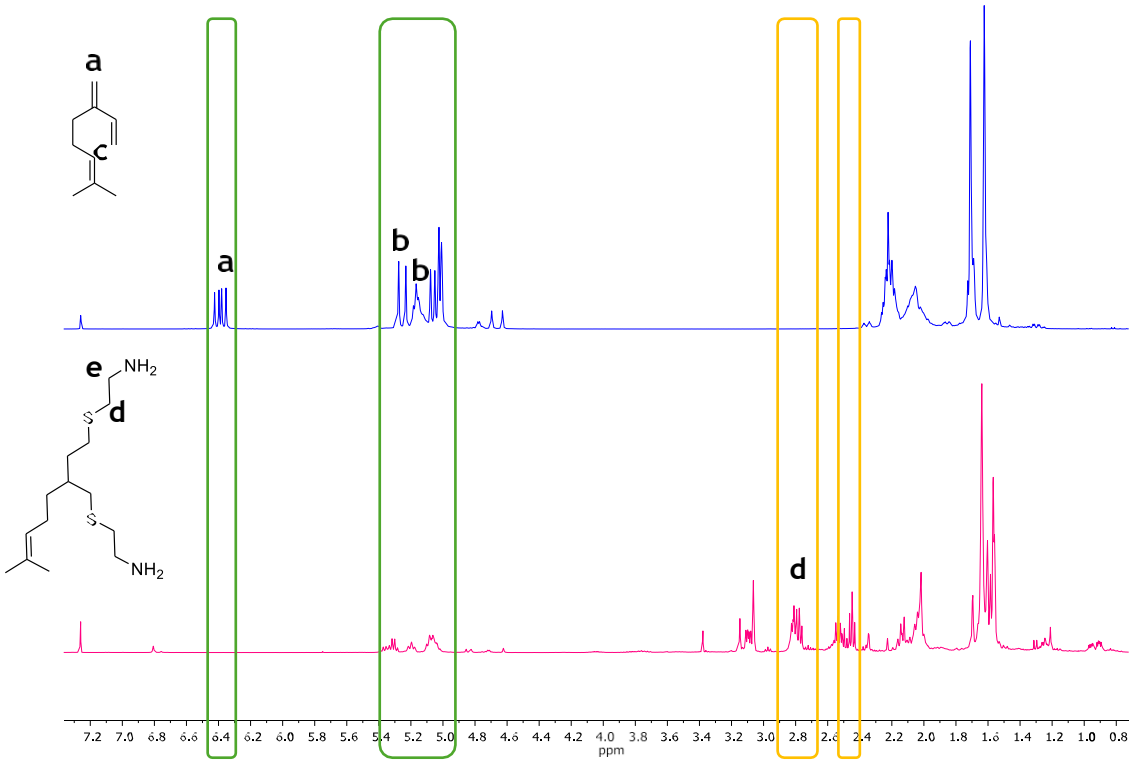

Figure 63. ^{1}H-NMR (400 MHz) proton spectrum in $CDCl_3$ (7.26 ppm) of myrcene before and after undergone thiol-ene photoreaction.

As in the case of myrcene, also linalool and geraniol possess internal unsaturations (one for linalool and two for geraniol). This can explain the presence of the monoamine in the final product. Nevertheless, geraniol has two internal double bonds, however, the one in β position to the OH, is more reactive due to the presence of the hydroxyl group as EWG.

Due to the high difficulty and large solvent waste created by the chromatographic separation of amines, the isolation of the single compounds from amine mixtures was not performed. From a sustainability and efficiency point of view, it is worth studying further the optimization of the thiol-ene process to achieve 100% functionalization of the double bonds. This could be also investigated by screening other wavelengths, solvents or in a flow reactor, as it was tested with HOSO (Chapter 2, Subchapter 2.4.1).

In the thiol-ene reaction of HOSO, the miscibility of the reactant was a crucial point to achieve. Therefore, the presence of an efficient solvent mixture and a proper amount of it was necessary for the purpose. This issue was not encountered in the case of terpenes as both CAHC and terpenes were soluble in EtOH. Therefore, in the latter case, the trend was found to be the opposite in comparison to the one experienced with vegetable oil. As decreasing the concentration of oil in the solvent media was reducing the conversion, the opposite was shown in the case of the thiol-ene reaction of terpenes.

1.5 CONCLUSION

In this second part of the work, a direct functionalization of the unsaturations present in vegetable oils and terpenes to achieve primary polyamines was investigated.

The study of the synthesis of vegetable oils led to optimization of the thiol-ene reaction on high oleic sunflower oil in terms of efficiency and sustainability. Full conversion of the double bonds was achieved within 7 h in an isopropanol/ethanol mixture replacing the unsafe dioxane. The use of a 2 W UV-LED and a valuable renewable polyamine was obtained in large scale. Moreover, the upscale synthesis was preliminary tested with an *in flow* thiol-ene approach.

With an adapted thiol-ene strategy, also terpene derived diamines were achieved from linalool and geraniol isomers and a mixture of di- and tri-amine was obtained from myrcene. Further studies could be carried out to achieve the total conversion of the unsaturations. Moreover, these molecules could be used as monomers for synthesizing different polymers such as epoxies, NIPUs or polyureas.

Through the *in flow* system, it was possible to scale up the reaction on a 2 g oil, reduce the reaction time to 6 h using a safe solvent, reaching > 99% conversion. Moreover, the UV LED employed was a low-power source of light, which is favourable for low energy consumption. Possibly, the reaction can be implemented using a faster flow rate or a lower concentration of the starting reaction mixture.

The etherification of oleic sunflower oil was successfully achieved in a short time. Full conversion was obtained in 30 minutes, with a trace of overoxidation (7% alcohol formation). Moreover, diverse pathways were tested for the purification process in order to use more sustainable solvents and reduce the amount of waste. The best strategy was achieved with the use of anisole. Nevertheless, the problem of the presence of polysiloxaane in the final product (formed via polymerization of the reducing agent) persisted.

1.6 EXPERIMENTAL DATA

Characterization methods

Thin Layer Chromatography (TLC)

TLC was performed on aluminium plates coated with silica gel of the type 60 F254 from Sigma Aldrich. The compounds on the plates were visualised via fluorescence quenching with 254 nm UV light or by staining with Seebach solution (2 g cerium(IV) sulfate, 5 g phosphomolybdic acid hydrate, 16 mL concentrated sulfuric acid, 200 mL water), vanillin solution (15 g vanillin, 2.5 mL concentrated sulfuric acid, 250 mL ethanol), or $KMnO_4$ staining solution (1.5 g $KMnO_4$, 10 g K_2CO_3, 1.25 mL 10% NaOH and 200 mL water) or ninhydrin solution (o.2 ninhydrin in 100 mL ethanol).

Flash Column Chromatography

Flash Column Chromatography was performed with silica gel 60 purchased from Sigma Aldrich. For automatic flash column chromatography, a Biotage® Isolera™ One Flash Column equipped with a UV-Vis detector (200 × 800 nm) with Biotage® Sfär Silica HC Duo Columns was used. All solvents were used in HPLC grade.

Nuclear Magnetic Resonance (NMR) Spectroscopy

^1H and ^{13}C NMR spectra were recorded at ambient temperature with a Bruker AVANCE DPX 400 spectrometer at 400 MHz for ^1H NMR and 101 MHz for ^{13}C NMR or with a Bruker AVANCE DPX 500 spectrometer at 500 MHz for ^1H NMR and 126 MHz for ^{13}C NMR. Chemical shifts δ are reported in ppm relative to the solvent signal of $CDCl_3$ (7.26 ppm for ^1H and 77.16 ppm for ^{13}C spectra) or DMSO-d_6 (2.50 ppm for ^1H and 39.52 ppm for ^{13}C spectra). Spin multiplicity and corresponding signal patterns were reported as follows: s = singlet, d = doublet, t = triplet, q = quartet, m = multiplet and br = broadened. Coupling constants (J) are reported in Hertz (Hz). For full assignment of the signals to the measured structure, ^1H-^1H Correlated Spectroscopy (^1H-^1H-COSY), ^1H-^{13}C Heteronuclear Single Quantum Coherence (^1H-^{13}C-HSQC), and ^1H-^{13}C Heteronuclear Multiple Bond Correlation (^1H-^{13}C-HMBC) were used.

Fourier-Transformation Infrared (FT-IR) Spectroscopy

FT-IR spectra were recorded using a Bruker Alpha-P instrument applying ATR technology in a range of $\tilde{\nu}$ = 400–4000 cm^{-1} with 24 scans per measurement.

High-Resolution Mass Spectrometry (HRMS)

Mass spectra were recorded on a Q Exactive (Orbitrap) mass spectrometer (Thermo Fisher Scientific, San Jose, CA, USA) equipped with an atmospheric pressure ionization source operating in the nebulizer assisted electrospray mode. Calibration of the instrument was done in the m/z-range 150–2000 using a standard containing caffeine, Met-Arg-Phe-Ala acetate and a mixture of fluorinated phosphazenes (Ultramark 1621) (all from Sigma-Aldrich). A constant spray voltage of 3.5 kV, a dimensionless sheath gas of 6 and a sweep gas flow rate of 2 were applied. The capillary voltage and the S-lens RF level were set to 68.0 V and 320 °C, respectively.

Gas Chromatography – Flame Ioniziation Detector (GC-FID)

GC Trace 1300 equipped with a FID detector (Thermo Fisher Scientific)

Electro spray ionization - Mass spectrometry (ESI-MS)

ESI-MS analysese were performed on a Linear Ion Trap mass spectrometer (LTQ, Thermo Fisher Scientific) Identification was based on full-scan MS covering *m/z 1*50–2000 and in MSn mode. Raw data were analysed by Xcalibur software (Thermo Fisher Scientific).

Size Exclusion Chromatography (SEC)

System I (Oligo SEC): A PSS SECcurity^2 SEC system based on Agilent Infinity 1260 II hardware was used for the measurements. The system is equipped with a refractive index detector SECcurity^2 RI, a column oven "(Bio)SECcurity^2 column compartment TCC6500", a "standard SECcurity^2" autosampler, and an isocratic pump "SECcurity^2 isocratic pump". Anhydrous tetrahydrofuran stabilized with 250 ppm butylated hydroxytoluene (BHT, ≥99.9%) was used at a flow rate of 1.0 ml min^{-1} and at 30 °C as mobile phase. The analysis was performed on the following column system: PSS SDV analytical precolumn (3 µm, 8 mm × 50 mm) with two PSS SDV analytical columns (3 µm, 8 mm × 300 mm, 1000 Å). For the calibration, narrow linear poly(methyl methacrylate) standards (Polymer Standards Service, PSS, Germany) ranging from 102 to 62200 Da were used. For the preparation of the samples,
2.00 mg of analyte was dissolved in 1.50 mL anhydrous tetrahydrofuran stabilized with 250 ppm butylated hydroxytoluene (BHT, ≥99.9%). All samples were filtered by syringe filter prior to use, to avoid plugging of the injection setup or the column.

Differential Scanning Calorimetry (DSC)

DSC measurements were performed on a Mettler Toledo DSC1 instrument equipped with a sample robot. Samples of 5–10 mg were loaded in a 100 µL aluminum crucible with pierced lid, and the measurements were performed under nitrogen atmosphere with a flow rate of 50 mL·min^{-1}. The DSC thermograms were recorded at a heating/cooling rate of 10 K·min^{-1} using the following heating/cooling program: first heating from 20 to 110 °C, then cooling from 110 to −70 °C, and a final heating step from −70 to 110 °C. The data from the last heating step are shown in the DSC curves.

Materials

High-Oleic Sunflower oil (Bio-Zentrale), linalool (97% Siga Aldrich), geraniol (98% Sigma Aldrich), myrcene (90% Sigma Aldrich), ethyl(2,4,6-trimethylbenzoyl) phenyl phosphinate (TPO-L, >95%, TCI), 2,2-dimethoxy-2-phenylacetophenone (DMPA, 99%, Thermo Scientific), Palladium(II)-Chloride (99.9%, Sigma Aldrich), Oxygen (99.999%, Air Liquide), Sodium sulfate anhydrous (Bernd Kraft GmbH), N,N-dimethylacetamide (99.5%, anhydrous, dried over molecular sieves, Thermo Scientific), dichloromethane (DCM ≥99%, Fisher Chemicals), chloroform (≥99.8%, Fisher Chemicals), Cyclohexane (≥99.5%, Honeywell) Ethylacetate (HPLC grade) 1,4-dioxane (Fluka Chemicals, 99.5%), ethanol (>99.8%, Fisher Chemicals), and propan-2-ol (>99.5%, Fisher Chemical) were used without further purification. Chloroform-d ($CDCl_3$, and DMSO-d6 99.8% atom-%D, Euriso-Top). Pd_3P catalysts supported on silica was synthetized by M.Sc. Arjun Neyyathala PhD student from Prof. Hanf group of research of the Institute of Inorganic chemistry of KIT.

Pressure reactor

Brand: Berghof, size 200 mL

Synthetic procedures

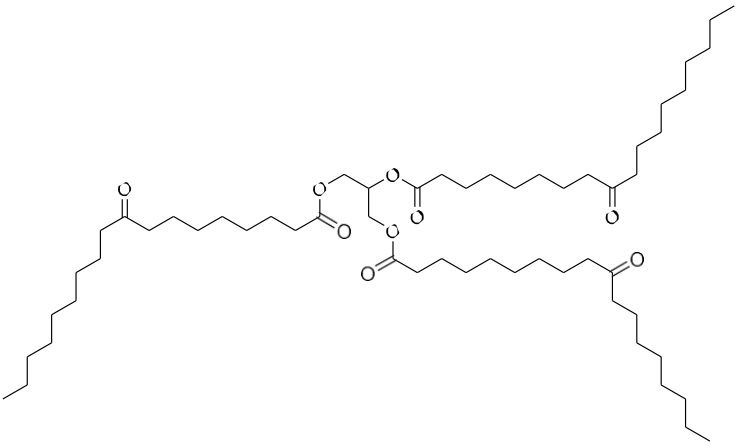

3-((10-oxooctadecanoyl)oxy)propane-1,2-diyl bis(9-oxooctadecanoate)
Chemical Formula: $C_{57}H_{104}O_9$
Molecular Weight: 933.45

- *3-((10-oxooctadecanoyl)oxy)propane-1,2-diyl bis(9-oxooctadecanoate)*
  Homogeneous catalysis

500 mg (0.56 mmol, 1.00 eq) of high oleic sunflower oil (HOSO, 85 % of monounsaturated fatty acid chains, average 3 double bonds per triglyceride, calculated *via* ^{1}H-NMR- from BioZenntrale) was weighted to a 10 mL glass vial. Subsequently, 3 mL DMAc/H2O (9:1 v/v) were added as a solvent mixture. Finally, 25 mg (0.14 mmol, 25.0 mol%) of $PdCl_2$ catalyst was added. The reaction mixture was placed in a pressure reactor ad the reactor chamber was filled with O_2 (10 bar, 3 conditioning cycles). The reaction was run for 24 hours under stirring at 70 °C. At the end, the crude was left cooling down at room temperature. For purification, the crude diluted with cyclohexane and washed with distilled water and saturated sodium chloride solution. Then, the cyclohexane phase was dried over sodium sulphate anhydrous, which was subsequently filtered and the solvent removed under vacuum. The product was obtained as a clear yellow oil. (Conversion double bods 62 %, yield: 95%)

TLC: Rf -Cyclohexane:EtOAc (8:2) = 0.57

^{1}H-NMR (400 MHz, CDCl3): δ (ppm) = 5.39-5.22 (CH=CH, m, 2H,), 5.19 (CH glycine unit, 1H,s), 4.23 (CH_2 glycine unit, 2H, dd), 4.07 (CH_2 glycine unit, 2H, dd), 2.27 (6H, CH, 6H, dt), 1.92 (CH_2, 6H,dp), 1.6 (CH_2, 6H, m) 1.19 (aliphatic H, 78 H, m), 0.81 (CH_3, 9H, t).

FT-IR ν [cm-1] = 2922 (νCH=CH, m), 2852 (s), 1742 (νC=O, s), 1555 (w), 1464 (w), 1376 (w), 1236 (w) , 1160 (νC-O ester, s), 1096 (w), 1026 (w), 966 (w), 861 (w), 721 (s), 450 (m).

ESI-HRMS= $C_{57}H_{104}O_9$ $[M+H]^+$ calculated: 933.45, found: 934.88.

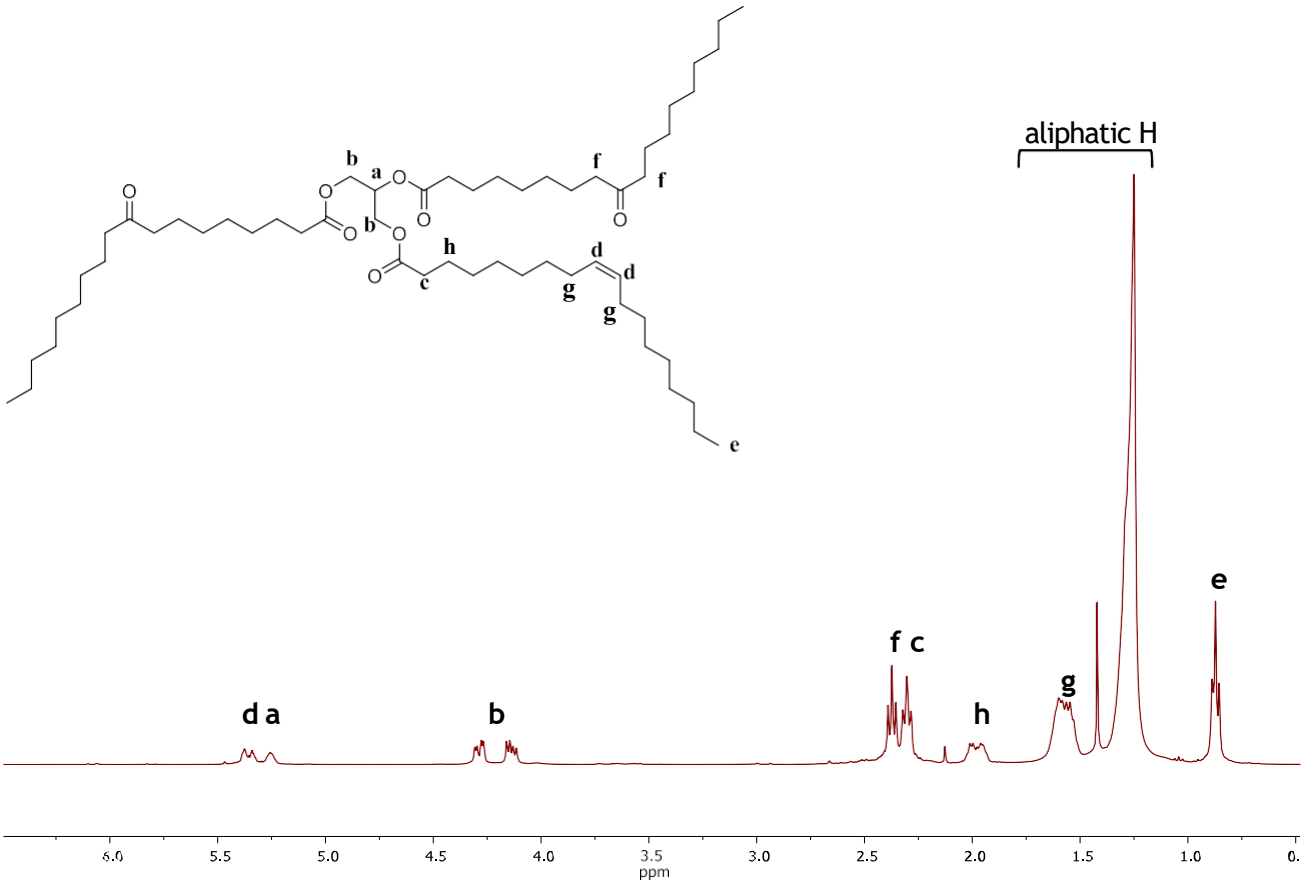

S 1. ^{1}H-NMR (400 MHz) proton spectrum in $CDCl_3$ (7.26 ppm) spectra of oxidized HOSO.

- *Methyl 9-oxooctadecanoate (or Methyl 10-oxooctadecanoate)*
  Heterogeneous catalysis- O_2 as sole oxidant

  In a 10 mL glass vial, methyl oleate 30 mg (0.1 mmol,1.00 eq) were weighted and the 5 mL of the solvent mixture were added. Subsequently, 2.5% mol of the catalyst was added (26.6 mg, 0.0025 mmol, 0.025 eq). The vial was placed in an autoclave at 80 °C under 10 bar O_2 atmosphere (3 conditioning cycles), 560 rpm, for 24 h. The crude was analyzed via GC-MS.

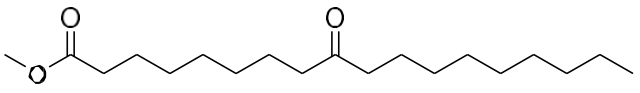

methyl 9-oxooctadecanoate
Chemical Formula: $C_{19}H_{36}O_3$
Molecular Weight: 312.49

- *Methyl 9-oxooctadecanoate (or Methyl 10-oxooctadecanoate)*
  Heterogeneous catalysis- $CuCl_2$ as cocatalyst

  In a 10 mL glass vial, methyl oleate 30 mg (0.1 mmol, 1.00 eq) were weighted and the 5 mL of the solvent mixture were added. Subsequently, 2.5% mol of the Pd_3P/SiO_2 (Pd 1% catalyst was added (26.6 mg, 0.0025 mmol, 0.025 eq) and 5% $CuCl_2$ co-catalyst (0.005 mmol, 0.05 eq.) The vial was placed in an autoclave at 80 °C under 10 bar O_2 atmosphere (3 conditioning cycles), 560 rpm, for 24 h. The crude was analyzed via GC-MS in EtOAc.

- *3-((10-oxooctadecanoyl)oxy)propane-1,2-diyl bis(9-oxooctadecanoate)- Heterogeneous catalysis- $CuCl_2$ as cocatalyst*

In a 10 mL glass vial, methyl oleate 88.5 mg of high oleic sunflower oil (HOSO, 85 % of monounsaturated fatty acid chains, average 3 double bonds per triglyceride, calculated *via* ^{1}H-NMR- from Bio-Zentrale) (0.1 mmol, 1.00 eq) were weighted and the 5 mL of the solvent mixture were added. Subsequently, 7.5% mol of the Pd_3P/SiO_2 (Pd 1%) catalyst was added (80 mg, 0.0075 mmol, 0.075 eq) and 15% $CuCl_2$ co-catalyst (0.0150 mmol, 0.15 eq.) The vial was placed in an autoclave at 80 °C under 10 bar O_2 atmosphere (3 conditioning cycles), 560 rpm, for 24 h. The crude was analyzed *via* NMR evaluating the forming integral at the 2.37 ppm peak corresponding at CH_2-(C=O)-CH_2 (4H, t). Reference peak: 0.88 ppm (-CH3, 3H, t).

^{1}H-NMR (400 MHz, CDCl3): δ (ppm), 3.66 (O=C-O-CH_3, 3H, s), 2.37 (CH_2-(C=O)-CH_2, 4H, t),1.97 ($CH_2C\mathbf{H}_2$-C=O, 2H, t), 1.61 ($C\mathbf{H}_2CH_2$-C=O, 2H, m), 1.25 (aliphatic H, s), 0.88 (-CH3, 3H, t).

GC-MS analyses

Retention times of molecules detected in the reaction mixture of Wacker oxidation of methyl oleate catalyzed by Pd_3P/SiO_2.

Methyl oleate	Epoxidate isomers	Ketone	Methyl oleate isomer
15.7 min	18.1-18.5 min	18.6 min	19.2 min

Compounds percentage were evaluated by the ratio of the registered products peaks in the GC-MS chromatograms.

- *Propane-1,2,3-triyl tris(10-((2-aminoethyl)thio)octadecanoate) with DMPA*

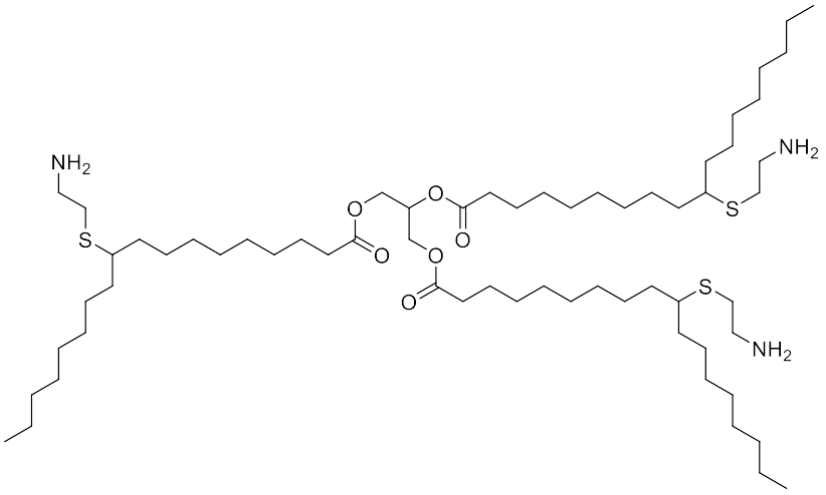

propane-1,2,3-triyl tris(10-((2-aminoethyl)thio)octadecanoate)
Chemical Formula: $C_{63}H_{125}N_3O_6S_3$
Molecular Weight: 1116.89

500 mg (0.56 mmol, 1.00 eq) high oleic sunflower oil (HOSO, 85 % of monounsaturated fatty acid chains, average 3 double bonds per triglyceride, calculated *via* ^{1}H-NMR- from Bio-Zentrale) were weighted in a 10 mL glass vial. The proper amount of the solvent mixture selected was added (1,4-dioxane: EtOH,7:3 or isopropanol: EtOH, 1:1), with a concentration of 0.04 g/mL or 0.28 g/mL of oil. 572.6 mg (5.04 mmol, 9.00 eq) of cysteamine hydrochloride (3.00 eq per double bond) The mixture was stirred for 30 minutes. Subsequently, 129.2 mg

(0.504 mmol, 0.3 eq) DMPA (0.1 eq per double bond) were added in the vial. The reaction was carried out under 365 or 405 nm UV LED-light, at room temperature for 7 hours. As the reaction ended, the solvent was removed under reduced pressure. Then, $CHCl_3$ was added (20 mL) and the crude washed one time with a basic solution of sodium carbonated and three times with distilled water. The organic phase was dried with sodium sulfate anhydrous and then filtered. The solvent was removed in vacuum. The product obtained was viscous liquid light-yellow product (Double bond conversion >99 %).

TLC: Red spot visible on the baseline revealed with ninhydrin solution. (EtOAc: MeOH, 9:1)

^{1}H–NMR (400 MHz, $CDCl_3$) δ 5.37 (CH=CH, 2H, m if present unreacted double bonds), 5.25 (CH glycerol unit, 1H, q), 4.08 – 4.34 (CH_2 glycerol unit,4 H, dd), 2.77 – 2.92 (C**H**$_2$NH$_2$, 6H, t), 2.47–2.71 (CHSC**H**$_2$, 6H, t), 2.22 – 2.38 (COCH2, 6H, t), 1.65 – 1.83 (s, -NH_2), 1.08 – 1.65 (CH_2 aliphatic protons, m), 0.87 (CH_3, 9H, t).

^{13}C–NMR (101 MHz, $CDCl_3$) δ 173.25, 68.89, 62.09, 45.90, 41.72, 35.07, 34.71, 34.02, 31.90, 29.67, 29.62, 29.31, 29.10, 26.85, 24.82, 22.68, 14.13.

DOSY- (500 MHz, $CDCl_3$) δ 68.89 (CH glyceryl structure), 62.10 (CH_2 glyceryl structure), 45.90 (C**H**-S), 41.71 (SH-CH_2-C**H**$_2$-NH_2), 35.07 (SH-C**H**$_2$-CH_2-NH_2), 14.13 (-CH_3).

FT-IR: ν [cm-1] = 2923 (ν N-H, w), 1740 (ν C=O, s), 1650 (δ N-H, m), 1604, 1462 (δ C-H, m) 1275 (ν C-N, m).

ESI-HRMS $C_{63}H_{125}N_3O_6S_3$ $[M+H]^+$= calculated: 1116.89, found: 1116.89.

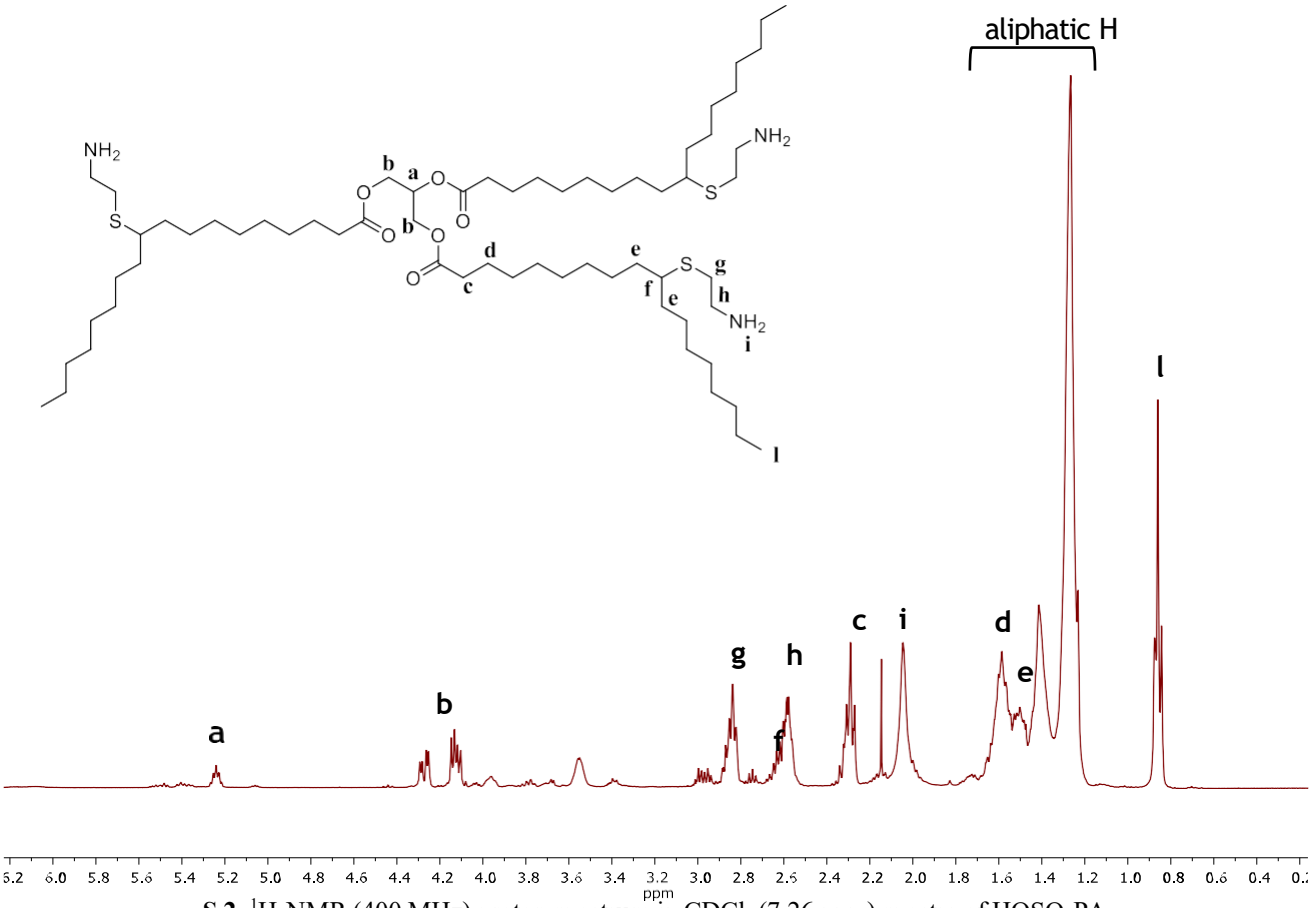

S 2. ^{1}H-NMR (400 MHz) proton spectrum in $CDCl_3$ (7.26 ppm) spectra of HOSO-PA.

- *Propane-1,2,3-triyl tris(10-((2-aminoethyl)thio)octadecanoate) with TPO-L*

500 mg (0.56 mmol) of high oleic sunflower oil (HOSO, 85 % of monounsaturated fatty acid chains, average 3 double bonds per triglyceride, calculated *via* ^{1}H-NMR from Rapuzel) were placed in a 10 mL glass vial. with cysteamine hydrochloride (CAHC, 3 equiv. per double bond, 5.08 mmol, 577.14 mg) and the correct amount of the solvent mixture chosen (Dioxane: EtOH,7:3 or Isopropanol: EtOH, 1:1), with a concentration of 0.28 g/mL of oil. The mixture was stirred for 30 min. Afterwards, a 2 wt% TPO-L solution was prepared in the solvent mixture chosen. The weight percentage was calculated considering the total weight of total oil and cysteamine salt, in the concentration of 1 mg/35 µL of oil. The reaction was stirred for 48 h at room temperature and irradiated by 405 nm LEDs. As the reaction ended, the solvent was removed under reduced pressure. Then, $CHCl_3$ was added (20 mL) and the crude washed one time with a basic solution of sodium carbonated and three times with distilled water. The organic phase was dried with sodium sulfate anhydrous and then filtered. The solvent was removed in vacuum. The product obtained was viscous liquid light-yellow product (Double bond conversion >99 %).

- *Propane-1,2,3-triyl tris(10-((2-aminoethyl)thio)octadecanoate) in flow*

2 g of high oleic sunflower oil (HOSO, 87% of oleic fatty acid chains, average 3 double bonds per triglyceride, calculated from ^{1}H-NMR, from Alnatura) and 2.31 g (20.3 mmol, 9 eq- 3 eq *per* double bond) of cysteamine hydrochloride were placed in a glass vial and 12 mL of isopropanol were added. The mixture was stirred for 30 min. After DMPA photoinitiator (174 mg, 0.3 eq- 0.1 eq *per* double bond) and the remaining solvent (2 mL) was added (total concentration 1g/7mL of oil). The reaction mixture was connected to a flow reactor placing the flask reaction mixture under stirring and fed to the UV chamber (365 nm, 16 W) via 1 mm diameter tube in a closed loop (Figure 1). The reaction was monitored via ^{1}H-NMR along the time.

- *(Z)-1-((1,3-bis(((Z)-octadec-9-en-1-yl)oxy)propan-2-yl)oxy)octadec-9-ene*

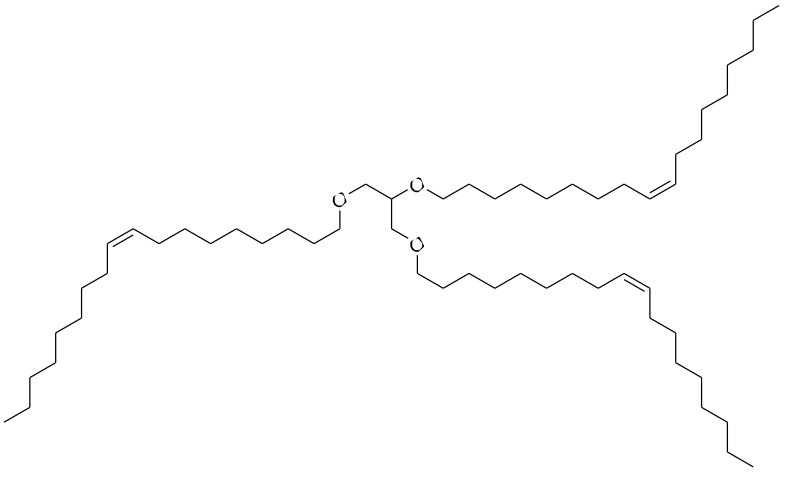

(*Z*)-1-((1,3-bis(((*Z*)-octadec-9-en-1-yl)oxy)propan-2-yl)oxy)octadec-9-ene
Chemical Formula: $C_{57}H_{110}O_3$
Molecular Weight: 843.50

500 mg (0.56 mmol, 1.00 eq) high oleic sunflower oil (HOSO, 85 % of monounsaturated fatty acid chains, average 3 double bonds per triglyceride, calculated *via* ^{1}H-NMR- from Bio-Zentrale) were weighted in a Schlenk glass vial. The oil was flushed with Ar for 30 minutes and slightly heated with a heat gun in order to remove dry it. Then, $GaBr_3$ was weighted in a glove box and placed in the Schlenk vial. The reaction mixture was placed under styrring at 80°C and the connected with a syringe pump in

order to add $SiHEt_3$ reducing agent (2.56 mL/min). The reaction was run for 1 h. Diverse work-up procedures were tested.

1) The crude reaction was stirred overnight in THF. After, the organic phase was washed with water three ties, dried with sodium sulfate anhydrous and filtered. The solvent removed under reduced pressure. The product was purified via column chromatography with the following solvent gradient: Cyclohexane:dietyl ether (8:2)- (8.5:1.5)-(9:1).

2) The crude reaction was stirred overnight in Et_2O. The same procedure as above was then applied. The product was purified via column chromatography with the following solvent gradient: Cyclohexane:dietyl ether (8:2)- (8.5:1.5)-(9:1).

3) The crude reaction was stirred overnight in anisole. The same procedure as above was then applied. Then anisole was removed by distillation.

Due to presence of polysiloxane in the final product, yields were not possible to calculate. Therefore, the introduction of the Q value was established (Equation 1).

$$Q = \frac{\int PS}{\int terminal\ CH_3} \qquad \textbf{Eq.1}$$

ETHOSO purification methods in different solvents and respective Q factors.

	Purification method	**Solvent**	**Q**
ETHOSO1	filtration	toluene	3,7
ETHOSO1	filtration + column	toluene	2,2
ETHOSO2	filtration	diethyl ether	6,6
ETHOSO2	filtration + column	diethyl ether	4,0
ETHOSO3	filtration + distillation	anisole	3,0

Q as the ratio of the integral of polysiloxane (0.07 ppm) divided by the integrals of terminal CH_3 groups at 0.88 ppm.

Product obtained as a clear liquid viscous substance. Quantitative conversion to ethers was achieved, however, the polysiloxane formed was not possible to be fully removed from the product (fine white solid).

TLC: 0.75 (Cycloexane:EtOAc 8:1)

^{1}H-NMR (400 MHz, $CDCl_3$) δ 5.34 (m, 6H, HC=CH), 3.45 (m, 1H, CH glycerine unit), 3.43 (m,4H, CH_2 glycerine unit), 2.77 (t, CH linolenic unit traces), 2.02 (m,12 H, **H**C-CH=CH-C**H**), 1.27 (m, 6H, O-CH_2), 56 (m, aliphatic protons), 0.88 (9H, CH_3).

^{13}C-NMR (101 MHz, $CDCl_3$): δ / ppm = 130.07, 130.06, 130.00, 129.98, 129.97, 78.03, 71.79, 70.99, 70.75, 32.06, 30.25, 29.93, 29.86, 29.82, 29.81, 29.77, 29.70, 29.68, 29.65, 29.64, 29.48, 29.44, 27.37, 26.29, 26.25, 22.84, 14.27.

FT-IR: ν [cm-1] = 3009 (ν CH=CH, w), 3000-2780 (ν C-H, w), 1471 (δ C-H, m), 1244 (ν C-O, m).

ESI-HRM $C_{57}H_{110}O_3$ [M+H]+ calculated: 843.8528, found: 843.8526.

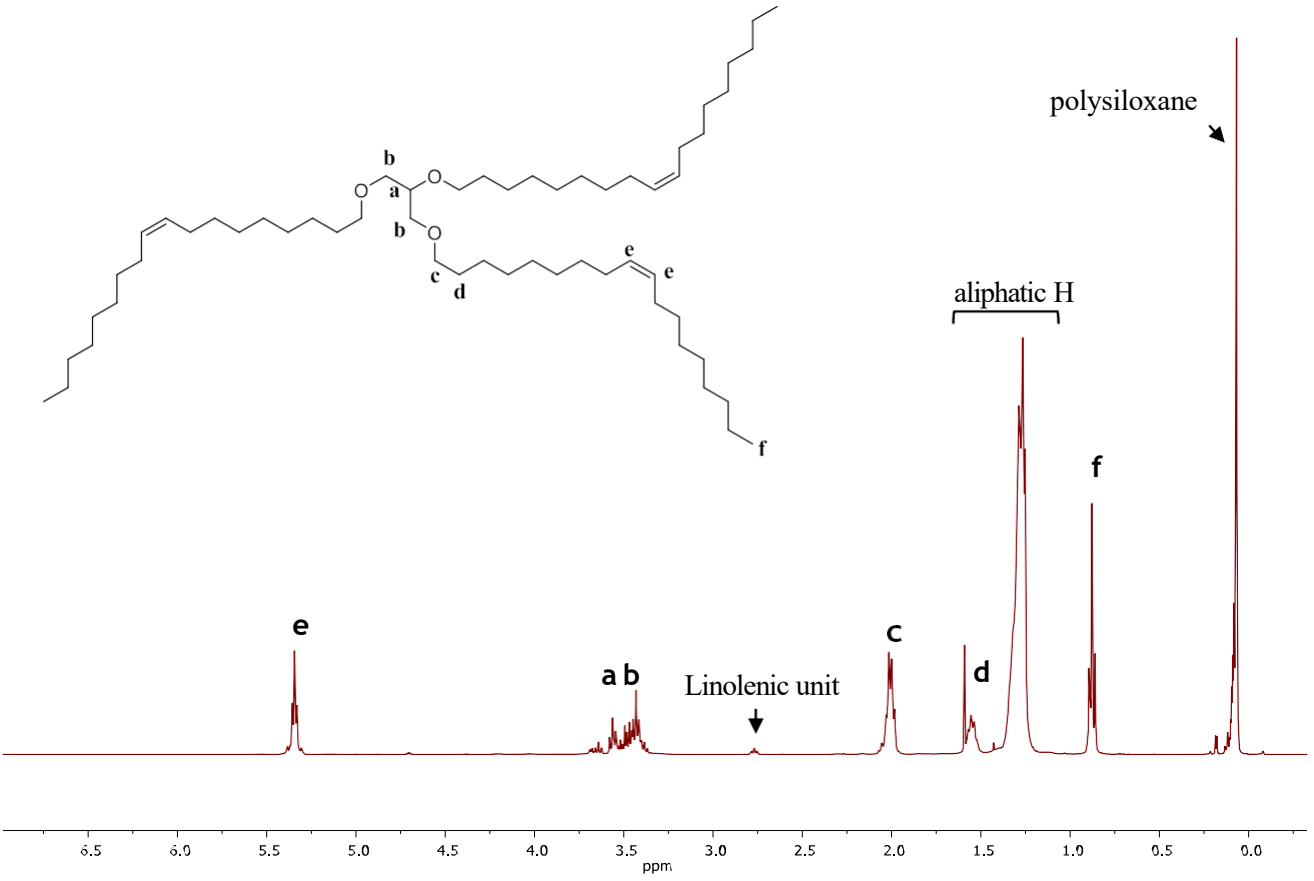

S 3.[1]H-NMR (400 MHz) proton spectrum in CDCl3 (7.26 ppm) spectra of ETHOSO.

- *16-((10-((2-aminoethyl)thio)octadecyl)oxy)-4,28-dioctyl-14,18-dioxa-3,29-dithiahentriacontane-1,31-diamine*

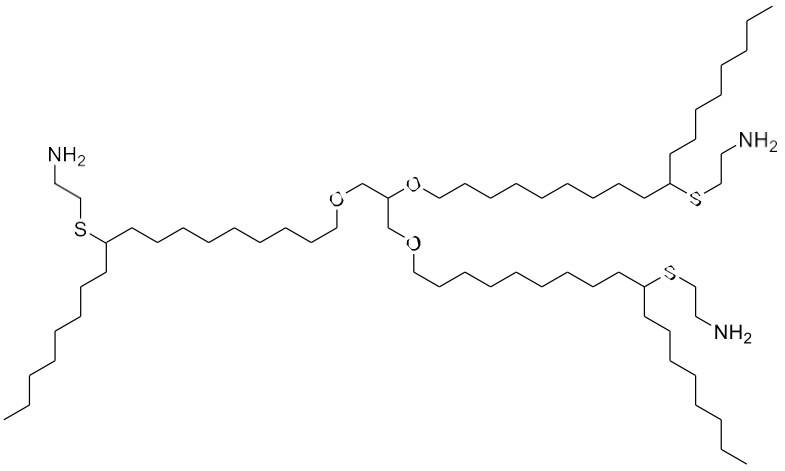

16-((10-((2-aminoethyl)thio)octadecyl)oxy)-4,28-dioctyl-14,18-dioxa-3,29-dithiahentriacontane-1,31-diamine

Chemical Formula: $C_{63}H_{125}N_3O_6S_3$

Molecular Weight: 1116.89

500 mg (0.56 mmol, 1.00 eq) high oleic sunflower oil ethers (HOSOET) were weighted in a 10 mL glass vial. The proper amount of the chosen solvent mixture selected was added (Table X). 572.6 mg (5.04 mmol, 9.00 eq) of cysteamine hydrochloride (3.00 eq per double bond) The mixture was stirred for 30

minutes. Subsequently, the chosen initiator was added (Table X). The reaction was carried out under 405 nm UV LED-light, at room temperature for 7 hours. As the reaction ended, the solvent was removed under reduced pressure. Then, $CHCl_3$ was added (20 mL) and the crude washed one time with a basic solution of sodium carbonated and three times with distilled water. The organic phase was dried with sodium sulfate anhydrous and then filtered. The solvent was removed in vacuum.

Different catalysts were testes (Table 16):

Table 14. Conversion of the double bonds (db) in different thiol-ene reaction conditions on high oleic sunflower oil ether (HOSOET).

	Initiator	Solvent	Conc HOSOET g/mL	Conversion db[a]	Amine functionality per TRG[b]
ETPA1	DMPA	Et_2O:EtOH (1:1)	0.36	53	Not measurable*
ETPA2	TPO-L	EtOAc	0.26	57	1.1
ETPA3	DMPA	Et_2O:EtOH (7:3)	0.26	86	0.8
ETPA4	Irgacure 2959	Et_2O:EtOH (7:3)	0.26	14	0.4
ETPA5	AIBN[b]	-	bulk	11	0.08

[a] Measured via ^{1}H-NMR, considering terminal -CH_3 (0.88 ppm, 9H). [b] Measured via ^{1}H-NMR, by the N- C**H**$_2$ integral at 2.85 ppm. *Overlapping signals. [b] Reaction temperature= 80°C.

- *2,2'-((2-(4-methylpent-3-en-1-yl)butane-1,4-diyl)bis(sulfanediyl))bis(ethan-1-amine)*

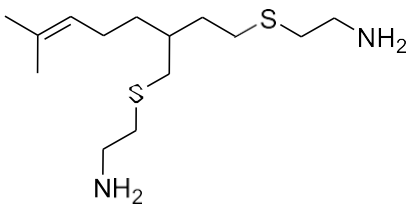

2,2'-((2-(4-methylpent-3-en-1-yl)butane-1,4-diyl)bis(sulfanediyl))bis(ethan-1-amine)
Chemical Formula: $C_{14}H_{30}N_2S_2$
Molecular Weight: 290.53

Diluted conditions. 200 mg (1.47 mmol, 1.00 eq) myrcene were weighted in a 10 mL glass vial and 3 mL of EtOH were added. Then, 1.5 g cysteamine hydrochloride (13.23 mmol, 9.00 eq, meaning 3.00 eq per double bond) was added and the reaction mixture was stirred for 30 minutes. Subsequently, a solution in 2 mL of EtOH of TPO-L photoinitiaor 1 %wt. of the total weight terpene + CAHC (17 mg, 0.054 mmol) was prepared and mixed with the previous reactants. The reaction was carried out under 405 nm UV LED-light (2W), at room temperature for 7 hours (0.04 g/mL of terpene).

Concentrated conditions. 200 mg (1.47 mmol, 1.00 eq) myrcene were weighted in a 10 mL glass vial and 15 g cysteamine hydrochloride (13.23 mmol, 6.00 eq, meaning 3.00 eq per double bond) were added. Subsequently, a solution in 700 µL of EtOH of TPO-L photoinitiaor 1 %wt. of the total weight terpene + CAHC (17 mg, 0.058 mmol) was prepared and mixed with the previous reactants. The reaction was carried out under 405 nm UV LED-light (2W), at room temperature for 7 hours (0.28 g/mL of terpene).

As the reaction ended, the solvent was removed under reduced pressure. Then, $CHCl_3$ was added (20 mL) and the crude washed one time with a basic solution of sodium carbonated and three times with distilled water. The organic phase was dried with sodium sulfate anhydrous and then filtered. The solvent was removed in vacuum. The product obtained was yellow viscous liquid. (Diluted condition yield: 10% Concentrated condition yield: 80%).

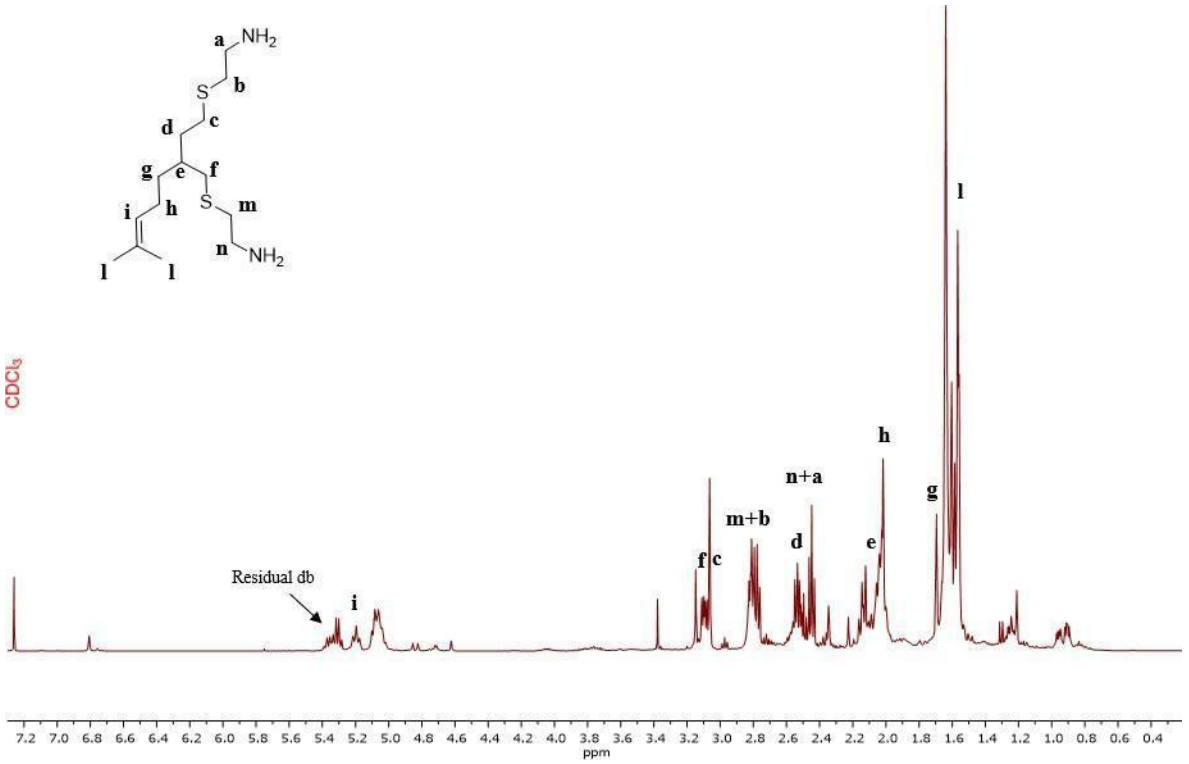

S 4. ^{1}H-NMR (400 MHz) proton spectrum in CDCl3 (7.26 ppm) spectra of myrcene amine.

TLC: Red spot visible on the baseline revealed with ninhydrin solution. (EtOAc: MeOH, 9:1)

^{1}H NMR (400 MHz, $CDCl_3$) δ 5.29 (residual myrcene CH=CH), 5.20 (CH=CH, 2H, m), 5.03 (residual myrcene CH=CH), 3.11(CH_2, 2H, m), 3.04 (CH_2, 2H, m), 2.80 (C**H**$_2$$NH_2$, 4H, t), 2.54 (SC**H**$_2$$CH_2NH_2$, 4H, t), 2.42 ($CH_2$, 2H, m), 2.32, 2.10 (CH,1H, m), 1.99 (NH), 1.86 (CH_2, 2H, m), 1.59 (-CH_3, 6H, m), 1.53.

FT-IR: ν [cm-1] = 3437-3118 (νN-H, w), 2905 (νC-H, s), 1646 (δN-H, m), 1590, 1456 (δC-H, m), 1270 (νC-N, m).

ESI-HRMS $C_{14}H_{30}N_2S_2$ $[M+H]^+$= diluted conditions, monoamine: calculated: 213.16 found: 214.0178 m/z

ESI-HRMS $C_{14}H_{30}N_2S_2$ $[M+H]^+$= concentrated conditions, diamine: calculated: 290.19 found: 291.0107 m/z. triamine: calculated: 367.21+[NH_3] found: 384.1991 m/z

- *1,6-bis((2-aminoethyl)thio)-3,7-dimethyloctan-1-ol (diamine from linalool)*

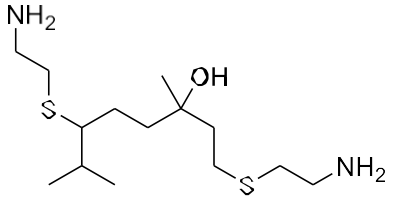

1,6-bis((2-aminoethyl)thio)-3,7-dimethyloctan-3-ol
Chemical Formula: $C_{14}H_{32}N_2OS_2$
Molecular Weight: 308.54

Concentrated conditions. 200 mg (1.47 mmol, 1.00 eq) linalool were weighted in a 10 mL glass vial and 1 g cysteamine hydrochloride (8.82 mmol, 6.00 eq, meaning 3.00 eq per double bond) were added. Subsequently, a solution in 700 µL of EtOH of TPO-L photoinitiaor 1 %wt. of the total weight terpene + CAHC (12 mg, 0.038 mmol) was prepared and mixed with the previous reactants. The reaction was carried out under 405 nm UV LED-light (2W), at room temperature for 7 hours (0.28 g/mL of terpene). As the reaction ended, the solvent was removed under reduced pressure. Then, $CHCl_3$ was added (20 mL) and the crude washed one time with a basic solution of sodium carbonated and three times with distilled water. The organic phase was dried with sodium sulfate anhydrous and then filtered. The solvent was removed in vacuum. Slightly yellow viscous liquid, yield= 42%.

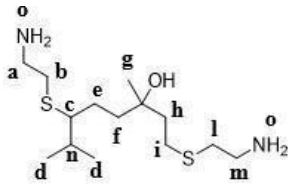

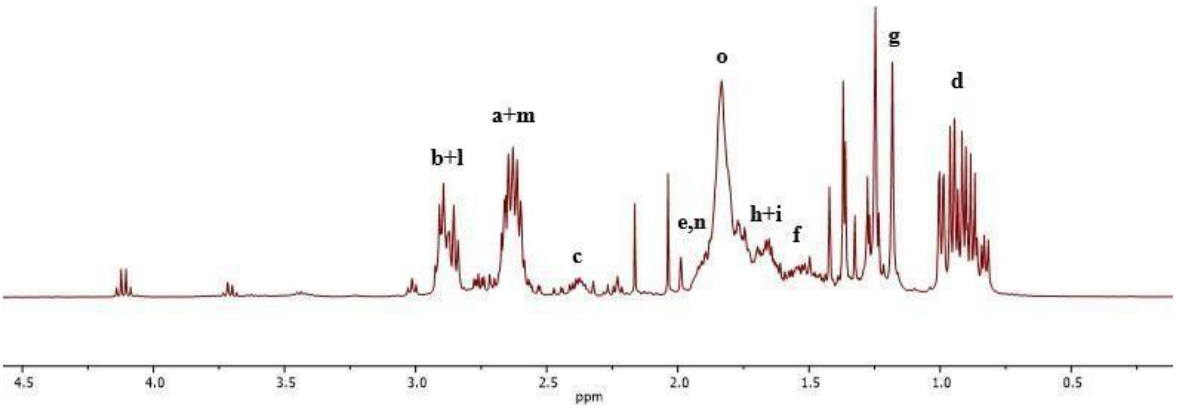

S 5. ^{1}H-NMR (400 MHz) proton spectrum in CDCl3 (7.26 ppm) spectra of linalol diamine.

TLC: Red spot visible on the baseline revealed with ninhydrin solution. (EtOAc: MeOH, 9:1)

^{1}H–NMR (400 MHz, $CDCl_3$) 2.89 (C**H**$_2$NH$_2$, 4H, t) 2.63 (SC**H**$_2$CH$_2$NH$_2$, 4H, t), 1.83 (CH, 1H, m), 1.77 (CH_2, 2H, m), 1.65 (NH), 1.37 (CH_2, 4H, m), 1.25 (-CH_3, 3H, s), 0.99, 0.95, 0.90, 0.87, 0.83 (-CH_3, 6H, m).

FT-IR: ν [cm-1] = 3400-3200 (νN-H, O-H, w), 1643 (δN-H, m), 1445 (δC-H, m), 1284 (νC-N, m).

ESI-HRMS $C_{13}H_{30}N_2OS_2$ $[M+H]^+$= monoamine calculated: 231.17, found: 232.1728 diamine calculated 308.20 m/z, found: 291.1920 – $[H_2O]$

- *1-((2-aminoethyl)thio)-6-((aminomethyl)thio)-3,7-dimethyloctan-3-ol (diamine from geraniol)*

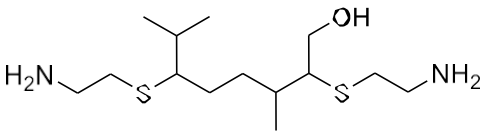

2,6-bis((2-aminoethyl)thio)-3,7-dimethyloctan-1-ol
Chemical Formula: $C_{14}H_{32}N_2OS_2$
Molecular Weight: 308.54

Concentrated conditions. 200 mg (1.47 mmol, 1.00 eq) geraniol were weighted in a 10 mL glass vial and 1 g cysteamine hydrochloride (8.82 mmol, 6.00 eq, meaning 3.00 eq per double bond) were added. Subsequently, a solution in 700 µL of EtOH of TPO-L photoinitiaor 1 %wt. of the total weight terpene + CAHC (12 mg, 0.038 mmol) was prepared and mixed with the previous reactants. The reaction was carried out under 405 nm UV LED-light (2W), at room temperature for 7 hours (0.28 g/mL of terpene). As the reaction ended, the solvent was removed under reduced pressure. Then, $CHCl_3$ was added (20 mL) and the crude washed one time with a basic solution of sodium carbonated and three times with distilled water. The organic phase was dried with sodium sulfate anhydrous and then filtered. The solvent was removed in vacuum. Yellow highly viscous liquid yield: 67%.

TLC: Red spot visible on the baseline revealed with ninhydrin solution. (EtOAc: MeOH, 9:1)

^{1}H–NMR (400 MHz, $CDCl_3$) δ: 5.43, 5.09, 4.16, 3.75, 3.72, 3.63, 3.02, 2.88, 2.76, 2.62, 1.84, 1.68, 1.60, 1.25, 0.99, 0.93.

FT-IR: ν [cm-1] = 3580-3070 (νN-H, O-H w), 2912 (νC-H, s), 1652 (δN-H, m), 1574, 1466 (δC-H, m), 1224 (νC-N, m).

ESI-HRMS $C_{13}H_{30}N_2OS_2$ $[M+H]^+$= monoamine calculated: 231.17, found: 232.1730 diamine calculated 308.20 m/z, found: 351.2134 m/z – [isopropyl]+.

2 CHAPTER 3:ISOCYANATE-FREE URETHANE BIS-CYCLIC CARBONATES (UBCS)

2.1 URETHANE BIS-CYCLIC CARBONATE (UBCS)SYNTHESIS

Different structural modifications are under investigation to improve the performances of cyclic carbonate monomers in aminolysis reactions to achieve PHU materials (Figure 64).[261]

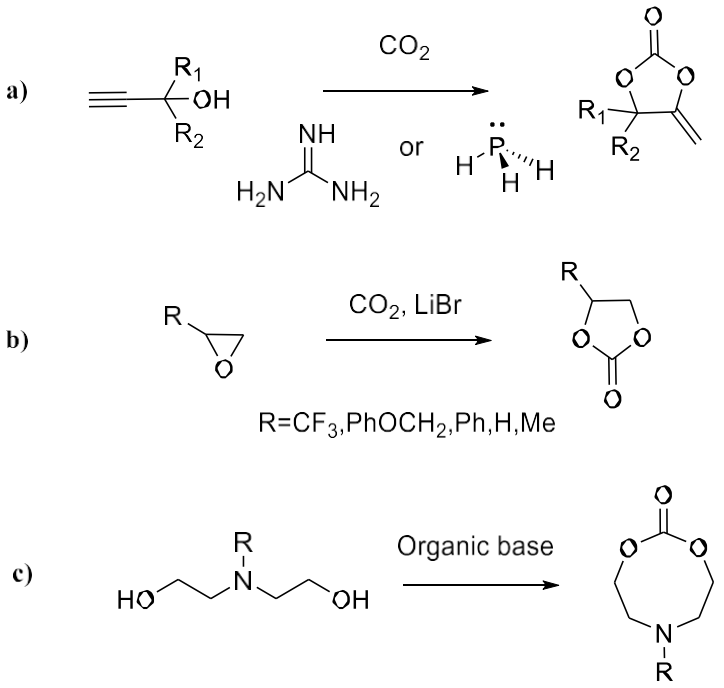

Figure 64. Examples of strategy to synthesize CC with enhanced reactivity. a)[262] b)[263] c)[264].

The most common strategy is to insert an electron-withdrawing (EWG) group close to the CC ring structure as an ester, ether or alkyl group.[110, 265, 266] Ester functions can be introduced in β position to the CC unit by using esters or carboxylic acids with glycerol carbonate.[266, 268] In a study by Cramail and coll., it was shown that 5-CCs with ester substituents in β position exhibit higher reactivity to same-size CCs with ether or alkyl group substituents and similar reactivity to 6-CCs (Chapter 1, Non-isocyanate polyurethanes).[265] As a drawback, the ester function can bring the formation of undesired products. In fact, the amidation reaction was reported as a side reaction during the aminolysis when an ester function was present.[269] This leads to lower molar mass PHU or lower crosslinking density and gel contents of PHU thermosets.[154, 266, 270, 271] The usual strategy to obtain urethane-linked polyfunctional cyclic carbonate monomers is by using isocyanates.[272–274] At present,

Nohra et *al.*[275] reported the only isocyanate-free synthetic pathway to achieve similar urethane cyclic carbonate (Figure 65).

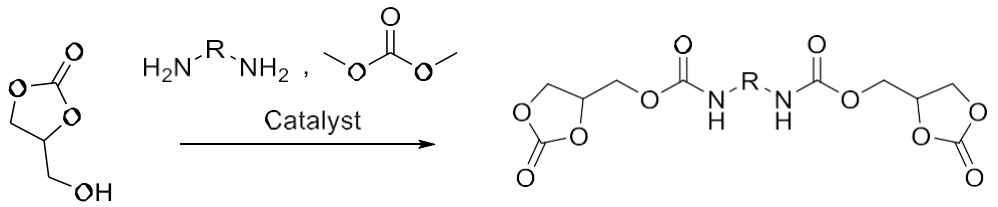

Figure 65. Isocyanate-free synthesis of bis-CC.[275]

The process involves diamines, glycerol carbonate and dimethyl carbonate *via* a catalytic reaction, being a greener method in comparison to the previously reported ones, for instance due to the low toxicity of the reactants and their renewable origin.[59, 276] However, in their study, no exploration of the production of polymeric materials was documented. To further investigate this unexplored topic, the synthesis of a CC bearing a urethane group in α position (urethane bis-cyclic carbonates-UBC) was developed more sustainably. Together with the design of the synthesis and the interest in the evaluation of the reactivity, the renewability of the starting compound was considered. Indeed, much attention is dedicated nowadays to avoiding petrol-based sources in general, and in particular to the CC synthesis.[277] In the frame of the EJD NIPU consortium, two novel UBC molecules following the above-mentioned requirements were designed together with the group of Caillol (ESR2 Federico Mundo) at Henkel Adhesive Technologies in Düsseldorf (Germany) as the industrial partner. Both PhDs conceptualised this project, as well as the practical syntheses, analyses and data evaluation. NMRs were run by the spectroscopy department at Henkel. Therefore, a defined attribution of tasks to a single PhD student is not possible as this was a close collaboration and different tasks were shared.

The selected starting compounds were 1,6-hexamethylene diamine (HA) as a medium aliphatic chain diamine and isophorone diamine (IPDA) as a cyclic compound. The structural chemical difference of the selected amine was chosen to evaluate how this dissimilarity will affect the reactivity and the final polymer properties. To evaluate the synthetic strategy, both isocyanate and isocyanate-free pathways were carried out. In the first case, 1,6-hexamethylene diisocyanate and isophorone diisocyanate were reacted with glycerol carbonate to achieve the corresponding UBCs. The reaction was monitored through FT-IR and the structures were confirmed by NMR. The attention was on the decreasing intensity of the N=C=O stretching band at 2250 cm^{-1} and consequent formation of the urethane stretching band (O-(C=O)-NH) at 1688 cm^{-1} and N-H stretching at 1519 cm^{-1}. For both monomers, 80 % yield was achieved.

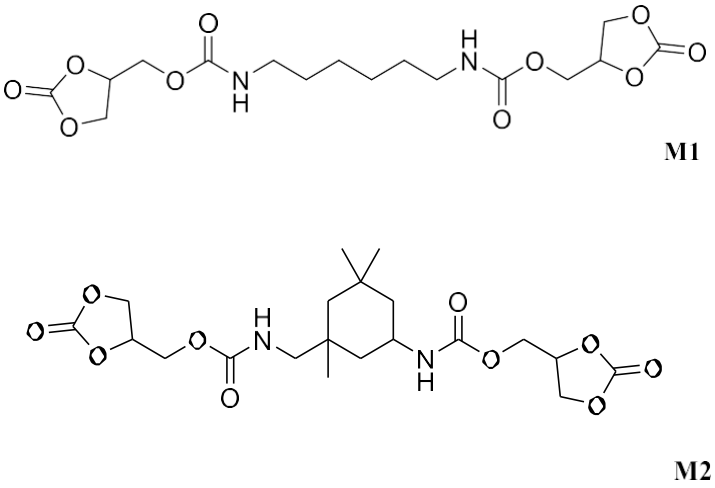

Figure 66. Structures of **M1** from HA and **M2** from IPDA.

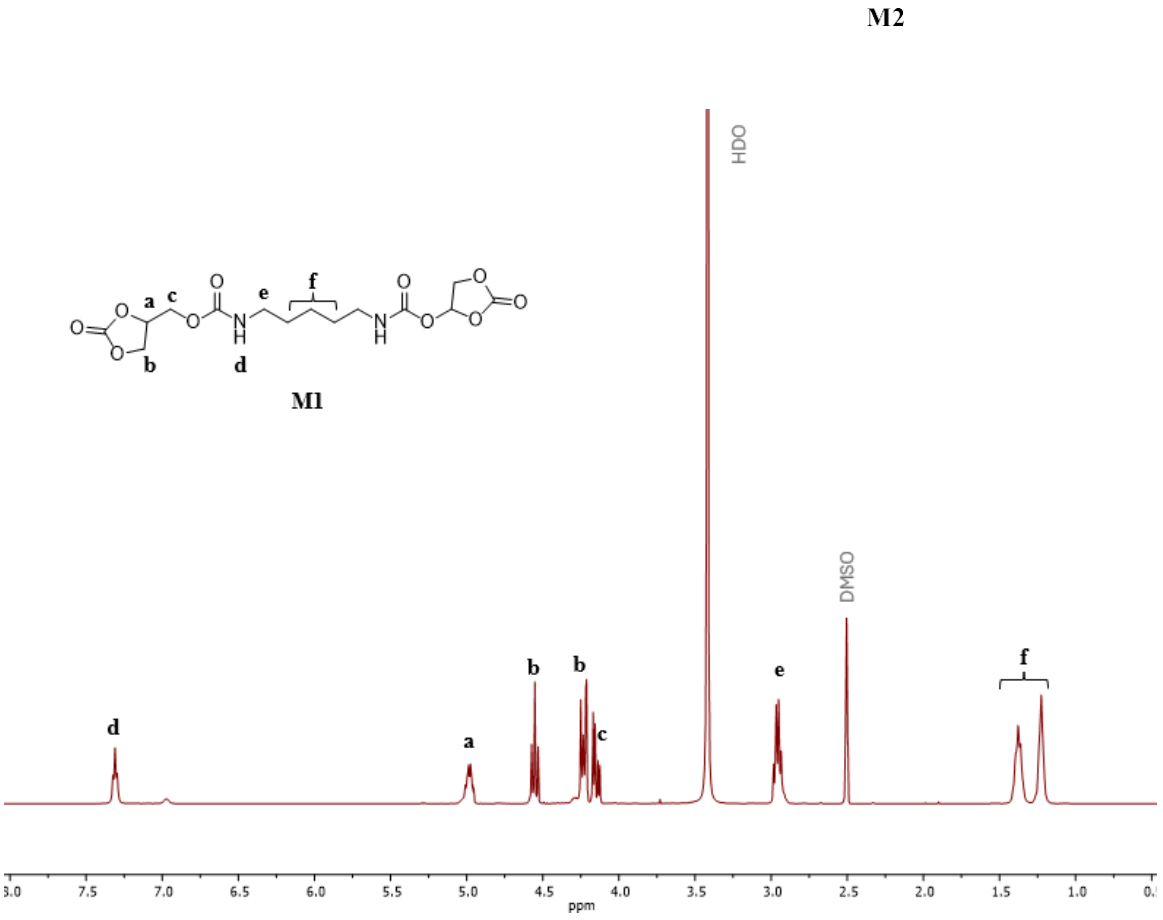

Figure 67. ^{1}H-NMR (400 MHz) proton spectrum of **M1** in DMSO (2.5 ppm).

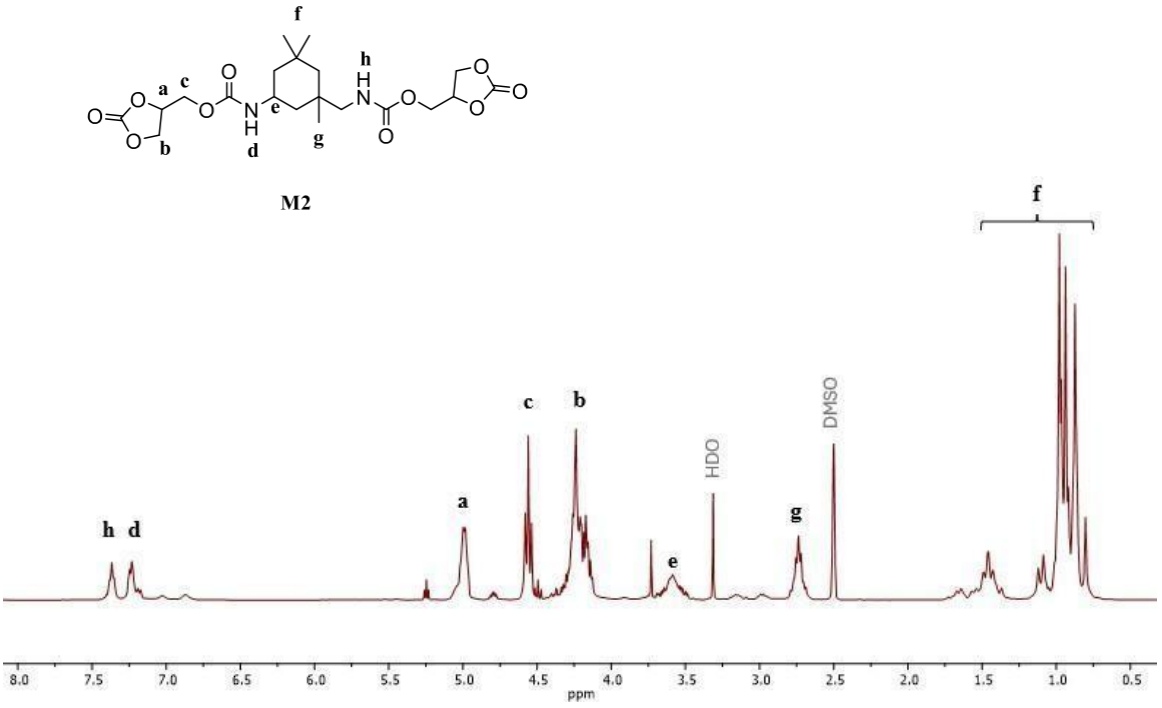

Figure 68. ^{1}H-NMR (400 MHz) proton spectrum of **M2** in DMSO (2.5 ppm).

The isocyanate-free reaction was designed as a two-step one-pot reaction. Firstly, the aminolysis reaction of glycerol carbonate (GC) and a chosen diamine was performed, resulting in dimeric diol species suitable for 5CC synthesis (Figure 69). In this case, the reaction was followed by IR regarding the band at 1766 cm^{-1} corresponding to the carbonyl of glycerol carbonate. At the same time, the appearance of the broad band of the OH groups (3318 cm^{-1}) and the carbamate group (O-(C=O)-NH 1688 cm^{-1} and N-H 1519 cm^{-1} was observed. The second step consists of the ring closure between dimethyl carbonate and the previously formed polyols *via* a potassium-tert-butoxide-catalyzed process (Figure 69). In this route, DMC acts as solvent and reactant, simultaneously. It is worth noticing that the unreacted excess of DMC can be easily recovered and reused.

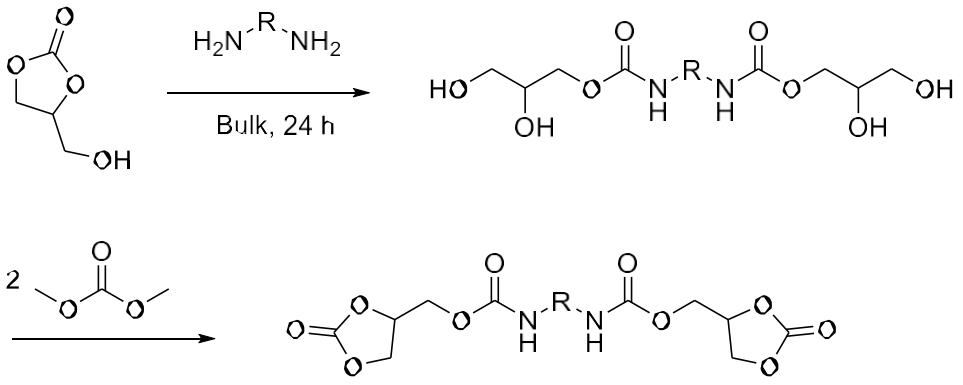

Figure 69. Two-step-one pot synthesis of isocyanate-free.

The disappearance of the OH bands and the characteristic cyclic carbonate stretching band (1766 cm^{-1}) were detected. All the structures were confirmed *via* NMR. Yields of 47% for **M1** and 68% for **M2** were obtained.

Achieving the same products through different pathways, enabled a sustainability comparison between the two. E-factors were calculated by considering the amines as the starting point of the process (isocyanates are generated from respective amines).

Table 15. E-factor values of the UBCs obtained *via* isocyanate and isocyanate-free synthetic routes

	E-factor Isocyanate route[a]	**E-factor Isocyanate-free route[b]**
M1	4.7	1.87
M2	16.61	1.16

[a]Synthetic pathway: amine-> isocyanate->cyclic carbonate [b] Synthetic pathway: Amine-> cyclic carbonate. For the isocyanate-route, the E-factors were calculated from literature HMDI[27] and IPDI[28] data.

It is obvious that the isocyanate-free route has an inferior environmental impact (Table 15). In fact, the two new processes present E-factor values of 2.5 and 14 times lower than the respective obtained from the syntheses *via* isocyanate. As a two-step synthesis from the amine, the isocyanate-based route leads to higher waste production compared to the two-step one-pot isocyanate-free pathway. Moreover, in the latter approach, safer chemicals are employed, such as DMC (LD50, oral, rabbit: 13000 mg/kg) in its dual action as solvent-reagent, preventing the need for additional chemicals. If compared with isocyanates such as IPDA (IPDI LD50, oral, rat = 1000 mg/kg), DMC is far less harmful. Notably, DMC can also be renewably obtained from methanol and urea. Looking at the current literature data, the E-factor values calculated in this study are 6 times lower than the average

E-factor values reported for the synthesis of mono-functional cyclic carbonate obtained by DMC and diols.

The reactivity of **M1** through aminolysis was studied. Two model amines were chosen, such as 1-hexylamine as a primary amine and *N*-methyl hexylamine as a secondary amine. Moreover, erythritol bis-CC (EBC), a biobased CC, was used as a benchmark to compare the reactivities and to understand the impact of urethane functionality in the structure. The reaction was monitored by FT-IR (Figure 70).

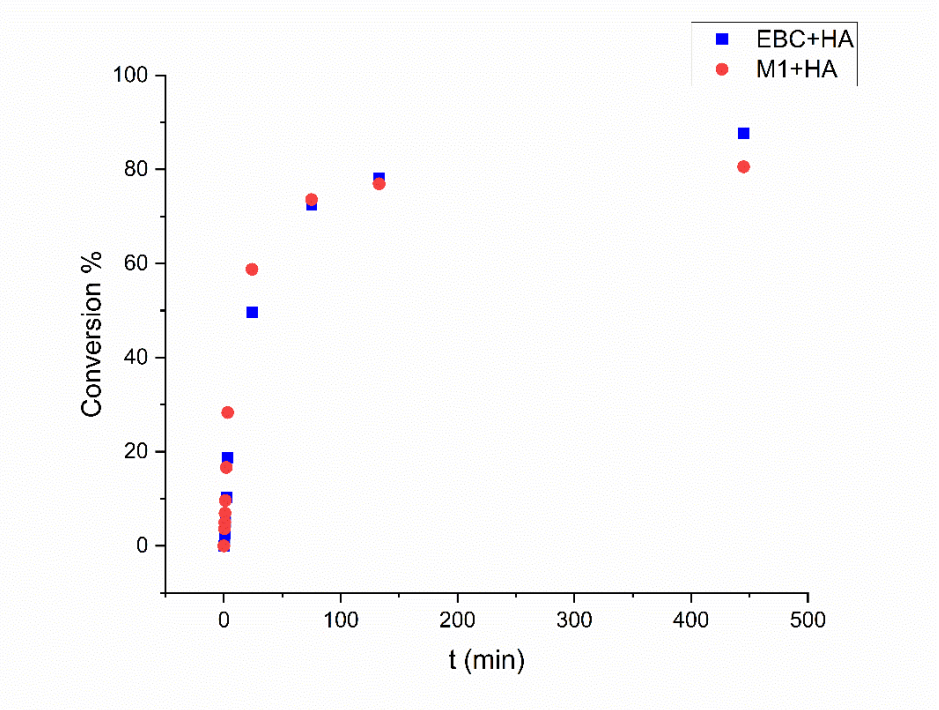

Figure 70. Conversion rates of **M1** and EBC with 1-hexylamine measured *via* FT-IR.

The reactions were run in DMSO at room temperature in a 1:1 ratio of functional groups (CC = [0.5 M] and amine = [1M]. In this case, little difference was observed between the reactivity of the two compounds. After 24 h of reaction, **M1** and EBC showed 59% and 50% conversion of the CC groups, respectively. Proceeding the reaction, after 18.5 days the monomers reached a maximum of 80% and 89% conversion of CC groups, respectively. The slightly lower conversion of **M1** can be attributed to higher H-bond density due to the greater presence of urethane groups in comparison to the polymer obtained from EBC.

2.2 PHU THERMOPLASTICS

To make use of **M1** and **M2**, diverse PHU thermoplastics were synthesized. Difunctional commercially available bio-biobased amines IPDA and *Priamine 1071*® and petrol-based *Jeffamine D230*® were chosen as co-monomers (Table 16, Figure 71).

Table 16. M1- and M2-based PHU and respective codes.

Monomers	Code	Monomers	Code
M1+*Jeffamine D230*®	**P1.1**	M2+*Jeffamine D230*®	**P2.1**
M1+LDA	**P1.2**	M2 +LDA	**P2.2**
M1+IPDA	**P1.3**	M2 +IPDA	**P2.3**
M1+***Priamine 1071*®**	**P1.4**	M2 +*Priamine 1071*®	**P2.4**

LDA=limonene diamine, IPDA= isophorone diamine

M1 resulted in being not miscible with the selected diamines, even with the help of heat (80-100 °C). Therefore, it was necessary to add a solvent to perform the polymerization. After a solubility test, DMF and DMSO proved to be the only feasible candidates. Oppositely, with **M2**, bulk polymerization was possible. Typically, a 1:1 ratio of the monomers was manually mixed and subsequently cured at 80 °C for 24 h. The resulting PHU were then characterized.

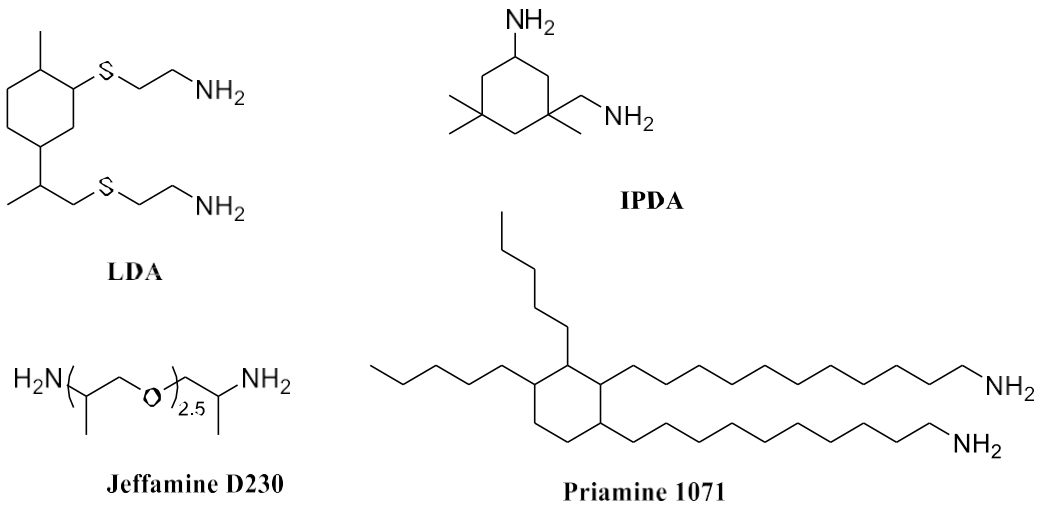

Figure 71. Set of amines employed for PHUs synthesis with **M1** and **M2**.

SEC analyses were possible only with thermoplastics derived from **M2** with the isophorone monomer due to the insolubility of the other polymers in the solvent of analysis (DMF). The samples were measured with a PMMA calibration method. It is relevant to know that PHUs do not have currently a comparable analogous polymer for calibration. This leads to poor molar mass reliability. Moreover, the presence of OH groups and urethane units in PHUs results in hydrogen bonding interactions with chromatographic columns.

Table 17. *Mn* and *Mw* obtained by SEC in DMF of the PHU thermoplastics obtained from M2 with four different diamines.

PHU	M_n g/mol	M_w g/mol	Đ
P2.1	4300	6000	1.41
P2.2	2900	4100	1.4
P2.3	2500	3100	1.23
P2.4	2500	4800	1.87

The SEC results of **P2** series showed only the formation of oligomers (Table 17). **P2.4** gave the higher M_n and M_w values with M_n = 4300 g/mol and M_w= 6000 g/mol and a dispersity of 1.4. This can be explained due to the large size amine molecule used for this polymer. TGA analyses were carried out to evaluate the degradation behaviour of the polymers until 600 °C. **P2.1** and **P2.2** were as resistant to high temperature, with a $T_{d,5\%}$ of about 200 °C. All the PHU were fully degraded at 600 °C and none of them was affected by heating earlier than 150°C. DSC analyses of **M1** and **M2** showed melting points of 115°C and 50.5°C, respectively. The DSC traces of the polymers revealed that the T_gs of the oligomers made from **M2** were higher in comparison to the ones made by **M1**. This feature can be explained by the rigidity of the structure of this monomer in comparison to the one of **M1**. For instance, **P2.3** displayed a T_g of 78.8 °C. Comparing same-amine PHU thermoplastics, it is noticeable that T_g of P2.4 (with Priamine) is higher than the analogous one with **M1** (20.2 °C and 9.8°C, Table 17). The low T_g*s* obtained can be attributed to the low molecular weight of the oligomer detected by SEC.

In order to investigate the possible applicability of the PHUs produced, lap shear tests were performed. **P2** polymers were tested because of the homogeneity of the mixture in bulk. Three adherent types were selected, such as softwood, PVC and aluminium. The uncured formulations were placed on the substrates and cured at 80°C for 24h. The *shear stress* defines the adhesion strength performance (Equation 5).

$$\tau = F_{max} w * L \quad \textbf{Eq.5}$$

F_{max} = the maximum force in the force-displacement curve
w = the width and the area of adhesion
L = length of the area of adhesion

Generally, the primary and secondary hydroxylic groups and the urethane units present on PHUs foster chemical interactions (hydrogen bonding and dipole forces) with the substrate, improving the adhesiveness. This is enhanced with wood adherent because of the abundance of cellulose and lignin OH, which interacts with the adhesive at the interface. As a consequence, the best performances were registered when wood was tested, followed by aluminum and PVC, in order (Table 18). The type of the specimen's failure was also examined. In all the three cases, a cohesive failure was displayed.

Table 18. Average force values (MPa) and breaking points (mm) calculated on five measurements conducted with P2.4 on wood, PVC and aluminium.

P2.4	Force (MPa)	Breaking point (mm)	Failure type
Wood	2.21± 0.36	0.42 ± 0.05	surface cohesive
Aluminum	1.69 ± 0.52	0.33 ± 0.11	adhesive/surface cohesive
PVC	0.63 ± 0.18	0.54 ± 0.10	adhesive cohesive

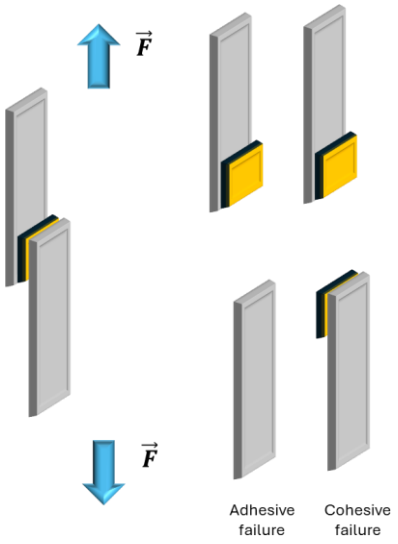

Figure 72. Representation of a specimen for lap shear tests and exemplification of adhesive and cohesive failures.

Considering the **P2.3** PHU, the density of the urethane and hydroxyl group is higher, due to the short chain of the two components. However, the shear stress values result in being lower than the above-mentioned P2.4 (Table 18). This outcome might be attributed to the rigidity of the polymer chain, due to the short and rigid structure of both UBC and amine monomers. Oppositely, in the case of **P2.4**, the long aliphatic chains of *Priamine® 1071* were promoting flexibility of the structure. Using **P2.3** adhesive, the type of failure was found to be cohesive for wood and aluminum (Table 19). Alternatively, it was adhesive-cohesive for PVC substrates.

Table 19. Average force values (MPa) and breaking points (mm) calculated on five measurements conducted with P2.3 on wood, PVC and aluminium.

P2.3	Force (MPa)	Breaking point (mm)	Failure type
Wood	1.45 ± 0.58	0.28 ± 0.09	surface cohesive
Aluminum	0.47 ± 0.13	0.16 ± 0.01	surface cohesive
PVC	0.26 ± 0.10	0.26 ± 0.12	adhesive cohesive

P2.2 and **P2.3** have similar backbone structures because of the diamine employed. Indeed, the first is made with limonene diamine (LDA) and the second with IPDA, which are both cyclic short-chain molecules, with the first being biobased and the second potentially biobased. The performance on wood and PVC of **P2.2** resulted in being inferior in comparison to **P2.3** (Table 20). Nevertheless, the values of shear stress obtained with aluminium were similar. All the substrates presented surface cohesive failure type.

Table 20. Average force values (MPa) and breaking points (mm) calculated on five measurements conducted with P2.2 on wood, aluminium and PVC.

P2.2	Force (MPa)	Breaking point (mm)	Failure type
Wood	0.73 ± 0.13	0.22 ± 0.03	surface cohesive
Aluminum	0.46 ± 0.18	0.16 ± 0.04	surface cohesive
PVC	0.08	0.025	surface cohesive

This project was carried as a preliminary study. Due to the short time available to investigate this novel topic, it was not possible to investigate further polymer formulations. In the future, it is planned to further examine the possibility of ameliorating the polymer synthesis with the use of

these UBCs. Moreover, with the monomer synthetic pathway performed, a library of new UBCs could be created.

2.3 CONCLUSION

Two novel UBC monomers were synthesized *via* isocyanate-free route resulting in new monomer structures through a more sustainable process. The comparison with the isocyanate-route synthesis displayed the lower environmental impact (E factors) of the first synthetic pathway. In this way, an efficient and safer process was proven to be a possible alternative. This route opens the to develop UBC monomers from biobased amines with different chemical structures to yield fully biobased building blocks.

Moreover, isocyanate-free oligomers were produced with the same aim of avoiding hazardous chemicals. Despite the low molecular weight achieved with the four diamines selected, the PHUs obtained showed good adhesive properties on lap shear tests, particularly when wood adherents were used.

2.4 Experimental Data

Characterization methods

Nuclear Magnetic Resonance spectroscopy (NMR)

NMR spectra were recorded using the following spectrometer hardware.

Bruker AVANCE 400

^{1}H-NMR (400 MHz), ^{13}C-NMR (101 MHz)

Bruker AVANCE 500

^{1}H-NMR (500 MHz), ^{13}C-NMR (126 MHz)

DMSO–d6, $CDCl_3$ and MeOD were used as solvents and their respective resonance signals served as reference for the chemical shift δ in parts per million: ^{1}H: $CDCl_3$ = 7.26 ppm, DMSO-d6 = 2.50 ppm; ^{13}C: $CDCl_3$ = 77.2 ppm, DMSO-d6 = 39.5 ppm. The spin multiplicity and corresponding signal patterns were abbreviated as follows: s = singlet, d = doublet, t = triplet, q = quartet, quint. = quintet, m = multiplet. Coupling constants J were noted in Hz. Furthermore, 2D NMR methods (e.g., heteronuclear single quantum coherence (HSQC), heteronuclear multiple bond correlation (HMBC) and correlated spectroscopy (COSY)) were carried out, if necessary, for signal assignment and structure elucidation.

Size exclusion Chromatography (SEC)

System I (Oligo SEC): A PSS SECcurity^2 SEC system based on Agilent Infinity 1260 II hardware was used for the measurements. The system is equipped with a refractive index detector SECcurity^2 RI, a column oven "(Bio)SECcurity^2 column compartment TCC6500", a "standard SECcurity^2" autosampler, and an isocratic pump "SECcurity^2 isocratic pump". Anhydrous tetrahydrofuran stabilized with 250 ppm butylated hydroxytoluene (BHT, ≥99.9%) was used at a flow rate of 1.0 ml min^{-1} and at 30 °C as mobile phase. The analysis was performed on the following column system: PSS SDV analytical precolumn (3 µm, 8 mm × 50 mm) with two PSS SDV analytical columns (3 µm, 8 mm × 300 mm, 1000 Å). For the calibration, narrow linear poly(methyl methacrylate) standards (Polymer Standards Service, PSS, Germany) ranging from 102 to 62200 Da were used. For the preparation of the samples,
2.00 mg of analyte was dissolved in 1.50 mL anhydrous tetrahydrofuran stabilized with 250 ppm butylated hydroxytoluene (BHT, ≥99.9%). All samples were filtered by syringe filter prior to use, to avoid plugging of the injection setup or the column.

Infrared spectroscopy

Infrared (IR) spectroscopy IR spectra were recorded on a Bruker alpha-p instrument in a frequency range of 3997.41 to 373.828 cm-1 applying KBr- and ATR technology.

Thin Layer Chromatography (TLC)

All thin layer chromatography (TLC) experiments were performed on silica-gel-coated aluminum foil (silica gel 60 F254, layer thickness: 0.25 mm, Sigma-Aldrich). Compounds were visualized by irradiation with a UV lamp (λ = 254 and 365 nm), by staining with Seebach solution (mixture of 5.00 g phosphomolybdic acid hydrate, 2.00 g cerium(IV)- sulfate, 16.0 mL concentrated sulfuric acid and 200 mL water) or vanillin staining solution (mixture of 8.60 g vanillin and 2.50 mL concentrated sulfuric acid and 200 mL ethanol), or KMnO4 staining solution (1.50 g $KMnO_4$, 10.0 g $K2CO_3$, 1.25 mL 10% NaOH and 200 mL water) or ninhydrin solution (0.2 ninhydrin in 100 mL ethanol).

Orbitrap Electrospray Ionization-Mass Spectrometry (ESI-MS)

Mass spectra were recorded on a Q Exactive (Orbitrap) mass spectrometer (Thermo Fisher Scientific, San José, CA, USA) equipped with an atmospheric pressure ionization source operating in the nebulizer assisted electrospray mode. The instrument was calibrated in the m/z-range 150-2000 using a standard containing caffeine, Met-Arg-Phe-Ala acetate (MRFA) and a mixture of fluorinated phosphazenes (Ultramark 1621, all from Sigma Aldrich). A constant spray voltage of 3.5 kV, a dimensionless sheath gas of 6, and a sweep gas flow rate of 2 were applied. The capillary voltage and the S-lens RF level were set to 68.0 V and 320 °C, respectively. For the interpretation of the spectra, molecular peaks [M]+ , peaks of pseudo molecules [M+H]+ , [M+NH4] + , [M+Na]+ and [M+K]+ and characteristic fragment peaks are indicated with their mass to charge ratio (m/z) and their intensity in percent, relative to the most intense peak (100%).

Differential scanning calorimetry (DSC)

DSC analyses were run with DSC Q2000 instrument. Samples were placed in aluminium pans and measured with a heating rate of 10 K min-1 over a temperature range from -40 to 120 and 250 °C, gas flow (nitrogen) of 50 mL/min.

Thermogravimetric Analysis (TGA)

TGA measurements were carried out on the TA Instruments TGA 5500 under nitrogen atmosphere using platinum TGA sample pans and with a heating rate of 10 K min-1 over a temperature range from -40 to 600 °C. Thanks to Théato research group (KIT) for the instrument availability.

Materials

Glycerol carbonate (Jeffsol) (99%) was supplied by Huntsmann. Isophorone diamine (mixture of isomers – 99%), dimethyl carbonate (99%), hexamethylene diamine (99%), isophorone diisocyanate (99%), hexamethylene diisocyanate (99%), potassium tert butoxide (99%), sodium carbonate (99%) were supplied by Sigma-Aldrich. 1-hexylamine (99%), N-methyl hexylamine (99%) were supplied by TCI. *N1,N6*-dimethyl-1,6 hexyldiamine (99%) was supplied by BLD Pharm. All reagents were used without further purification.

Synthesis procedures

- *2-oxo-1,3-dioxolan-4-yl ((2-oxo-1,3-dioxolan-4-yl)methyl) pentane-1,5-diyldicarbamate* (**M1**) from isophorone diisocyanate.

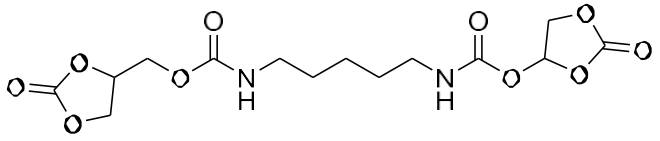

2-oxo-1,3-dioxolan-4-yl ((2-oxo-1,3-dioxolan-4-yl)methyl) pentane-1,5-diyldicarbamate
Chemical Formula: $C_{14}H_{20}N_2O_{10}$
Molecular Weight: 376.32

28.7g glycerol carbonate (243 mmol, 2eq) was dropped in a three-neck 500 mL round bottom flask conditioned with nitrogen with a dropping funnel and heated at 80°C. Then, 20.2 g of 1,6-hexamethylene diisocyanate (120 mmol, 1 eq) was added through the dropping funnel. The reaction was carried out at 80°C for 16.5h under mechanical stirring. The product was obtained as a white solid. (97% yield). Solubility tests showed that the compound was insoluble in methanol, ethyl acetate and dichloromethane and soluble in DMSO and DMF at room temperature. Consequently, purification was performed by recrystallization in ethyl acetate at 80°C. After recrystallization, 80% yield of the pure product was recovered.

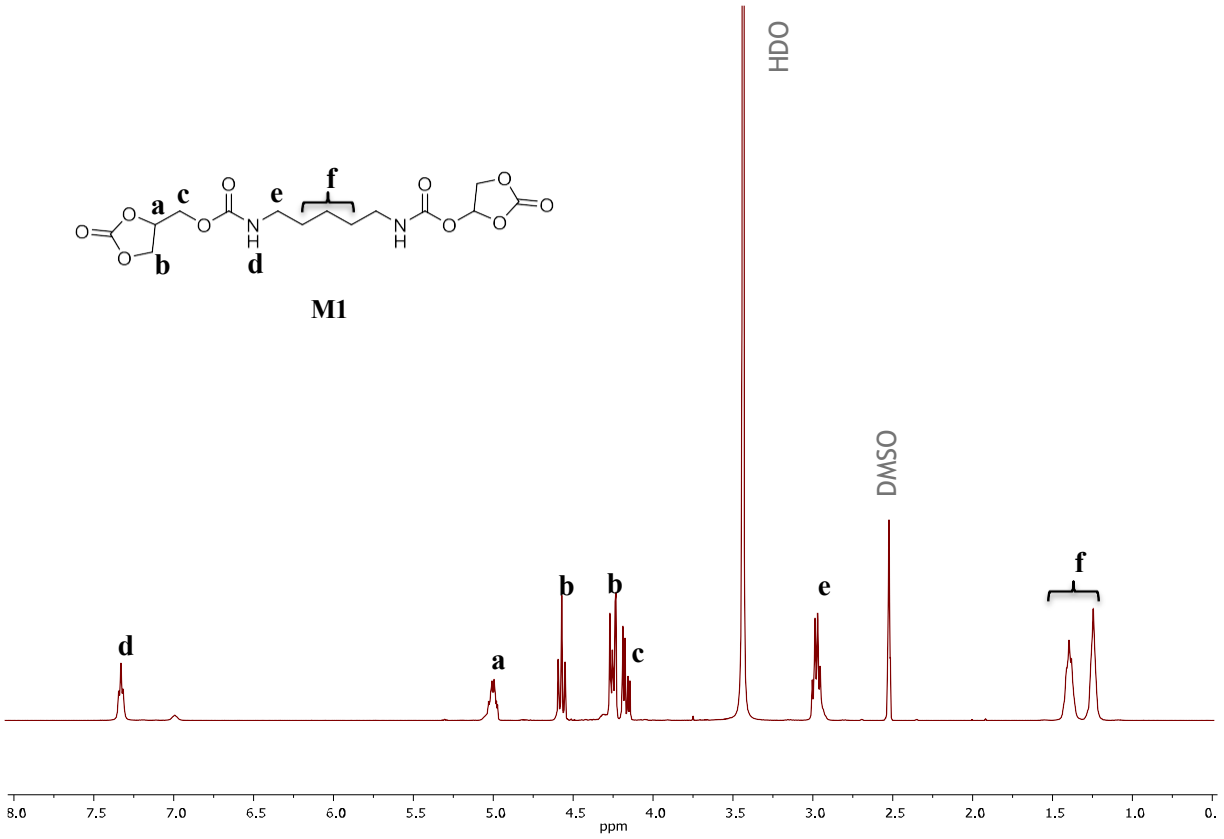

S 6. ^{1}H-NMR (400 MHz) of **M1** in DMSO (2.5 ppm).

^{1}H-NMR (400 MHz, DMSO-d6 δ 7.28 (J = 5.5 Hz, 2H, t), 4.95 (J = 11.2, 8.6, 2.6 Hz, 2H, ddd), 4.58 – 4.46 (2H, m), 4.23 – 4.17 (4H, m), 4.12 (J = 12.6, 5.0 Hz, 2H, dd), 2.93 (J = 13.0, 6.6 Hz, 4H, dd), 1.40 – 1.28 (4H, m), 1.20 (4H, s).

^{13}C-NMR (101 MHz, DMSO) δ 156.05, 155.14, 75.29, 66.30, 63.47, 29.64, 26.30.

FT-IR v [cm-1]: 3340 (vN-H, m), 2937-2870 (vC-H, m), 1783 (vC=O of CC, s), 1688 (vNH-**C=O**, s), 1521, 1477, 1398, 1338, 1259, 1218, 1166, 1146, 1045, 999, 770, 714.

- *(2-oxo-1,3-dioxolan-4-yl)methyl(3,3,5-trimethyl-5-(((((2-oxo-1,3-dioxolan-4-yl)oxy)carbonyl)amino)methyl)cyclohexyl)carbamate* (**M2**) from isophorone diisocyanate
-

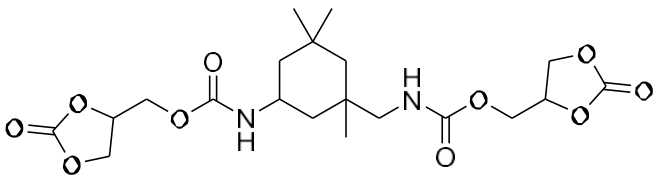

(2-oxo-1,3-dioxolan-4-yl)methyl (3,3,5-trimethyl-5-(((((2-oxo-1,3-dioxolan-4-yl)methoxy)carbonyl)amino)methyl)cyclohexyl)carbamate
Chemical Formula: $C_{20}H_{30}N_2O_{10}$
Molecular Weight: 458,46

26.7g of isophorone diisocyanate (120 mmol, 1eq.) and glycerol carbonate (28,7 g, 243 mmol, 2 eq.) were placed in a 500 mL round bottom flask and the reaction run at 80°C for 36 h under stirring. The product was obtained as a transparent brittle solid (80% yield).

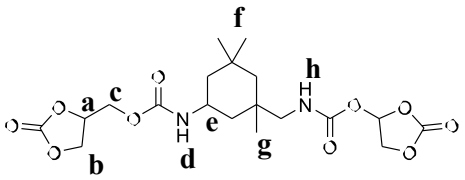

M2

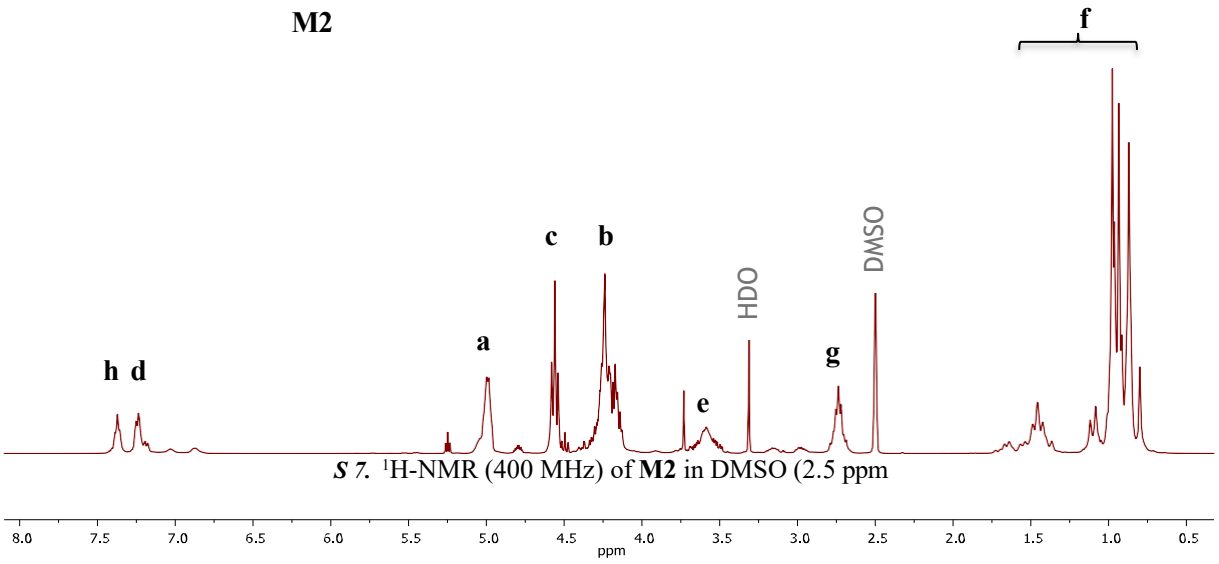

S 7. ^{1}H-NMR (400 MHz) of **M2** in DMSO (2.5 ppm

^{1}H-NMR (400 MHz, DMSO-d6) δ 7.34 (J = 5.8 Hz, 1H, t), 7.20 (J = 10.1 Hz, 1H, t), 5.03 – 4.90 (2H, m), 4.53 (J = 8.5 Hz, 4H, t), 4.27 – 4.11 (4H, m), 3.60 – 3.50 (1H, m), 2.76 – 2.64 (2H, m), 1.52 - 0.68 (15H, m).

^{13}C-NMR (101 MHz, DMSO-d6) δ 156.77, 156.66, 155.25, 155.09, 149.05, 77.43, 75.31, 74.48, 66.28, 63.40, 61.03, 55.43, 54.79, 49.03, 47.84, 46.99, 46.06, 45.76, 44.56, 41.61, 36.86, 36.71, 36.23, 35.36, 34.97, 31.93, 31.81, 31.72, 30.23, 27.87, 27.68, 27.45, 23.53.

FT-IR v [cm-1]: 3333 (νN-H, m), 2953 (νC-H, m), 1785 (νC=O of CC, s), 1703 (νNH-**C=O**, s), 1526, 1240, 1166, 1090, 1045, 1020, 765, 708.

3340 2937-2870 1783 1688 1521, 1477 1398, 1338, 1259, 1218, 1166, 1146, 1045, 999, 770, 714.

ESI-MS m/z $C_{20}H_{30}N_2O_{10}$ $[M+H]^+$= calculated 458.46, found: 459.46

- *2-oxo-1,3-dioxolan-4-yl ((2-oxo-1,3-dioxolan-4-yl)methyl) pentane-1,5-diyldicarbamate* (**M1**) from 1,6 hexamethylene diamine, glycerol carbonate and dimethyl carbonate

Isocyanate-free **M1** was synthesized in a one-pot two step procedure.

1) 23.2g of 1,6-hexamethylendiamine (200 mmol, 1 eq) and 47.2 g of glycerol carbonate (400 mmol, 2 eq) were placed in a round bottom flask and the reaction was run for 3 hours, 50°C under stirring. (During the reaction, the temperature was increasing up to 65°C due to the exothermicity of the reaction).

2) 2,35 g of sodium carbonate (22 mmol, 5 wt.% compared to glycerol carbonate) and 36 g of dimethyl carbonate (36g, 400 mmol, 34 mL, 2eq) were added to the reaction mixture. The reaction was carried out for 16 h at 75°C under mechanical stirring. At the end of the reaction time, the mixture was cooled down to room temperature. 1g of the crude reaction mixture was recrystallized in EtOAc under reflux conditions and magnetic stirring. After 2h, the solution slowly cooled down and a white solid

precipitated. The solid was filtered and dried under reduced pressure (Yield 47%). For product analyses and attribution see "*-oxo-1,3-dioxolan-4-yl ((2-oxo-1,3-dioxolan-4-yl)methyl) pentane-1,5-diyldicarbamate* (**M1**) from isophorone diisocyanate").

- *(2-oxo-1,3-dioxolan-4-yl)methyl(3,3,5-trimethyl-5-(((((2-oxo-1,3-dioxolan-4-yl)oxy)carbonyl)amino)methyl)cyclohexyl)carbamate* (**M2**) from isophorone diamine, glycerol carbonate, and dimethyl carbonate.

Isocyanate-free **M2** was synthesized in a one-pot two step procedure

1) 94,5 g of glycerol carbonate (800 mmol, 2 eq.) and 68 g of isophorone diamine (400 mmol, 1 eq.) were placed in a 500 mL three-neck round bottom flask. The reaction was run for 24h at 50°C under stirring. at 50°C. (During the reaction, the temperature was increasing up to 65°C due to the exothermicity of the reaction). After 2h, the reaction mixture drastically increases the viscosity. Consequently, to facilitate the diffusion and increase the conversion of the reagents, 25 mL of MeOH were added to the reaction mixture.

2) 2.3 g potassium tert-butoxide (20 mmol, 0,05 eq.) and 85 g of dimethyl carbonate (950 mmol, 2.4 eq) were added to the reaction mixture The reaction was carried out for 16 h at 75°C under mechanical stirring. Note. A distillation apparatus was connected to the three-neck round bottom flask to recover the MeOH and the DMC evaporating from the reaction mixture. A solid white compound was obtained. A chromatographic separation with 100% ethyl acetate as a mobile phase was performed and a solid compound was yielded (68% yield). For product analyses and attribution see *(2-oxo-1,3-dioxolan-4-yl)methyl(3,3,5-trimethyl-5-(((((2-oxo-1,3-dioxolan-4-yl)oxy)carbonyl)amino)methyl)cyclohexyl)carbamate* (**M2**) from isophorone diisocyanate

Estimation of E-factor (Equation 1) of **M1**

$$E-factor = \frac{weight\ of\ raw\ aterials - weight\ of\ desired\ product}{weight\ of\ desired\ product} \quad \textbf{Eq.1}$$

Reagents	MW (g/mol)	mmol	g
Glycerol carbonate	118.09	240	28
Hexamethylene diisocyanate	161.21	125	20.18
Phosgene	90.08	155	14.05
Hexamethylene diamine	116.21	1170	136
Methanol	32.04	470	15.44
HCl	36.46	770	28
Hexamethylene diamine chlorohydrate	189.13	1330	251.63
Amylbenzene	148.25	1715	254.24

Theoretic yield	48.48 g
Experiental yield	38.78 g
E factor	4.71

Estimation of E-factor (Equation 1) of **M2**

Reagents	MW (g/mol)	mmol	g
Glycerol carbonate	118.09	240	28
Isophorone diisocyanate	222.3	120	26.68
Phosgene	90.08	424	38.25
Isophorone diamine	170.29	128	21.89
Chloroform	119.38	5798	692.3

Theoretic yield	55.0 g
Experiental yield	44.3 g
E factor	16.61

Model reactions

Model reactions between **M1** with HA and EBC with HA were performed and monitored via FT-IR. Aliquots were taken at different time intervals. Conditions: room temperature, [bis-CC] = 0.5 M and [HA] = 1M in DMSO under continuous stirring.
M1 or **EBC** (1 mmol, 1 eq.) and HA (2 mmol, 2 eq.) were added into a glass vial with 2 mL of DMSO. Evaluation of the absorbance associated to the cyclic carbonate carbonyl stretch disappearance at 1785 cm^{-1} over time (Equation 2). Transmittance was converted in absorbance and the conversion was calculated from absorbance values.

$$Conv.CC = 1 - \frac{Abs\ \nu(C=O)CC_{t=0}}{Abc\ \nu(C=O)CC_t} \qquad \textbf{Eq.2}$$

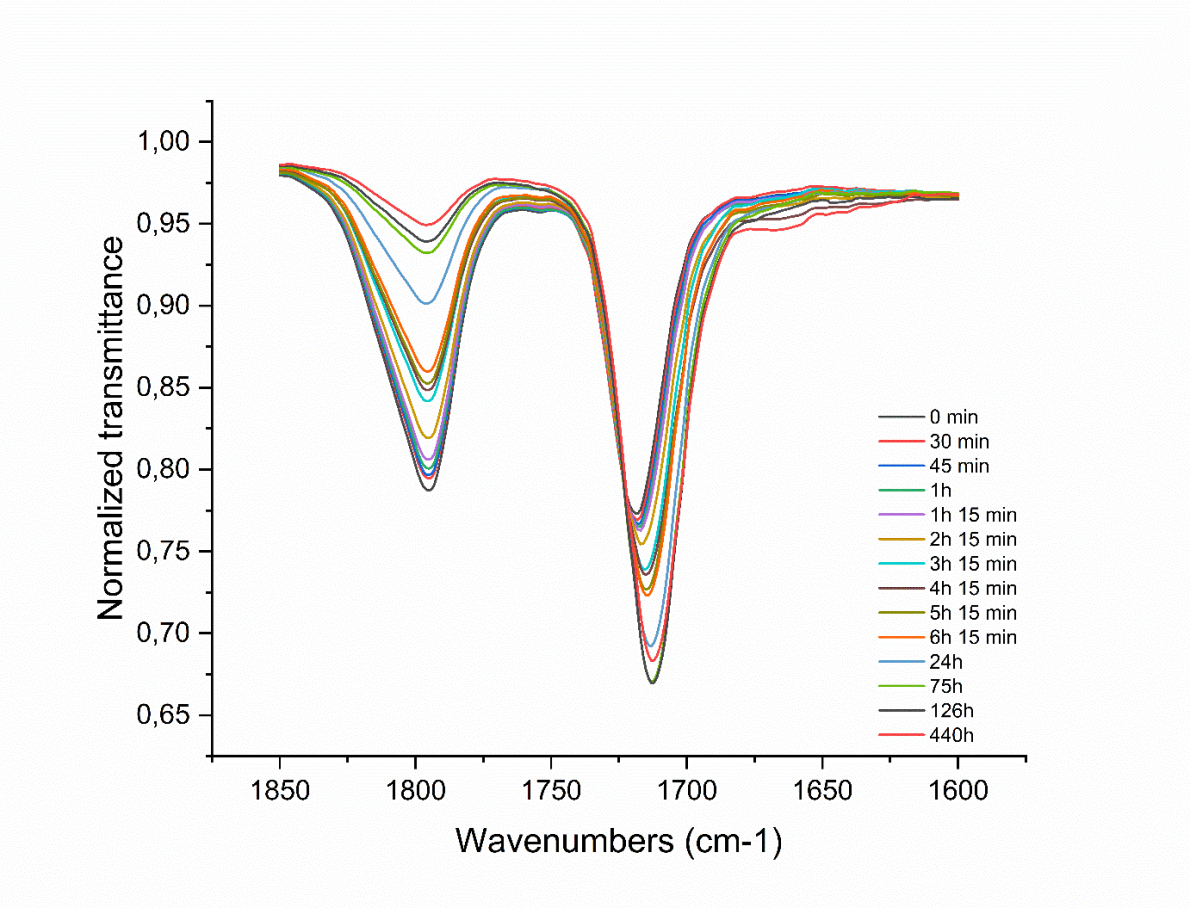

S 8. *FT-IR measurements of **M1**+1-hexylamine (HA) at different reaction time (0 min- 440 h).*

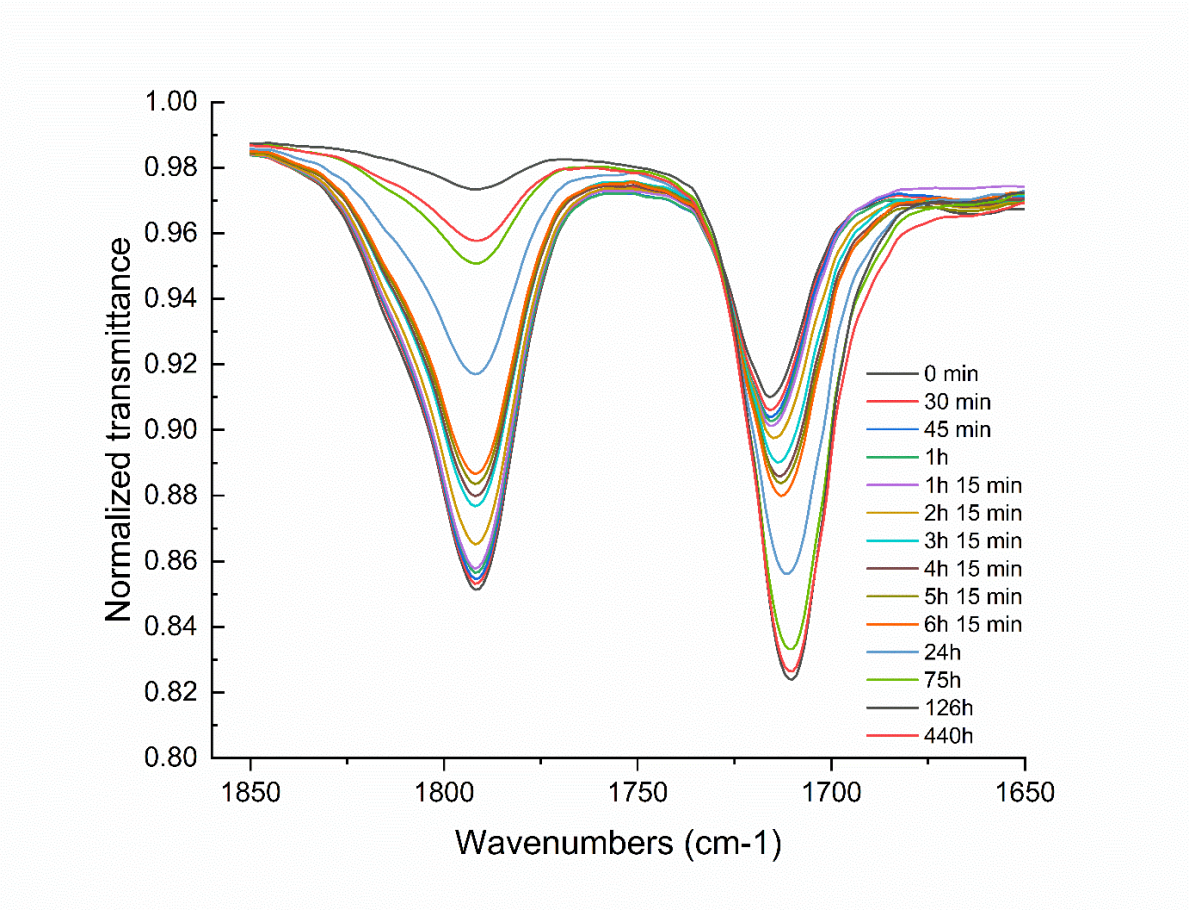

S 9. FT-IR measurements of erythritol bis-cyclic carbonate (EBC)+1-hexylamine (HA) at different reaction time (0 min- 440 h).

Thermoplastics

Thermoplastics PHUs were synthesized mixing equimolar amount of cyclic carbonate to amino groups of **M2** and a proper amine (i.e. *Priamine 1071*®, limonene diamine, *Jeffamine D230*®, isophorone diamine) at room temperature without any additional solvent. The curing process was performed at 80°C for 24 h. The obtained PHUs were characterized via DSC, SEC, FT-IR and their MW evaluated via SEC and NMR.

- Molecular weights measurements and calculations

SEC analyses were performed in DMF (Table 21).

Table 21. Mn and Mw obtained by SEC in DMF of the PHU thermoplastics obtained from M2 with four different diamines (equimolar ration of primary amino groups and cyclic carbonate groups) compared with the calculations of polymer MWs obtained *via* ^{1}H-NMR.

PHU	M_n g/mol	M_w g/mol	^{1}H-NMR MW g/mol	$Đ$
P2.1	4300	6000	4100	1.41
P2.2	2900	4100	3400	1.4
P2.3	2500	3100	2300	1.23
P2.4	2500	4800	2500	1.87

The polymers molecular weights were also evaluated by ^{1}H-NMR (Table 21). The calculation was made by the ratio of a known integral: 2N**H** urethane peaks between 7.32-6.84 ppm (2 groups for each polymer repeating unit, R.U.) and the signal of C**H** of the cyclic carbonate terminal at 4.98 ppm (Equation 3). The, the number of R.U. was multiplied for the MW of the specific R.U. of the thermoset evaluated (Equation 4).

$$Number\ of\ R.U. = \frac{\int CH\ of\ CC}{\int NH\ /2} \qquad \textbf{Eq.3}$$

$$Polymer\ MW = \frac{\int CH\ of\ CC}{\int NH} * MW_{R.U.} \qquad \textbf{Eq. 4}$$

Table 22. Detailed calculations of polymer MWs via ^{1}H-NMR.

PHU	Integral urethane	Integral termials	Number R.U.	MW *per* R.U. (g/mol)	^{1}H-NMR MW kg/mol
P2.1	24.22	2	6	685.78	4.1
P2.2	20.37	2	5	694.97	3.4
P2.3	16.46	2	4	574.74	2.3
P2.4	10.55	2	2.5	939.44	2.5

[1]H-NMR of **P2.1-P2.4** in DMSO

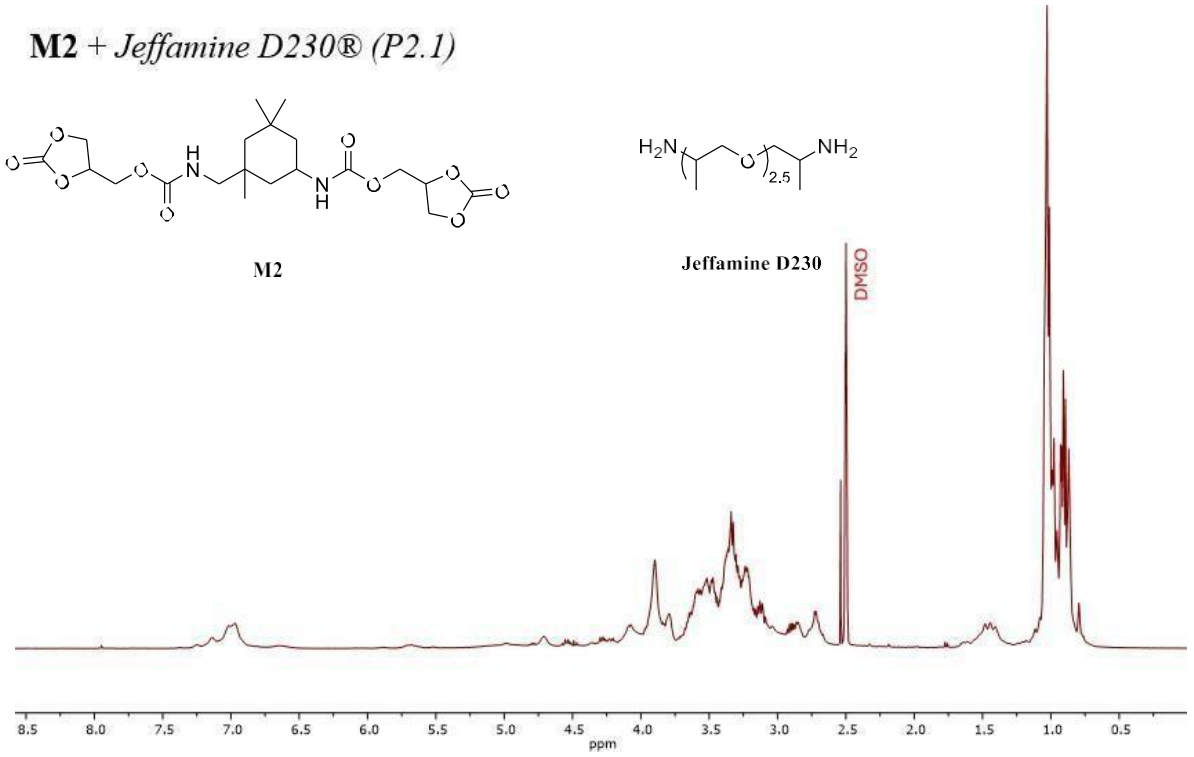

S 10. [1]H-NMR (400 MHz) in DMSO of P2.1.

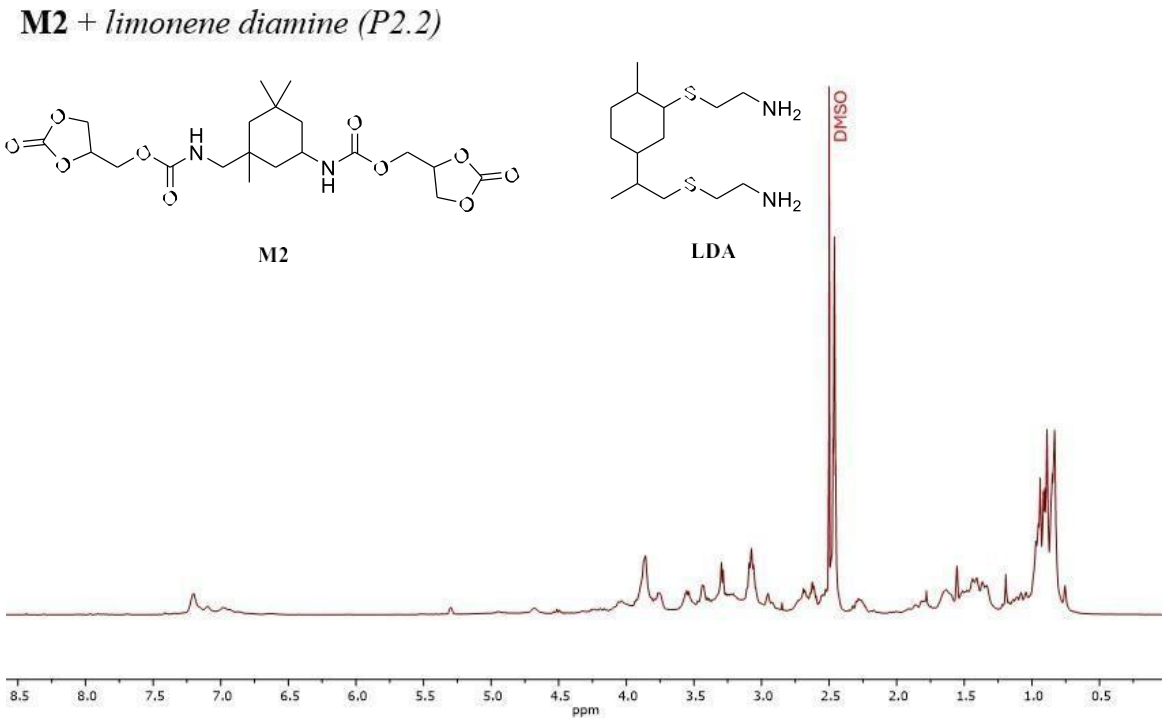

S 11.[1]H-NMR (400 MHz) in DMSO of P2.2.

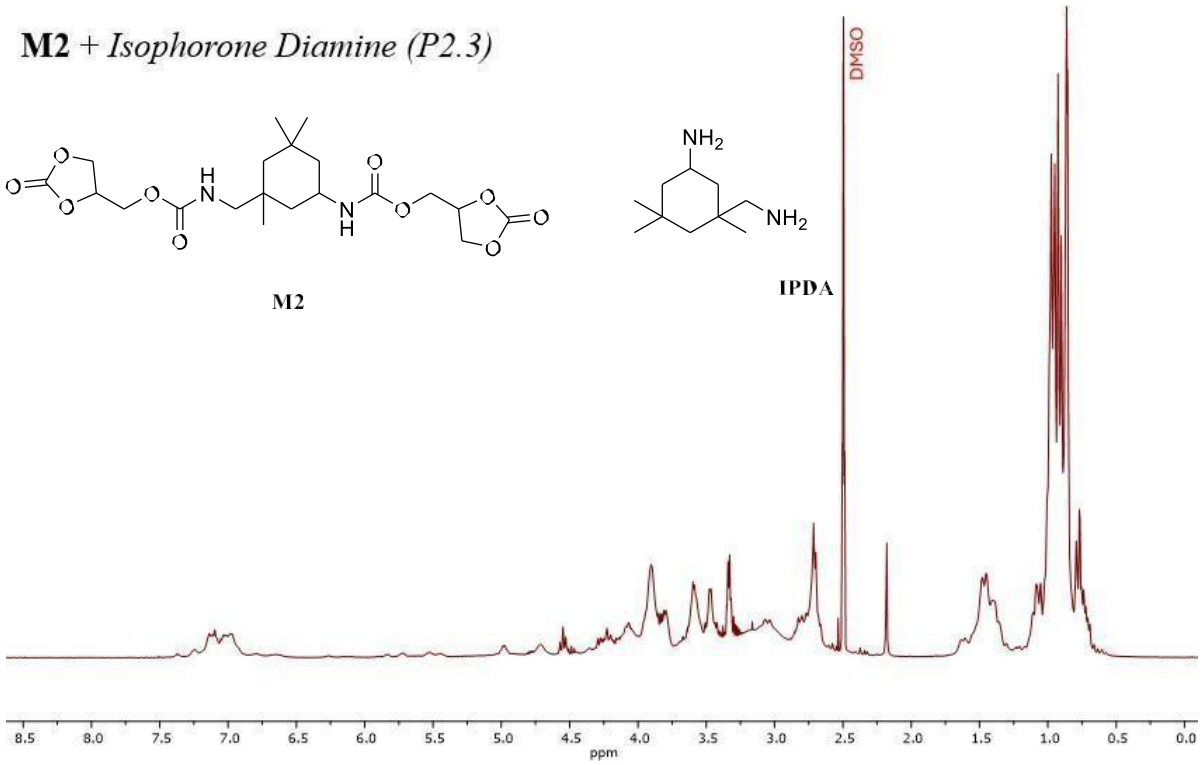

S 12.[1]H-NMR (400 MHz) in DMSO of P2.3.

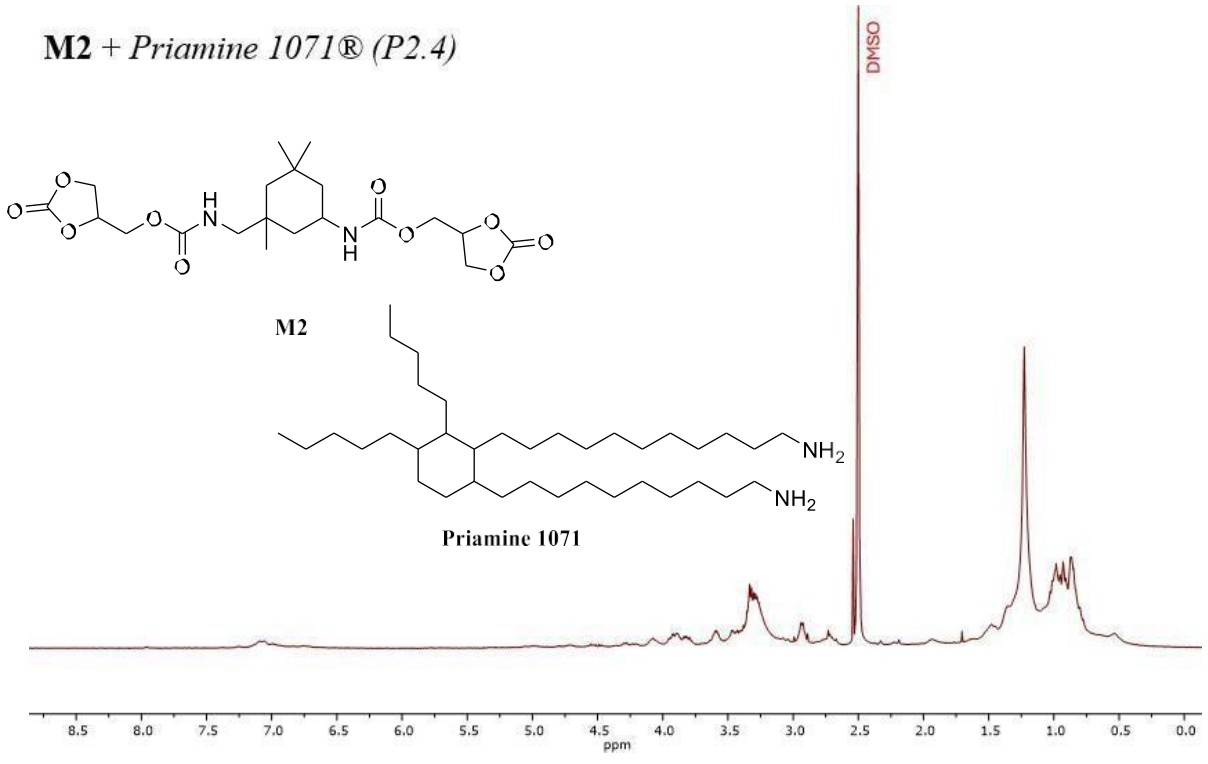

S 13.[1]H-NMR (400 MHz) in DMSO of P2.4.

Lap shear tests (Adhesive tests)

Specimen details: Aluminium, Berch wood and PVC 100 mm*2.5 mm substrates were used.

Specimen preparation. The uncured ad freshly prepared PHUs formulation (ca. 200 mg) was spread on a surface area of the adherent equal to of 13 mm*25 mm and glued together with a second piece of adherent (Figure 9). Later, the specimens were placed into an oven at 80°C for curing for 24 h. After cooling down at room temperature the samples were ready to be tested.

Substrate glued area dimensions (left) and adhesive application (right):

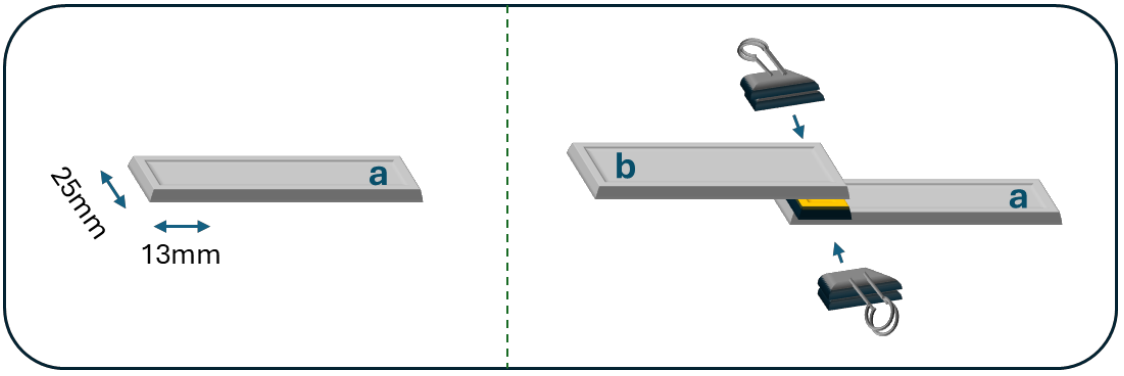

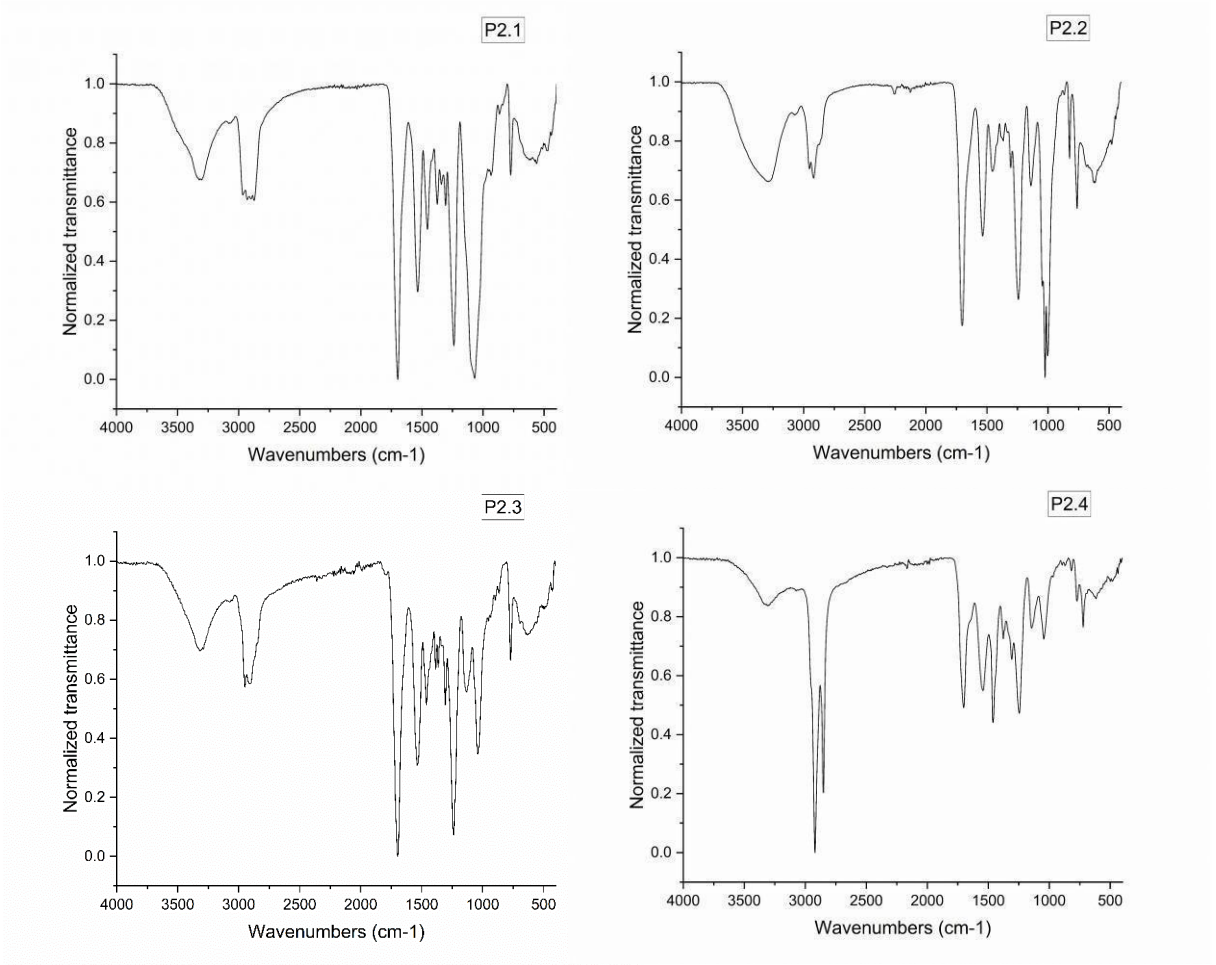

S 14. FT-IR of the four thermoplastics synthetized from M2. P2.1= M2+Jeffaine D230®; P2.2 M2+ limonene diamine (LDA); P2.3: M2+isophorone diamine (IPDA): P2.4: M2+ Priamine 1071®.

3 CHAPTER 4: NOVEL BIO-BASED VINYLOGOUS URETHANES (VUS)

3.1 VINYLOGOUS URETHANES (VUS)

With the discovery of dynamic networks by Bowman (2005)[278] and Leibler (2011),[279] covalent adaptable networks (CANs) became a great innovation in the field of polymer chemistry. CANs are nowadays considered to possess the potential to overcome some limitations of thermoset materials, while displaying similar properties. Indeed, thermosets are essential polymeric materials in everyday human life, exhibiting excellent mechanical and thermal properties. However, they are non-recyclable and non-reshapable due to their covalent crosslinking. As mentioned in the first chapter, the reuse, recycling or sustainable degradation of materials is crucial to conform to the circular economy model. Unlike thermosets, the dynamic nature of CANs allows for the control of its chemical connections through external stimuli (i.e. light, heat, solvent). Specifically, these bonds can interchange by two types of mechanisms: dissociative or associative (Figure 73).[280]

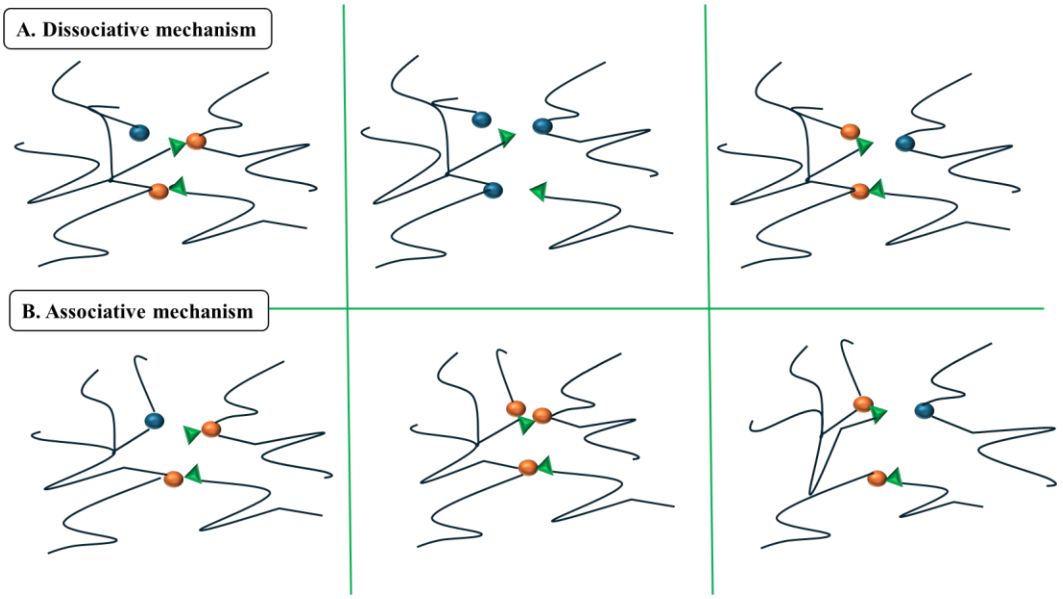

Figure 73. Representation of A) dissociative and B) associative dynamic mechanisms in CAN materials.[280]

Figure 73A illustrates the dissociative mechanism, which consists of a temporary decrease of crosslinking and its subsequent reformation. Differently, polymers exhibiting an associative behaviour (Figure 73B) present a simultaneous break of the bonds with the formation of another linkage. CANs with associative dynamics of covalent bonds are called vitrimers.[280] The first example was represented by Bowman *via* a transesterification reaction between an epoxy resin and a carboxylic acid crosslinker.[2] Due to their associative nature, the crosslinking density of vitrimers remains always constant, which translates into steady performances of the material. Moreover, vitrimers are processable materials due to continuous and simultaneous debonding and re-bonding

of the chemical network.[281, 282] Further, the rate of the linkage exchange can be regulated through different parameters, such as the temperature or the presence of a suitable catalyst.

In the last decade, numerous manuscripts describing the use of sustainable building blocks for the production of CANs were published,.[283, 285] In the field of NIPUs, vinylogous urethanes (VUs) can be considered as isocyanate-free vitrimers analogous to PUs (Figure 74). Developed for the first time by Du Prez *and coll.,* VUs are commonly synthesized by a transamination reaction between di- or multifunctional acetoacetate containing monomers and amines.[286]

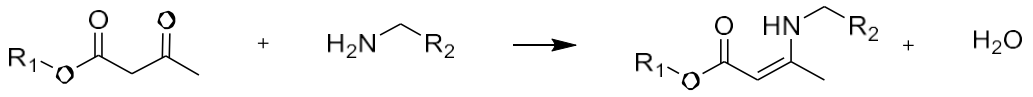

Figure 74. General reaction scheme for the synthesis of vinylogous urethanes.

The main advantages of VUs are their ease of production on a large scale, resistance to hydrolysis (oppositely to esters) and high stability to elevated temperatures. In particular, the latter point can be explained by the peculiar increase in the network exchange mechanism with rising temperature.[267] With the aim of developing new polyVUs, diverse biobased acetoacetate monomers by transesterification reaction and amines *via* thiol-ene reaction (Chapter 2) were synthesized. Taking advantage of this, the produced building blocks and some commercially available ones, different polymers were generated. The curing of the materials was followed, and their physical and mechanical properties evaluated.

3.1.1 Monomer syntheses

The procedure for the synthesis of acetoacetates was inspired by existing scientific literature and a procedure previously used at Henkel (Figure 75).[287, 288]

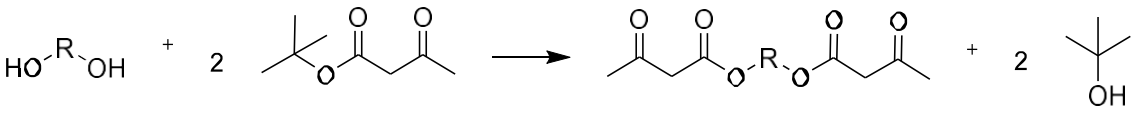

Figure 75. General transesterification reaction scheme for the synthesis of a polyacetoacetate.

Di- and tri-acetoacetates were synthesized *via* transesterification of *tert*-butyl acetoacetate (TBAA) with castor oil (CoAcAc), 1,4-butanediol (BuAcAc), and glycerol (GlyAcAc) (Figure 76).

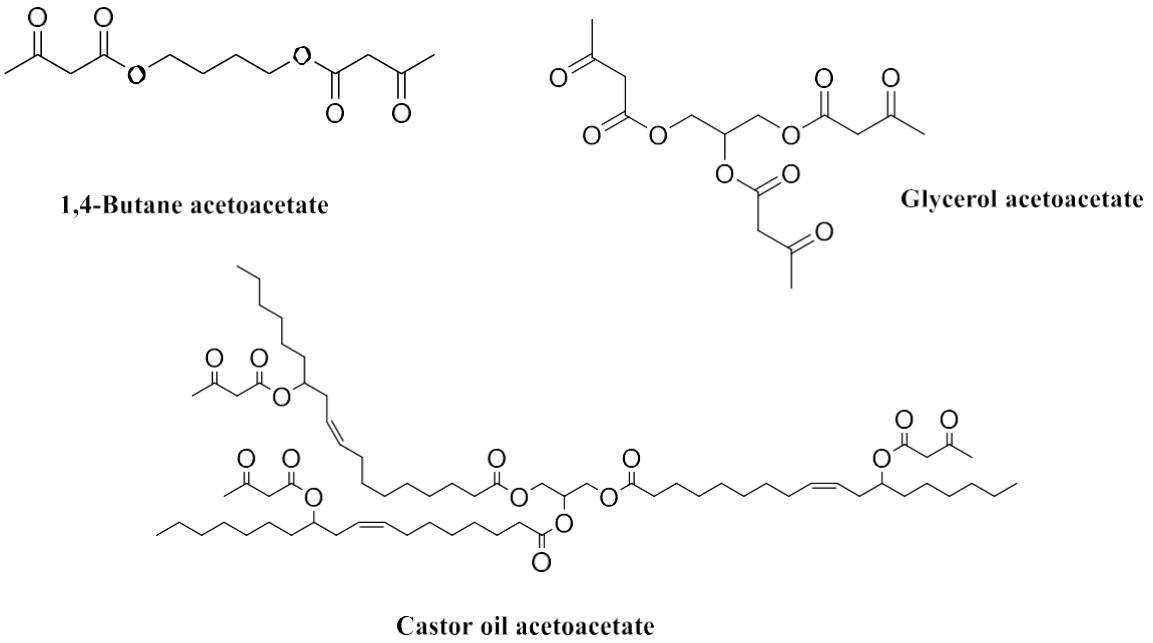

Figure 76. Chemical structures of castor oil acetoacetate (CoAcAc), 1,4-butane acetoacetate (BuAcAc), and glycerol acetoacetate (GlyAcAc).

A distillation apparatus was used to remove *tert*-butanol, a reusable side product, and a specific temperature for each starting molecule was chosen to conduct the reaction. The syntheses were performed without solvent and the reaction time was optimised to 3 h. The progress of the reaction was monitored by FT-IR until no O-H stretching bend (3500-3000 cm^{-1} region) was detectable (Figure 77, further spectra can be found in the Experimental section).

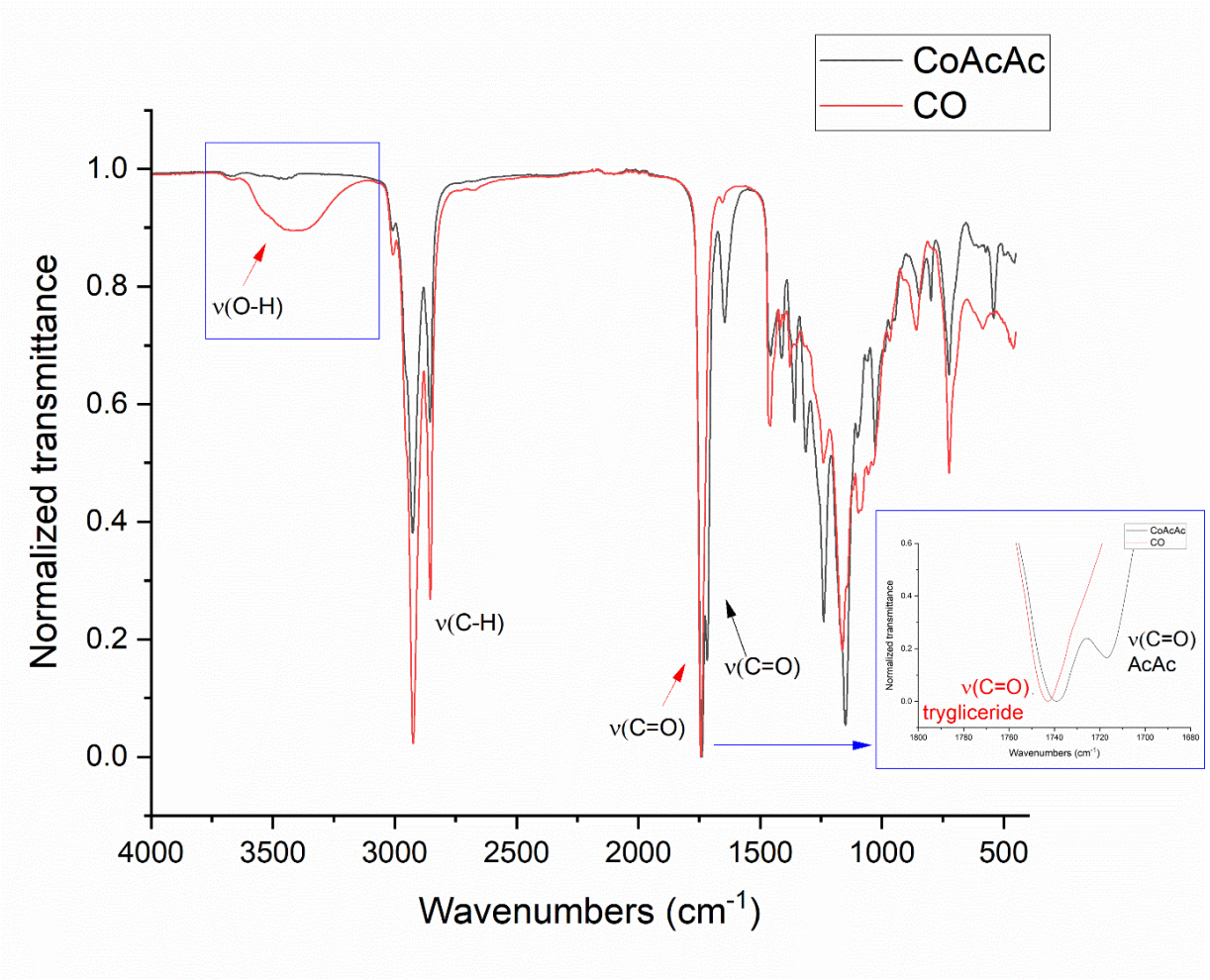

Figure 77. FT-IR spectra of castor oil acetoacetate (CoAcAc-black line) and castor oil (CO-red line). In the blue boxes the details relative to peaks proving the successful reaction.

It was possible to achieve high yields for all the three acetoacetate compounds: quantitative yield for CoAcAc, and GlyAcAc, 93% for 1,4-BuAcAc (more information in the Experimental data). The colour of the final monomer from orange to yellow it´s attributed to the impurities present in the TBAA, which presented a yellow colour. In fact, it is reported that the colour of TBAA could be from transparent to yellow. It was performed one reaction with CO and a transparent TBAA (Sigma Aldrich) and, unlike the previous outcome, the final product was clear. The limonene polyamines necessary for subsequent polyVUs synthesis was prepared *via* thiol-ene reaction under UV irradiation at 365 nm (Figure 78). Thiol-ene reaction is an efficient click reaction known for the efficient and fast functionalization of unsaturated compounds (see Chapter 3).[289, 290] In the literature, a variety of applications of thiol-ene chemistry were shown for polymerization approaches or monomer synthesis to produce polyols and amines.[291, 292] Limonene was chosen as a short-chain aliphatic building block, which was already reported by Meier *and coll*.[45]

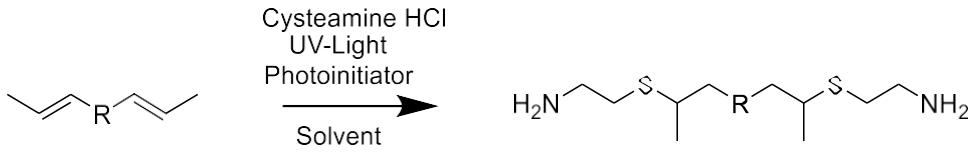

Figure 78. General reaction scheme for polyamine synthesis *via* thiol-ene photoinitiated reaction.

3.1.2 Fully and partially bio-based vinylogous urethane formulations

The three acetoacetates derived from castor oil, 1,4-butanediol, and glycerol (i.e. CoAcAc, BuAcAc and GlyAcAc, respectively) were combined with petroleum- as well as bio-based commercially available polyamines to obtain vinylogous urethane polymers (VUs, Table 23, Figure 79).

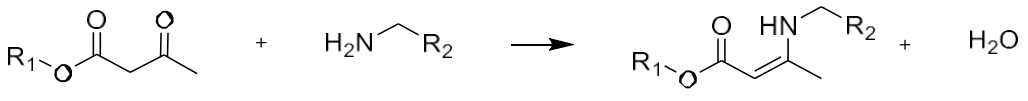

Figure 79. General scheme for the synthesis of polyvinylogous urethanes.

Equimolar amount of amine: acetoacetate groups were used. The commercial amines used for this project were the following: isophorone diamine (IPDA), *Jeffamine D230®, Jeffamine T403®, Priamine 1071®* and LDA (Figure 80).

While mixing the two components, the pot life of each formulation was determined (Table 23). Pot life is defined as the time between the moment when the components of a formulation (i.e. adhesive, coating) are placed in contact and mixed, until the viscosity increases to the point where the formulation can no longer be applied to a surface (i.e. not workable in terms of mixing and spread). This is a crucial parameter to establish possible future application of the material, because it indicates the duration for which the mixture remains applicable. The determination of the pot life was performed using a chronometer, while manually mixing the calculated amounts of the two adhesive components at room temperature in a plastic container with a flat wood stick.

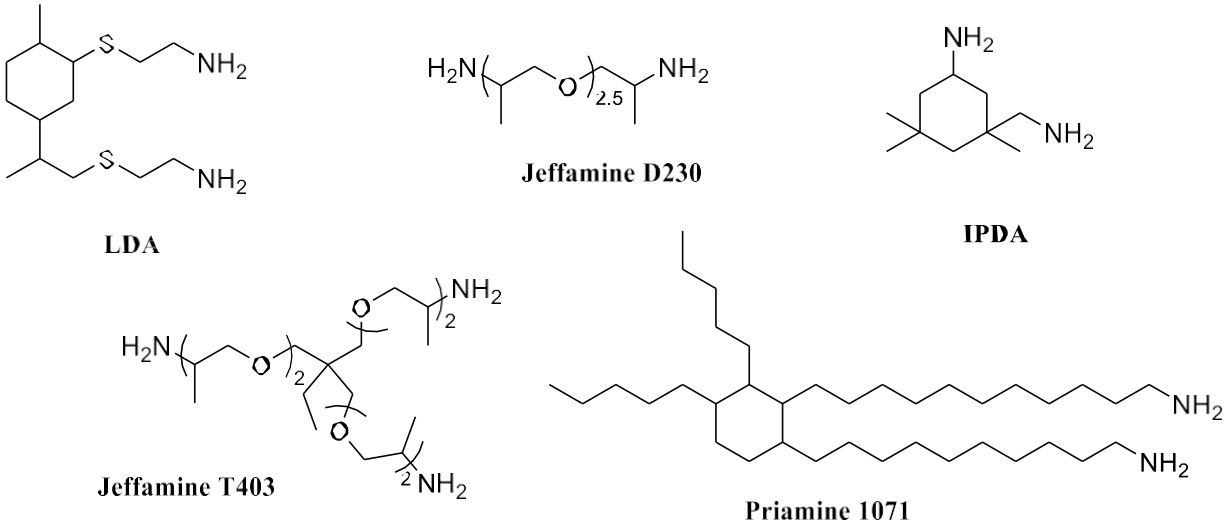

Figure 80. Chemical structures of co-monomer pluriamines: limonene diamine (LDA), *Jeffamine D230®,* isophorone diamine (IPDA), *Jeffamine T403® and Priamine 1071®.*

Table 1. VU formulations and their corresponding pot lives.

Code	Acetoacetate	Amine	Pot Life
VU1	CoAcAc	IPDA	2-5 min
VU2	GlyAcAc	*Jeffamine D230®*	20-25 min
VU3	GlyAcAc	*Priamine 1071®*	55 s
VU4	1,4-BuAcAc	*Jeffamine T430®*	40 min
VU5	CoAcAc	LDA	-
VU6	GlyAcAc	LDA	<1 min

The water formed during enamine formation remains trapped inside the network, but, due to its small amount, it is not expected to trigger a depolymerization or affect the material properties.[274] Spontaneous evaporation of water was noticed in the samples at room temperature. This could be observed at macroscopic level by the change of light incidence on the material. In fact, after evaporation of water, the materials shifted from opaque to transparent (Figure 81-left). To accelerate the process, samples were placed in the oven at 80°C overnight (Figure 81-right). Higher temperatures led to bubble formation and therefore inhomogeneity of the cross-linked materials. With the help of an optical microscope, it was possible to observe the bubbles formed by the evaporation of water. In Figure 82, the materials on the left appear opaque due to the presence of

trapped H_2O, while the same polymers are transparent after removal of H_2O, on the right in Figure 82.

Figure 81. Pictures of vinylogous urethane materials. *Top*: **VU2** before (left) and after drying in oven 80°C (right). *Bottom*: **VU3** before (left) after two weeks at rt (right).

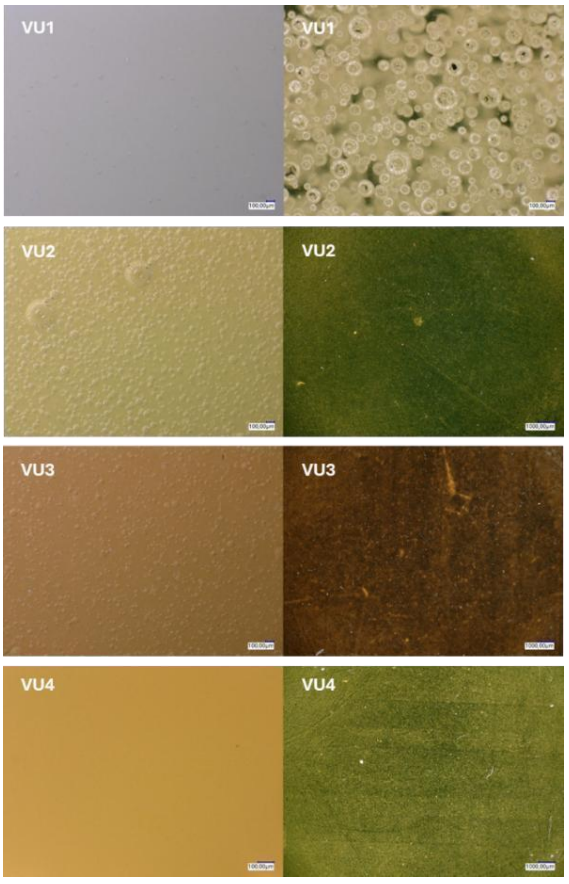

Figure 82. Optical microscopy pictures of **VU1-VU4** before (left) and after drying (right).

The curing process was monitored by FT-IR. In particular, the attention was focused on the appearance of the C=C stretching signal at 1590 cm^{-1} and the shift to lower wavenumbers of the two peaks corresponding to the carbonyl stretching of the acetoacetate group, from about 1740 and 1710 cm^{-1} to about 1650 cm^{-1} (Figure 83). It is worth noting that no solvent, no catalyst or heating was needed for the synthesis of VUs. Monitoring the disappearance of the acetoacetate peaks at about 1740 and 1710 cm^{-1} in FT-IR analyses, it was possible to determine that all the formulations were cured after 5 h at room temperature.

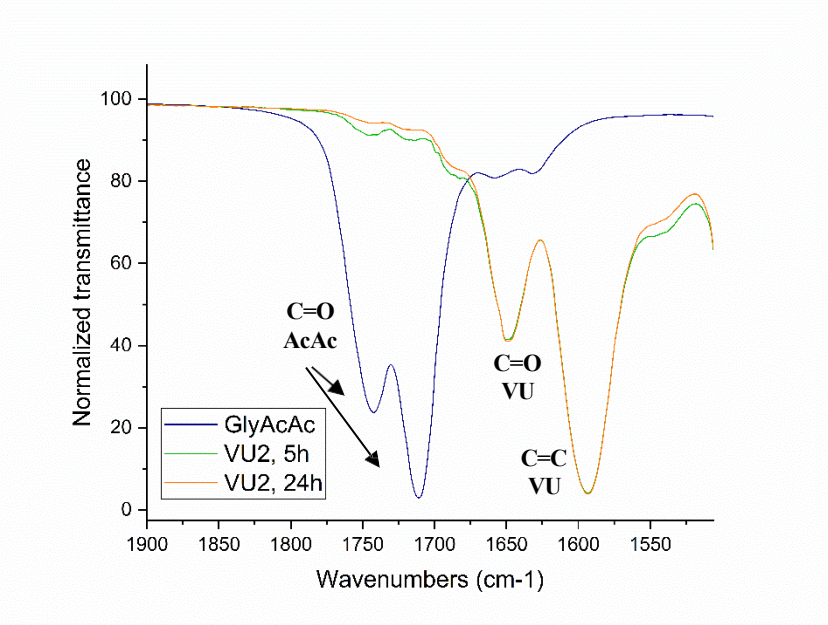

Figure 83. Details of GlyAcAc (blue line) and **VU2** (yellow line) FT-IR spectra in the carbonyl and double bond stretching region.

Shore A and Shore D durometer were employed to measure the relative hardness of the obtained materials (Table 24). Generally, materials can be divided as follows (Figure 85):

- **Shore 00:** Used for soft and flexible materials (gels, soft foams, flexible rubbers).
- **Shore A:** Rubbers and flexible/semi-rigid plastics.
- **Shore D:** Hard/semi-rigid plastics and rubbers.

The use of Shore A or D instruments depends on the empirical hardness of the polymer (Figure 84), since the force applied to the sample is different. For the vinylogous urethane materials analyzed in this work, a force of 12.5 N and 50 N was applied for Shore A and D hardness testing, respectively. Due to the high density of ester linkages and high hydrogen bonding density the materials prepared using *Jeffamine D230*® as co-monomer resulted in being stiff._**VU5,** obtained from the flexible CoAcAc, displayed a softer structure compared to **VU6**, which had a higher crosslink density due to the use of the lower-molecular-weight acetate (GlyAcAc), leading to a very lower inter-crosslinking space and a rigid chemical network structure. Considering these observations, it stands to reason that the vitrimers incorporating monomers with long aliphatic chains such as CoAcAc

(**VU1** and **VU5**) resulted in softer structure with a Shore A hardness typical of flexible rubbers (Table 24). Similarly, the combination of *Priamine 1071*® and the short trifunctional GlyAcAc was also generating a flexible material (**VU3**), even though not as much as the prior. This can be attributed to the higher aliphatic character of the CoAcAc in comparison to P1071.Morover, the measurements were performed on hydrated (H) and dried (D) sample. The presence of water did not influence strongly the hardness values (Table 24). However, a high increase in hardness was detected for sample **VU2-H** to **VU-D**, with Shore D values of 2 and 12, respectively.

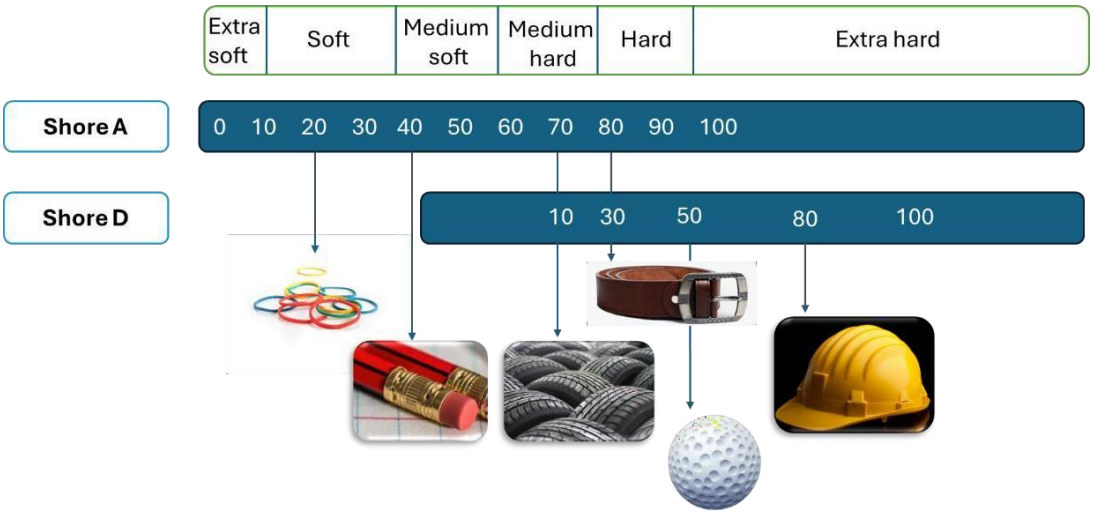

Figure 84. Shore A and Shore D hardness scales, with examples of common material hardness values.[275]

Thermal analysis by DSC showed glass transition temperature (T_g) values between -3 and -10 °C for **VU1**, **VU3,** and **VU4** (Table 24), close to room temperature for **VU2** (35 °C) and higher for **VU6** (65 °C). The vinylogous urethanes **VU2** and **VU6,** prepared from GlyAcAc and a relatively rigid amine (i. e. D230 and LDA) exhibited higher T_g values because of a rigid and highly cross-linked polymer network. As expected, the T_gs of non-dried samples were lower compared to the dried analogues, due to the plasticizing effect of water.

Table 2. T_g and $T_{d,5\%}$ values of vinylogous urethane formulations, with and without water trapped in the material.

	AcAc	Amine	T_g (°C) Dried	T_g (°C) Hydrated	$T_{d,5\%}$ (°C) Dried
VU1	CoAcAc	IPDA	-9		330
VU2	GlyAcAc	*Jeffamine D230®*	35		287 (H)
VU3	GlyAcAc	*Priamine 1071®*	-10	-7	308
VU4	BuAcAc	*Jeffamine T430®*	-3	-5	287
VU5	CoAcAc	DLA	25		160
VU6	GlyAcAc	DLA	65		190

Degradation temperatures at 5% weight loss of VU dried samples. Measured by TGA analyses.

TGA was measured to evaluate the degradation profile of the obtained materials (Table 24). **VU1-VU4** samples showed high temperature resistance, with temperatures at 5% mass loss ($T_{d,5\%}$) values from 260 to 330 °C. Lower performances were displayed by polymers using LDA as monomers, with *a* $T_{d,5\%}$ of 160 °C for **VU5** and 190 °C for **VU6.**

The crosslinking density was evaluated *via* swelling tests in THF (Table 25). In particular, the swelling index ranged from 150 (**VU6-H**) to 290% (**VU4-H**), while the gel contents were high (90% - 98%) for all the formulations, indicating good cross-linking and showing that a minimal fraction of the materials dissolved in the THF.

Table 3. Swelling index and gel content values of vinylogous urethane formulations, with and without water trapped in the material.

	AcAc	Amine	Shore A	Shore D	Swelling index (%)	Gel content (%)
			12.5 N	50 N		
VU2- H	GlyAcAc	*Jeffamine D230®*		2	188	95
VU3-H	GlyAcAc	*Priamine 1071®*	12.2		208	93
VU4-H	1,4-BuAcAc	*Jeffamine T430®*	8.9		290	90
VU5-H	CoAcAc	DLA	2			
VU6-H	GlyAcAc	DLA		36	1500	62
VU1-D	CoAcAc	IPDA	5.5		236	94
VU2-D	GlyAcAc	*Jeffamine D230®*		11.8	205	94
VU3-D	GlyAcAc	*Priamine 1071®*	10.3		288	92
VU4-D	1,4-BuAcAc	*Jeffamine T430®*	11.1			

H=containing trapped water; D=dried. Values of hardness measured with durometers Shore A (12.5 N applied) and shore D (50 N applied).

NMR and SEC of the residual solvent from the swelling tests were recorded. The ^{1}H-NMR of **VU1** showed traces of the CoAcAc structure. Similarly, the spectra of the other VUs showed traces of the respective monomers (Figure 85, further spectra in the experimental section).

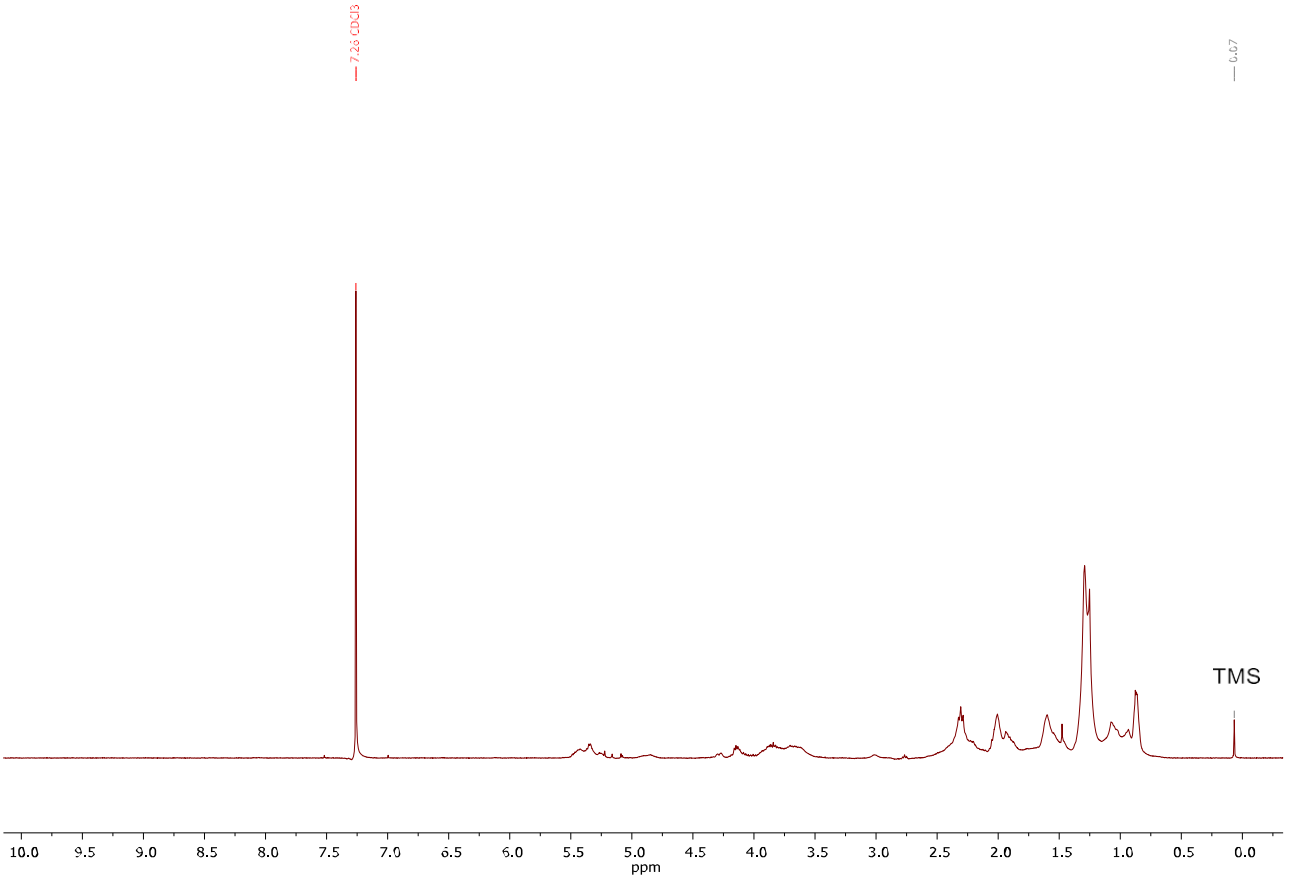

Figure 85. ^{1}H-NMR ($CDCl_3$) of residue found in THF after swelling tests for the **VU1** sample.

SEC of the soluble residues from the swelling tests were recorded employing a PMMA calibration standard. The *Mn* values indicated the presence of small oligomers (Figure 86). Typically, the highest values obtained refer to formulations involving large monomers, such as **VU1** (CoAcAc) and **VU3** (P1071), with *Mn* equal to 2100 g/mol and 1200 g/mol, respectively.

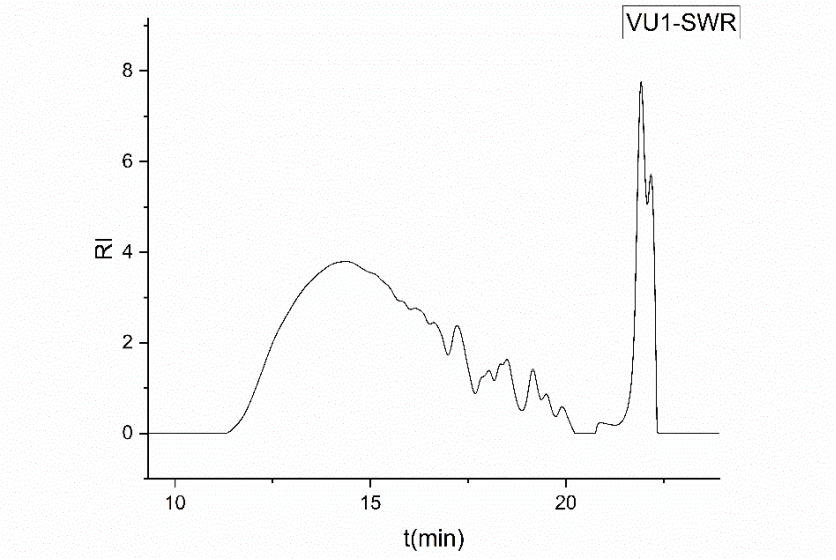

Figure 86. SEC chromatogram of **VU1** residues found in solvent (THF) after swelling test. Retention time detail from 10 to 25 min (measured in THF). System signal peak at 22 min.

Tensile tests were also measured for **VU1-VU4** samples (Table 26, Figure 87).

Table 4. Mechanical properties of vinylogous urethane formulations.

	AcAc	Amine	Elongation at break (%)	Stress at break (MPa)	E_{mod}
VU1	CoAcAc	IPDA	69±11	0.18±0.01	0.3
VU2	GlyAcAc	JD230	98±18	11±3	1405
VU3	GlyAcAc	P1071	12±9	8.8±0.4	3.4
VU4	BuAcAc	JT430	40±11	0.55±0.12	1.6

Analyzing the stress-strain curves reported in Figure 65, different mechanical behaviours were noticed. The stress-strain profile depends on the molecular structure, microstructure, temperature and strain-rate. When the last two parameters are fixed in the measurements, the stress profile is mostly influenced by the polymer structure. **VU1** displayed a large elastic region up to the yielding point, followed by a short plastic deformation before fracture, revealing a stress-strain profile comparable to PMMA (Figure 65).[276] A completely different profile was displayed by **VU2**, which exhibited a much harder and tougher structure, characterized by lower elongation at yield, followed by prolonged yielding and strain hardening before the breaking point. **VU4** did not show any significant deviation from a linear direct proportionality between stress and strain, until fracture, and presented values of elongation and stress at break similar to polystyrene (Figure 87).[295]

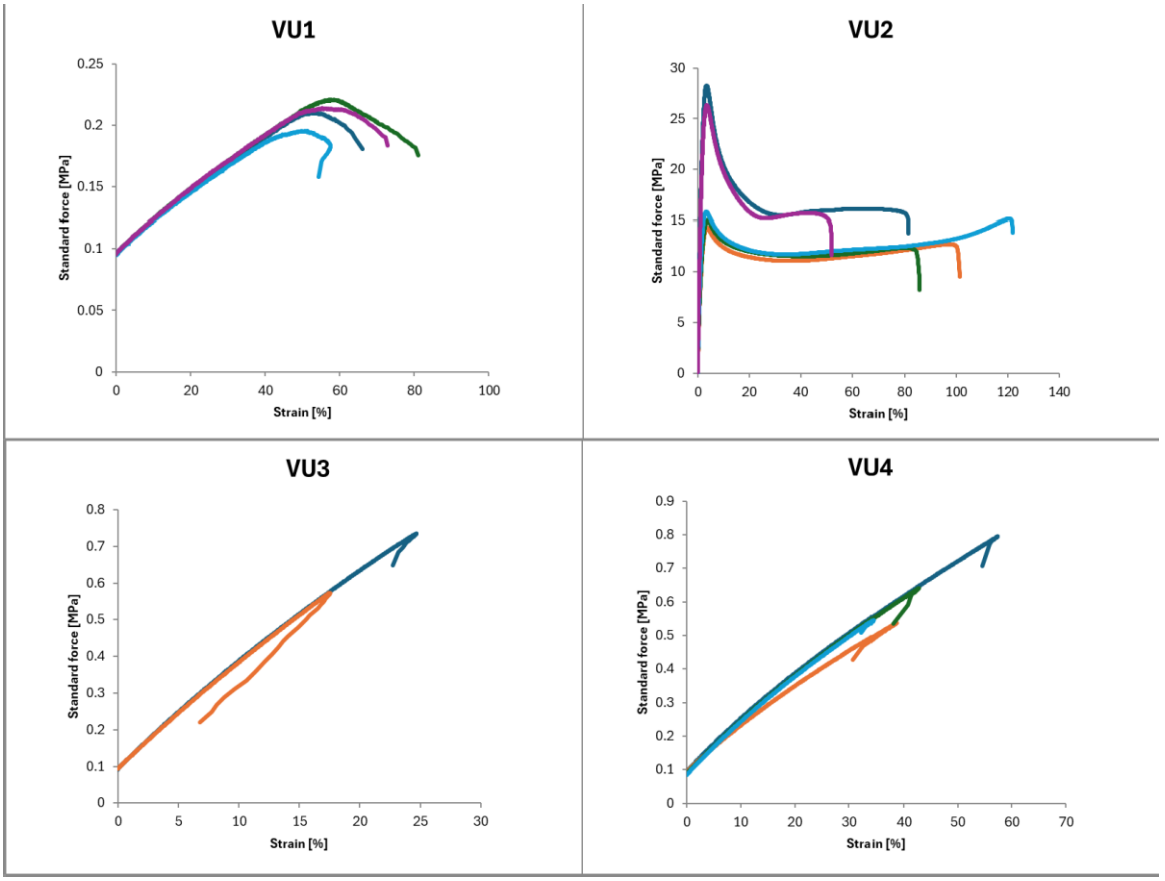

Figure 87. Stress-strain profiles of **VU1-VU4**.

In order to test the vitrimeric nature of the network, reprocessing of the materials were performed using a hot press. The tests were performed by PhD candidate Timo Sehn from Meier research group during his permanence at the Laboratory of Organic Polymers (LCPO, University of Bordeaux, France) supervised by Prof. Dr. Llevot. The materials were cut in small pieces and heated to 130 °C and subjected to a pressure of 30 bar for 30 minutes (Figure 88).

Figure 88. *Left:* VUs cut in pieces. *Right:* VUs after hot press treatment.

After this process, the materials showed the ability of being re-build. The lighter colours shown by the reprocessed materials (Figure 88, right side). were due to the reduced thickness in comparison to the staring pieces (about 1 mm). To better evaluate the outcome of the treatment and the re-born network, TGA and DSC were again performed and compared with the virgin thermosets.

Table 5. *Tg* and *Td,5%* values of **VU1-VU4** before and after reprocessing process.

VU	T_g (°C) before reprocessing	T_g (°C) after reprocessing	$T_{d,5\%}$ (°C) before reprocessing	$T_{d,5\%}$(°C) after reprocessing
VU1	-9	-20	330	307
VU2	35	27	287	262
VU3	-10	-12	308	288
VU4	-3	29	287	266

From an empirical point of view, the material achieved after the reprocessing process displayed a solid and uniform composition. Form the analyses, a slight decrease in degradation temperature (at 5% wt. weight loss) was detected by thermogravimetric analyses, indicated a good reconstruction of the chemical network. Parallelly, DSC analyses showed a decrease in T_g values (Table 27), indicating less cross-linking density. To obtain more insights about the network dynamics, rheological mechanical tests (i.e. tensile tests) and rheological analyses should be performed. In the frame of this work, further investigation was not possible due to lack of time and equipment unavailability.

Lap-shear adhesion tests were performed (Table 28) to evaluate the adhesive properties of the vinylogous urethane formulations. Three different substrate materials were chosen: PVC, birch softwood and aluminium (Figure 89).

Table 6. Lap-shear strength of vinylogous urethane formulations with different substrate materials.

	Strain Stress (Mpa)		
	PVC	**Wood**	**Alu**
VU1	1.40 ±0.06	1.93 ±0.12	0.71 ±0.05
VU2	0.72 ±0.15	8.49 ±0.86	2.04 ±0.53
Failure Type	A	SF! Fiber tear	A
Failure Type	AC	SC	AC
VU3	0.69 ±0.15	0.81 ±0.50	0.32 ±0.09
Failure Type	AC	SC	A
VU4	1.28 ±0.10	2.45 ±0.16	0.75 ±0.24
Failure Type	AC	SC	A
VU5	3.30 ±0.43	0.90 ±0.77	0.91 ±0.26
Failure Type	SF! Stock-break	SC	AC
VU6	0.34 ±0.13		
Failure Type	A		

Legend: A= adhesive, SC= surface cohesive, AC=adhesive cohesive, SF!= substrate failure

Note. Stress-strain values were obtained calculating the average of 5 measurements for each material.

All the formulations showed the best performances on wood substrates. This result was explained from both a chemical and a physical perspective. Firstly, analyzing the chemical composition at the

interface between wood and adhesive, the presence of -OH and -COOH groups on the softwood surface and -NH and C=O within the VU glues allowed hydrogen bonding, as well as possibly covalent bond formation at the interface.[277,278] Secondly, the porous nature of the substrate permits the adhesive to penetrate its structure more efficiently.[279] Good adhesion performances were also evident by the type of failure observed, which resulted in being cohesive for all wood samples.

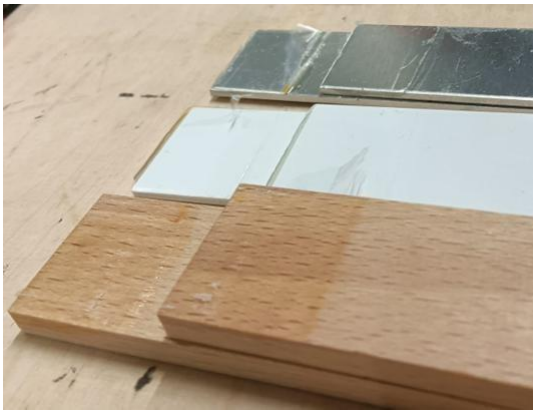

Figure 89. Substrates used for lap shear tests: Aluminium, PVC and softwood (from top to bottom).

Commonly, as the number of exchangeable bonds increases, the higher the strength of the adhesion. Among all the VUs, the best performance on wood was registered by **VU2** (8.48 MPa). **VU2** was composed of GlyAcAc and an ether diamine (JD230). The first permits high crosslinking density as a short-chain and tri-functional compound. In this case, the strong adhesiveness resulted in a substrate failure, termed “fibres tear” (Figure 90a).

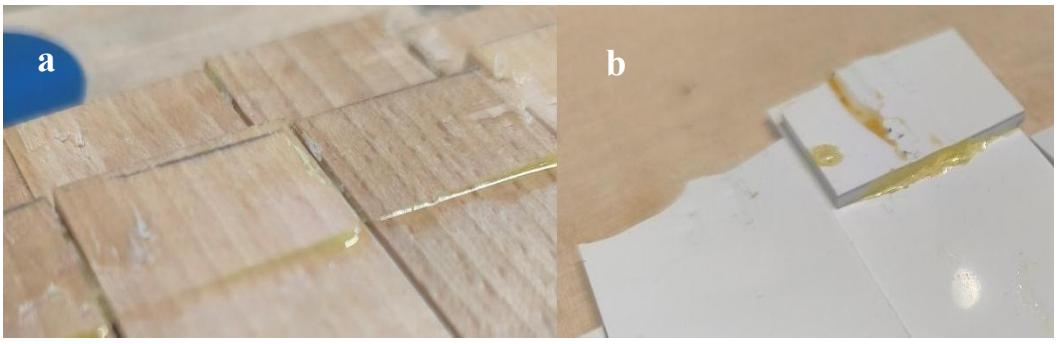

Figure 90. Substrate failures: a) fibre tears of wood and b) stock-break of PVC.

Most of the measurements on aluminium substrates showed poor performance and mostly adhesive type of failure, indicating that these VU formulations are rather unsuitable to glue aluminium. It is worth mentioning that no pre-treatment of the aluminium specimens was performed. In order to enhance the interaction between the adhesive and the metal, a pre-treatment might be required.[280] A similar polarity between substrate and adhesive guarantees the best wetting of the substrate

(interfacial defect model and the fracture energy model of adhesion), which is a key parameter for strong adhesion.[300] This explains why the performances on PVC were also not excellent. Once again, the best result using PVC was obtained by **VU5**, showing a lap-shear strength two to three times higher than the values achieved by other formulations. An excellent performance was observed for this formulation on PVC substrate, showing another type of substrate failure defined "stock-break failure" since the substrate material did not withstand the applied stress, resulting in premature breakage (Figure 90b).

Usually, also plastic materials, likewise to metals, need surface pre-treatments.[16] Usually, the ultimate layer on the surface is called the weak boundary layer due to the presence of low molecular chains of the polymer. Adhesive-cohesive failure was the most observed failure type in the case of PVC adherents. **VU1** and **VU5** are analogous formulations containing both CoAcAc with IPDA the first and DLA the second, respectively. IPDA and DLA are diamines with comparable chemical structures. Better performances were recorded for the wood adherent for **VU1**, similar stress strains for aluminium in both formulations and definitively better performance of **VU5** for PVC was observed. A polyurethane made with a canola oil-derived polyol cured with pMDI hardener (polymethylene diphenyl diisocyanate) was tested as wood adhesive and compared with a commercial adhesive PU. The results showed a 3.9 and 4.9 MPa shear strength, respectively. In comparison, **VU1** and **VU5** containing vegetable oil-derived acetoacetate showed lower performances on wood such as 1.93 Pa and 0.83 MPa (Table 28). Moreover, on the same substrate, the adhesive **VU2** showed a greater performance with a shear strength equal to 8.5 MPa. In the frame of vinylogous urethane adhesive, a lignin-based adhesive was recently reported.[301] The best performance registered on wood was 4.4 MPa when the specimen was hot-pressed at 170°C for 30 minutes. Caillol *and coll.* reported a PHU adhesive exhibiting a 15 MPa shear stress on wood with a formulation based on two polyfunctional cyclic carbonate and 1,3-cyclohexanebis(methylamine).[302]

3.2 CONCLUSION

Three biobased acetoacetates were synthetized and combined with different commercial and synthetized di- and tri- amines. The differences of the chemical structure of the monomers and their combination gave reason to the final physical, chemical and mechanical properties of the polyvinylogous urethanes (polyVUs) obtained. Due to the dynamic nature of this class of

thermosets, polyVUs belong to the class of CANs (Covalent Adaptable Network materials). Considering the advantage of CANs in comparison to normal thermosets, i.e. the possibility to be recycled, reprocessing tests of the produced polyVUs were performed (the reprocessing was performed by PhD Candidate Timo Sehn at LCPO laboratory of the University of Bordeaux). A relation between T_g and reprocessing was observed, leading to easier reprocessing process for materials with lower T_g values. DSC analyses displayed values of T_g between -3 and 65 °C. High resistance to temperature was observed by TGA analyses with the lower $T_{d,5\%}$ registered above 300°C for all the formulation except the ones containing LDA, displaying a $T_{d,5\%}$ equal to 160°C (with CoAcAc) and 190 °C (with GlyAcAc). Lap shear tests displayed the best performances of all the formulations on softwood substrate. Moreover, differences in the adhesive properties were showed according to the chemical structure and free OH density present in the polyVUs network. As outlook, biodegradability and biocompatibility tests can give a wider view on the perspective of applicability of the developed materials.

3.3 EXPERIMENTAL DATA

Characterization methods

Nuclear Magnetic Resonance spectroscopy (NMR)

NMR spectra were recorded using the following spectrometer hardware.

Bruker AVANCE 400

1H NMR (400 MHz), 13C-NMR (101 MHz)

Bruker AVANCE 500

1H NMR (500 MHz), 13C-NMR (126 MHz)

DMSO–d6, $CDCl_3$ and MeOD were used as solvents and their respective resonance signals served as reference for the chemical shift δ in parts per million: 1H: $CDCl_3$ = 7.26 ppm, DMSO-d6 = 2.50 ppm; 13C: $CDCl_3$ = 77.2 ppm, DMSO-d6 = 39.5 ppm. The spin multiplicity and corresponding signal patterns were abbreviated as follows: s = singlet, d = doublet, t = triplet, q = quartet, quint. = quintet, m = multiplet. Coupling constants J were noted in Hz. Furthermore, 2D NMR methods (e.g., heteronuclear single quantum coherence (HSQC), heteronuclear multiple bond correlation (HMBC) and correlated spectroscopy (COSY)) were carried out, if necessary, for signal assignment and structure elucidation.

Size exclusion Chromatography (SEC)

System I (Oligo SEC): A PSS SECcurity^2 SEC system based on Agilent Infinity 1260 II hardware was used for the measurements. The system is equipped with a refractive index detector SECcurity^2 RI, a column oven "(Bio)SECcurity^2 column compartment TCC6500", a "standard SECcurity^2" autosampler, and an isocratic pump "SECcurity^2 isocratic pump". Anhydrous tetrahydrofuran stabilized with 250 ppm butylated hydroxytoluene (BHT, ≥99.9%) was used at a flow rate of 1.0 ml min^{-1} and at 30 °C as mobile phase. The analysis was performed on the following column system: PSS SDV analytical precolumn (3 µm, 8 mm × 50 mm) with two PSS SDV analytical columns (3 µm, 8 mm × 300 mm, 1000 Å). For the calibration, narrow linear poly(methyl methacrylate) standards (Polymer Standards Service, PSS, Germany) ranging from 102 to 62200 Da were used. For the preparation of the samples, 2.00 mg of analyte was dissolved in 1.50 mL anhydrous tetrahydrofuran stabilized with 250 ppm butylated hydroxytoluene (BHT, ≥99.9%). All samples were filtered by syringe filter prior to use, to avoid plugging of the injection setup or the column.

Infrared spectroscopy

Infrared (IR) spectroscopy IR spectra were recorded on a Bruker alpha-p instrument in a frequency range of 3997.41 to 373.828 cm-1 applying KBr- and ATR technology.

Thin Layer Chromatography (TLC)

All thin layer chromatography (TLC) experiments were performed on silica-gel-coated aluminum foil (silica gel 60 F254, layer thickness: 0.25 mm, Sigma-Aldrich). Compounds were visualized by irradiation with a UV lamp (λ = 254 and 365 nm), by staining with Seebach solution (mixture of 5.00 g phosphomolybdic acid hydrate, 2.00 g cerium(IV)- sulfate, 16.0 mL concentrated sulfuric acid and 200 mL water) or vanillin staining solution (mixture of 8.60 g vanillin and 2.50 mL concentrated sulfuric acid and 200 mL ethanol), or KMnO4 staining solution (1.50 g $KMnO_4$, 10.0 g $K2CO_3$, 1.25 mL 10% NaOH and 200 mL water) or ninhydrin solution (0.2 ninhydrin in 100 mL ethanol).

Orbitrap Electrospray Ionization-Mass Spectrometry (ESI-MS)

Mass spectra were recorded on a Q Exactive (Orbitrap) mass spectrometer (Thermo Fisher Scientific, San José, CA, USA) equipped with an atmospheric pressure ionization source operating in the nebulizer assisted electrospray mode. The instrument was calibrated in the m/z-range 150-2000 using a standard containing caffeine, Met-Arg-Phe-Ala acetate (MRFA) and a mixture of fluorinated phosphazenes (Ultramark 1621, all from Sigma Aldrich). A constant spray voltage of 3.5 kV, a dimensionless sheath gas of 6, and a sweep gas flow rate of 2 were applied. The capillary voltage and the S-lens RF level were set to 68.0 V and 320 °C, respectively. For the interpretation of the spectra, molecular peaks [M]+ , peaks of pseudo molecules [M+H]+ , [M+NH4] + , [M+Na]+ and [M+K]+ and characteristic fragment peaks are indicated with their mass to charge ratio (m/z) and their intensity in percent, relative to the most intense peak (100%).

Differential scanning calorimetry (DSC)

DSC analyses were run with DSC Q2000 instrument. Samples were placed in aluminium pans and measured with a heating rate of 10 K min-1 over a temperature range from -40 to 120 and 250 °C, gas flow (nitrogen) of 50 mL/min.

Thermogravimetric Analysis (TGA)

TGA measurements were carried out on the TA Instruments TGA 5500 under nitrogen atmosphere using platinum TGA sample pans and with a heating rate of 10 K min-1 over a temperature range from -40 to 600 °C. Thanks to Théato research group (KIT) for the instrument availability.

Tensile tests

Tensile tests were performed by the Automated Laboratory at Henkel Adhesive and Technologies department (Düsseldorf). The equipment for tensile tests was a Zwicks (Z050 frame) with respective Loadcells XForce HP 2.5Measurement specifications. Pre-load= 0.1 MPa, Test speed: 10 mm/in. Begin of Young´s modulus determination 0.05%; end of Young´s modulus determination 0.25%.

Lap shear tests

The tests were conducted on a Zwick 100. The set-up consists of two jaws holding the edges of the specimen. When the experiment started, a tensile load was applied until bonding failure.

Materials

Isophorone diamine (IPDA) (Sigma Aldrich), *Priamine 1071*® (Cargill), *Jeffamine D230*® (Evonik), *Jeffamine T430*® (Evonik), castor oil, R-(+)-limonene, glycerol, 1,4-butanediol, tert-butyl acetoacetate (Acros Organics), sodium sulphate anhydrous (Sigma Aldrich). Solvents: tetrahydrofuran (THF), chloroform ($CHCl_3$), isopropanol (i-PrOH), ethanol (EtOH) from Acros Organics.

Synthesis and characterization

- *Synthesis of 2-(((Z)-11-((3-oxobutanoyl)oxy)octadec-8-enoyl)oxy)propane-1,3-diyl (9Z,9'Z)-bis(12-((3-oxobutanoyl)oxy)octadec-9-enoate)- (castor oil acetoacetate)*

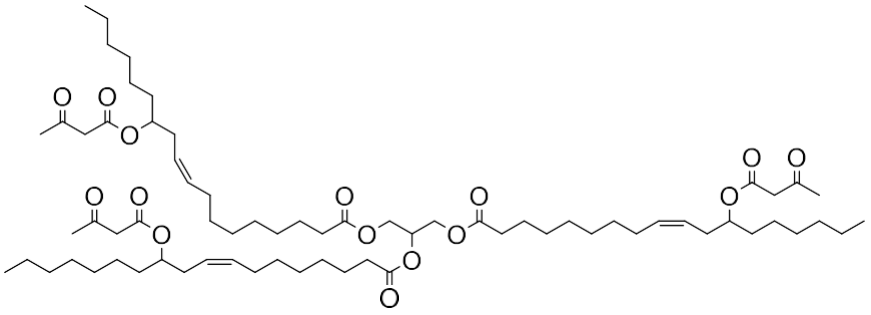

2-(((Z)-11-((3-oxobutanoyl)oxy)octadec-8-enoyl)oxy)propane-1,3-diyl (9Z,9'Z)-bis(12-((3-oxobutanoyl)oxy)octadec-9-enoate)

(Castor acetoacetate)
Chemical Formula: C69H116O15
Molecular Weight: 1185.67

A 250 mL three-neck round bottom flask, equipped with a stirring bar and a thermocouple, was charged with castor oil (60 g, 0.064 mol, 1 eq) and tert-butyl acetoacetate (30.506 g, 0.193 mol, 3 eq). The flask was connected to a distillation apparatus (vacuum applied: 200-250 mbar). The reaction mixture was stirred at 130 °C for 3 h, until no more tert-butanol evolved (orange viscous liquid, >99% recovered yield). Note. The colour is due to impurities already present in the tert-butyl acetate, the colour of which is reported to be from colourless to yellow.

Castor oil acetoacetate (CoAcAc) ^{1}H-NMR in $CDCl_3$.

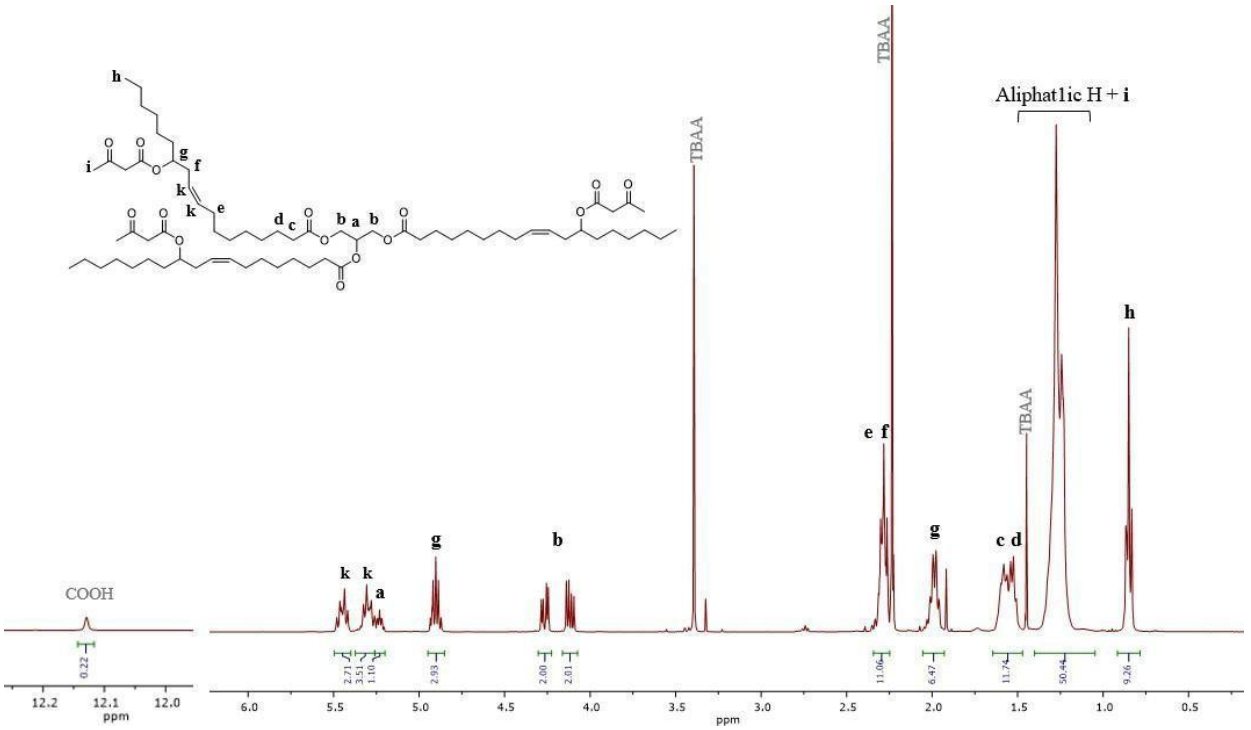

S 15. ^{1}H NMR (400 MHz) in $CDCl_3$ of CoAcAc reaction mixture after three-hour reaction.

^{1}H NMR (400 MHz, $CDCl_3$) δ (ppm) 5.44 and 5.31(CH=CH, 6H, m), 5.23 (CH glycerin unit, 1H, m), 4.90 (CH, 3H,m) 4.26 (CH_2 glycerin unit, 2H, dd), 4.12 (CH2 glycerin unit, 2H, dd),2.28 (CH-CH=CH-CH, 12 H, m) ,1.98 (C=O CH_2C=O, 6H, m), 1.52 (C**H**$_2$$CH_2$-C=OO 6H, m) 1.58 ($CH_2$-C=OO 6H, m)1.27,1.24 (aliphatic H), 0.85(-CH_3, t, 9H). Reaction mixture after three-hour reaction.

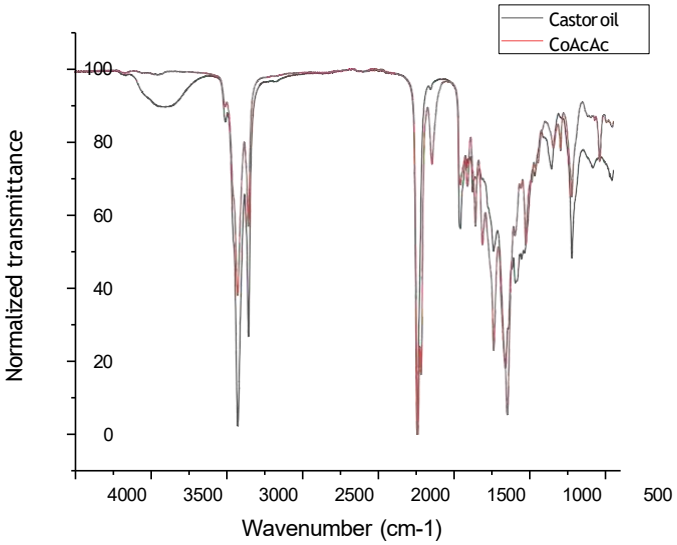

S 16. Castor oil (CO) vs castor oil acetoacetate (CoAcAc) full FT-IR spectra.

FT-IR ν^{-1} [cm^{-1}]: 3000-2700 (νC-H, m), 1738 and1718 (νC=O acetoacetate, s), 1146 (νC-O alkoxy, s.).

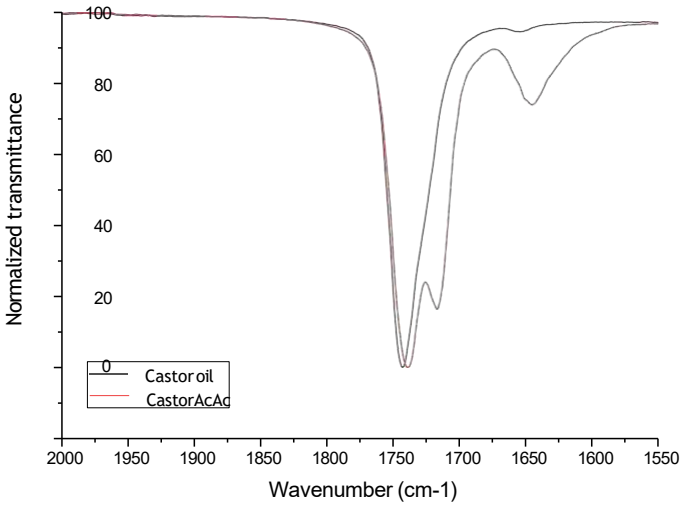

S 17. Castor oil (CO) vs castor oil acetoacetate (CoAcAc) FT-IR spectra details of carbonyl bands stretching vibrations (FT-IR).

- *Synthesis of propane-1,2,3-triyl tris(3-oxobutanoate)-(glycerol acetoacetate)*

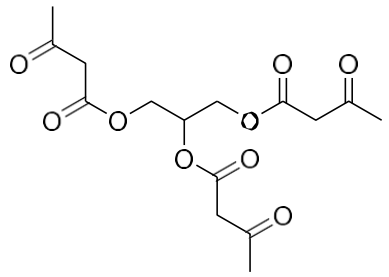

propane-1,2,3-triyl tris(3-oxobutanoate)
(Glycerol acetoacetate)
Chemical Formula: $C_{15}H_{20}O_9$
Molecular Weight: 344.32

A 500 mL three-neck round bottom flask, equipped with a stirring bar and a thermocouple, was chanrged with glycerol (50 g, 0.543 mol, 1 eq) and tert-butyl acetoacetate (257.67 g, 1.63 mol, 3 eq). The flask was connected to a distillation apparatus (vacuum applied: 200-250 mbar). The reaction mixture was stirred at 110 °C for 3 h, until no more tert-butanol evolved (yellow viscous liquid, >99% yield).

Glycerol acetoacetate (GlyAcAc) ^{1}H-NMR in $CDCl_3$.

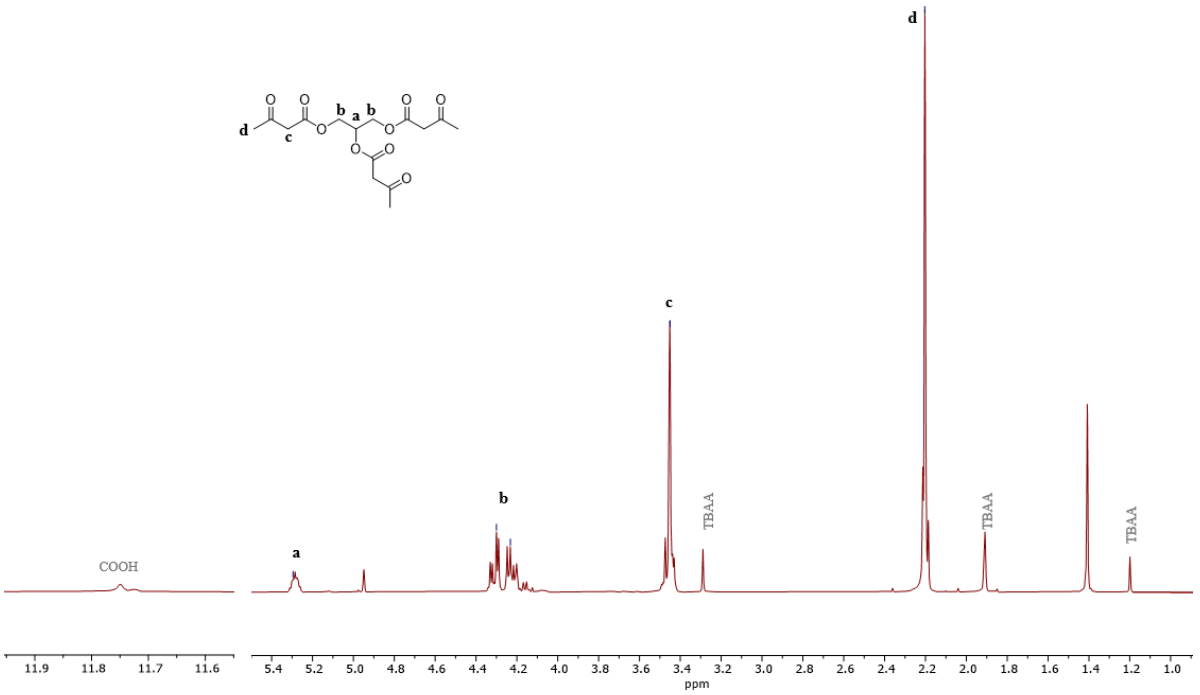

S 18. ^{1}H NMR (400 MHz) in $CDCl_3$ of GlyAcAc reaction mixture after three-hour reaction.

^{1}H NMR (400 MHz, $CDCl_3$) δ (ppm) 5.30 (CH glycerin unit, 1H, m), 4.30-4.23 (CH_2 glycerin unit, 4H, dd), 3.45 (CH, 3H, s), 2.20 (CH_3, 9H, s). Reaction mixture after three-hour reaction.

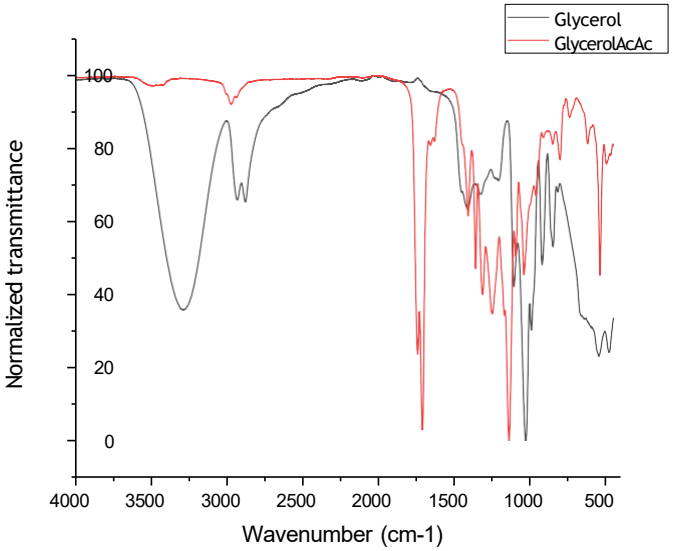

S 19. Glycerol vs glycerol acetoacetate (GlyAcAc) full FT-IR spectra.

FT-IR ν^{-1} [cm^{-1}]: 3000-2700 (νC-H, m), 1743, 1709 (νC=O, s, acetoacetate), 1238 (νC-O acyl, s) 1147 (νC-O alkoxy, s).

- *Synthesis of butane-1,4-diyl bis(3-oxobutanoate)-(1,4-butane acetoacetate)*

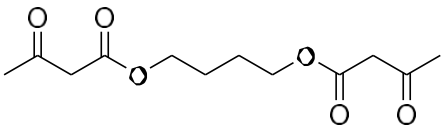

butane-1,4-diyl bis(3-oxobutanoate)
(1,4-butane acetoacetate)
Chemical Formula: $C_{12}H_{18}O_6$
Molecular Weight: 258.27

A 500 mL three-neck round bottom flask, equipped with a stirring bar and a thermocouple, was charged with castor oil (50 g, 0.555 mol, 1 eq), tert-butyl acetoacetate (174.54 g, 1.11 mol, 3 eq). The flask was connected to a distillation apparatus (vacuum applied: 200-250 mbar). The reaction mixture was stirred at 120 °C for 3 h, until no more tert-butanol evolved (yellow liquid, 93% yield).

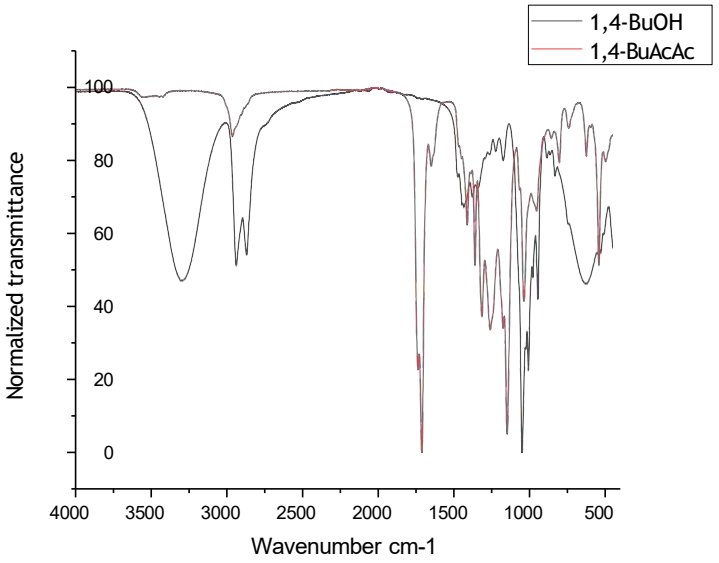

S 20. 1,4-Butanediol vs 1,4-butaneacetoacetate (BuAcAc) full FT-IR spectra.

FT-IR ν^{-1} [cm^{-1}]: 3000-2700 (νC-H, m), 1735 and 1707 (νC=O acetoacetate, s), 1252 (νC-O acyl, s) 1143 (νC-O alkoxy, s).

- *Synthesis of 2-((2-(3-((2-aminoethyl)thio)-4-methylcyclohexyl)propyl)thio) ethan-1-amine-(limonene diamine)*

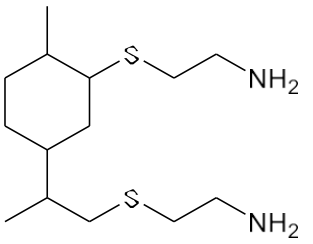

2-((2-(3-((2-aminoethyl)thio)-4-methylcyclohexyl)propyl)thio)ethan-1-amine
(Limonene diamine)
Chemical Formula: $C_{14}H_{30}N_2S_2$
Molecular Weight: 290.53

35 g of D-limonene (0.26 mol, 1 eq), cysteamine hydrochloride (202.9 g, 1.54 mol, 6 eq), and 2-hydroxy-2-methylpropiophenone (0.847g, 5.14 mmol, 0.02 eq) were dissolved in about 300 mL were dissolved in about 300 mL isopropanol. The UV LED was completely immersed in a suited flask. The mixture was exposed to a UV lamp 365 nm for 24 h. After that time the solvent was evaporated under reduced pressure. The crude mixture was dissolved in chloroform and subsequently washed with saturated sodium carbonate solution and two to three aqueous workups untill neutral pH was achieved. Water residues were removed with anhydrous sodium sulfate and the chloroform was removed under reduced pressure. Yellow viscous liquid, 87% conversion). Note: the amount of solvent indicated was necessary to allow the UV LED to be immersed in the reaction mixture.
^{1}H NMR (400 MHz, Chloroform-*d*): δ = 5.29 (ddt, *J* = 4.6, 3.4, 1.8 Hz, C**H**=C), 2.85 – 2.73 (m, -S-C**H**2-CH2-, 4H), 2.58 – 2.43 (m, 4H, -S-CH2-C**H**2), 2.28 (ddt, *J* = 14.8, 12.4, 8.4 Hz, 1H, C**H**-S) , 2.0 – 1.2 (8H ring), 0.97 – 0.93 (m, 3H, - CH3), 0.89 (dd, *J* = 6.9, 1.1 Hz, 3H, -CH3).

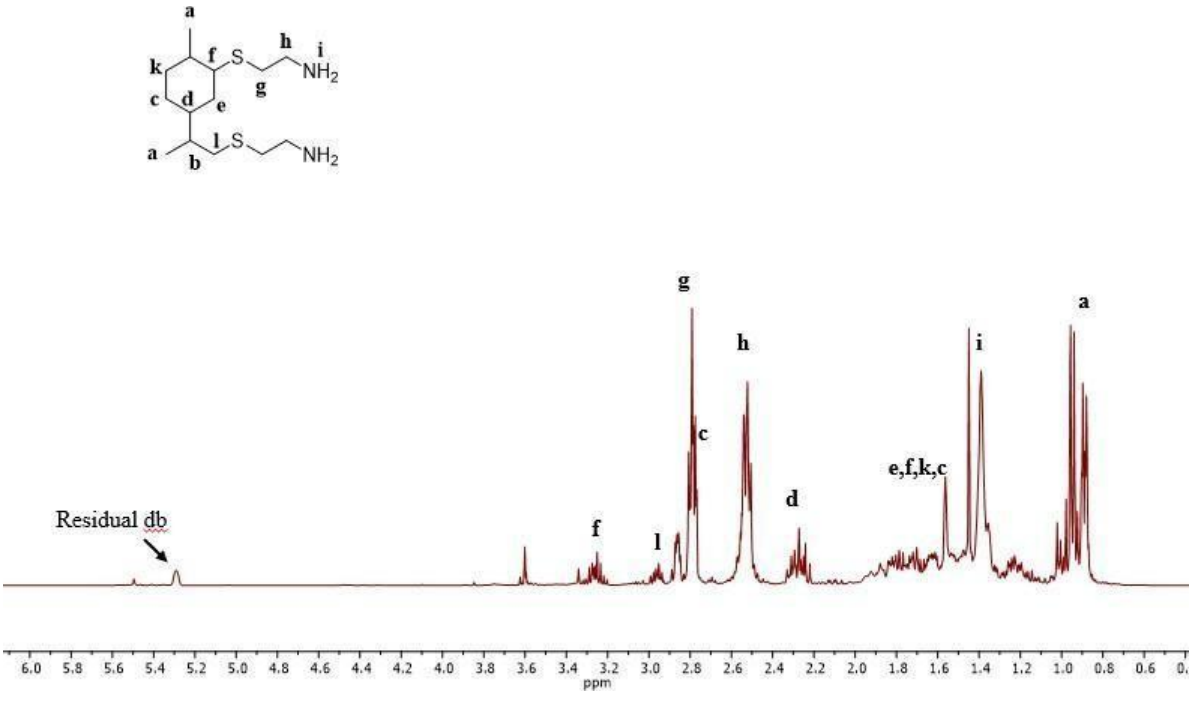

S 21. ^{1}H-NMR (400 MHz) in $CDCl_3$ of limonene diamine.

- ***VU1-*** *CastorAcAc+ isophorone diamine*

Castor oil acetoacetate (60 g, 0.051 mol, 1 eq) was weighed in a plastic container for a speed mixer. Afterwards, isophorone diamine (12.9 g, 0.076 mol, 1.5 eq) was added and the mixture was placed in a speed mixer and mixed for 30 sec. reaching 300 mbar of vacuum plus 30 sec. of non-mixing and reaching ambient pressure.

FT-IR ν^{-1} [cm^{-1}]: 3287 (N-H str.), 2928, 2848 (C-H str), 1646 (C=O str), 1605 (C=C str).

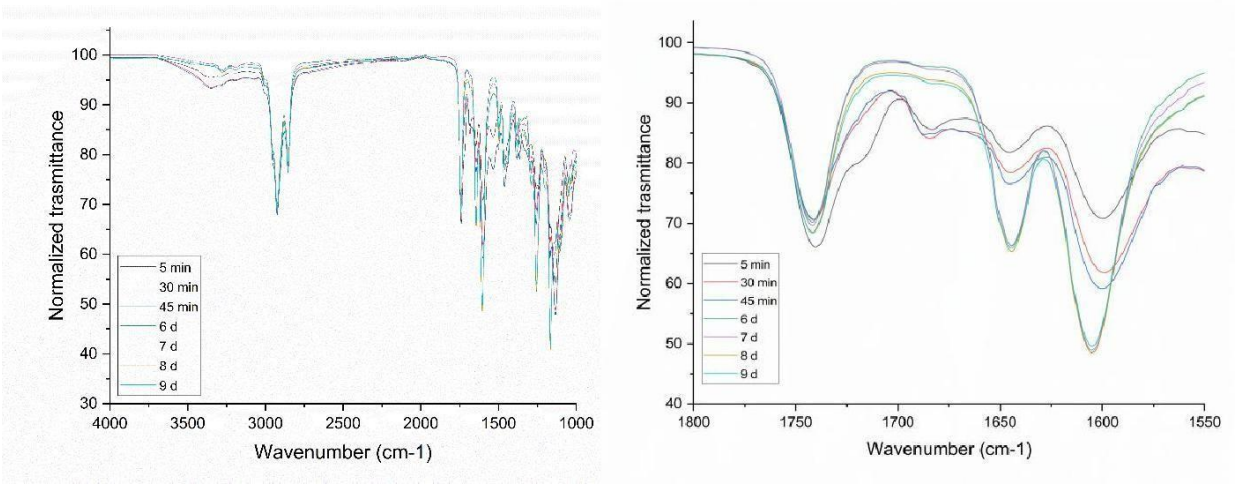

S 22. VU1 full FT-IR spectrum at different curing times (left). VU1detail carbonyl stretching zone at different curing times (right).

- ***VU2-*** *GlycerolAcAc + Jeffamine D230*

Glycerol acetate (20 g, 0.058 mol, 1 eq) was weighed in a plastic container for a speed mixer. After, Jeffamine D230 (20 g, 0.087 mol, 1.5 eq) was added and the mixture was placed in a speed mixer and mixed for 30 sec reaching 300 mbar of vacuum plus 30 sec of non-mixing and reaching ambient pressure. The samples were cured at room temperature and the curing was monitored along the time by FT-IR.

FT-IR ν^{-1} [cm^{-1}]: (N-H str.), (C-H str), 1652 (C=O str), 1594 (C=C str).

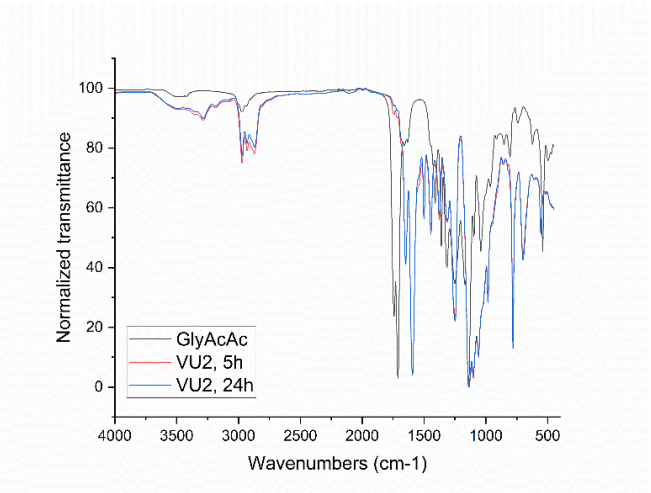

S 23. *VU2* full FT-IR spectrum at 5h and 24h.

- ***VU3****- GlycerolAcAc + Priamine 1071*

Glycerol acetate (15 g, 0.043 mol, 1 eq) was weighed in a plastic container for a speed mixer. After, Priamine 1071 (42.5 g, 0.065 mol, 1.5 eq) was added and the mixture was placed in a speed mixer and mixed for 30 sec reaching 300 mbar of vacuum plus 30 sec of non-mixing and reaching ambient pressure. The samples were cured at room temperature and the curing was monitored along the time by FT-IR.

FT-IR v^{-1} [cm^{-1}]: 3354 (N-H str.), 2922, 2959 (C-H str), 1656 (C=O str), 1605 (C=C str).

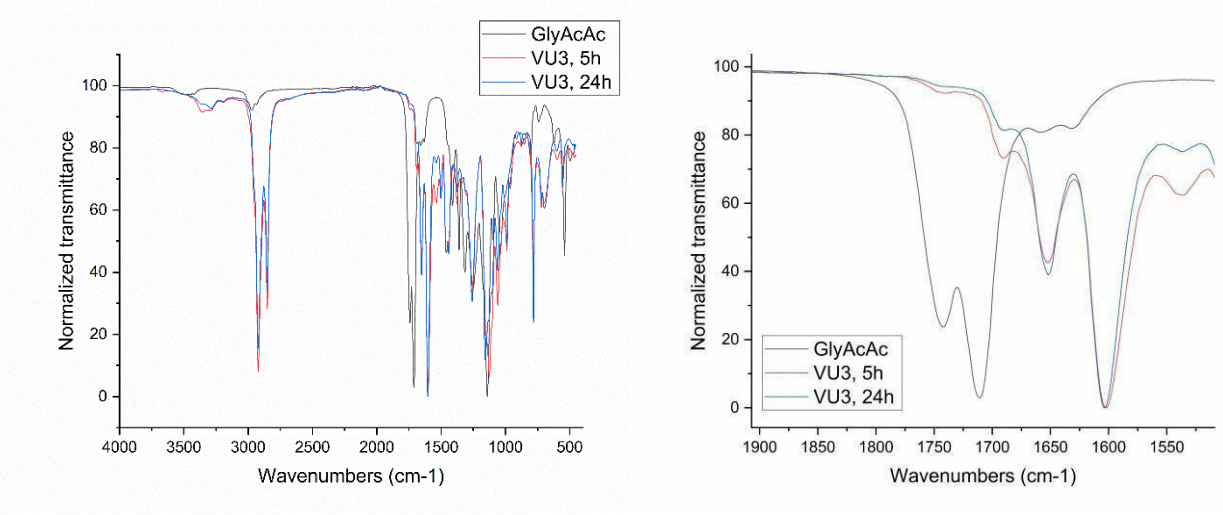

S 24. *VU3* full FT-IR spectrum at 5h and 24h curing times (left). *VU3* detail carbonyl stretching zone at different curing times (right).

- ***VU4****- 1,4-ButAcAc + Jeffamine T430*

The acetoacetate (20 g, 0.077 mol, 1 eq) was weighed in a plastic container for a speed mixer. After, the amine (22.5 g, 0.087 mol, 0.66 eq) was added and the mixture was placed in a speed mixer and mixed for 30 sec reaching 300 mbar of vacuum plus 30 sec of non-mixing and reaching ambient pressure. The samples were cured at room temperature and the curing was monitored along the time by FT-IR.

FT-IR v^{-1} [cm^{-1}] : 3338 (N-H str.), 2973-2860 (C-H str), 1657 (C=O str), 1588 (C=C str).

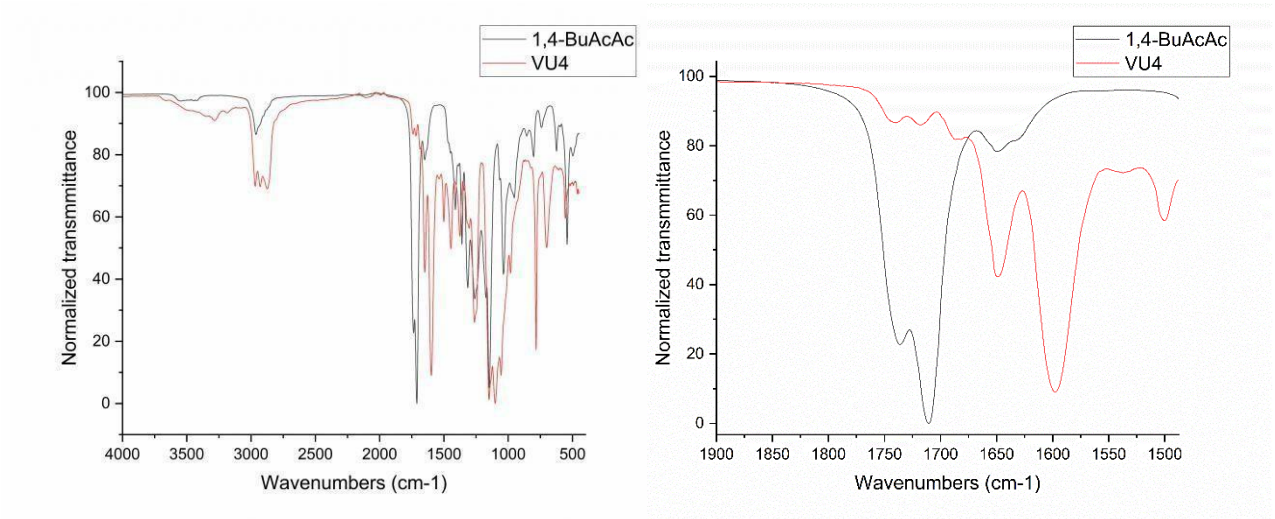

S 25. *VU4* full FT-IR spectrum after 24h curing time (left). *VU4* detail carbonyl stretching zone (right).

- ***VU5***- *CastorAcAc + limonene diamine*

Castor oil acetoacetate (10 g, 0.008 mol, 1 eq) was weighed in a plastic container for a speed mixer. After, limonene diamine (3.7 g, 0.012 mol, 1.5 eq) was added and the mixture was placed in a speed mixer and mixed for 30 sec reaching 300 mbar of vacuum plus 30 sec of non-mixing and reaching ambient pressure. The samples were cured at room temperature and the curing was monitored along the time by FT-IR.

Lap shears note: the curing process was 16 h long at room temperature plus 5 h at 80 °C in the oven to accelerate the curing process.

FT-IR ν^{-1} [cm^{-1}] : 3350 (N-H str.), 2957-2858 (C-H str), 1650 (C=O str), 1585 (C=C str).

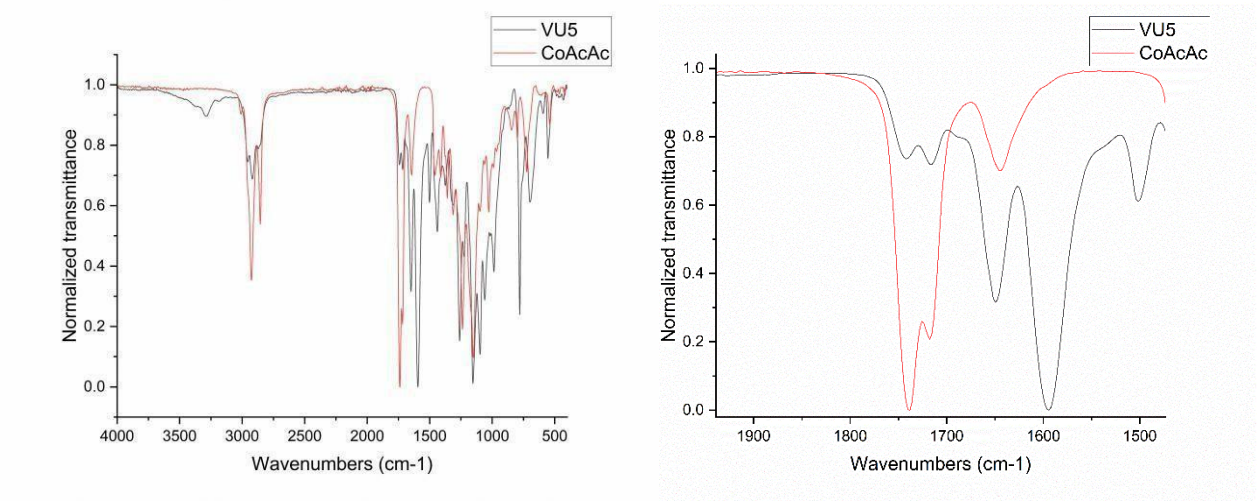

S 26. *VU5* full FT-IR spectrum after 24h curing time (left). *VU5* detail carbonyl stretching zone (right).

- ***VU6***- *GlycerolAcAc + limonene diamine*

Glycerol acetoacetate (5 g, 0.014 mol, 1 eq) was weighed in a plastic container for a speed mixer. After, limonene diamine (6.3 g, 0.022 mol, 1.5 eq) was added and the mixture was placed in a speed mixer and mixed for 30 seconds reaching 300 mbar of vacuum plus 30 sec of non-mixing and reaching ambient pressure.The samples were cured at room temperature and the curing was monitored along the time by FT-IR.

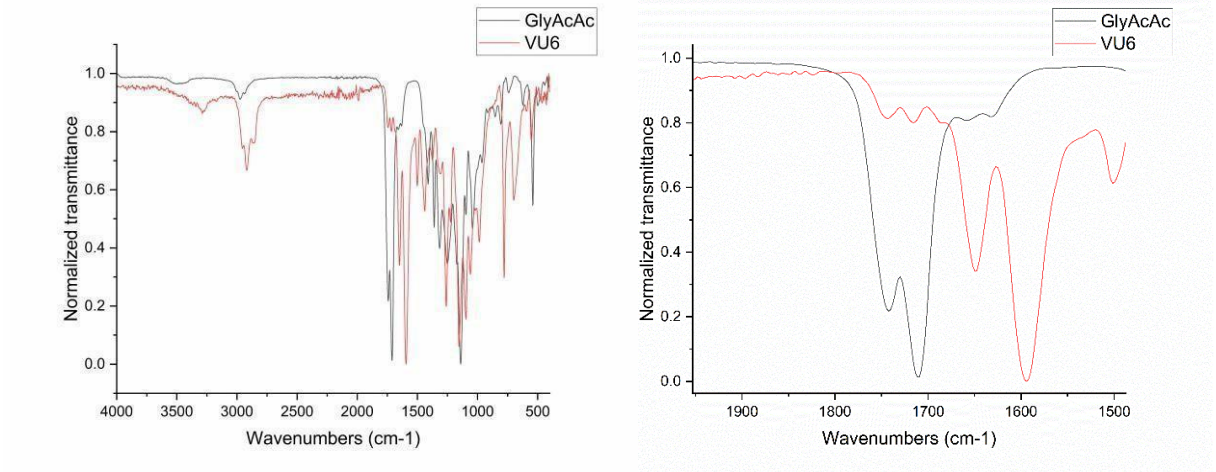

S 27. *VU6* full FT-IR spectrum after 24h curing time (left). *VU6* detail carbonyl stretching zone (right).

Pot life. To measure the pot life of the mixture, the same procedure was repeated mixing manually, while monitoring the time.

Curing. The samples were cured at room temperature and the curing was monitored along the time by FT-IR

Swelling tests. About 500 mg of each sample were placed in THF (100g/5mL) for 24h. After, the swelling index was calculated as follows:

$$SI = \frac{W_s - W_0}{W_0} . 100$$

where W_s is the weight of the swollen material and W_o corresponds to the initial weight of the material.

Afterwards the solvent was removed and the saple placed in oven at 50°C for 24 h. Subsequently, gel contents were calculated as follows:

$$Gel\% = \frac{W_d}{W_o} . 100$$

where W_d is the weight of the dried material after being swollen and W_o corresponds to the initial weight of the material.

SEC measurement of soluble fractions after swelling tests (SWR)

Table 29. Molecular weights registered for the solvent residue from swelling tests of VUs by GPC (THF).

	Mn	**Mw**	**Mz**	***Đ***
VU1	2.1E+3	8.3E+3	1.94E+4	3.9
VU2	6.4E+2	1.1E+3	1.8E+3	1.7
VU3	1.2E+3	2.1E+3	3.2E+3	1.8
VU4	1.0E+3	2.1E+3	3.6E+3	2.0
VU5	5.2E+3	1.9E+4	4.4E+4	3.6
VU6	6.3E+2	1.5E+3	3.0E+3	2.4

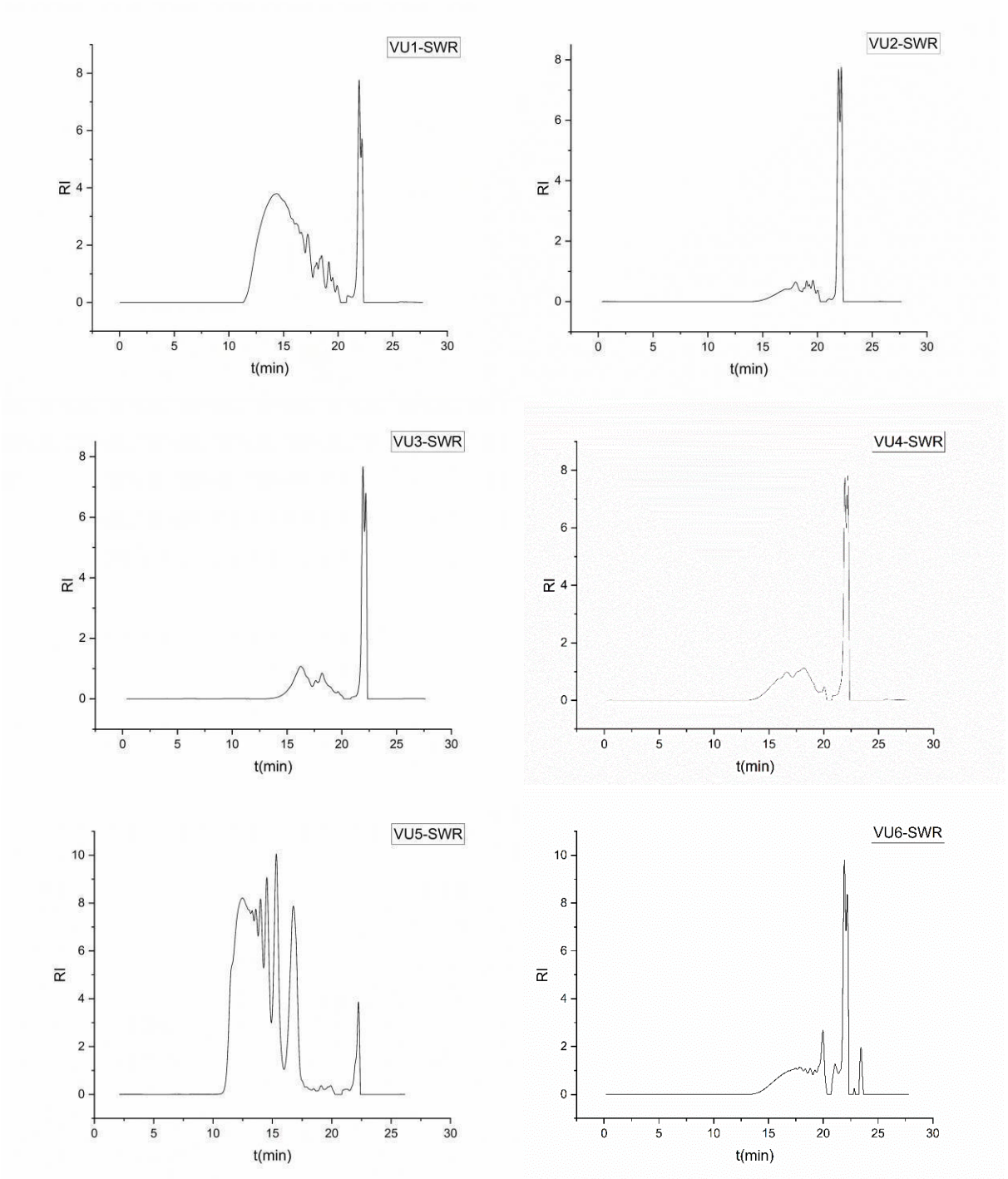

S 28. SEC chromatograms of *VU1*-*VU6* residues found in solvent (THF) after swelling test (measured in THF). System signal peak at 22 min.

Lap shear preparation. The aluminium and PVC adherents were cleaned wiping the surface with EtOH. The glueing area of the substrate was delimited and marked (13 mm in length). 200 mg of the formulation was placed on this area (13 mm* 25 mm) and glued with the second adherent. Subsequently, two office clips were placed on both sides of the junction area (Figure 91). The samples were measured 24 h after curing at room temperature.

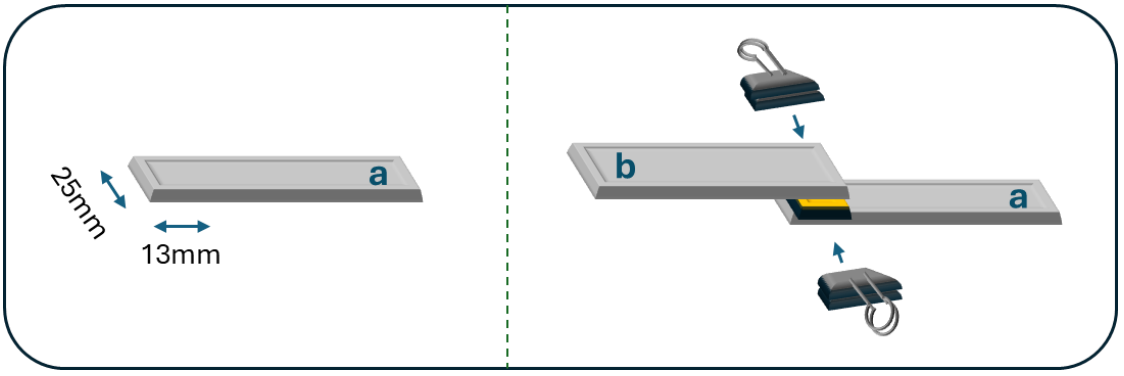

Figure 91. Substrate dimensions (left) and adhesive application (right).

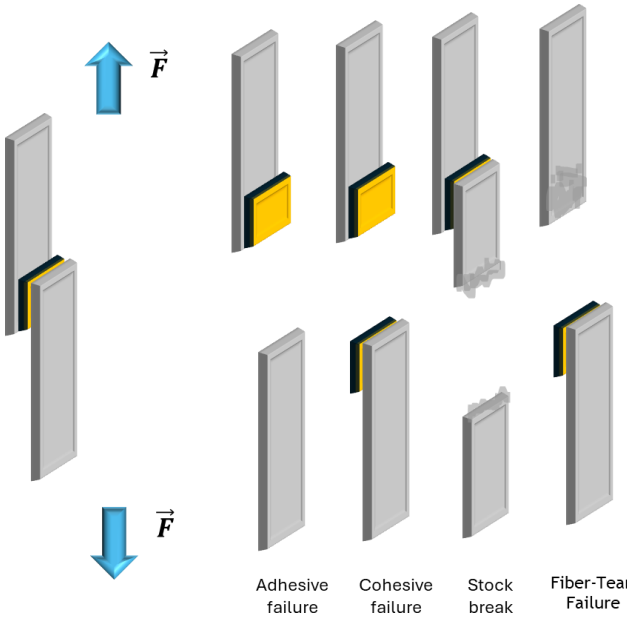

Figure 92. Scheme of force direction during the test and possible types of failures.

DSC measurements

DSC measurement **VU1-VU6**: three circles -40 to 200 °C.

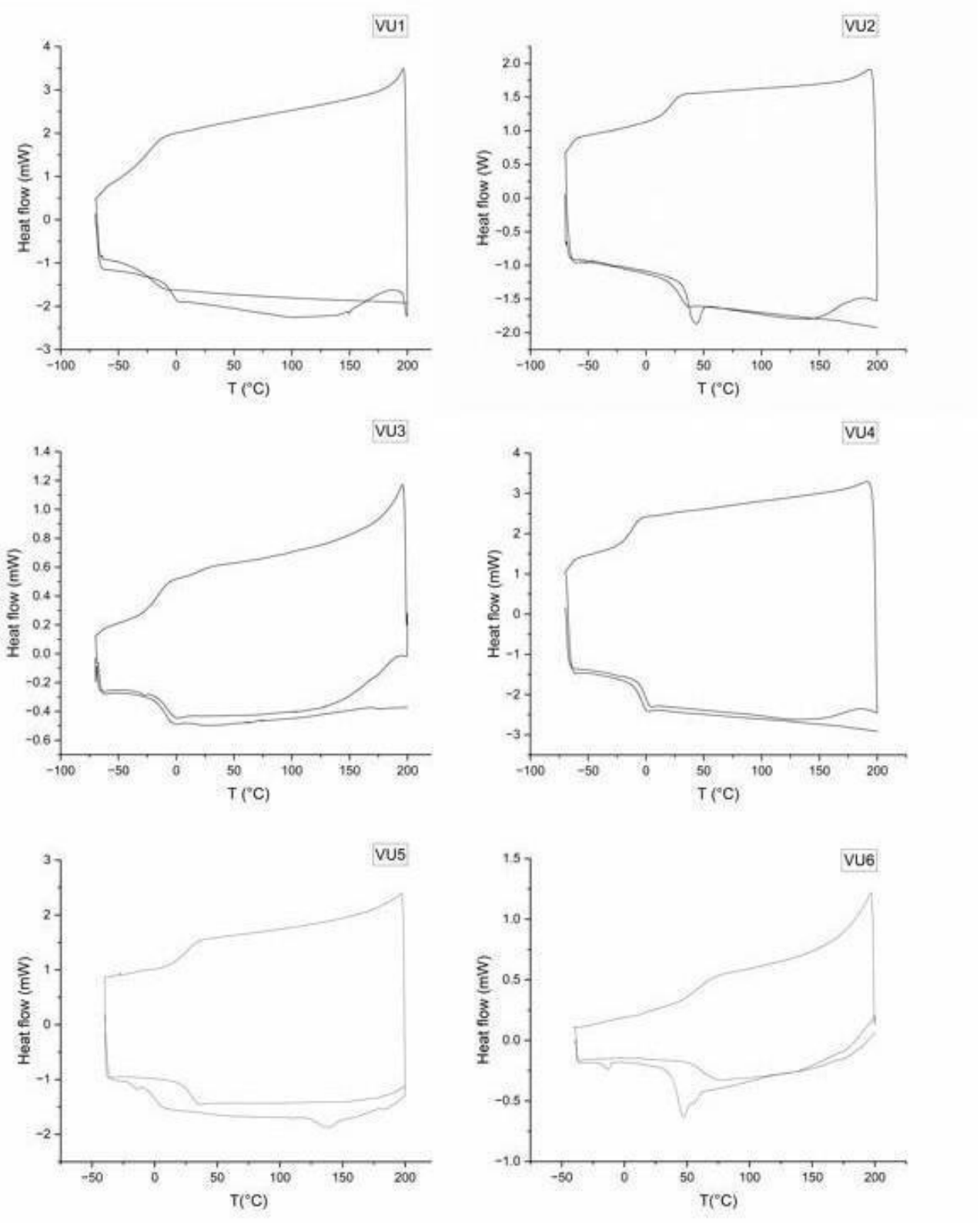

S 29. DSC measurement VU1-VU6: three circles -40 to 200 °C.

TGA measurements

TGA measurements of *VU1-VU6* from room temperature to 600°C. D= Dried, H=hydrated. No substantial difference was found in dried and hydrated samples, except for initial loss of water.

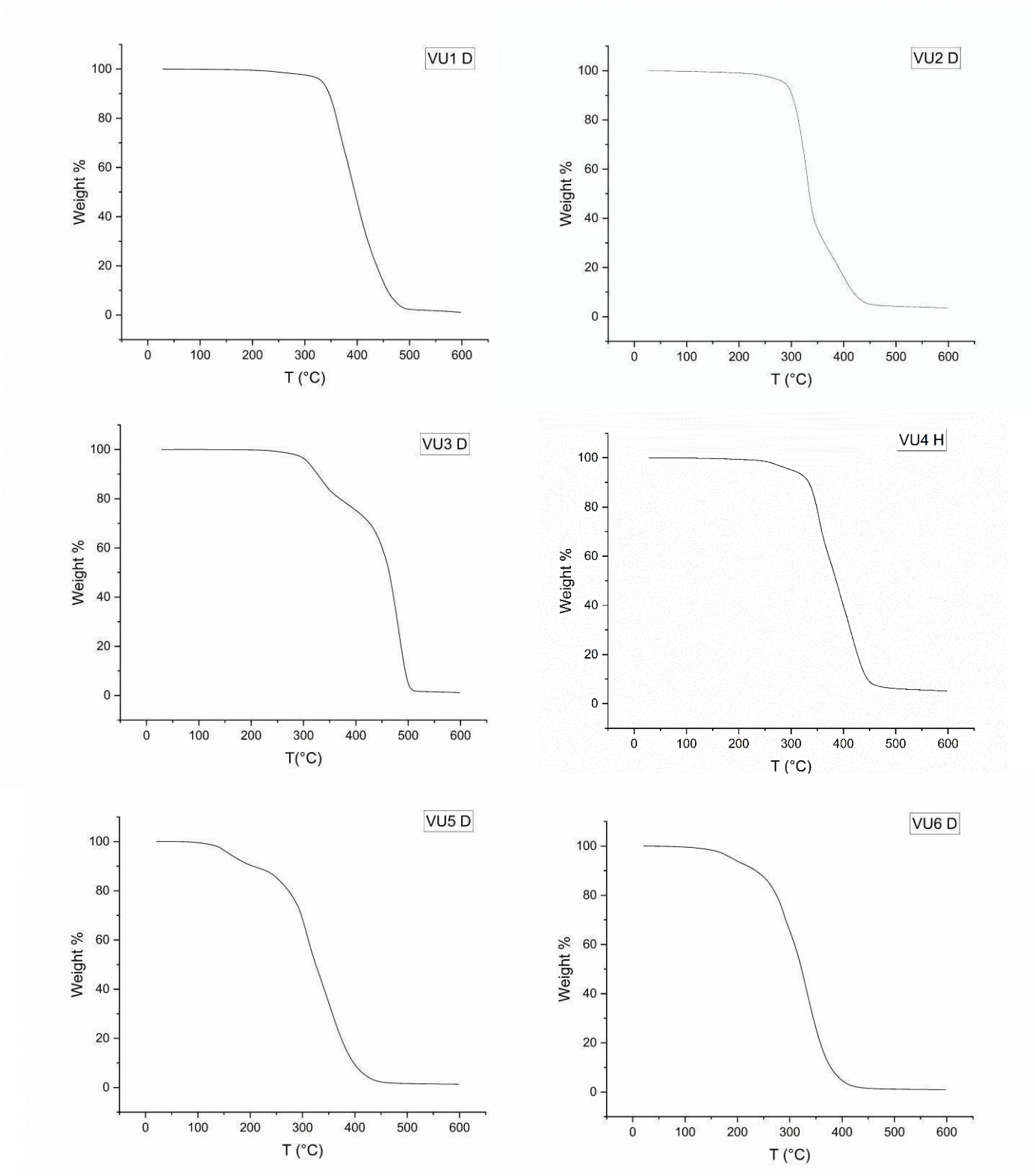

S 30. TGA measurements of *VU1-VU6* from room temperature to 600°C.

Tensile tests

Sample specifications. Standard dog bones shapes were manufactured with the follow dimensions: length 40 mm x width 10 mm x thickness 2 mm.

Stress-strain profiles of **VU1-VU4**.

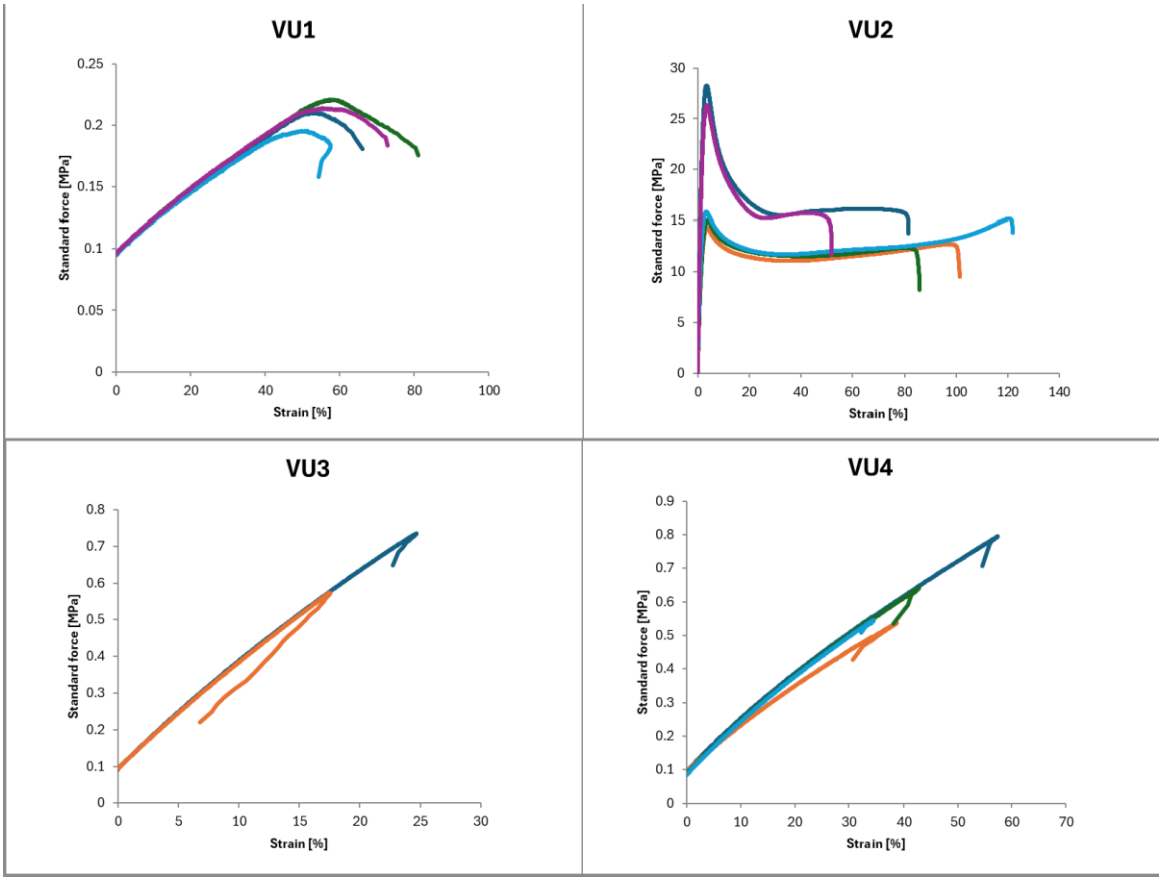

S 31. Stress-strain profiles of VU1-VU4.

DSC analyses *VU1-VU4* after reprocessing (R)

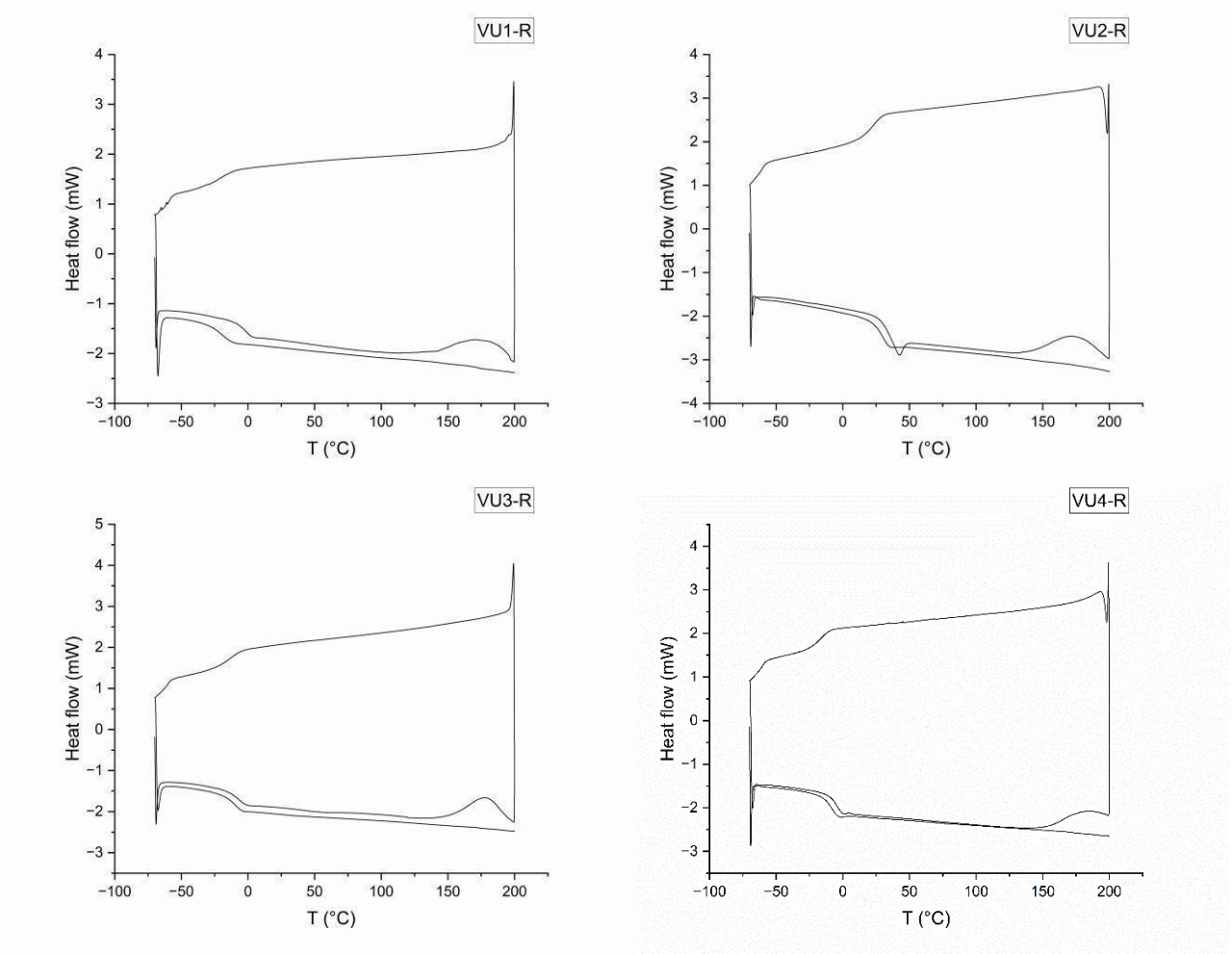

S 32. DSC analyses *VU1-VU4* after reprocessing (R).

4 CHAPTER 5: BIO-BASED POLY(HYDROXYURETHANE)S (PHUS)

4.1 PHU SYNTHESIS

In recent years, with the aim of developing more sustainable alternatives to petrol-based PU, diverse strategies were designed to produce PU-like polymers.[303, 304] Among the different strategies, the polyaddition reaction between di- or polyamines and bis- or polycyclic carbonates is the most explored.[154] The aminolysis reaction generates the so-called poly(hydroxyurethane)s (PHUs).[305] The structural difference between PUs and PHUs is the presence of primary and/or secondary hydroxy groups, which are absent in PU chains. The type of OH groups formed depends on the path of the ring-opening after the nucleophilic attack by the amine on the cyclic carbonate unit (Chapter 1, Figure 7).[306, 307] In PHUs, the presence of OH groups lead to increased hydrogen bonding and increased hydrophilicity, resulting in distinct properties in comparison to PUs (i.e. improved adhesive properties). Although this synthetic pathway is preferred to the isocyanate-based one of PUs, weaknesses of this approach are still present (Chapter 1). Firstly, the reactivity of cyclic carbonates towards aminolysis is limited. Usually, the reaction is slow and tough conditions are needed. [308–310] This translates into long reaction times or incomplete conversions. Consequently, different research groups are studying the synthesis of activated CC (ACC) to perform more efficient polymerization reactions.[311, 312] Due to these limitations, usually, PHUs show limited molecular weights. This can be also attributed to the reactivity of the monomers and the high H bond density.[313] Another way to overcome PHU limitations is to produce hybrid PHUs *via* co-polymerization or prepolymer formation strategies.[314, 315] The tuning of the reactivity and the presence of diverse functional groups can contribute to synthesis and properties improvements.[316] The newly formed NIPUs need to be fully investigated, as PHUs are a new advancing class of materials, compared to the well-established PU.

4.2 VEGETABLE OIL AND ERYTHRITOL-BASED PHUS

The previously synthesized polyamines (PAs) from HOSO and linseed oil (LO) were employed as a monomer together with a bio-sourced sugar-based cyclic carbonate. Due the presence of linoleic chains in LO (Figure 94), a higher degree of unsaturation is present (6 double bonds on average). A functionalization with 4 primary amino groups per triglyceride was achieved *via* the described photoinitiated thiol-ene reaction (Figure 1 and 2, Chapter 1, thiol-ene).

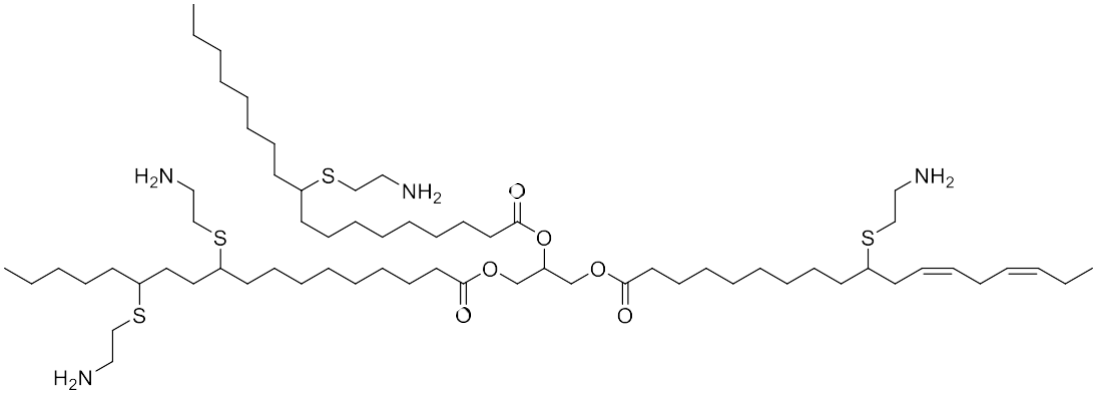

Figure 94. Chemical structure of linseed oil polyamine.

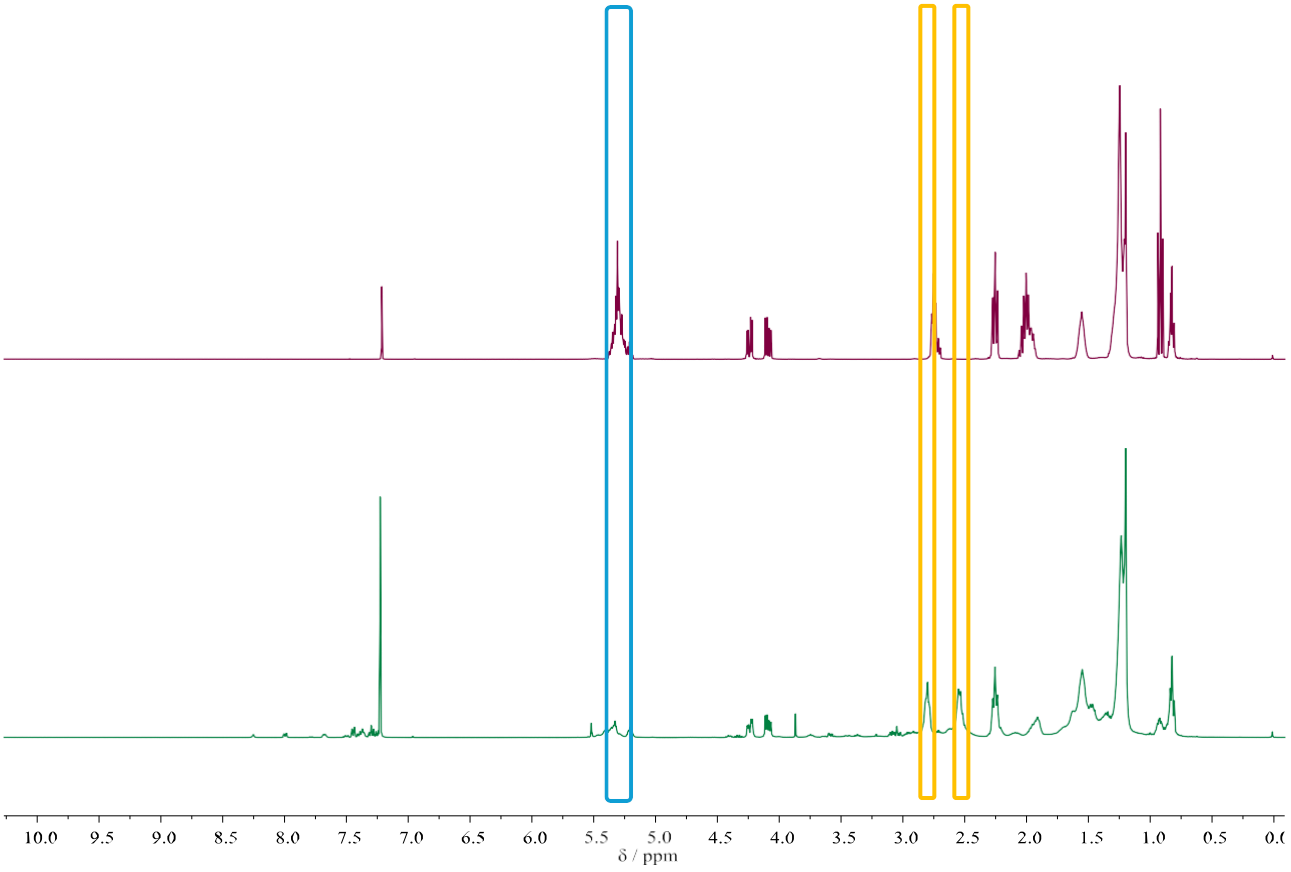

Figure 95. ^{1}H-NMR (400 MHz) of linseed oil (top) and linseed oil polyamine (LO-PA) in $CDCl_3$ (7.26 ppm). The blue box shows the decreasing in intensity of the double bonds peak. Yellow boxes indicate the two CH_2 groups of the alkyl chain of the linked cysteamine chain (bottom).

With the obtained vegetable oil polyamines, fully bio-based PHUs were produced. before that, a model reaction was carried out between HOSO-PA and propylene carbonate as CC benchmark. The conversion profile was screened along the time (Figure 96). Due to the liquid-viscous nature of the vegetable oil-

derived triamine and the liquid mono-CC, the reaction was carried out in bulk condition at 80°C under magnetic stirring.

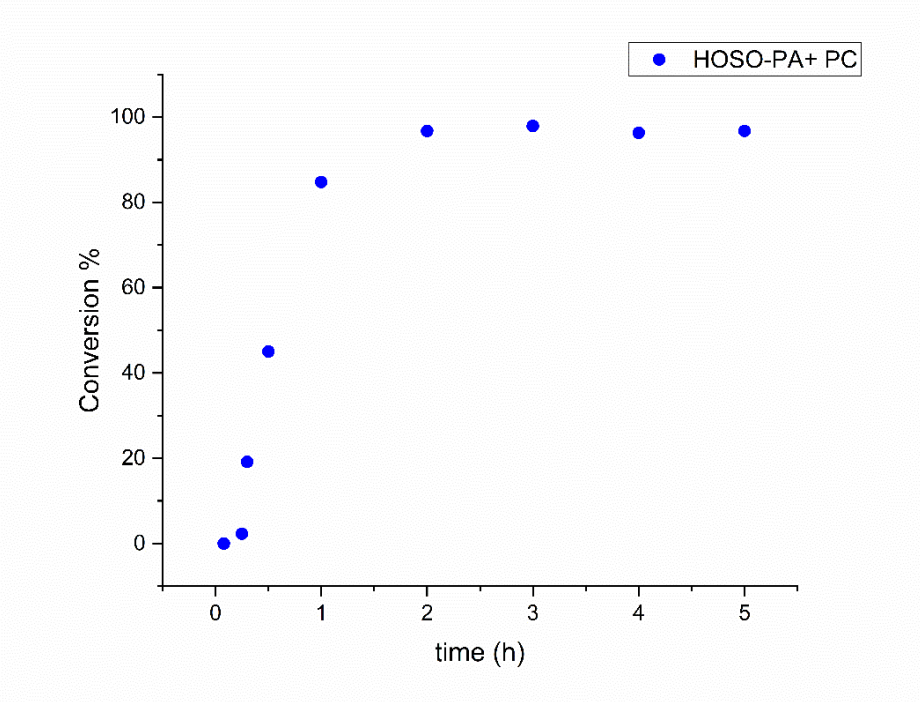

Figure 96. Conversion profile of the model reaction between high oleic sunflower oil polyamine and propylene carbonate.

The conversion monitoring was performed *via* proton NMR ($CDCl_3$) of different aliquots collected at determined time intervals. The evolution of the urethane NH proton peak at 6.0 ppm was monitored. As shown in the graphic (Figure 73), the kinetic plateau was reached already after two hours, with a maximum conversion detected at 5 hours, equal to 97%. Following, the subsequent step was to test bicyclic carbonates to synthesize fully biobased PHUs. Erythritol bis-carbonate CC (EBC) was used as a renewable comonomer, it can be easily obtained from erythritol and dimethyl carbonate straightforwardly (Figure 97).[77]

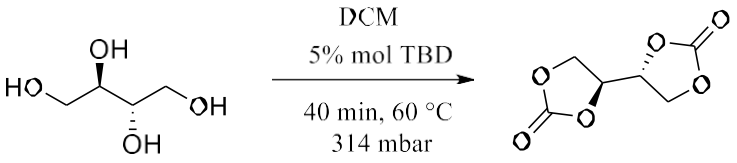

Figure 97. Synthesis of erythritol bicyclic carbonate (EBC) from erythritol and dimethyl carbonate (DCM).[77]

Erythritol is a natural sugar commonly used in the food and pharmaceutical sectors.[317] Due to its importance, improvements in its biological production on an industrial-scale have been carried out.[318] Due to its abundance in nature, it can be considered as a renewable feedstock.[76] A second long chain bis

carbonated monomer was tested to evaluate the difference in final properties of the PHUs obtained, namely 1,6-henadiol bis(cyclo carbonate) (HCC, Figure 98).

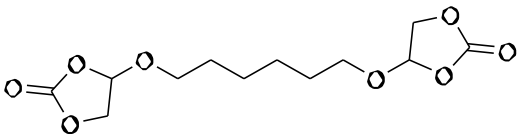

Figure 98. Chemical structure of 1,6-henadiol bis(cyclo carbonate) (HCC).

Firstly, the reactivity of HOSO-PA was evaluated with a model compound, such as propylene carbonate. It was known, from previous kinetic studies, that vegetable oil CC monomers presented a low conversion rate.[300] Therefore, a similar behaviour was expected. Unfortunately, some problems were encountered on performing these studies. The tests were carried out directly in deuterated solvent to being able to perform NMR analysis efficiently. Solubility issues were encountered performing the reaction in DMSO, leading to consequent unbalance of stoichiometric ratio between amine and carbonate groups. Therefore, the analysis was not valid to evaluating the kinetics. Alternatively, the same experiment was repeated in THF lowering the temperature to 80 °C, facing the same problem. In chloroform the amine is soluble, and the propylene carbonate is miscible, however the reaction could be only run at room temperature. Eventually, a model kinetic analyses was not possible.

The polymerization reactions were carried out in bulk condition at 100°C in an inert atmosphere (Ar) for 24 h. The equivalents of CC and -NH_2 were maintained at a 1:1 ratio. Four different thermosets were synthesized by combining of HOSO-PA or LO-PA with EBC or HCC (Table 30).

Table 30. Swelling index and gel content values calculated after swelling tests of PHU1-PHU4 in THF. T_gs registered *via* DSC analyses of PHU1, PHU2 and PHU4. Degradation temperatures at 5% wt. loss observed in TGA analyses registered until 600°C of PHU1, PHU2 and PHU4 samples.

Code	Amine	CC	Swelling index	Gel content	T_g (°C)	$T_{d,5\%}$ (°C)
PHU1	LO-PA	EBC	235	75	-20	242
PHU2	LO-PA	HCC	366	65	-6	202
PHU3	HOSO-PA	EBC	-	-	-	-
PHU4	HOSO-PA	HCC	1021	64	-26	266

The thermosets obtained with LO-PA (**PHU1** and **PHU2**) resulted in being solid gummy brown materials. Oppositely, with HOSO-PA, **PHU3** showed a honey-like consistency. **PHU4** obtained with HCC displayed a sticky-gummy brown feature.

FT-IR analyses were carried out to evaluate the PHU linkage formations. As an example, **PHU1** versus EBC FT-IR spectra are displaced in Figure 74 (further IR spectra can be found in the experimental section). The formation of the broad band in the 3000-3500 cm^{-1} region attributed to the O-H (primary and secondary hydroxyl group typical of PHU) and N-H stretching (Figure 74) can be noticed. Moreover, the formation of urethane linkages is observed in the region of 2000-1000 cm^{-1}. The O-C=O stretching vibration can be found at 1702 cm^{-1}, differently from the same vibration of the cyclic carbonates at 1759 cm^{-1}. Additionally, the C-N stretching appears at 1530 cm^{-1} (together with the N-H bending) and 1459 cm^{-1} (Figure 99).

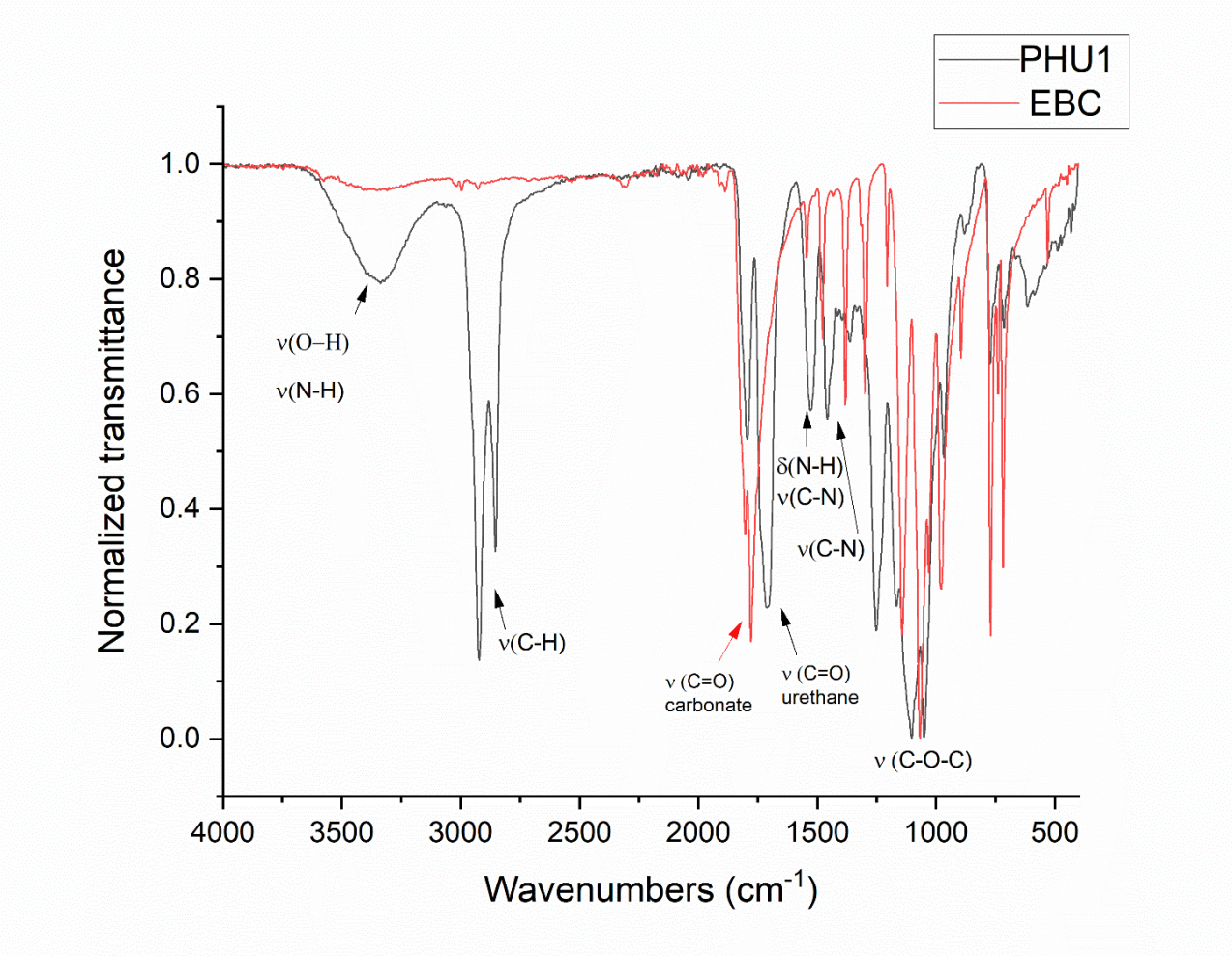

Figure 99. FT-IR of **PHU1** (black line) in comparison to erythritol biscarbonate (EBC, red line) with important vibrational band indicated.

To evaluate the crosslinking, swelling test were performed in THF. It was observed that the swelling index was particularly high for **PHU4** (Table 30). For **PHU2** and **PHU4**, indices of 235 and 366 were obtained. **PHU3** showed a complete dissolution in THF, indicating an incomplete crosslinking. All samples showed the presence of soluble components, as colouring of the solvent was observed. These residuals were further analysed by GPC (Figure 100). A similar gel content of about 65% was found for **PHU2** and **PHU4**, while for **PHU1** the gel content was 75% (Table 30).

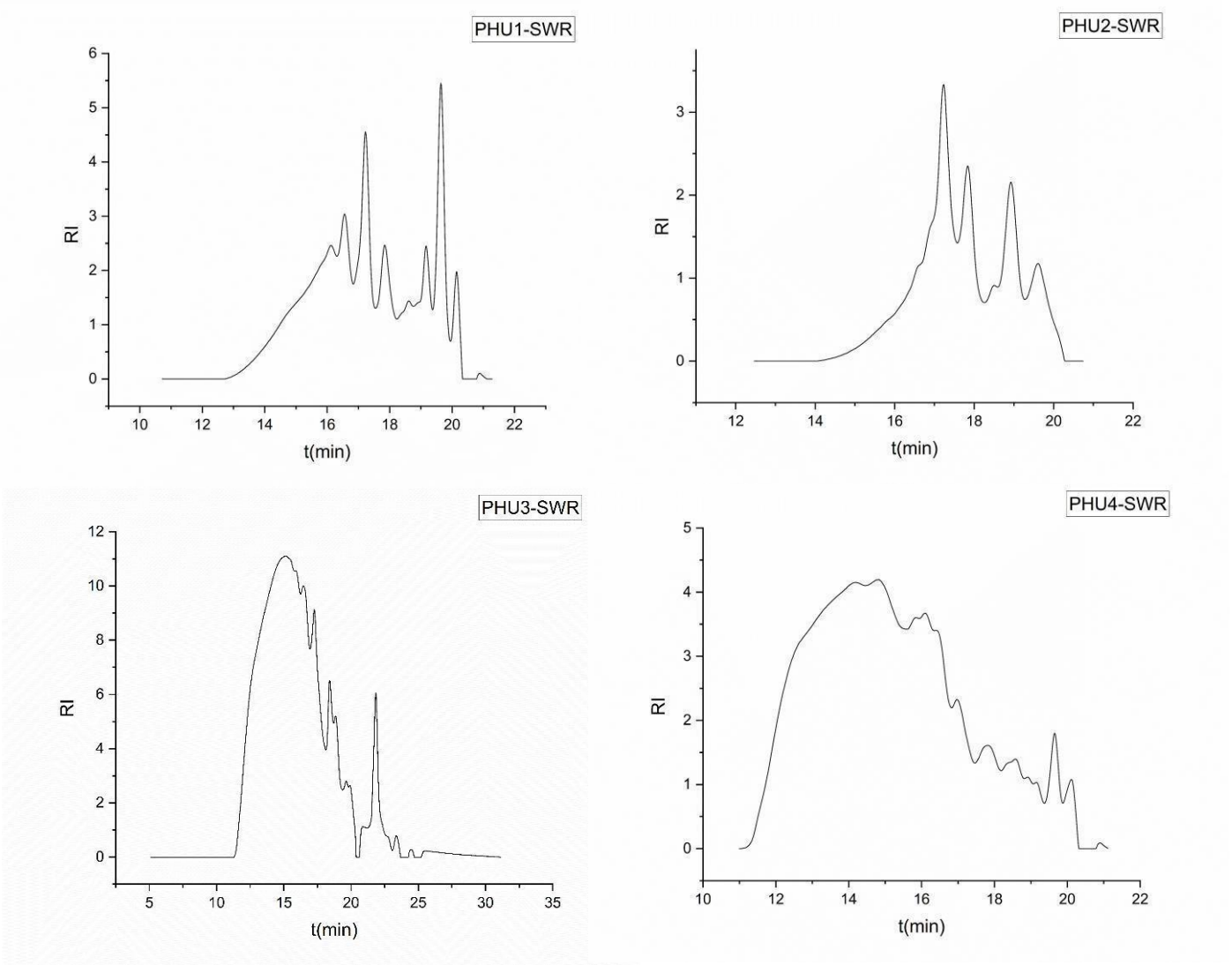

Figure 100. SEC (in THF) of the soluble part of **PHU1** to **PHU4** after swelling tests. SWR=swelling test residue

The DSC of the samples **PHU1**, **PHU2 and PHU4** were analysed (Figure 101). It was not possible to perform the analysis of the sample **PHU3** due to the liquid-viscous behaviour of the sample. All the thermoset exhibited T_g values below zero, i.e. -20 for **PHU1**and -26 °C for **PHU4**. A higher T_g was observed for **PHU2**, i.e. -6 °C. These values might be explained by the high aliphatic nature of all the thermosets, which does not allow strong interactions between the polymer chains, a low degree of cross-linking and a large mesh size in the network.

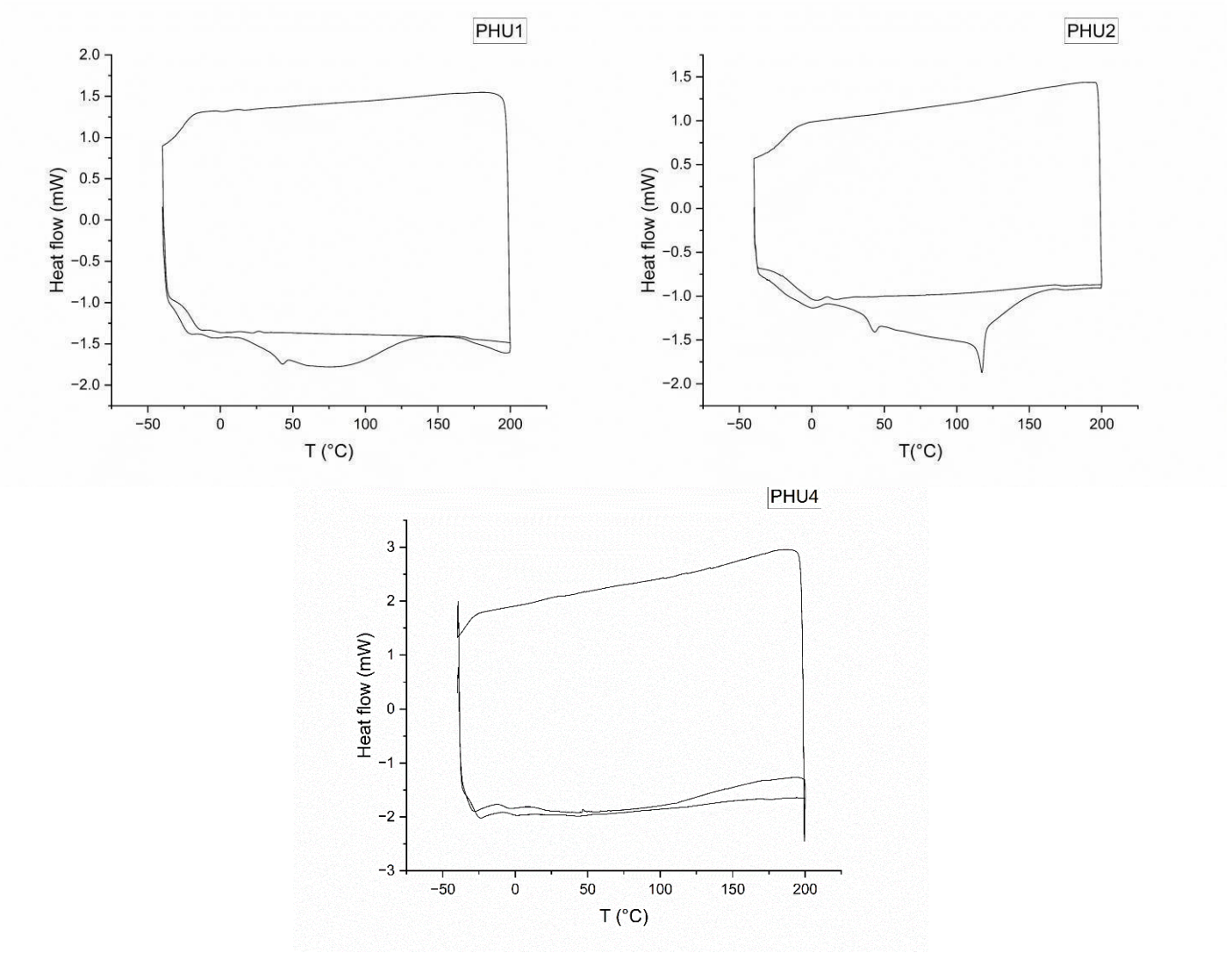

Figure 101. DSC analyses of **PHU1**, **PHU2** and **PHU4** from -40 °C to 200 °C (3 cyrcles).

By TGA analyses, **PHU1**, **PHU2** and **PHU4** were shown to resist temperatures above 200 °C (Table 30). In fact, **PHU2** showed 5% wt. loss at 202 °C, followed by **PHU1** (242 °C, Table 30). The highest degradation temperature at 5% weight loss was registered for **PHU4**, equal to 266°C. All the sample showed full degradation at 500 °C (Figure 102).

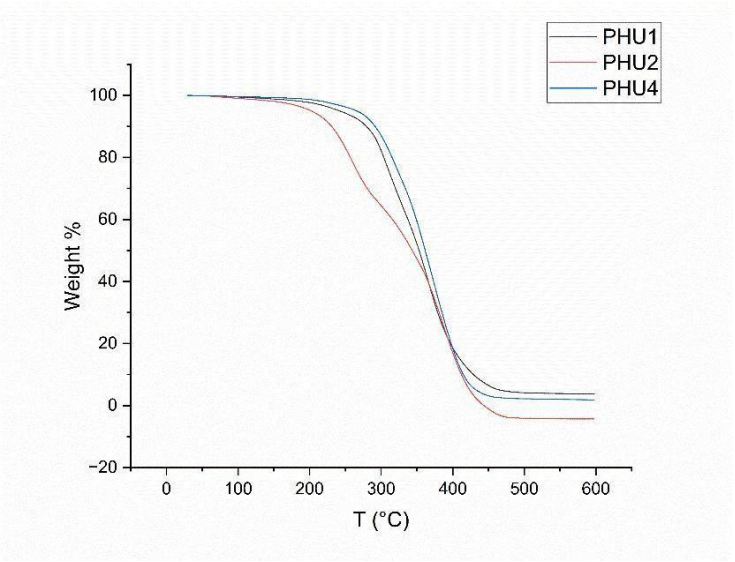

Figure 102. TGA analyses of **PHU1**, **PHU2** and **PHU4**.

4.3 VEGETABLE OIL AND LIGNIN-BASED PHUS

To broaden the research scope, other thermosets were developed employing lignin based-CC as co-monomer together with the HOSO-PA. In collaboration with a PhD student colleague, Celeste Libretti from the group of Prof. Dr. Meier, fully biobased thermosets were produced. Different formulations with diverse amounts of cyclic carbonate functionalized lignin (CCFL) were tested. As also shown in a previous publication, the intrinsic aromatic nature of lignin led to highly brittle materials. In order to tune the properties of the final thermosets, a tri-component thermoset was developed by Celeste Libretti using HOSO-PA, EBC and CCFL. The stiff structure of lignin was balanced with the presence of the long aliphatic chains present in the HOSO and LO-PA. and EBC was used as a co-monomer. A reference material consisting of EBC with HOSO-PA was previously described. Moreover, the blank test of CCFL and HOSO-PA yet exhibited a fragile structure.

Table 31. Thermoset compositions, their T_g and decomposition temperatures at 5%wt measured by DSC and TGA, respectively.

	LC %wt.	CCFL eq.	EBC eq.	HOSO-PA eq.	T_g (°C)	$T_{d,5\%(°C)}$
T1	26	0.15	0.85	1	-30-60	287
T2	38	0.25	0.75	1	20-80	290
T3	56	0.50	0.50	1	80-120	301
T4	67	0.75	0.25	1	90-130	307

LC= lignin content. CC:NH_2 groups were always kept 1:1 molar ratio. TBD catalyst was used in 0.1 eq in all the entries.

The molar ratio of CC and amino groups was maintained 1:1. The compositions developed contained 26% wt. (**T1**) of CCFL, 38% wt. (**T2**), 56% wt. (**T3**) ad 67% wt.(**T4**) of CCFL (Table 32). Consecutively also the EBC:CCFL content was modulated according to this parameter (i.e. **T4**= EBC 0.75 eq and CCFL 0.25 eq; Table 31). Curing time was established to be optimal after 2.5 days at 150°C. The curing process was monitored by FT-IR.

All the samples were analysed by DSC, TGA and WCA. Moreover, it was possible to measure DMA of **T2**. All thermosets presented a higher thermal stability. Lignin is responsible of thermal stability and this was evident from TGA analyses. While increasing in CCFL content, the degradation temperature was also increasing ($T_{d,5\%}$ = 287 °C, for **T2**; $T_{d,5\%}$ = 307 °C for **T4,** Table 32). The evaluation of the T_g resulted to be difficult due to the broad T_g step in the curve, due to the heterogeneity of the material. The heating speed was increased in order to obtain a clearer thermal transition (from 10 to 30 K/min), however with no visible improvement. It was thought to perform DMA analyses in order to obtain a clearer T_g value, however it was only possible to measure DMA of **T2** due to the material brittleness (Figure 103, Table 32).

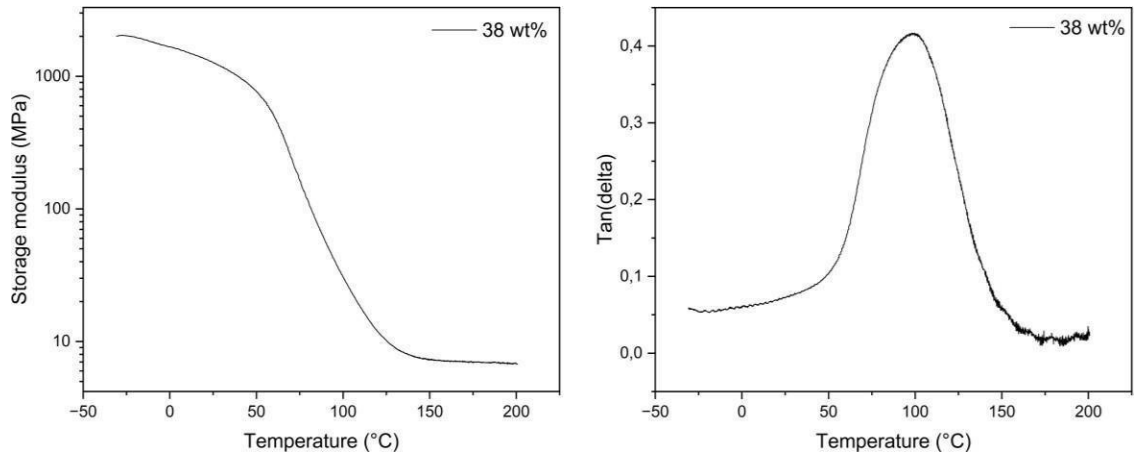

Figure 103. T2 (38 wt% lignin content) DMA analysis. Storage modulus (E') curve against temperature for the, left side). Curve of the tan (δ) against temperature (right).

The material showed a storage modulus below T_g from 1970 MPa at - 30 °C to 1220 MPa at 25 °C. Subsequently, the modulus dropped to a minimum equal to E' = 5.72 ± 2.41 MPa at 150 °C (Table 32). The T_g (or α relaxation temperature, T_α) causes a large change in the material's elasticity, resulting in a decrease of the storage modulus and a peak in the tan(δ) curve. This is mainly attributed to the aromatic unit present and to the crosslinking density. The glass transition can be measured from the onset of the storage modulus or the temperature at the maximum of the tan(δ) peak. Storage modulus vs temperature usually gives the lowest value of T_g and it is often a good indicator of when the mechanical strength of the material starts to fail. Knowing this value is crucial for future application of the material. In the second graphic, (Figure 80, right) a T_g of 97.3 °C (max peak tan(δ), Table 32) was detected.

Table 32. DMA analysis results of **T2** (38 wt.% lignin content).

wt% lignin	$E'_{-30°C}$ (MPa)	$E'_{25°C}$ (MPa)	$E'_{150°C}$ (MPa)	Tg (°C) Onset E'	Tg (°C) Max tan δ
38	1970 ± 386	1220 ± 223	5.72 ± 2.41	55.2 ± 2.4	97.3 ± 4.1

Results are the average of three measurements.

Water contact angle (WCA) analyses were conducted to evaluate hydrophobic character of the thermosets (static single-drop measurements). Due to aromaticity of lignin and the elevated aliphatic character of HOSO-PA the polymer is expected to be quite hydrophobic. With the amount of HOSO-PA being constant for all the thermosets, it was concluded that the hydrophobic character of the materials was increasing proportionally with the crescent amount of lignin present. Similarly, the lignin content is contributing to the crosslinking. In fact, it was noticed that the highest gel content was obtained for the **T4** composition (98%). Moreover, the lowest was obtained for **T2**. CCFL (79%). As expected, the swelling index value and the gel content displayed an opposite behaviour.

4.4 Conclusion

The synthesis and optimization of vegetable oil polyamines gave the chance to develop new poly(hydroxyurethane)s (PHUs). In this specific case, PHUs from renewable resources were obtained. Two different biobased cyclic carbonates (CC) were tested as co-monomers, such as the erythritol biscarbonate (EBC) and 1,6-hexanediol bis(cyclo carbonate) (HCC). It was noticed that the higher amine functionalities present in LO-PA showed better crosslinking, even though higher GC are desirable for thermoset materials The aliphatic nature of the amines give reason of the low T_g measured (-26 to -6). A quite high resistance to degradation of the PHUs was displayed by TGA analyses, having a starting degradation at temperatures >200°C. A third component might be useful to improve the crosslinking network and T_g values of thermoset deriving from vegetable oils amines. As a consequence, using HOSO-PA and EBC thermosets were developed with lignin cyclic carbonates (CCFL) in the described collaborative project. Comprehensively, a trend in T_g, and wettability properties was observed in relation to the lignin content. Generally, keeping the amount of amine fixed, the main differences between the polymeric material properties resulted from the level of aromatics present in the final material. Among the different formulations, the 36% wt. lignin content resulted to be the best due to the chemical structure balance resulting in stiffness, low brittleness, crosslinking density (GC = 87%) and T_g (97°C).

As future perspectives, biocompatibility and biodegradability tests would be interesting to investigate. Moreover, mechanical tests, such as lap shear and tensile tests, could help to establish possible applications of these new fully bio-based thermosets.

4.5 EXPERIMENTAL DATA

Characterization methods

NMR analyses

All NMR characterizations have been performed on a Bruker advance 400 MHz spectrometer equipped with a cryoprobe. ^{1}H spectra result from 16 scans acquisitions while ^{13}C spectra were obtained from 1000 scans. The analyses were performed in $CDCl_3$ or DMSO-d6.

FTIR analyses

Fourier Transform InfraRed (FTIR) spectra were recorded on a Bruker-VERTEX 70 instrument (400 to 4000 cm-1, 4 cm-1 resolution, 32 scans, DLaTGS MIR) equipped with a Pike GladiATR optical design diamond crystal) for attenuated total reflectance (ATR).

Size Exclusion Chromatography (SEC)

SEC measurements were performed in THF on a PSS SECcurity^2 GPC system based on Agilent infinity 1260 II hardware. The system was equipped with an autosampler SECcurity^2, a SECcurity^2 isocratic pump, a column oven (Bio)SECcurity^2 column compartment TCC6500, and a refractive index detector SECcurity^2 RI. Analysis was performed using two PSS SDV analytical columns (3 µm, 300 × 8.0 mm^2, 1000 Å) with a PSS SDV analytical precolumn (3 µm, 50 × 8.0 mm^2). The flow rate for measurements was set to 1 mL·min^{-1}. The system was calibrated with narrow linear poly(methyl methacrylate) standards (Polymer Standards Service, PSS, Germany) ranging from 102 to 62200 Da.

Differential Scanning Calorimetry (DSC)

DSC measurements were performed on a Mettler Toledo DSC1 instrument equipped with a sample robot. Samples of 5–10 mg were loaded in a 100 µL aluminum crucible with pierced lid, and the measurements were performed under nitrogen atmosphere with a flow rate of 50 mL·min^{-1}. The DSC thermograms were recorded at a heating/cooling rate of 10 K·min^{-1} using the following heating/cooling program: first heating from 20 to 110 °C, then cooling from 110 to −70 °C, and a final heating step from −70 to 110 °C. The data from the last heating step are shown in the DSC curves.

Thermogravimetric Analysis (TGA)

TGA measurements were carried out on the TA Instruments TGA 5500 under nitrogen atmosphere using platinum TGA sample pans and with a heating rate of 10 K min-1 over a temperature range from -40 to 600 °C. Thanks to Théato research group (KIT) for the instrument availability.

Materials

Organosolv beech wood lignin was kindly donated by the Fraunhofer Center for Chemical Biotechnological Processes CBP (Leuna, Germany). 1,6-henadiol bis(cyclo carbonate) (HCC) was kindly provided by the laboratory of Chemistry of Liege University from Dr. Bruno Grignard. High oleic sunflower oil (Rapunzel), high oleic sunflower oil (Alnatura), 4-(hydroxymethyl)-1,3-dioxolan-2-one (glycerol carbonate, 90%, BLDPharm), 2,2-dimethoxy-2-phenylacetophenone (DMAP, 99%, Thermo Scientific), ethyl(2,4,6-trimethylbenzoyl) phenyl phosphinate (TPO-L, >95%, TCI), N-hydroxy-5-norbornene-2,3-dicarboxylic acid imide (NHND, 97%, Alfa Aesar), Chromium(III) acetylacetonate (99.99% trace metal basis, Sigma Aldrich), meso erythritol (99%, Alfa Aesar), dimethyl carbonate (anhydrous, > 99%, Sigma-Aldrich), 1,8-diazabicyclo[5.4.0]undec-7-ene (DBU, > 98%, Fluorochem), 1,5,7-triazabicyclo[4.4.0]dec-5-ene (TBD, > 98%, TCI Chemicals), pyridine (≥99%, Sigma Aldrich), N,N-dimethylacetamide (99.5%, anhydrous, dried over molecular sieves, Thermo Scientific), dichloromethane (DCM ≥99%, Fisher Chemicals), chloroform (≥99.8%, Fisher Chemicals),

1,4-dioxane (Fluka Chemicals, 99.5%), ethanol (>99.8%, Fisher Chemicals), and propan-2-ol (>99.5%, Fisher Chemical) were used without further purification. Deuterated solvents (DMSO-d6 and CDCl3) were purchased from Eurisotop.

General PHU synthesis procedures

Equimolar NH2:CC group of the two monomers (HOSO-PA or LO-PA with EBC or HCC) were weighed in a Schlenk flask and flushed with argon. The reaction mixture was placed in an oil bath and kept stirring at 100 °C for 24 h.

***PHU1**- Linseed oil polyamine (LO-PA) and erythritol bis-cyclic carbonate (EBC)*

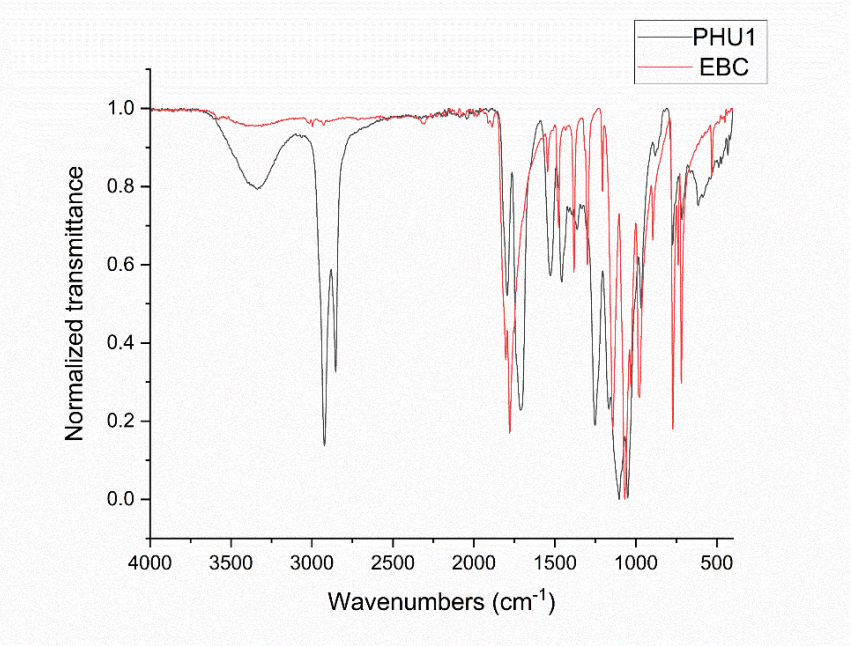

S 33. PHU1 FT-IR Vs erythritol biscarbonate (EBC).

***PHU2**- Linseed oil polyamine (LO-PA) and 1,6-hexa(cyclo carbonate) (HCC)*

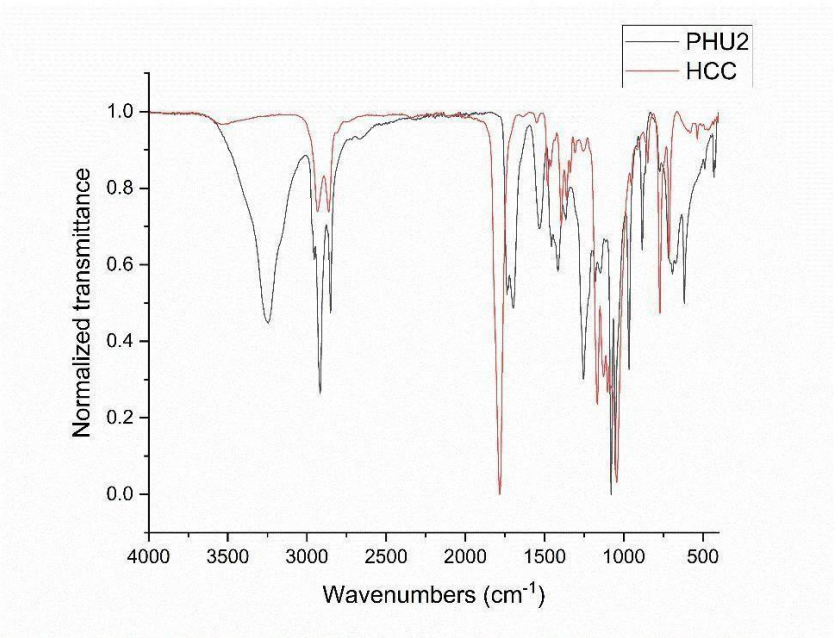

S 34. *PHU2 FT-IR Vs 1,6-hexa(cyclo carbonate) (HCC).*

***PHU3**- High oleic sunflower oil triamine (HOSO-PA) and erythritol bis-cyclic carbonate (EBC)*

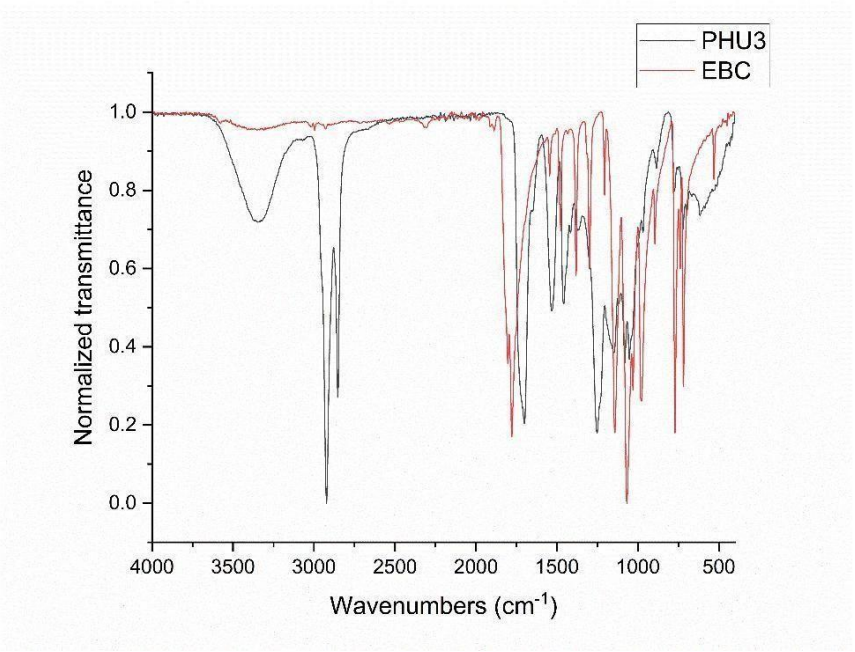

S 35. PHU3 FT-IR Vs erythritol biscarbonate (EBC).

***PHU4**- High oleic sunflower oil triamine (HOSO-PA) and 1,6-hexa(cyclo carbonate) (HCC)*

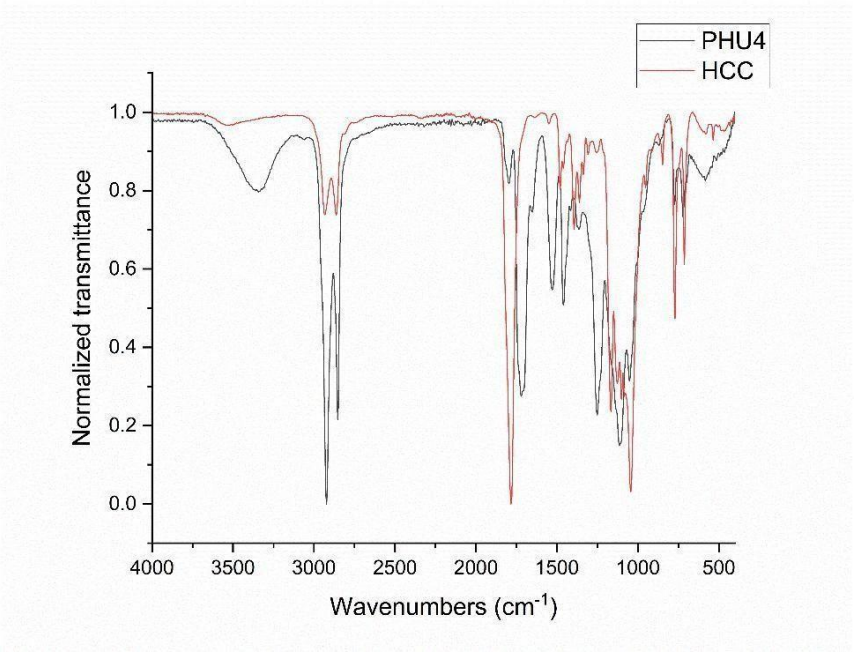

S 36. PHU4 FT-IR Vs 1,6-hexa(cyclo carbonate) (HCC).

Swelling tests. About 500 mg of each sample were placed in THF (100g/5mL) for 24h. After, the swelling index was calculated as follows:

$$SI = \frac{W_s - W_0}{W_0} . 100$$

where W_s is the weight of the swollen material and W_o corresponds to the initial weight of the material.

Afterwards the solvent was removed and the saple placed in oven at 50°C for 24 h. Subsequently, gel contents were calculated as follows:

$$Gel\% = \frac{W_d}{W_o}.100$$

where W_d is the weight of the dried material after being swollen and W_o corresponds to the initial weight of the material.

Figure 104. Swollen (left) and dry (right) samples of **PHU1** (56), **PHU2** (57) **PHU4** (58). The PHU samples were placed in THF for 24h, afterwards the solvent was removed (swollen samples, left) and the samples dried in oven for 50°C for 24h.

SEC measurement of soluble fractions after swelling tests (SWR)

Table 33. Molecular weights registered for the solvent residue from swelling tests of PHUs by GPC (THF).

	Mn	**Mw**	**Mz**	***Đ***
PHU1	8.2E+2	2.3E+3	4.9E+3	2.8
PHU2	7.8E+2	1.3E+3	2.1E+3	1.7
PHU3	2.5E+2	7.1E+3	1.0E+5	2.8
PHU4	2.1E+3	9.5E+3	2.5E+4	4.8

GPC analyses (residue swelling tests-SWR)

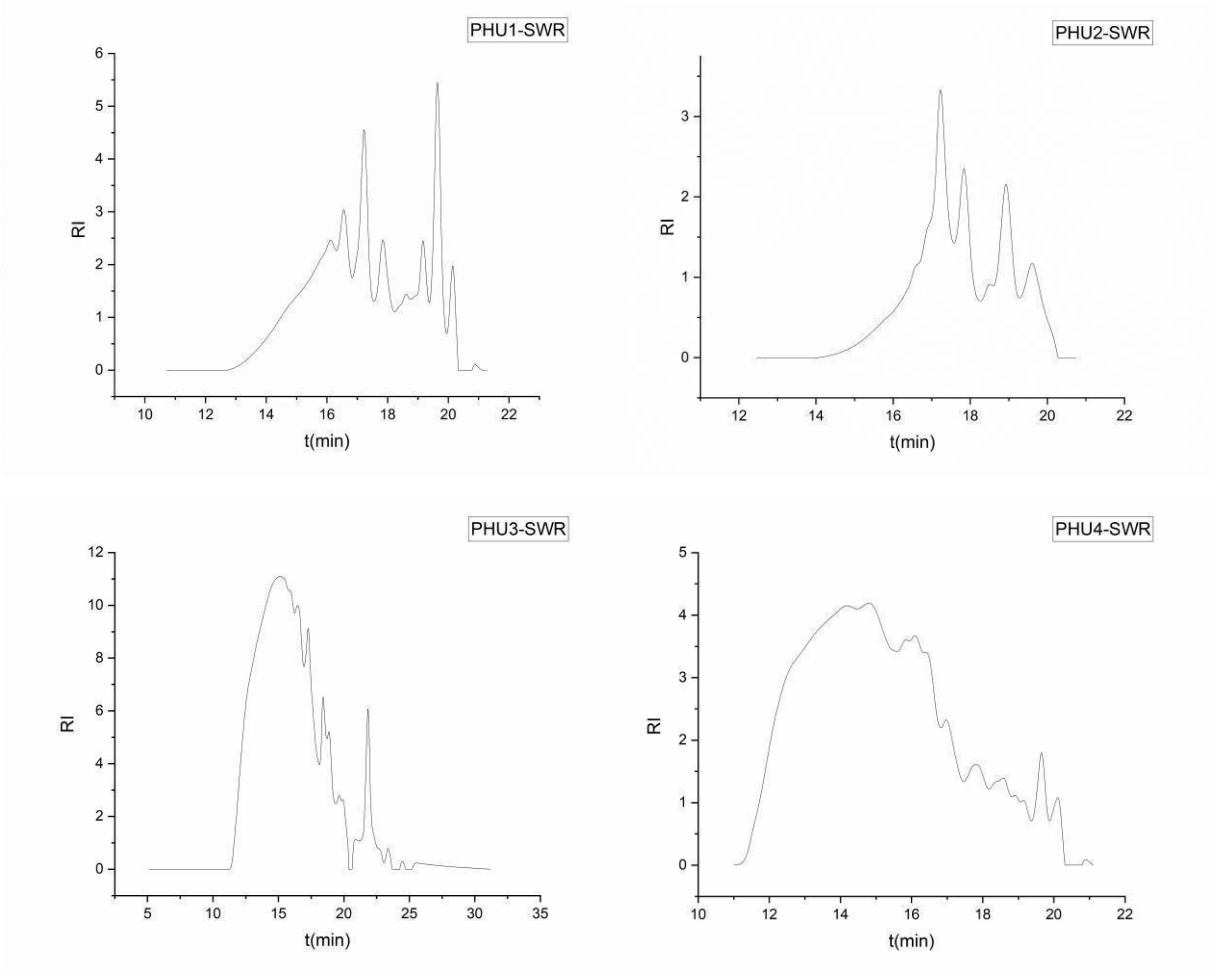

S 37. PHU1-PUH4 GPC analyses of residues after swelling tests-SWR.

DSC analyses

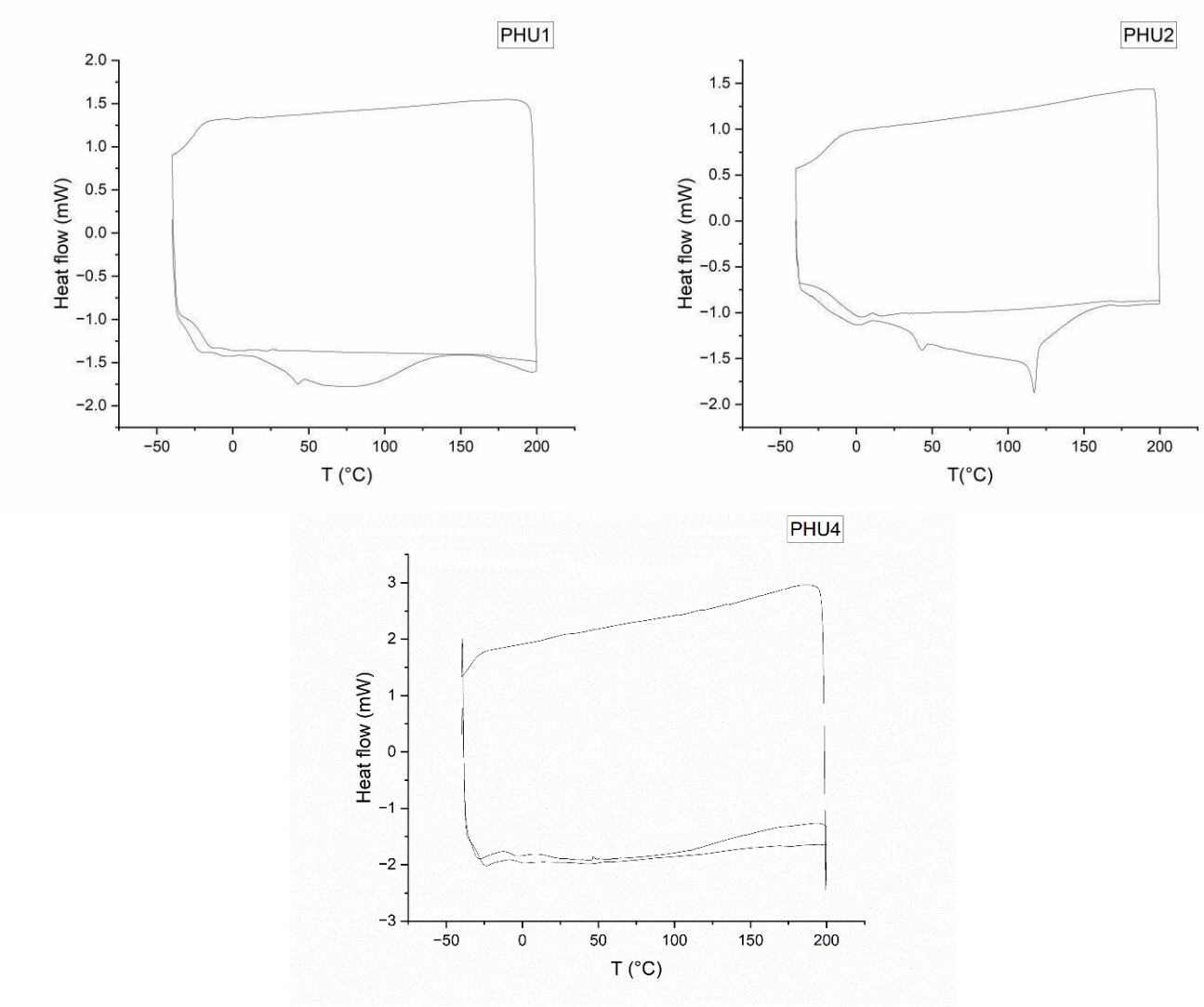

S 38. PHU1-PUH4 DSC analyses (-30 – 200°C).

TGA analyses

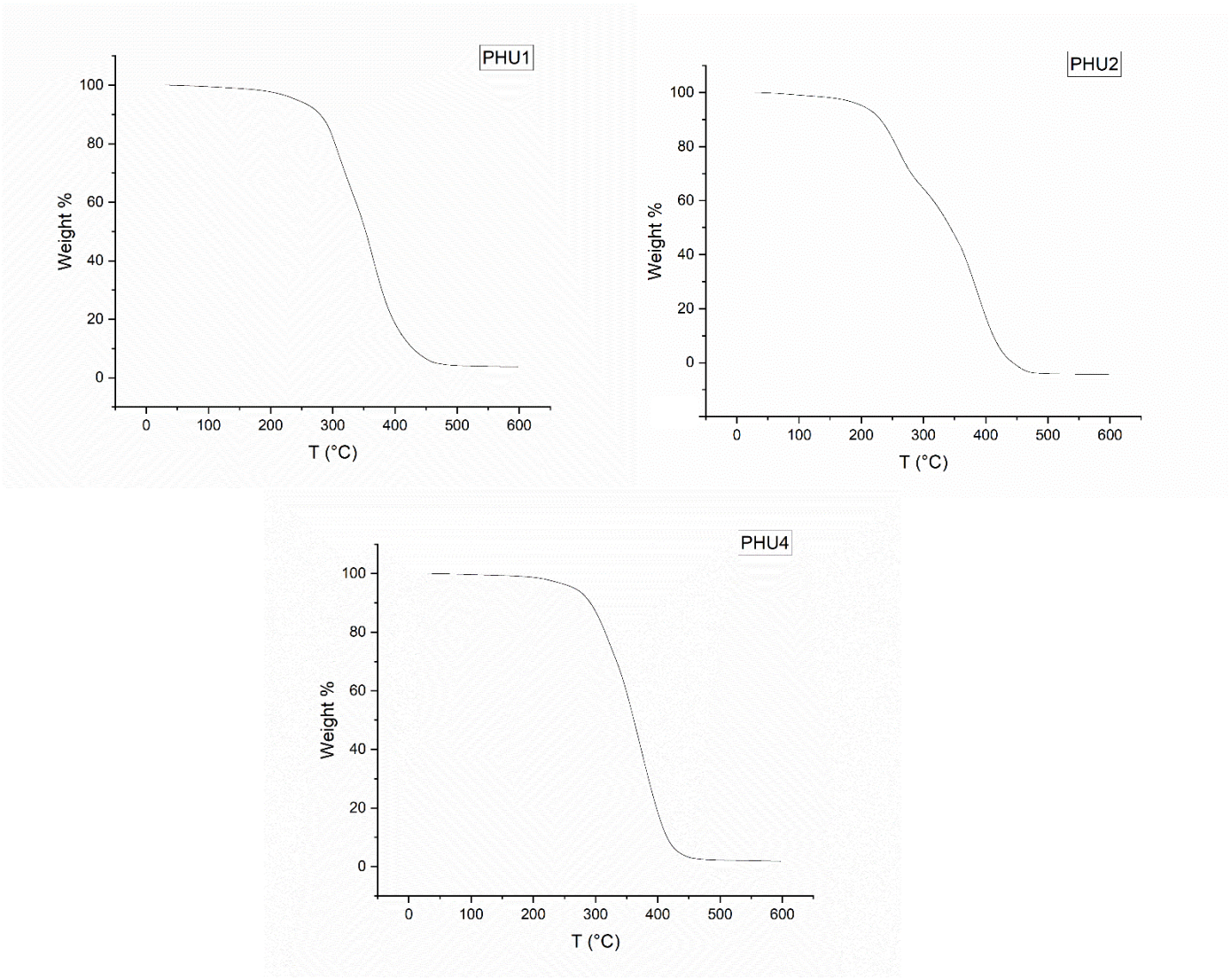

S 39. PHU1-PUH4 TGA analyses (25 – 600°C).

5 CHAPTER 6: FULLY AND PARTIALLY BIO-BASED EPOXY RESINS

5.1 EPOXY RESINS

Epoxy resins are versatile materials finding applications in various fields such as construction,[320] automotive,[321] electronic,[322] marine[323], and others.[324–326] An epoxy resin can be defined as a molecule containing a minimum number of two epoxy rings, or it can also indicate a material derived from the previous. In the second case, epoxy rings are not anymore present in the structure after reacting with a second component, such as an amine hardener. Epoxy resins were discovered by Prileschajew in 1909,[327] while the first commercialised product was launched in 1938 by De Trey Frères company (Zurich, Switzerland).[328] A widely exploited difunctional epoxy is the diglycidyl ether of bisphenol A (DGEBA), usually obtained by the diglycidylation of bisphenol A (BPA) with epichlorohydrin in the presence of a base (sodium hydroxide).[329] Indeed, the most frequent and effective strategy to achieve epoxy-functionalized compounds is to react hydroxy-containing molecules with epichlorohydrin.[329] To minimize the impact of the synthesis, bio-based epichlorohydrin from glycerol has been developed by Solvay (Epicerol®). In recent years, different regulations have been introduced by the European Commission restricting the use of bisphenols in different production sectors such as cosmetics,[330] food,[331] toys,[332] or paper printing.[96] The high safety concern is due to the toxicity of this class of molecules, specifically for the human endocrine system, and the adverse effects on the environment.[333, 334] In 2021, REACH included three bisphenols (BPA, BPB and 2,2-bis(4'-hydroxyphenyl)-4-methylpentane) to the list of substances of very high concern (SVHC).[335] Major attention was pointed to food containers, since often food cans are coated with epoxy resins as anticorrosion agents, which can release monomers to the food contained.[336] The tolerable daily intake (TDI) of bisphenol A equals 0.2 ng/kg of body weight per day.[337] Diverse scientific studies investigated the toxic effects of this compound.[338] Due to the high relevance of bisphenols in polymers production (polycarbonates and epoxy resins), diverse groups researched for less hazardous and bioderived alternatives.[325,338–340] Examples are diglycidyl derived from isosorbide,[341] soybean oil,[342] or resorcinol.[343] However, their synthetic pathway involves the classic epichlorohydrin route.[329] Due to the toxicity of epichlorohydrin,[120, 121] alternative pathways have been developed to synthesize epoxies.[119] A different synthetic approach is the epoxidation of olefins with peracids. Gross *et al*. performed an esterification reaction between adipic acid and allyl alcohol followed by an epoxidation reaction using meta-chloroperoxybenzoic acid (mCPBA) with an overall 52% yield.[344] Moreover, also mCPBA is a chemical of concern due to its high toxicity (acute toxicity- category 4). Also, epoxidized vegetable oils are generated *via* the peroxidation reaction of their double bonds.[345] The conversion of palm olein to the epoxidized product was achieved by in-situ formation of peracetic acid or performic acid with high conversion (95.5%).[346]

Enzymatic pathways were also investigated to carry out the epoxidation of diverse unsaturated fatty

acids. Warwel *and coll.*[347] employed an immobilized *Candida antarctica* lipase reaching major yields between 68-91%. More recently, modified gallic and vanillic acids where epoxidized with the same enzyme in moderately harsh conditions (toluene, 48h).[348]

During the epoxy resin formation, two reaction mechanisms can occur between the epoxy and the specific functional group of the co-monomer:[349] Chain-growth and step-growth polymerization, of which the first can be distinguished into cationic and anionic pathways (Figure 105). Chain-growth polymerization occurs in four steps (initiation, propagation, chain transfer and termination). During the initiation step, a cation or an anion is generated (active centre of the polymerization) by chemical reaction or light irradiation. These ions subsequently generate primary chains, which continue growing over time by the subsequent addition of monomers (propagation). During this process, the centre of the polymerization is always present at the end of the chain. At the end, this process is interrupted by a chain transfer or a termination step.

1)Cationic chain-growth polymerization

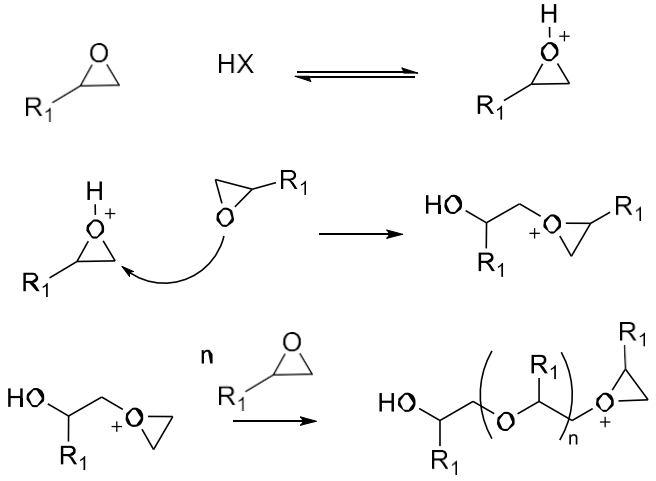

2)Anionic chain-growth polymerization

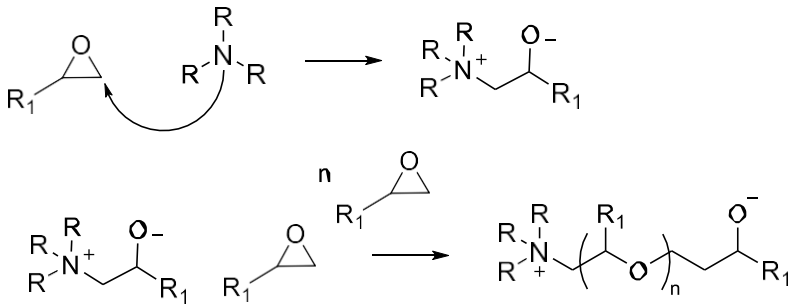

Figure 105. Representation of epoxide-based chain-growth polymerizations; 1) cationic and 2) anionic pathways.[350]

Commonly, anionic polymerization takes place with imidazole derivatives and tertiary amines (alkali hardeners). Cationic chain-growth is usually initiated by oxonium and onium salts and BF_3 complexes.[328]

Step-growth polymerizations advance step-by-step by consecutive addition of monomers (Figure 106). The number of functional groups and the ratio between these functionalities with the one of the monomers are the controlling factors of the polymerization. Step-growth polymerization occurs, for instance when using acids, isocyanates, thiols, phenols and amines.[349] The main difference between the two mechanism is the kinetic of the process.[351–353]

Step-growth polymerization

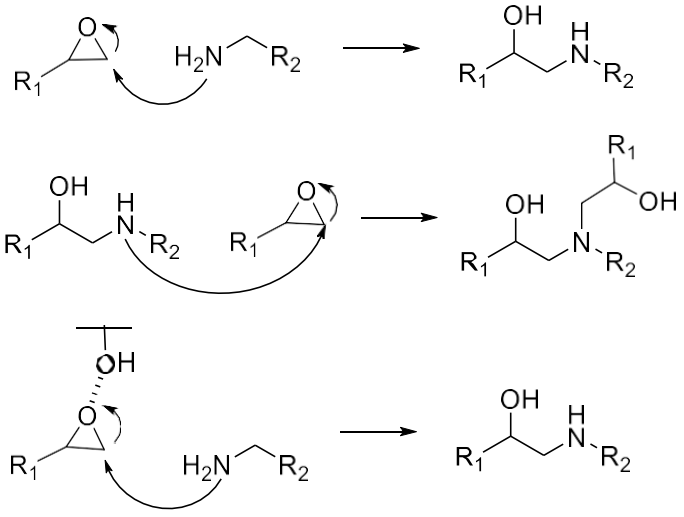

Figure 106. Representation of epoxy and amino groups reaction in step-growth polymerization.[350]

The compounds reacting with epoxides are commonly called *hardeners* or *crosslinkers,* which act as nucleophiles.[156] To obtain linear epoxy polymers, the two monomers have to present functionality of 2. Differently, to achieve crosslinked material, one of the two components of the polymeric system has to possess functionality > 2.

Polyfunctional amines are the most extensively employed crosslinkers. The reactivity of the amine increases with its nucleophilic character as follows: primary > secondary > tertiary and aliphatic > cycloaliphatic > aromatic. In the case of a primary amine, the resulting secondary amine after first reaction with an epoxide is more reactive and can add a second equivalent of epoxide, whereby the secondary amine is less reactive than the primary one. For instance, aromatic secondary amines are 2-5 times less reactive than the aromatic primary ones. Commonly, primary amines are used for low-curing temperature applications, such as adhesives and coatings. Alternatively, secondary amines are employed to build composite materials. Attention should be placed on the nature of the amine, which can have hazardous characteristics.[354–356] Additionally, amines contribute to the

yellowing of the materials, particularly the aromatic ones.[357, 358] During the reaction mechanism between epoxy and amine groups, hydroxyl groups catalyse the reaction through the formation of a trimolecular complex, which assists the nucleophilic attack of the amine. The reaction has an autocatalytic effect due to the continuous formation of secondary OH during the ring opening when the epoxy-amine bond has formed.[359, 360] Moreover, the process is exothermic, therefore this phenomenon helps the progress of the reaction.[156] When an excess of epoxy is present, another etherification reaction with OH group might happen, resulting in a change of epoxy:amine ratio.

As a result, the thermoset material obtained possesses a high T_g value, displaying characteristic mechanical, thermal and chemical properties.[349] Certainly, the final material properties are highly dependent on the structure and reactivity of the monomers.[361, 362]

Fully biobased examples of epoxy resins have been published in the recent literature.[343,363–365] Unfortunately, the majority of these resins use epichlorohydrin to incorporate epoxide groups. Cramail and Wang employed a commercially available epoxidized soybean oil derived by the oxidation of unsaturation, without the need for epichlorohydrin to obtain hybrid epoxy-NIPU materials.[263, 264]

1. Novel bio-based epoxy resins: a comparative study

With the aim to develop novel biobased epoxy resins and to compare their performances with petroleum-based ones, a comparative study was carried out. This work was performed at Henkel Adhesives and Technology, as Henkel was the assigned as industrial partner in the frame of the NIPU-EJD consortium.

Two diglycidyl ethers were chosen for their structure similarity and different sources. As such, diglycidyl ethers from bisphenol-A (DGEBA) and isosorbide (DGEISO) were selected, a petroleum-based and a bio-based epoxy, respectively (Figure 107).

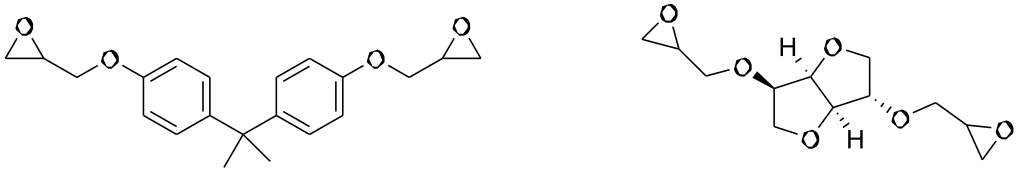

DGEBA DGEISO

Figure 107. Chemical structured of diglycidyl ether from bisphenol A (DGEBA) and isosorbide (DGEISO).

As mentioned previously, DGEBA is a crucial building block for epoxy production, but undesired due to hazardousness. As a consequence, analogous materials to the existing ones need to be studied to achieve polymers with similar or better performances. A set of amine hardeners was chosen to react with the abovementioned epoxies (Table 34).

Table 34. Sourcing of amines employed in this study.

Bio-based	Petrol-based	Production
Priamine 1071®		Commercial
Castor oil triamine		Synthesized in lab
IPDA[347]	IPDA	Commercial
LDA		Synthesized in lab

Priamine 1071® and castor oil triamine (COTA) were chosen as comparable long aliphatic di- and tri-amine (Figure 108). COTA was not reported in any study prior to this one. It was synthesized *via* a thiol-ene photoinitiated reaction (Chapter 2, thiol-ene). *Priamine 1071*® is part of a series of biobased commercially available amines derived from fatty acids by Cargill.[366] Moreover, isophorone diamine (IPDA) and limonene diamine (LDA) were selected as short cycloaliphatic amines with similar chemical structures (Figure 4). IPDA is a potentially biobased amine, which was renewably produced at first by Evonik starting from bioderived acetone.[367] LDA was synthesized similarly to COTA *via* thiol-ene reaction (Chapter 1, thiol-ene). *Priamine*® and IPDA have already been extensively studied to develop more sustainable polymers.[349–352]

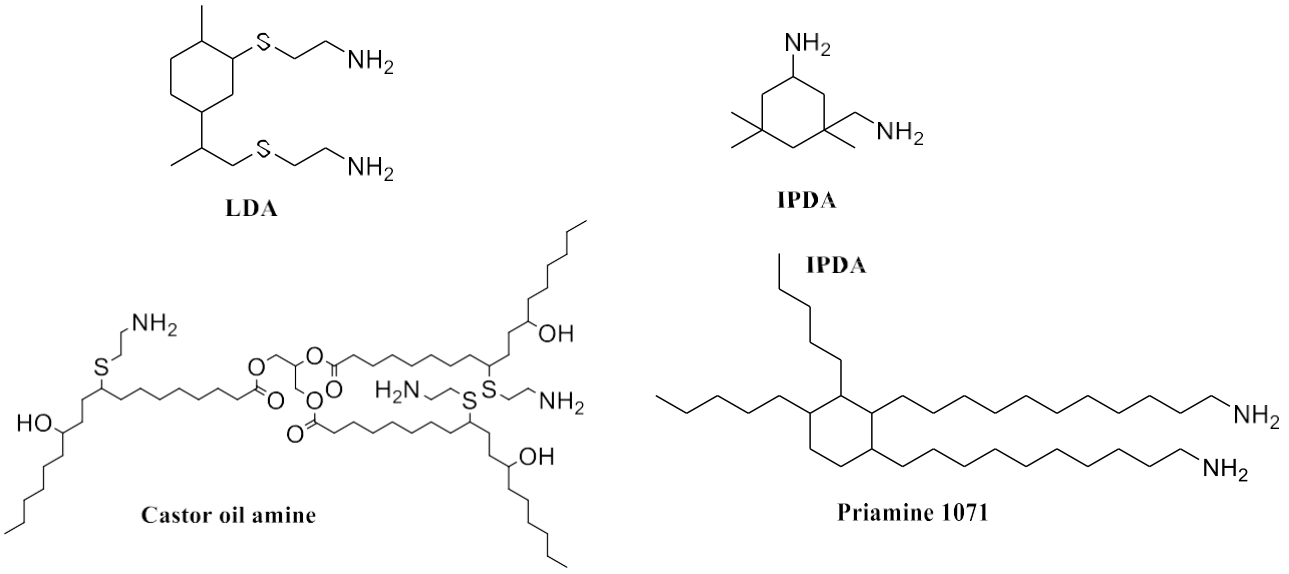

Figure 108. Polyamine hardeners selected for epoxy resin curing.

As a first step, the epoxy equivalent weight of the diglycidyl monomer was evaluated by NMR using an internal standard (Equation 6, Figure 109 and 110).

$$EW = \frac{\int IntSt * H_{function}}{\int function * H_{IntSt}} * \frac{m_{function}}{m_{IntSt}} * MW_{IntSt} \qquad \textbf{Eq.6}$$

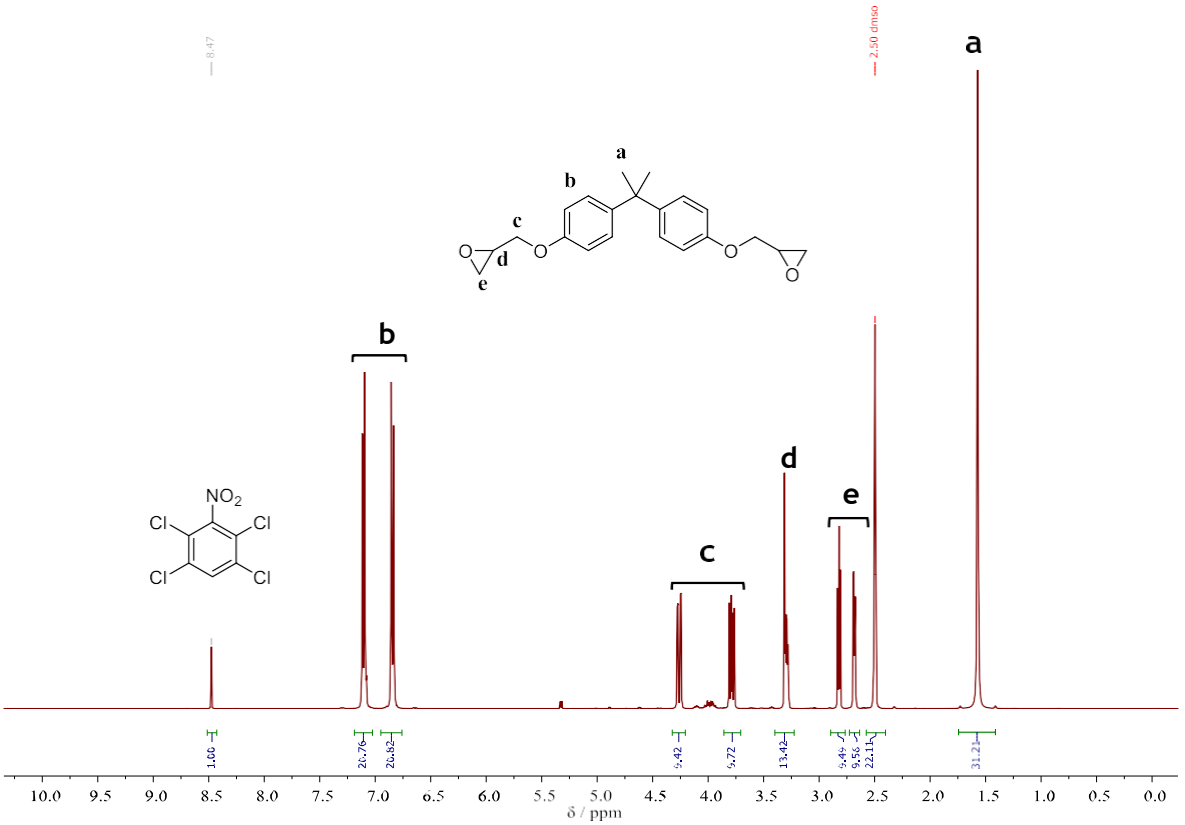

Figure 109. [1]H-NMR (400 MHz; DMSO-d6, 2.5 ppm) spectrum of bisphenol A diglycidyl ether (DGEBA) with 1,2,4,5- tetrachloro-3-nitrobenzene as internal standard (8.5 ppm) for the calculation of epoxy content (EEW). 4.27 ppm peak from DGEBA was used for the calculation.

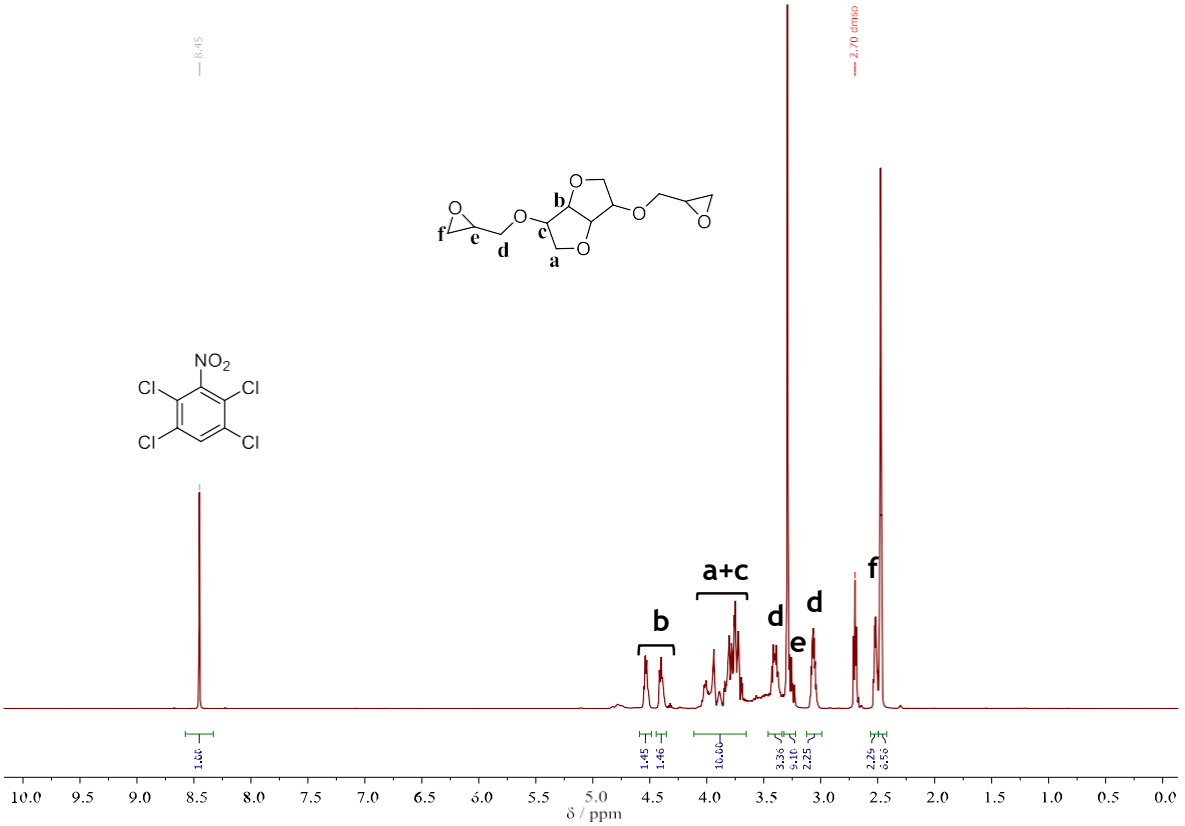

Figure 110. ^{1}H-NMR (400 MHz; DMSO-d6, 2.5 ppm) spectrum of isosorbide diglycidyl ether (DGEISO) with 1,2,4,5-tetrachloro- 3-nitrobenzene as internal standard (8.5 ppm) for the calculation of epoxy content (EEW). 3.06 ppm peak from DGEISO was used for the calculation.

Subsequently, the thermosets were formulated in equimolar amounts of epoxy/amino groups. The curing process was monitored by FT-IR (Figure 11, further spectra can be found in the experimental section).

Table 35. Shore A and Shore D hardness values for six epoxy resin formulations and swelling index and gel content of six epoxy resin formulations measured in THF.

	Epoxy	Amine	Shore A	Shore D	Swelling index	Gel content
			12.5 N	50 N		
Ep1	DGEBA	IPDA		failure	failure	failure
Ep2	DGEBA	COTA	13.4		195	86
Ep4	DGEBA	DLA		47	104	95
Ep5	DGEISO	IPDA		failure	91	82
Ep7	DGEISO	DLA	13		62	91
Ep8	DGEISO	COTA	19		153	88

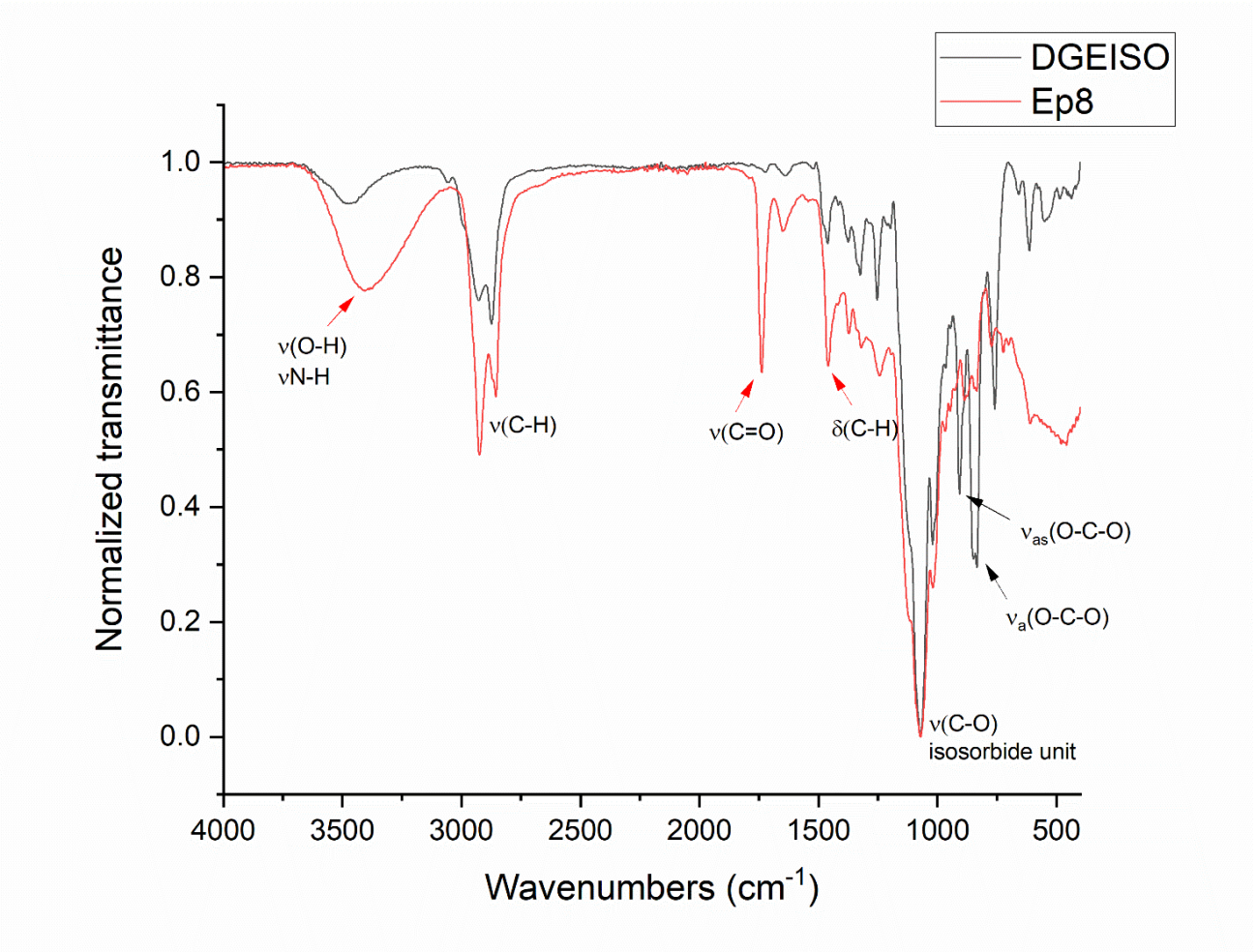

Figure 111. FT-IR of the starting isosorbide dyglicidyl ether (black line) and **Ep8** (red line).

The 830 cm^{-1} vibrational peak represents the O-C-O symmetric stretching of the epoxy unit. Similarly, 900 cm^{-1} displays the O-C-O asymmetric stretching typical of epoxy groups. Those two vibrations are no longer present in the spectrum of **Ep8**. Moreover, the formation of the C=O band at 1740 cm^{-1} and the O-H and N-H stretching indicate the curing in **Ep8**. The C-O stretching units (1079 and 1011 cm^{-1}) and C-H (2932 and 2874 cm^{-1}) can be found in both spectra.

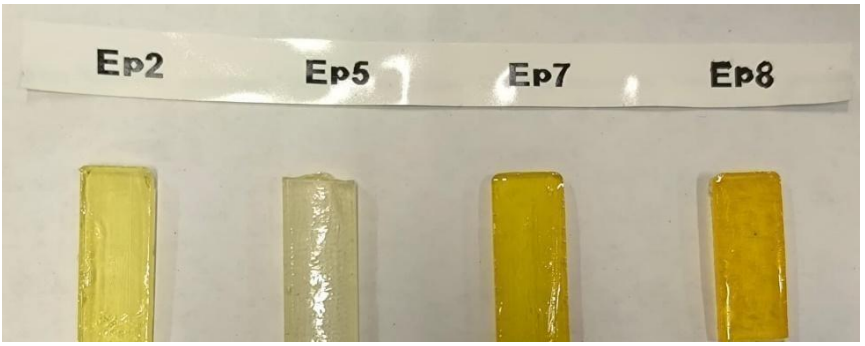

Figure 112. Picture of samples of the epoxy resins obtained. From left to right: **Ep2**, **Ep6**, **Ep7** and **Ep8**.

Hardness, crosslinking, adhesive, tensile and thermal properties of the materials were evaluated. The hardness of the materials was measured by referring to a relative scale established by numerical values of shores (1-100 scale). The measurements were performed by shore A and shore D durometers. The first was used for measuring soft materials and it applies a 12.5 N force on the sample. Differently, shore D evaluates hard materials imposing a 50 N force on the sample (Table 35). Presenting a short cyclic primary amine as a hardener (IPDA), the epoxies **Ep1** and **Ep5** were glassy materials. The rigidity of the amine chemical structure reflected in macroscale on the material hardness. Hence, the durometer tests failed in both cases because the material was immediately broken as the instrument probe was in contact with the surface. In comparison, the epoxy materials synthesized with the similar LDA monomer, generated slightly softer material, even still very rigid. This can be attributed to the presence of the pendant amino group chains ($NH_2(CH_2)_2S$-), which enhance the aliphatic character. The thermoset **Ep4** displayed a 47 Shore D value that is comparable to hard elastomers, such as vulcanized rubbers (Table 35). Oppositely, the thermoset obtained with DGEISO and DLA (**Ep7**) displayed a softer nature, with a Shore A of 13 (Table 35). **Ep2** and **Ep8** were produced with COTA. The resin **Ep8** resulted in a higher hardness of few points in comparison to the respective one formulated with DGEBA. **Ep3** and **Ep6** produced with *Priamine 1071*® showed uncomplete curing and a liquid viscous state, therefore the samples were not measured.

The crosslinking was evaluated by performing swelling tests in THF. Because of the glassy nature of **Ep1**, it was not possible to perform the swelling test due to its brittleness and therefore the impossibility of obtaining a defined piece of specimen. The higher SI obtained was detected for **Ep2** and **Ep8** equal to 195 and 153, respectively (Table 35). This can be explained by the higher mesh-size of the network due to the presence of a long-chain aliphatic crosslinker as COTA in both formulations. Comparing the formulations with DLA (short cyclic aliphatic), the partially biobased **Ep4** showed almost double the value in comparison with the fully biobased one (**Ep7,** Table 35). All the formulations showed a high gel content between 82% and 95% (Table 35). **Ep7** and **Ep4** showed similar GC (91 and 95, respectively, Table 35). Reasonably, **Ep4** had the highest GC value because of the short chain crosslinker (DLA) with the aromatic DGEBA and the reactivity of the primary amino groups. Comparing IPDA and DLA formulations with DGEISO, the difference in gel content might be attributed to the different reactivity of the amino group. In fact, while the amino groups in DLA have comparable reactivity, the two groups present in IPDA show different ones. Most probably, the -NH_2 connected to a primary carbon (high reactive) reacted earlier starting the network formation and, in a later stage, the -NH_2 linked to a secondary carbon (less reactive) finalizing the network.[369-371]The soluble parts were measured by SEC after the swelling tests. In all the cases, only very small mass values were detected, probably due to some monomer leak (Figure 113).

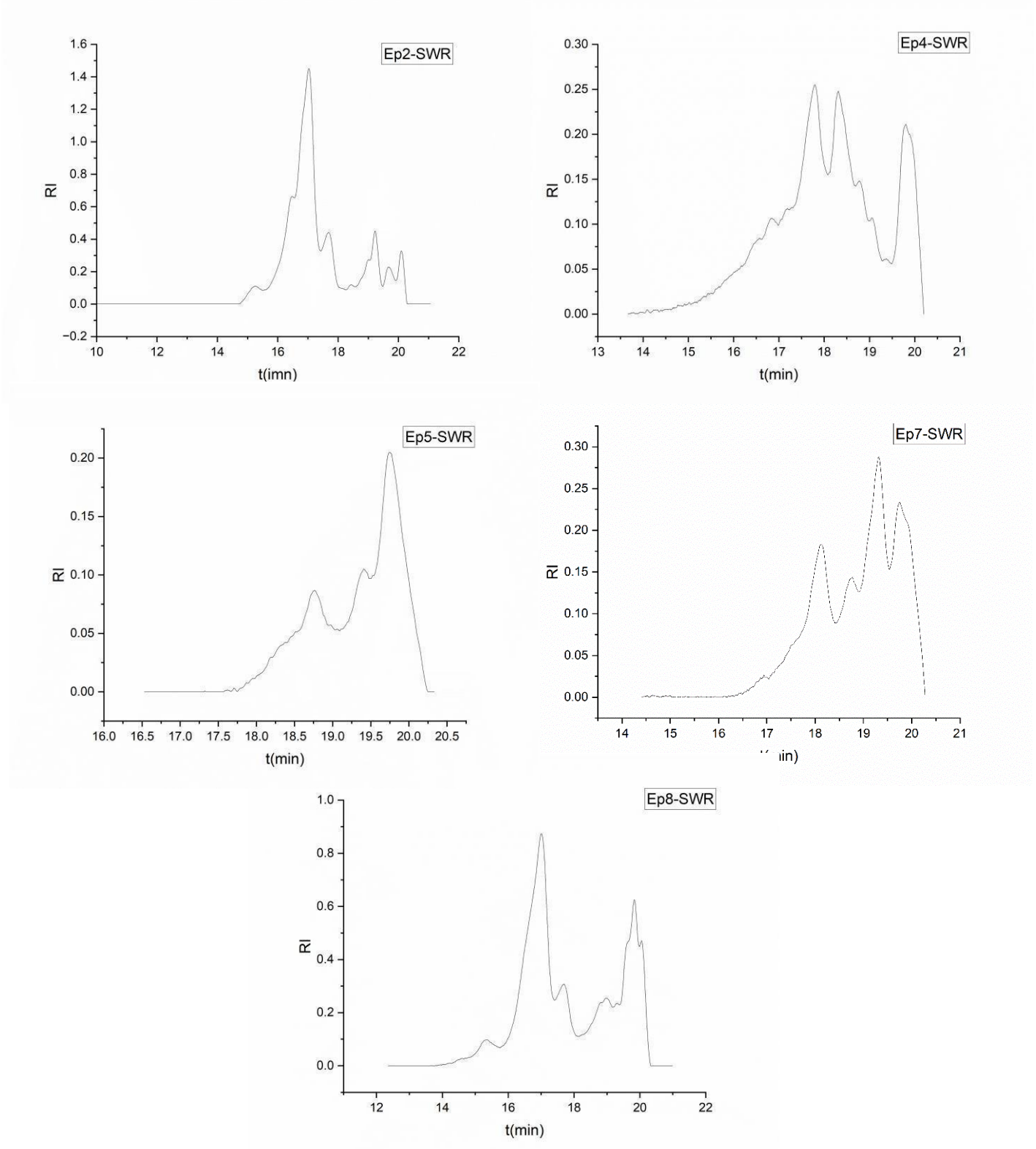

Figure 113. SEC (in THF) of the soluble residue recovered after swelling tests in THF of Ep2, Ep4, Ep5, Ep7, Ep8. SWR= swelling test residue.

DSC analyses were performed for all the samples. A 99.5 °C T_g was detected for **Ep1** (Table 35), which can be attributed to the rigidity of IPDA and the quite high crosslinking density (gel content = 86, Table 35). The second highest value obtained was detected in **Ep5 (**T_g = 59 °C), the analogous

composition substituted with DGEISO (Table 35). The difference in the two values might be linked to the aromatic units present in the DGEBA monomer, responsible of increasing the stiffness of the polymer chain and the possible π orbital interactions of the benzine rings withing different polymer segments. **Ep4** and **Ep7**, having DLA as co-monomer, showed comparable T_g values (36 °C and 29 °C, respectively). The difference between the two values, can also be attributed to the aromaticity of DGEBA, as previously. The lowest T_g was measured for the sample **Ep8** with a T_g equal to -5 °C, which displays 26.5 degrees less than the corresponding **Ep2**, which displays a T_g of 21.2 °C. Due to the great aliphatic nature of the COTA (common co-monomer in **Ep2** and **Ep8)** the determining factor affecting the T_g were attributed to the aromatic units in DGEBA.

The thermal degradation behaviour was evaluated by TGA. **Ep1** and **Ep5** displayed the highest thermal resistance with $T_{d,\ 5\%}$ of 360 °C and 328, respectively, and 50% degradation at about 400 °C. Similarity to these materials, **Ep2** showed a $T_{d,5\%}$ above 300°C and 391°C $T_{d,50\%.}$ Slightly lower values were obtained for $T_{d,50\%}$ for the formulation with DLA.

Tensile tests were also performed (Figure 114). It was not possible to manufacture dogbone samples of **Ep1** and **Ep2** due to the material rigidity. **Ep2 a**nd **Ep5** resulted in a very stiff materials with a Young´s modulus of about 2000 and 3000 MPa. Consequently, the elongation at break was low (1.4 and 1.5 %, respectively). Oppositely, **Ep7** registered a lower E_{mod} equal to 6.6 MPa. The sample displayed a wide linear plastic region, leading to elongation at break values of about 27.3 % (Table 36, Figure 114).

Table 36. T_gs and thermal degradation temperatures measured by DSC and TGA for six epoxy resin formulations. Elongation and stress at break and Young´s modulus (E_{mod}) obtained by ensile tests of epoxy resins.

	Epoxy	Amine	T_g (°C)	$T_{d,5\%}$ (°C)	Elongation at break (%)	Stress at break (MPa)	E_{mod} (MPa)
Ep1	DGEBA	IPDA	99	362	/	/	/
Ep2	DGEBA	COTA	21	310	1.4	20.0	1793
Ep4	DGEBA	DLA	36	231	/	/	/
Ep5	DGEISO	IPDA	59	328	1.5	43.0	3134
Ep7	DGEISO	DLA	29	171	27.3	1.3	6.6
Ep8	DGEISO	COTA	-5	219	/	/	/

$T_{d,5\%}$ decomposition temperature at 5% weight loss.

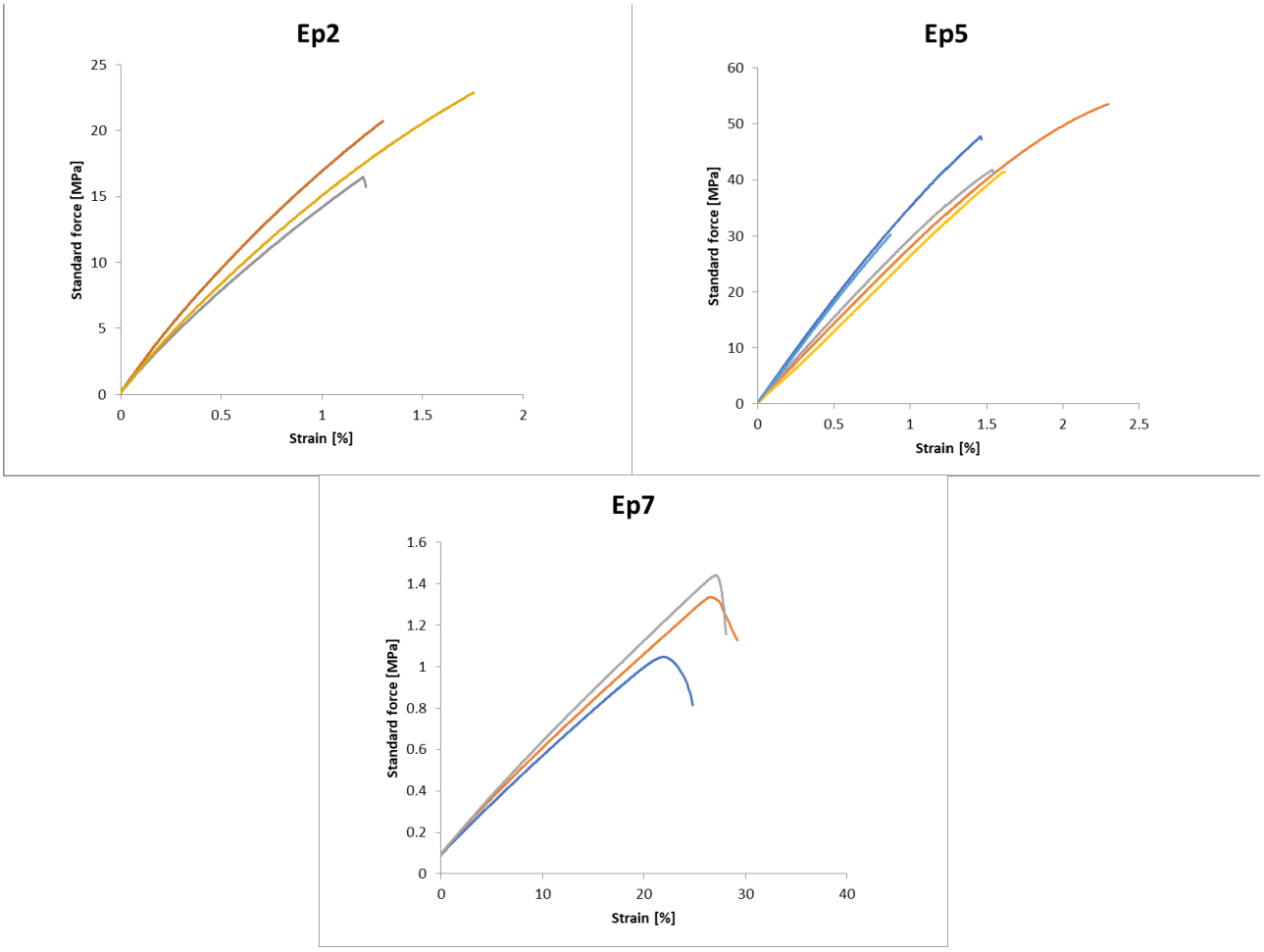

Figure 114. Tensile tests of **Ep2**, **Ep5** and **Ep7**.

Lap shear tests were performed to evaluate adhesive properties (Table 37). Three different substrates were selected to study the adhesive performances on diverse materials. Aluminium, softwood and PVC were chosen.

Table 37. Lap shear tests of six epoxy formulations on three different adherents: wood, aluminium and PVC.

	Epoxy	Amine	Adherent	Shear strength (Mpa)	Break (mm)
Ep1	DGEBA	IPDA	Wood	1.23±0.26	0.24±0.03
			Alu	1.20±0.41	0.21±0.03
			PVC	0.47±0.02	0.28± 0.02
Ep2	DGEBA	COTA	Wood	12.2±0.6	1.38±0.09
			Alu	3.5±0.9	0.33±0.05
			PVC	0.88±0.19	0.38±0.05
Ep4	DGEBA	DLA	Wood	1.81±0.21	0.34±0.04
			Alu	1.50±0.16	0.30±0.4
			PVC	0.99±0.13	0.48±0.03
Ep5	DGEISO	IPDA	Wood	10.75±0.85	1.23±0.12
			Alu	2.09±0.60	0.28±0.01
			PVC	0.77±0.17	0.37±0.01
Ep7	DGEISO	DLA	Wood	7.62±0.85	0.99±0.10
			Alu	3.23±0.32	0.37±0.02
			PVC	1.60±0.37	0.65±0.4
Ep8	DGEISO	COTA	Wood	1.6±0.2	0.38±0.06
			Alu	0.64±0.1	0.28±0.04
			PVC	0.61±0.06	0.60±0.14

As previously explained in Chapters 3 and 4, the hydroxyl group present on the surface of the wood substrate (cellulose and lignin) improve the chemical interaction (hydrogen bond and dipole forces) at the interface of the adhesive and the adherent. This gives reason to the highest values measured for tests performed on wood samples. Among the epoxies with IPDA, the **Ep5** formulation with DGEISO showed 9-times the shear stress in comparison to the analogous with DGEBA, equal to about 11 MPa shear stress. Similarly, the highest registered value over all samples was observed for **Ep2** with the petroleum-based DGEBA and COTA with 12.2 MPa. An inferior performance was exhibited by the comparable fully biobased **Ep8** (1.6 MPa). Oppositely, the fully biobased **Ep7** formulated with DLA manifested a 7.6 MPa shear stress with respect to the 1.8 MPa value of **Ep4.** Generally, aluminium and PVC exhibited poorer performances when compared against wood, with PVC as the lowest.

5.2 CONCLUSION

Fully and partially bio-based epoxy resins were produced in order to compare the performances to the petroleum-based bisphenol A diglycidyl ether and the isosorbide diglycidyl ether. The latter was chosen as a possible alternative to DGEBA for possible future epoxy formulation with a high biobased carbon content. What is playing a difference in properties of the final materials is prevalently the presence of the aromatic units presents in DGEBA in comparison to DGEISO. This leads to stiff materials resulting in higher T_gs. Hence, the T_g of materials obtained with DGEISO are mostly above room temperature. It can be noticed that a great influence is played by the amine hardener nature. All the epoxies displayed a high gel content (86-95) and good resistance to degradation at high temperature ($T_{d,5\%}$ from about 200 to >300°C). Best adhesive properties were recorded on wood substrate with the fully biobased **Ep5** consisting of DGEISO and IPDA overpassing the analogous petrol-based made of DGEBA and IPDA **(Ep1).** Generally, all the formulations with DGEISO showed higher performances of shore stress on wood adherents in comparison to the respective epoxies containing DGEBA.

5.3 EXPERIMENTAL DATA

Characterization methods

Nuclear Magnetic Resonance spectroscopy (NMR)

NMR spectra were recorded using the following spectrometer hardware.

Bruker AVANCE 400

^{1}H-NMR (400 MHz), ^{13}C-NMR (101 MHz)

Bruker AVANCE 500

^{1}H-NMR (500 MHz), ^{13}C-NMR (126 MHz)

DMSO–d6, $CDCl_3$ and MeOD were used as solvents and their respective resonance signals served as reference for the chemical shift δ in parts per million: ^{1}H: $CDCl_3$ = 7.26 ppm, DMSO-d6 = 2.50 ppm; ^{13}C: $CDCl_3$ = 77.2 ppm, DMSO-d6 = 39.5 ppm. The spin multiplicity and corresponding signal patterns were abbreviated as follows: s = singlet, d = doublet, t = triplet, q = quartet, quint. = quintet, m = multiplet. Coupling constants J were noted in Hz. Furthermore, 2D NMR methods (e.g., heteronuclear single quantum coherence (HSQC), heteronuclear multiple bond correlation (HMBC) and correlated spectroscopy (COSY)) were carried out, if necessary, for signal assignment and structure elucidation.

Gel Permeation Chromatography (GPC)

System I (Oligo SEC): A PSS SECcurity^2 SEC system based on Agilent Infinity 1260 II hardware was used for the measurements. The system is equipped with a refractive index detector SECcurity^2 RI, a column oven "(Bio)SECcurity^2 column compartment TCC6500", a "standard SECcurity^2" autosampler, and an isocratic pump "SECcurity^2 isocratic pump". Anhydrous tetrahydrofuran stabilized with 250 ppm butylated hydroxytoluene (BHT, ≥99.9%) was used at a flow rate of 1.0 ml min^{-1} and at 30 °C as mobile phase. The analysis was performed on the following column system: PSS SDV analytical precolumn (3 µm, 8 mm × 50 mm) with two PSS SDV analytical columns (3 µm, 8 mm × 300 mm, 1000 Å). For the calibration, narrow linear poly(methyl methacrylate) standards (Polymer Standards Service, PSS, Germany) ranging from 102 to 62200 Da were used. For the preparation of the samples,
2.00 mg of analyte was dissolved in 1.50 mL anhydrous tetrahydrofuran stabilized with 250 ppm butylated hydroxytoluene (BHT, ≥99.9%). All samples were filtered by syringe filter prior to use, to avoid plugging of the injection setup or the column.

Infrared spectroscopy (FT-IR)

Infrared (IR) spectroscopy IR spectra were recorded on a Bruker alpha-p instrument in a frequency range of 3997.41 to 373.828 cm-1 applying KBr- and ATR technology.

Thin Layer Chromatography (TLC)

All thin layer chromatography (TLC) experiments were performed on silica-gel-coated aluminum foil (silica gel 60 F254, layer thickness: 0.25 mm, Sigma-Aldrich). Compounds were visualized by irradiation with a UV lamp (λ = 254 and 365 nm), by staining with Seebach solution (mixture of 5.00 g phosphomolybdic acid hydrate, 2.00 g cerium(IV)- sulfate, 16.0 mL concentrated sulfuric acid and 200 mL water) or vanillin staining solution (mixture of 8.60 g vanillin and 2.50 mL concentrated sulfuric acid and 200 mL ethanol), or KMnO4 staining solution (1.50 g $KMnO_4$, 10.0 g $K2CO_3$, 1.25 mL 10% NaOH and 200 mL water) or ninhydrin solution (0.2 ninhydrin in 100 mL ethanol).

Differential scanning calorimetry (DSC)

DSC analyses were run with DSC Q2000 instrument. Samples were placed in aluminium pans and measured with a heating rate of 10 K min-1 over a temperature range from -40 to 200 °C, gas flow (nitrogen) of 50 mL/min.

Thermogravimetric Analysis (TGA)

TGA measurements were carried out on the TA Instruments TGA 5500 under nitrogen atmosphere using platinum TGA sample pans and with a heating rate of 10 K min-1 over a temperature range from -40 to 600 °C. Thanks to Théato research group (KIT) for the instrument availability.

Tensile tests

Tensile tests were performed by the Automated Laboratory at Henkel Adhesive and Technologies department (Düsseldorf). The equipment for tensile tests was a Zwicks (Z050 frame) with respective Loadcells XForce HP 2.5 kN. Measurement specifications. Pre-load= 0.1 MPa, Test speed: 10 mm/in. Begin of Young´s modulus determination 0.05%; end of Young´s modulus determination 0.25%.

Lap shear tests

The tests were conducted on a Zwick 100. The set-up consists of two jaws holding the edges of the specimen. When the experiment started, a tensile load was applied until bonding failure.

Materials

Epikote™ Resin 828 (Westlake Epoxy), KDBM-1041 (KUKDO), isophorone diamine (IPDA) (Sigma Aldrich), *Priamine 1071*® (Cargill), *Jeffamine D230*® (Evonik), *Jeffamine T430*® (Evonik), castor oil, R-(+)-limonene (), cysteamine hydrochloride (). Solvents: tetrahydrofuran (THF), chloroform ($CHCl_3$), isopropanol (i-PrOH), ethanol (EtOH) from Acros Organics.

Synthesis and characterization

- *Synthesis of propane-1,2,3-triyl tris(9-((2-aminoethyl)thio)-12-hydroxyoctadecanoate)-(castor oil triamine)*

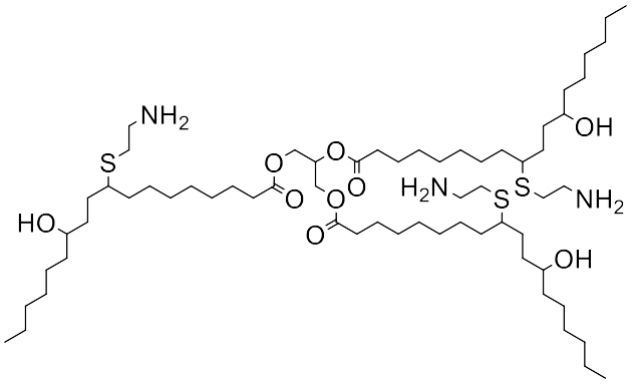

propane-1,2,3-triyl tris(9-((2-aminoethyl)thio)-12-hydroxyoctadecanoate)
(Castor oil triamine)
Chemical Formula: $C_{63}H_{125}N_3O_9S_3$
Molecular Weight: 1164.89

20 g of castor oil (0.02 mol, 1 eq), cysteamine hydrochloride (25.4 g, 0.19 mol, 9 eq), and 2-hydroxy-2-methylpropiophenone (1.05 g, 6.43 mmol, 0.3 eq) were dissolved in about 300 mL isopropanol. The UV LED was completely immersed in a suited flask. The mixture was exposed to a UV lamp 365 nm for 24 h. After that time, the solvent was evaporated under reduced pressure. The crude mixture was dissolved in chloroform and subsequently washed with saturated sodium carbonate solution and two to three aqueous workups until neutral pH was achieved. Water residues were removed with anhydrous sodium sulfate and the chloroform was removed under reduced pressure. (from yellow to orange viscous liquid 12 g, 46% yield, >99 % conversion).

Note: the amount of solvent indicated was necessary to allow the UV-lamp to be immersed in the reaction mixture.

^{1}H-NMR (400 MHz, Chloroform-*d*): δ = 5.57 – 5.39 (m, C**H**=C**H**), 5.24 (pd, *J* = 5.0, 0.0 Hz, 1H, CH2-C**H**-CH2), 4.27 (dd, *J* = 11.9, 4.3 Hz, 2H, C**H**2-CH-C**H**2), 4.12 (dd, *J* = 11.8, 6.0 Hz, 2H, C**H**2-CH-C**H**2), 2.88 – 2.79 (m, 6H, C**H**2-CH2-NH2), 2.59 (d, *J* = 1059.5 Hz, 6H, CH2-C**H**2-NH2), 2.04 (s, 6H, -NH2), 2.30 (td, *J* = 8.9, 7.5, 4.1 Hz, 6H), 1.14-1.69 (m, 87H aliphatics), 0.86 (t, 9H, -CH3).

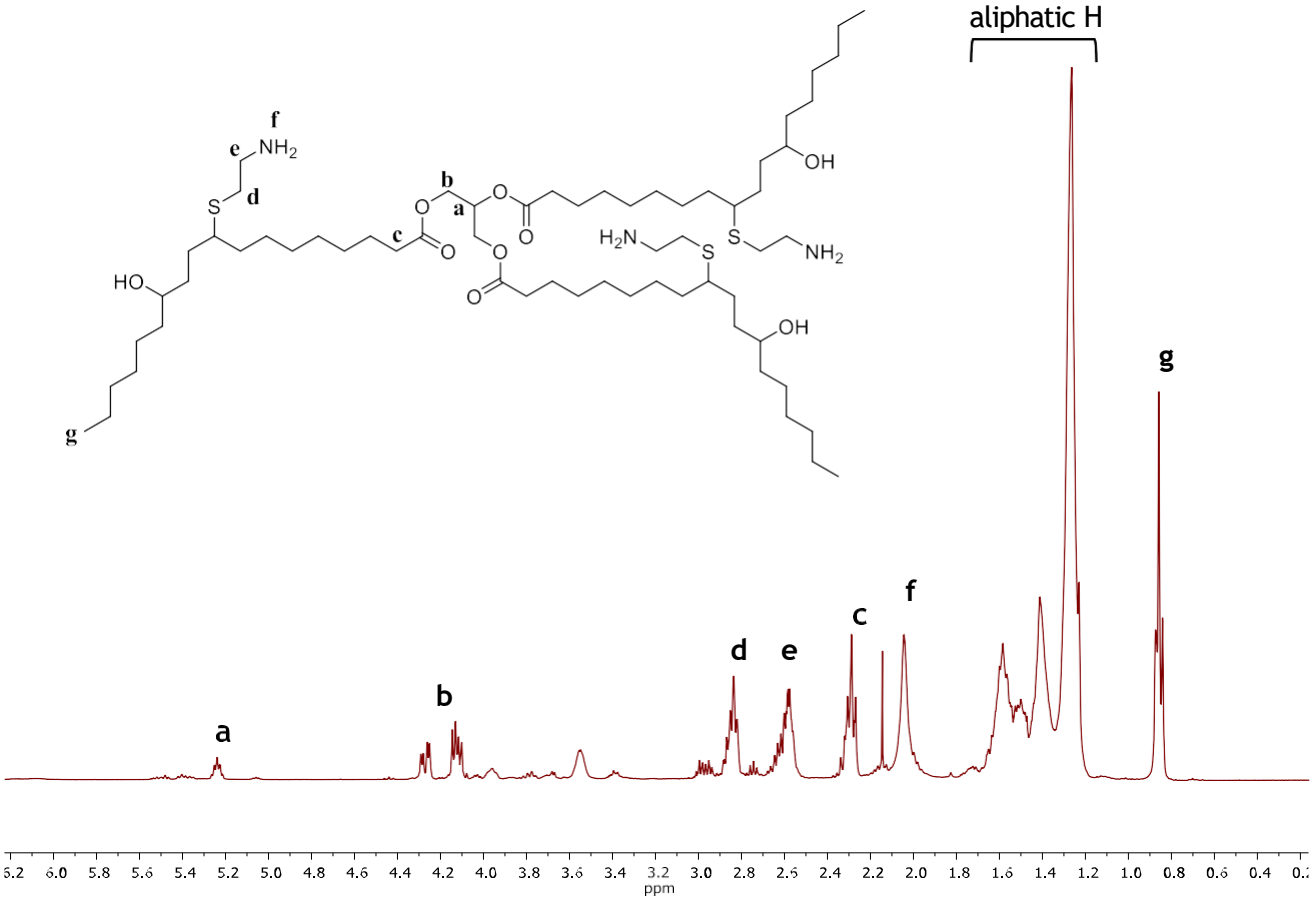

S 40. ^{1}H-NMR (400 MHz) of castor oil triamine in CDCl3/MeOH.

- *Synthesis of 2-((2-(3-((2-aminoethyl)thio)-4-methylcyclohexyl)propyl)thio) ethan-1-amine-(limonene diamine)*

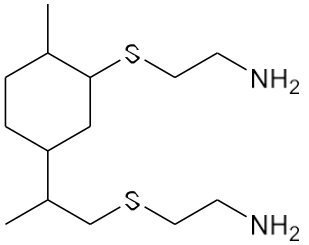

2-((2-(3-((2-aminoethyl)thio)-4-methylcyclohexyl)propyl)thio)ethan-1-amine
(Limonene diamine)
Chemical Formula: $C_{14}H_{30}N_2S_2$
Molecular Weight: 290.53

35 g of D-limonene (0.26 mol, 1 eq), cysteamine hydrochloride (202.9 g, 1.54 mol, 6 eq), and 2-hydroxy-2-methylpropiophenone (0.847g, 5.14 mmol, 0.02 eq) were dissolved in about 300 mL were dissolved in about 300 mL isopropanol. The UV LED was completely immersed in a suited flask. The mixture was exposed to a UV lamp 365 nm for 24 h. After that time the solvent was evaporated under reduced pressure. The crude mixture was dissolved in chloroform and subsequently washed with saturated sodium carbonate solution and two to three aqueous workups untill neutral pH was achieved. Water residues were removed with anhydrous sodium sulfate and the chloroform was removed under reduced pressure. Yellow viscous liquid, 87% conversion). Note: the amount of solvent indicated was necessary to allow the UV LED to be immersed in the reaction mixture.

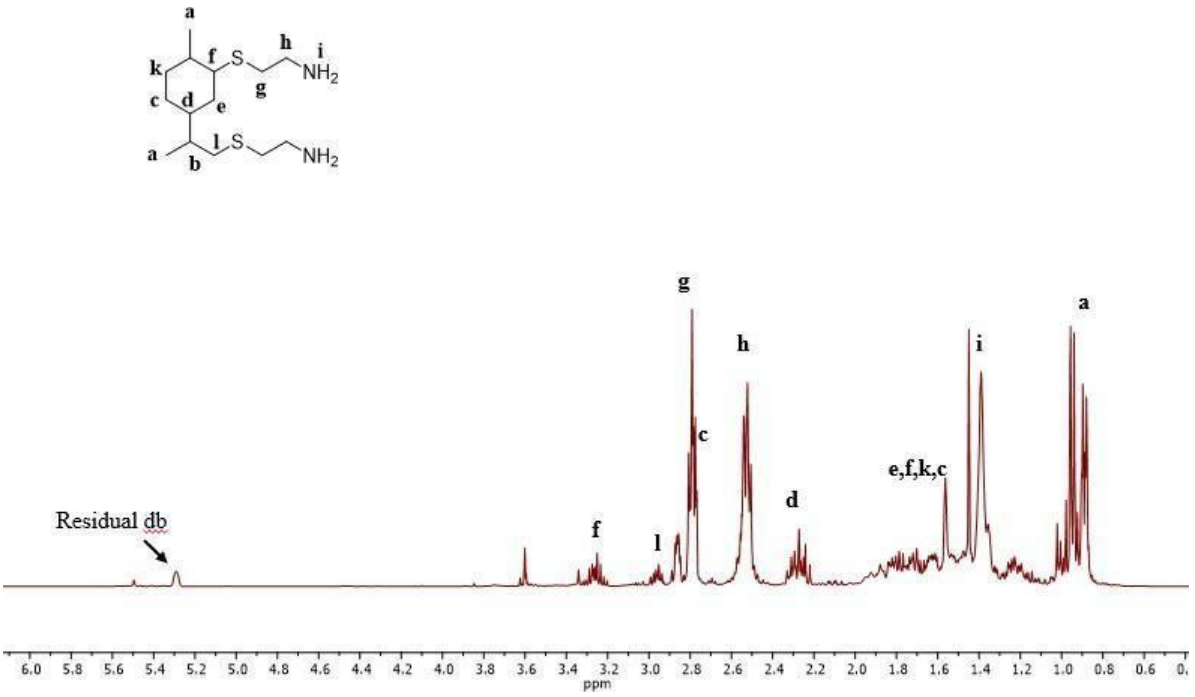

S 41. [1]H-NMR (400 MHz) of limonene diamine in $CDCl_3$.

[1]H NMR (400 MHz, Chloroform-*d*): δ = 5.29 (ddt, *J* = 4.6, 3.4, 1.8 Hz, C**H**=C), 2.85 – 2.73 (m, -S-C**H**2-CH2-, 4H), 2.58 – 2.43 (m, 4H, -S-CH2-C**H**2), 2.28 (ddt, *J* = 14.8, 12.4, 8.4 Hz, 1H, C**H**-S), 2.0 – 1.2 (8H ring), 0.97 – 0.93 (m, 3H,- CH3), 0.89 (dd, *J* = 6.9, 1.1 Hz, 3H, -CH3).

Curing. The samples were cured at room temperature and the curing was monitored along the time by FT-IR.

Epoxy equivalent weight calculate by NMR with 1,2,4,5-tetrachloro-3-nitrobenzene as internal standard in DMSO-d6:

$$EW = \frac{\int IntSt * H_{function}}{\int function * H_{IntSt}} * \frac{m_{function}}{m_{IntSt}} * MW_{IntSt}$$

EW (DGEBA)= 370

EW (DEISO) = 322

- ***EP1-*** *Diglycidyl ether bisphenol A + isophorone diamine (IPDA)*
  4.0 g (10.8 mmol) of diglycidyl ether bisphenol A and IPDA (1.92g, 11.3 mmol) were mixed in a ratio 1:1 of epoxy to amine group.

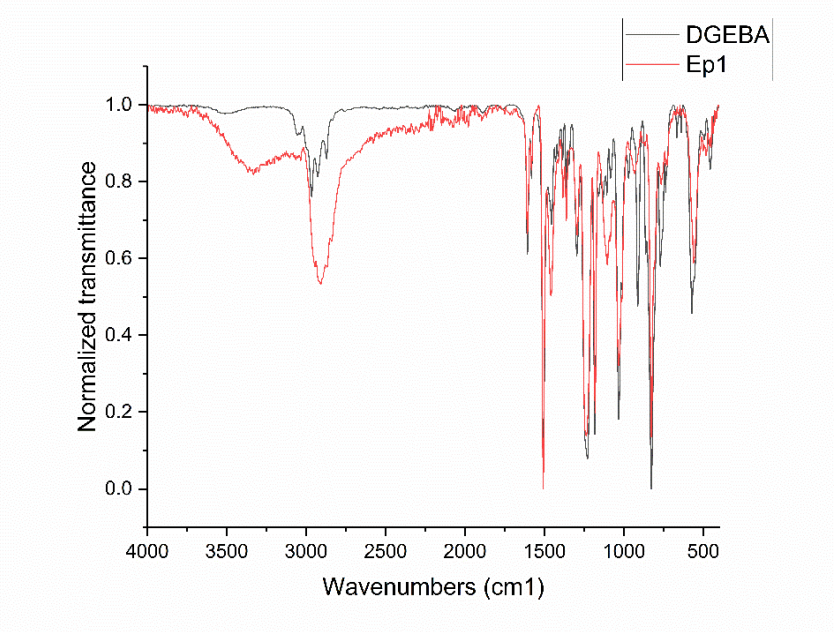

S 42. EP1 FT-IR Vs DGEBA.

- ***EP2-*** *Diglycidyl ether bisphenol A + limonene diamine (DLA)*
  4.0 g (0.01 mol) of diglycidyl ether bisphenol A and DLA (3.12 g, 0.01 mol) were mixed in a ratio 1:1 of epoxy to amine group.

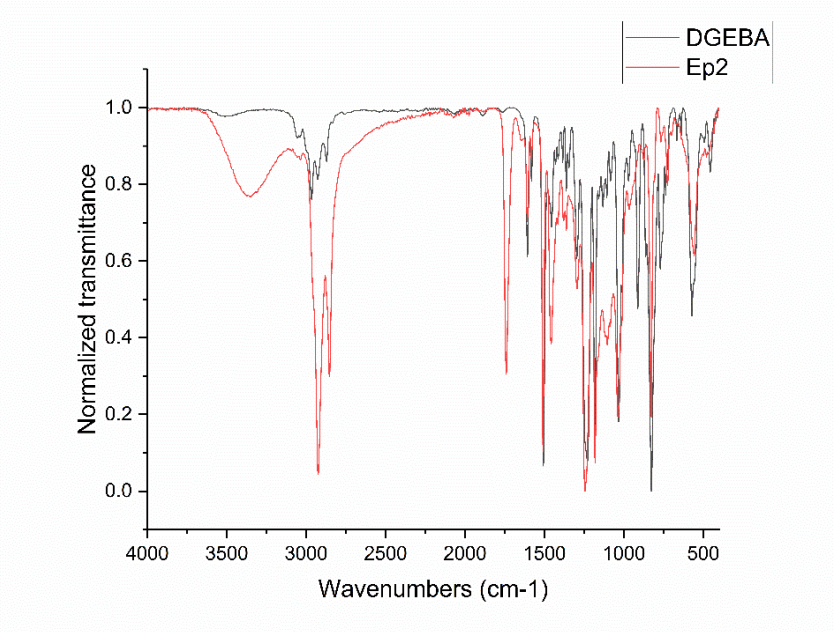

S 43. EP2 FT-IR Vs DGEBA.

EP3- *Diglycidyl ether bisphenol A + Priamine 1071® (P1071)*
4.0 g (0.01 mol) of diglycidyl ether bisphenol A and *Priamine 1071®* (7 g, 0.01 mol) were mixed in a ratio 1:1 of epoxy to amine group.

- ***EP4-*** *Diglycidyl ether bisphenol A + castor oil triamine (COTA)*
  1.0 g (2.7 mmol) of diglycidyl ether bisphenol A and COTA (2.07 g, 1.7 mmol) were mixed in a ratio 1:1 of epoxy to amine group.

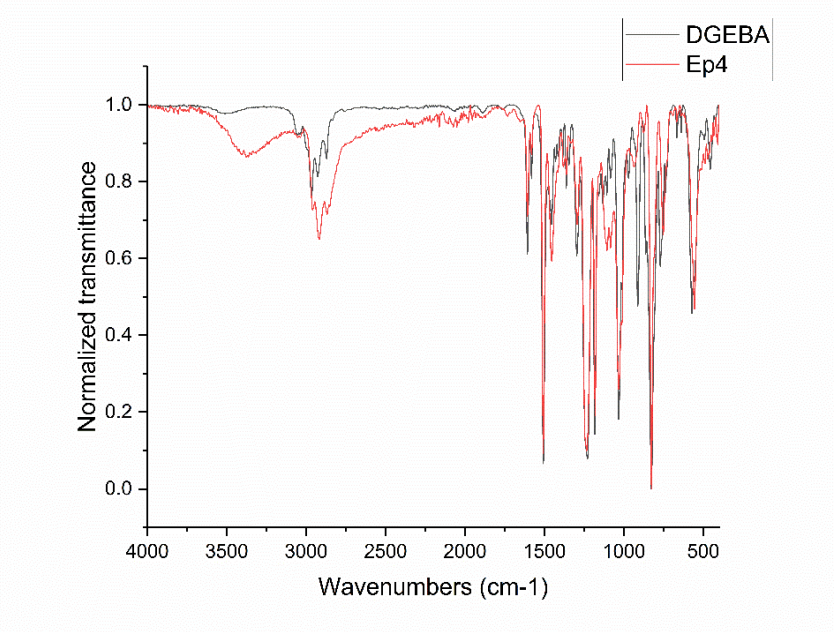

S 44. EP3 FT-IR Vs DGEBA.

- ***EP5-*** *Isosorbide diglycidil ether + isophorone diamine (IPDA)*
  5.0 g (15.5 mmol) of isosorbide diglycidyl ether and IPDA (2.64 g, 15.5 mmol) were mixed in a ratio 1:1 of epoxy to amine group.

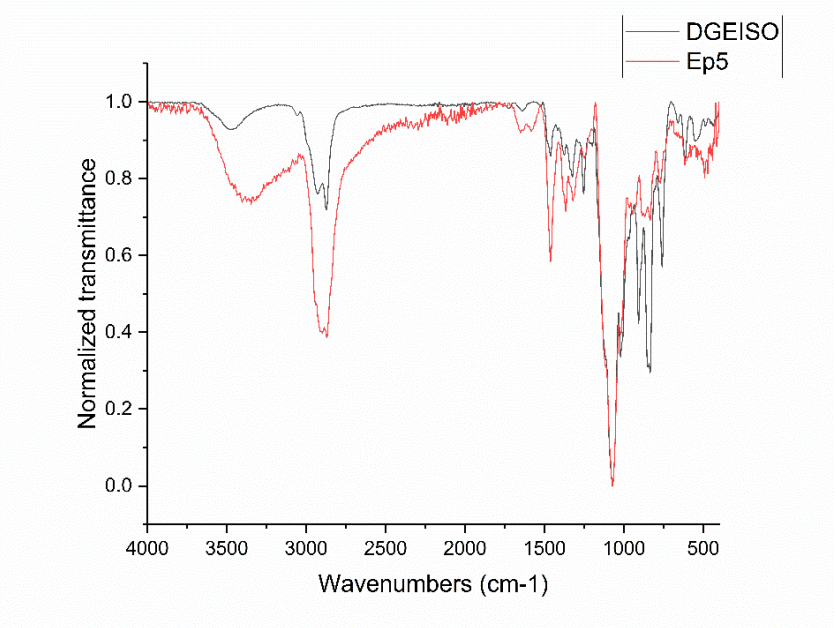

S 45. EP5 FT-IR Vs DGEISO.

- ***EP6-*** *Isosorbide diglycidyl ether + castor oil triamine (COTA)*
  3.0 g (9.3 mmol) of isosorbide diglycidyl ether and COTA (7.14 g, 6.13 mmol) were mixed in a ratio 1:1 of epoxy to amine group.
- ***EP7-*** *Isosorbide diglycidil ether + Priamine 1071® (P1071)*

5.0 g (15.5 mmol) of isosorbide diglycidyl ether and *Priamine 1071*® (10.0 g, 15.4 mmol) were mixed in a ratio 1:1 of epoxy to amine group.

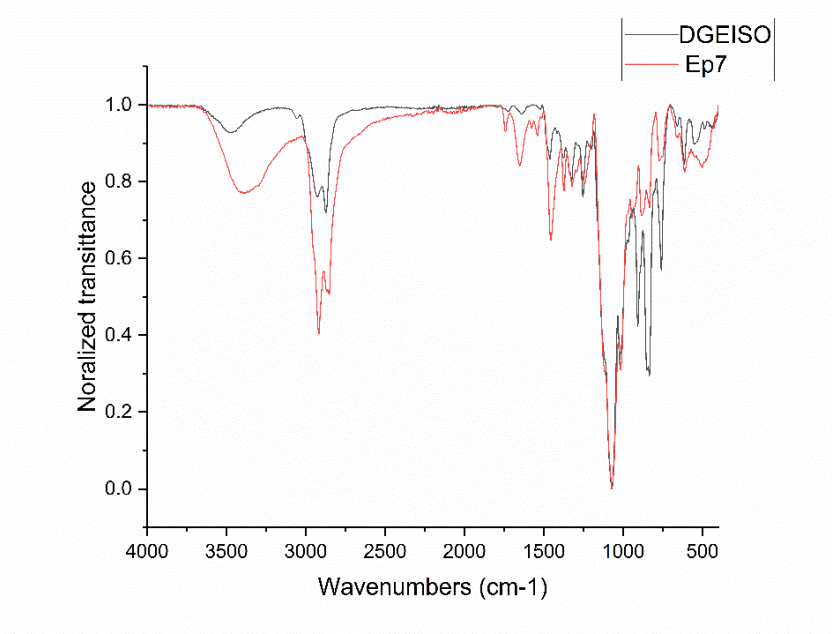

S 46. EP7 FT-IR Vs DGEISO.

- ***EP8-*** *Isosorbide diglycidil ether + limonene diamine (DLA)*
  4.0 g (12.4 mmol) of isosorbide diglycidyl ether and DLA (3.6 g, 12.4 mmol) were mixed in a ratio 1:1 of epoxy to amine group.

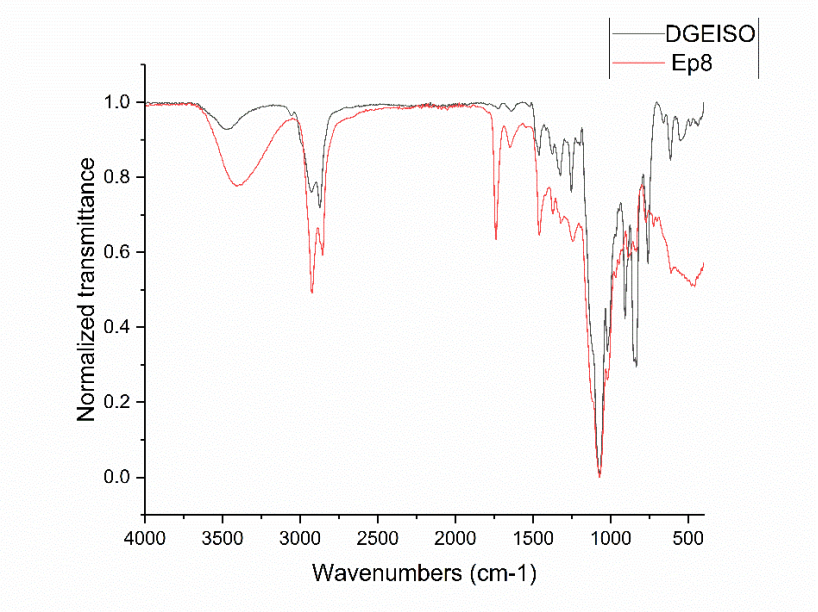

S 47. EP8 FT-IR Vs DGEISO.

TGA analyses

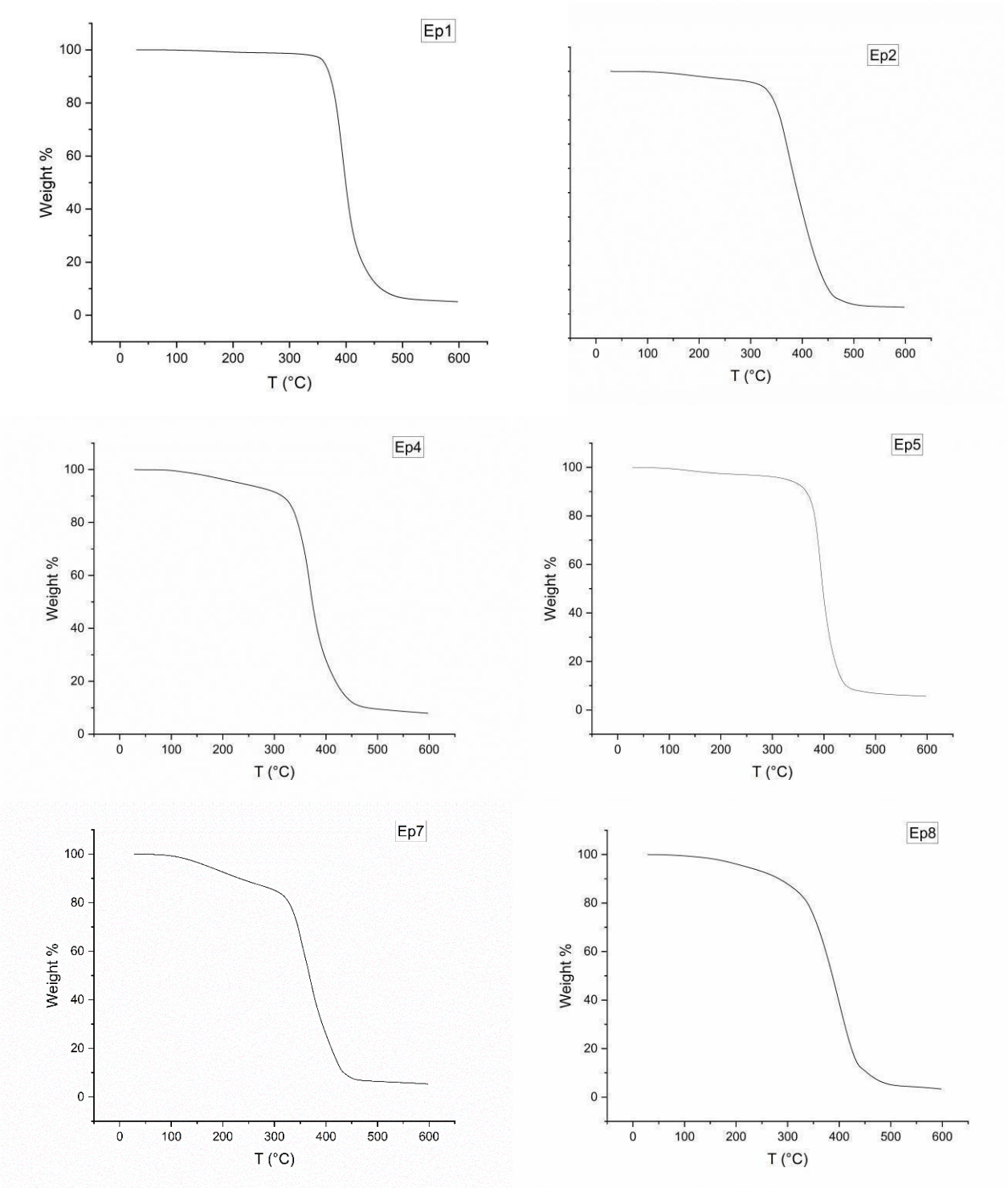

S 48. Ep1, Ep2, Ep4, Ep5, Ep7, Ep8 TGA analyses (25 − 600°C).

DSC analyses

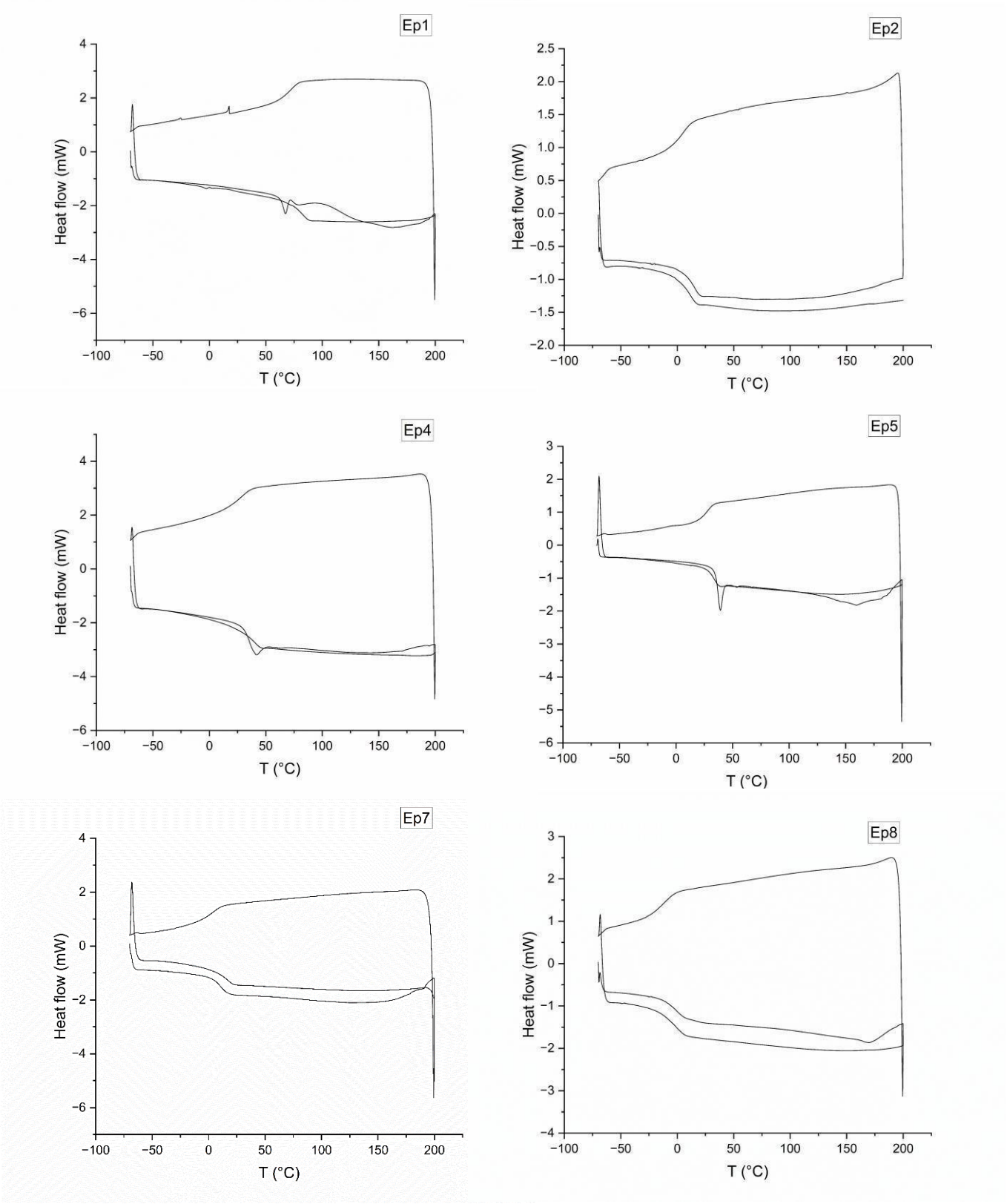

S 49. Ep1, Ep2, Ep4, Ep5, Ep7, Ep8 DSC analyses (-30 − 200°C).

Swelling tests. About 500 mg of each sample were placed in THF (100g/5mL) for 24h. After, the swelling index was calculated as follows:

$$SI = \frac{W_s - W_0}{W_0} . 100$$

where W_s is the weight of the swollen material and W_o corresponds to the initial weight of the material.

Afterwards the solvent was removed and the sample placed in oven at 50°C for 24 h. Subsequently, gel contents were calculated as follows:

$$Gel\% = \frac{W_d}{W_o} . 100$$

where W_d is the weight of the dried material after being swollen and W_o corresponds to the initial weight of the material.

SEC measurements of soluble parts after swelling tests (SWR)

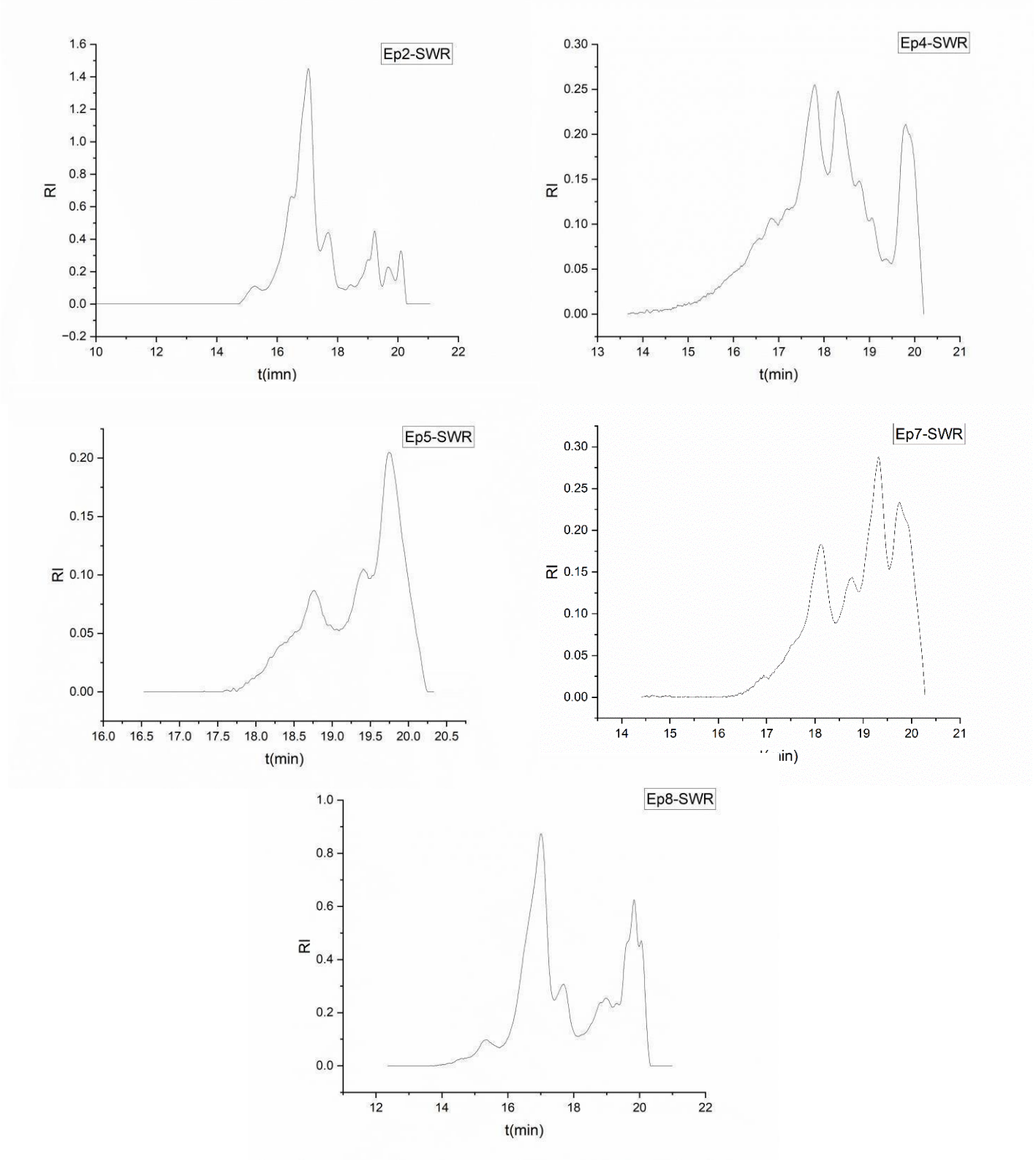

S 50. SEC (in THF) of the soluble residue recovered after swelling tests in THF of Ep2, Ep4, Ep5, Ep7, Ep8. SWR= swelling test residue.

Lap shear preparation. The aluminium and PVC adherents were cleaned wiping the surface with EtOH. The glueing area of the substrate was delimited and marked (13 mm in length). 200 mg of the formulation was placed on this area (13 mm* 25 mm) and glued with the second adherent. Subsequently, two office clips were placed on both sides of the junction area (Figure 7). The samples were measured 24 h after curing at room temperature.

Tensile tests

Sample specifications. Standard dog bones shapes were manufactured with the follow dimensions: length 40 mm x width 10 mm x thickness 2 mm.

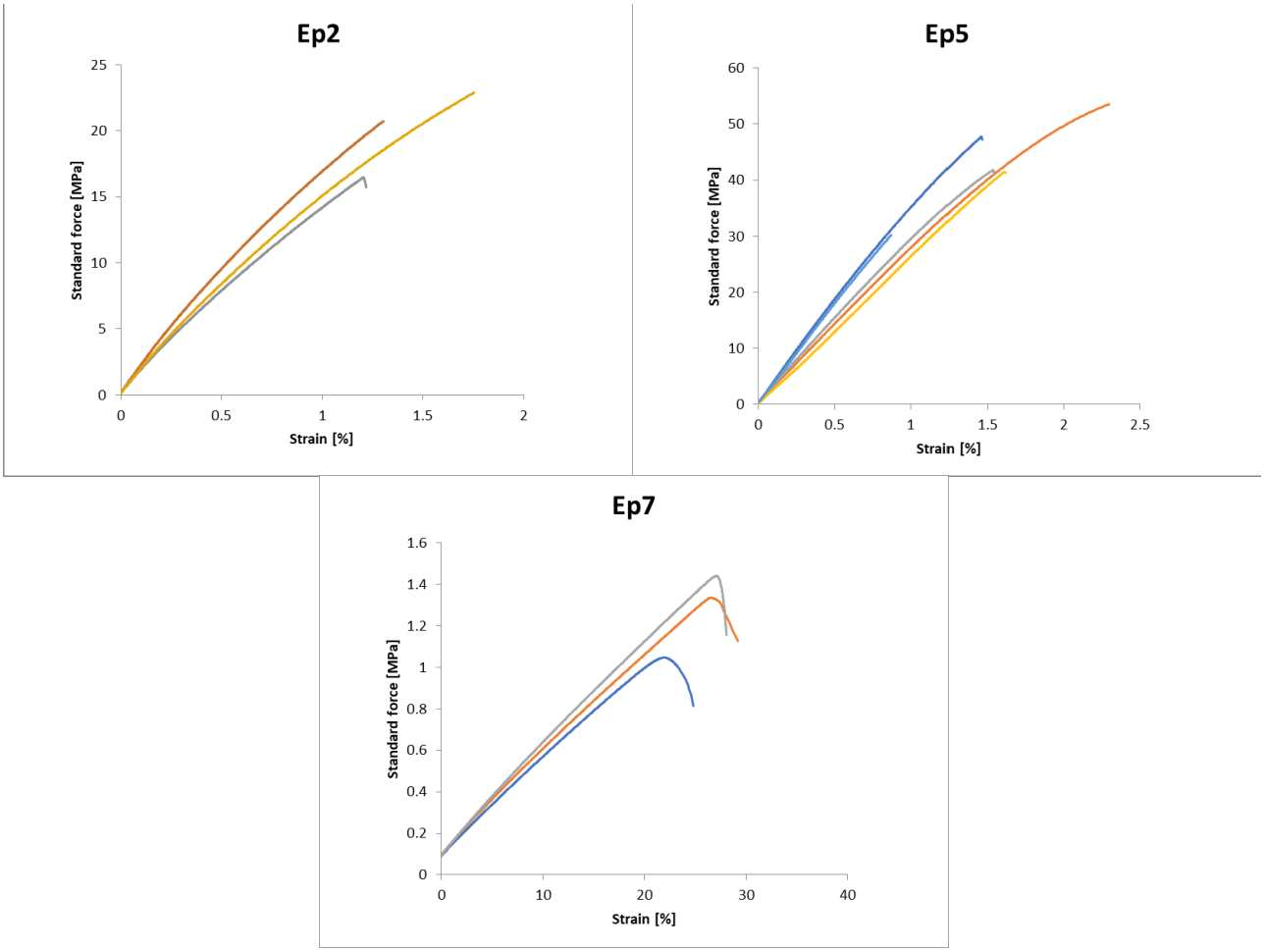

S 51. Tensile tests of Ep2, Ep5 and Ep7.

6 General conclusion

With the aim of contributing to the transition to a more sustainable chemistry and promoting a circular economy model, this research work aimed to the development of novel biobased polyamines for the production of non-isocyanate polyurethanes (NIPUs). A central point of the study was the design and optimization of the synthesis procedures with the purpose of optimizing the sustainability of the processes. This involved the design of greener process which follow the 12 principles of green chemistry as the maximum extent possible. Specifically, this research was successfully able to respect the principles in relation to the choice of suitable renewable feedstock, the avoidance of toxic chemicals as far as possible, targeting high atom economy, minimizing wastes and synthetic steps, use of catalysts.

Starting from vegetable oils and terpene compounds, diverse polyamines from small to midsize were achieved. Two main pathways were investigated such as: 1) catalytic oxidation followed by reductive amination and direct functionalization by thiol-ene click photoinitiated reaction. Even though, the reductive amination resulted unsuccessful, the oxidation pathway was studied and implement in heterogeneous and homogenous catalysis, with the second having a great accomplishment in term of reaction efficiency. The thiol-ene reaction prove to be an effective strategy to achieve polyamine from unsaturated compound, but not free from challenges due to the high number of parameters to evaluate and control to the successful reaction outcome. Moreover, this reaction was also implemented for a scale up process in a *in flow* fashion.

Taking advantage of these novel molecules, different biobased NIPUs were produced and characterized together with sugar- and lignin-based bis-cyclic carbonates *via* aminolysis reaction. The three monomers employed allowed to balance their different chemical structures, as such the aliphatic nature of the long chain vegetable oil-based polyamine, the rigid structure of lignin and the small-size erythritol bicyclic carbonate. The study of the optima ratio between the three components was crucial to achieve good results in the final thermoplastic properties.

Moreover, along the research path, new projects drove to the development of additional useful monomers for polyurethane-analogous materials, such as urethane bis-cyclic carbonates (UBCs) and acetoacetate. The synthesis was designed *via* isocyanate-free fashion and the reactivity of the UBCs obtained were further investigated. Additionally, the isocyanate-free route and the and isocyanate-based one were compered in terms of *Environmental Impact*. The two new UBC monomer were synthetized and preliminary test on their polymerization were performed.

Subsequently, three biobased acetoacetates were produced and combined with polyamines with chemical structural diversity giving birth to polyvinylogous urethanes (polyVUs). The materials achieved were characterized *via* TGA, DSC and IR. Furthermore, swelling, tensile and adhesives tests were carried out to evaluate the performances of the polymers. Particularly, the adhesive lap share tests run on wood suberates showed high strength-stress values. The dynamic intrinsic nature of polyVUs, allowed the successful reprocessing of the materials produced.

Finally, a comparative study was carried out in the frame of bio-based epoxy materials with the aim of investigating alternatives to bisphenol A diglycidyl ether for the development of a new generation of epoxy resins. Bisphenol A diglycidyl ether and an isosorbide-based diglycidyl ether were employed to create epoxy resins with a set of different amines. The thermosets were evaluated via TGA, DSC and IR. swelling, Also, swelling, tensile and adhesives tests were measured. It was observed that the aromatic nature of bisphenol A diglycidyl ether was playing a kye role in the final polymer performances.

7 REFERENCES

(1) Hansen, J.; Johnson, D.; Lacis, A.; Lebedeff, S.; Lee, P.; Rind, D.; Russell, G. Climate Impactof Increasing Atmospheric Carbon Dioxide. *Science* **1G81**, *213* (4511), 957–966. https://doi.org/10.1126/science.213.4511.957.

(2) Holme, P.; Rocha, J. C. Networks of Climate Change: Connecting Causes and Consequences. *Appl Netw Sci* **2023**, *8* (1), 10. https://doi.org/10.1007/s41109-023-00536-9.

(3) Bertazzi, P. A. Long-Term Effectsof Chemical Disasters. Lessons and Results from Seveso. *Scienceof The Total Environment* **1GG1**, *10c* (1), 5–20. https://doi.org/10.1016/0048-9697(91)90016-8.

(4) Ridings, J. E. The Thalidomide Disaster, Lessons from the Past. In *Teratogenicity Testing: Methods and Protocols*; Barrow, P. C., Ed.; Humana Press: Totowa, NJ, 2013; pp 575–586. https://doi.org/10.1007/978-1-62703-131-8_36.

(5) Erythropel, H. C.; Zimmerman, J. B.; de Winter, T. M.; Petitjean, L.; Melnikov, F.; Lam, C. H.; Lounsbury, A. W.; Mellor, K. E.; Janković, N. Z.; Tu, Q.; Pincus, L. N.; Falinski, M. M.; Shi, W.; Coish, P.; Plata, D. L.; Anastas, P. T. The Green ChemisTREE: 20 Years after Taking Root with the 12 Principles. *Green Chem.* **2018**, *20* (9), 1929–1961. https://doi.org/10.1039/C8GC00482J.

(6) Cheng, H. N.; Gross, R. A. Sustainability and Green Polymer Chemistry—An Overview. In *Sustainability & Green Polymer Chemistry Volume 1: Green Products and Processes*; ACS Symposium Series; American Chemical Society, 2020; Vol. 1372, pp 1–11. https://doi.org/10.1021/bk-2020-1372.ch001.

(7) Peer Reviewed: Design Throughthe 12 Principles of Green Engineering. *Environ. Sci. Technol.* **2003**, *37* (5), 94A-101A. https://doi.org/10.1021/es032373g.

(8) Sheldon, R. A. The EFactor at 30: APassion for Pollution Prevention. *Green Chem.* **2023**, *25* (5), 1704–1728. https://doi.org/10.1039/D2GC04747K.

(9) Rizos, V.; Tuokko, K.; Behrens, A. The Circular Economy: AReview of Definitions, Processes and Impacts. *CEPS Papers* **2017**.

(10) *THE 17 GOALS | Sustainable Development*. https://sdgs.un.org/goals (accessed 2024-12- 11).

(11) Silva, A. C. Q.; Silvestre, A. J. D.; Vilela, C.; Freire, C. S. R. Natural Polymers-Based Materials: A Contribution to a Greener Future. *Molecules* **2022**, *27* (1), 94. https://doi.org/10.3390/molecules27010094.

(12) Ali, S. S.; Abdelkarim, E. A.; Elsamahy, T.; Al-Tohamy, R.; Li, F.; Kornaros, M.; Zuorro, A.; Zhu, D.; Sun, J. Bioplastic Production in Terms of Life Cycle Assessment: A State-of-the- Art Review. *Environmental Science and Ecotechnology* **2023**, *15*, 100254. https://doi.org/10.1016/j.ese.2023.100254.

(13) Mohanty, A. K.; Wu, F.; Mincheva, R.; Hakkarainen, M.; Raquez, J.-M.; Mielewski, D. F.; Narayan, R.; Netravali, A. N.; Misra, M. Sustainable Polymers. *Nat Rev Methods Primers* **2022**, *2* (1), 1–27. https://doi.org/10.1038/s43586-022-00124-8.

(14) Wang, S.; Chen, B.; Sun, Z.; Long, X.; Xue, M.; Yu, H.; Sun, M.; Wang, Y. The Booming Non-Food Bioeconomy Drives Large Share of Global Land-Use Emissions. *Global Environmental Change* **2023**, *83*, 102760. https://doi.org/10.1016/j.gloenvcha.2023.102760.

(15) Castro-Muñoz, R.; Díaz-Montes, E.; Gontarek-Castro, E.; Boczkaj, G.; Galanakis, C. M. A Comprehensive Review on Current and Emerging Technologies toward the Valorization of Bio-Based Wastes and by Products from Foods. *Comprehensive Reviews in Food Science and Food Safety* **2022**, *21* (1), 46–105. https://doi.org/10.1111/1541-4337.12894.

(16) A. Koutinas, A.; Vlysidis, A.; Pleissner, D.; Kopsahelis, N.; Garcia, I. L.; K. Kookos, I.; Papanikolaou, S.; Him Kwan, T.; Ki Lin, C. S. Valorization of Industrial Waste and By- Product

Streamsvia Fermentation for the Production of Chemicalsand Biopolymers. *Chemical Society Reviews* **2014**, *43* (8), 2587–2627. https://doi.org/10.1039/C3CS60293A.
(17) Kessler, B.; Weusthuis, R.; Witholt, B.; Eggink, G. Production of Microbial Polyesters: Fermentation and Downstream Processes. *Advances in biochemical engineering/biotechnology* **2001**, *71*, 159–182. https://doi.org/10.1007/3-540-40021-4_5.
(18) Saravanan, A.; Senthil kumar, P.; Vo, D.-V. N.; Jeevanantham, S.; Bhuvaneswari, V.; Anantha Narayanan, V.; Yaashikaa, P. R.; Swetha, S.; Reshma, B. A Comprehensive Review on Different Approaches for CO2 Utilization and Conversion Pathways. *Chemical Engineering Science* **2021**, *23c*, 116515. https://doi.org/10.1016/j.ces.2021.116515.
(19) Pires da Mata Costa, L.; Micheline Vaz de Miranda, D.; Couto de Oliveira, A. C.; Falcon, L.; Stella Silva Pimenta, M.; Guilherme Bessa, I.; Juarez Wouters, S.; Andrade, M. H. S.; Pinto, J. C. Capture and Reuse of Carbon Dioxide (CO2) for a Plastics Circular Economy: A Review. *Processes* **2021**, *S* (5), 759. https://doi.org/10.3390/pr9050759.
(20) Pellis, A.; Malinconico, M.; Guarneri, A.; Gardossi, L. Renewable Polymers and Plastics: Performance beyond the Green. *New Biotechnology* **2021**, *c0*, 146–158. https://doi.org/10.1016/j.nbt.2020.10.003.
(21) *What is natural capital?*. European Investment Bank. https://www.eib.org/en/stories/nature-environment-pollution (accessed 2024-09-09).
(22) Moshood, T. D.; Nawanir, G.; Mahmud, F.; Mohamad, F.; Ahmad, M. H.; AbdulGhani, A. Sustainability of Biodegradable Plastics: New Problem or Solution to Solve the Global Plastic Pollution? *Current Research in Green and Sustainable Chemistry* **2022**, *5*, 100273. https://doi.org/10.1016/j.crgsc.2022.100273.
(23) Malafeev, K. V.; Apicella, A.; Incarnato, L.; Scarfato, P. Understanding the Impact of Biodegradable Microplastics on Living Organisms Entering the Food Chain: AReview. *Polymers* **2023**, *15* (18), 3680. https://doi.org/10.3390/polym15183680.
(24) Ülger-Vatansever, B.; Onay, T. T.; Demirel, B. Evaluation of Bioplastics Biodegradation under Simulated Landfill Conditions. *Environ Sci Pollut Res* **2024**, *31* (12), 17779–17787. https://doi.org/10.1007/s11356-023-30195-3.
(25) Van Roijen, E. C.; Miller, S. A. A Review of Bioplastics at End-of-Life: Linking Experimental Biodegradation Studies and Life Cycle Impact Assessments. *Resources, Conservation and Recycling* **2022**, *181*, 106236. https://doi.org/10.1016/j.resconrec.2022.106236.
(26) Clark, R. A.; Shaver, M. P. Depolymerization within a Circular Plastics System. *Chem. Rev.* **2024**, *124* (5), 2617–2650. https://doi.org/10.1021/acs.chemrev.3c00739.
(27) Østergaard, P. A.; Duic, N.; Noorollahi, Y.; Kalogirou, S. Renewable Energy for Sustainable Development. *Renewable Energy* **2022**, *1SS*, 1145–1152. https://doi.org/10.1016/j.renene.2022.09.065.
(28) Curran, M. A. Life Cycle Assessment: AReview of the Methodology and Its Application to Sustainability. *Current Opinion in Chemical Engineering* **2013**, *2* (3), 273–277. https://doi.org/10.1016/j.coche.2013.02.002.
(29) A, A.; Ligthart, T. *Data Certification for LCAComparisons: Inventory of Current Status and Strength and Weakness Analysis.*; 2002.
(30) Environment, U. N. *Publications & data*. https://www.unep.org/publications-data (accessed 2024-09-11).
(31) *European Bioplastics e.V.* European Bioplastics e.V. https://www.european- bioplastics.org/ (accessed 2024-09-17).
(32) EUBIO_Admin. *Feedstock*. European Bioplastics e.V. https://www.european-bioplastics.org/bioplastics/feedstock/ (accessed 2024-09-11).
(33) Standards, E. *Searchfor an expression "EN 17228:201S."* https://www.en-standard.eu. https://www.en-standard.eu/search/?q=EN+17228%3A2019 (accessed 2024-09-11).

(34) de Freitas Netto, S. V.; Sobral, M. F. F.; Ribeiro, A. R. B.; Soares, G. R. da L. Concepts and Forms of Greenwashing: A Systematic Review. *Environmental Sciences Europe* **2020**, *32* (1), 19. https://doi.org/10.1186/s12302-020-0300-3.

(35) *Global vegetable oil production 2023/24*. Statista. https://www.statista.com/statistics/263978/global vegetable-oil-production-since- 2000-2001/ (accessed 2024-07-18).

(36) Schlagermann, P.; Göttlicher, G.; Dillschneider, R.; Rosello-Sastre, R.; Posten, C. Composition of Algal Oil and Its Potential as Biofuel. *Journal of Combustion* **2012**, *2012* (1), 285185. https://doi.org/10.1155/2012/285185.

(37) *Vegetable oils consumption worldwide 2023/24*. Statista. https://www.statista.com/statistics/263937/vegetable-oils-global-consumption/ (accessed 2024-09-10).

(38) Petrović, Z. S.; Javni, I.; Ionescu, M. Biological Oils as Precursors to Novel Polymeric Materials. *j renew mater* **2013**, *1* (3), 167–186. https://doi.org/10.7569/JRM.2013.634112.

(39) Biermann, U.; Bornscheuer, U. T.; Feussner, I.; Meier, M. A. R.; Metzger, J. O. Fatty Acids and Their Derivatives as Renewable Platform Molecules for the Chemical Industry. *Angew Chem Int Ed* **2021**, *c0* (37), 20144–20165. https://doi.org/10.1002/anie.202100778.

(40) Ray, D.; Mistri, E. Use of Fatty Acids to Develop Green Polymers and Composites. In *Green Solvents I: Properties and Applications in Chemistry*; Mohammad, A., Ed.; Springer Netherlands: Dordrecht, 2012; pp 299–330. https://doi.org/10.1007/978-94-007-1712- 1_10.

(41) Firdaus, M. Thiol-Ene (Click) Reactions as Efficient Tools for Terpene Modification. *Asian J. Org. Chem.* **2017**, *c* (12), 1702–1714. https://doi.org/10.1002/ajoc.201700387.

(42) Sawpan, M. A. Polyurethanes from Vegetable Oils and Applications: A Review. *JPolym Res* **2018**, *25* (8), 184. https://doi.org/10.1007/s10965-018-1578-3.

(43) Kolb, N.; Winkler, M.; Syldatk, C.; Meier, M. A. R. Long-Chain Polyesters and Polyamides from Biochemically Derived Fatty Acids. *European Polymer Journal* **2014**, *51*, 159–166. https://doi.org/10.1016/j.eurpolymj.2013.11.007.

(44) Lebarbé, T.; Grau, E.; Gadenne, B.; Alfos, C.; Cramail, H. Synthesis of Fatty Acid-Based Polyesters and Their Blends with Poly(l-Lactide) as a Way To Tailor PLLA Toughness. *ACS Sustainable Chem. Eng.* **2015**, *3* (2), 283–292. https://doi.org/10.1021/sc500648g.

(45) Firdaus, M.; Meier, M. A. R. Renewable Polyamides and Polyurethanes Derived from Limonene. *Green Chem.* **2013**, *15* (2), 370–380. https://doi.org/10.1039/C2GC36557J.

(46) Echeverri, D. A.; Inciarte, H. C.; Cortés, N.; Estenoz, D. A.; Polo, M. L.; Rios, L. A. Synthesis of a Renewable Polyamine from Canola Oil by Photocatalyzed Thiol-Ene Addition of Cysteamine under Green Conditions. *Journal of Applied Polymer Science* **2023**, *140* (28), e54036. https://doi.org/10.1002/app.54036.

(47) Thin Wai, P.; Jiang, P.; Shen, Y.; Zhang, P.; Gu, Q.; Leng, Y. Catalytic Developments in the Epoxidation of Vegetable Oils and the Analysis Methods of Epoxidized Products. *RSC Advances* **201G**, *S* (65), 38119–38136. https://doi.org/10.1039/C9RA05943A.

(48) Galià, M.; de Espinosa, L. M.; Ronda, J. C.; Lligadas, G.; Cádiz, V. Vegetable Oil-Based Thermosetting Polymers. *European Journal of Lipid Science and Technology* **2010**, *112* (1), 87–96. https://doi.org/10.1002/ejlt.200900096.

(49) Montero de Espinosa, L.; Ronda, J. C.; Galià, M.; Cádiz, V. A New Enone-Containing Triglyceride Derivative as Precursor of Thermosets from Renewable Resources: Enone-Containing Triglyceride Derivative. *J. Polym. Sci. APolym. Chem.* **2008**, *4c* (20), 6843– 6850. https://doi.org/10.1002/pola.22992.

(50) Xia, Y.; Larock, R. C. Vegetable Oil-Based Polymeric Materials: Synthesis, Properties, and Applications. *Green Chem.* **2010**, *12* (11), 1893. https://doi.org/10.1039/c0gc00264j.

(51) *Flavoursand Fragrances: Chemistry, Bioprocessing and Sustainability*; Berger, R. G., Ed.; Springer Berlin Heidelberg: Berlin, Heidelberg, 2007. https://doi.org/10.1007/978-3-540- 49339-6.
(52) Pichersky, E.; Raguso, R. A. Why Do Plants Produce so Many Terpenoid Compounds? *New Phytol* **2018**, *220* (3), 692–702. https://doi.org/10.1111/nph.14178.
(53) *Terpenes Market Research Report [2024-2032]*. https://www.businessresearchinsights.com/market-reports/terpenes-market-105622 (accessed 2024-09-10).
(54) Helfrich, E. J. N.; Lin, G.-M.; Voigt, C. A.; Clardy, J. Bacterial Terpene Biosynthesis: Challenges and Opportunities for Pathway Engineering. *Beilstein J. Org. Chem.* **201G**, *15* (1), 2889–2906. https://doi.org/10.3762/bjoc.15.283.
(55) Fordjour, E.; Mensah, E. O.; Hao, Y.; Yang, Y.; Liu, X.; Li, Y.; Liu, C.-L.; Bai, Z. Toward Improved Terpenoids Biosynthesis: Strategies to Enhance the Capabilities of Cell Factories. *Bioresources and Bioprocessing* **2022**, *S* (1), 6. https://doi.org/10.1186/s40643-022-00493-8.
(56) Mosquera, Marta. E. G.; Jiménez, G.; Tabernero, V.; Vinueza-Vaca, J.; García-Estrada, C.; Kosalková, K.; Sola-Landa, A.; Monje, B.; Acosta, C.; Alonso, R.; Valera, M. Á. Terpenes and Terpenoids: Building Blocks to Produce Biopolymers. *Sustainable Chemistry* **2021**, *2* (3), 467–492. https://doi.org/10.3390/suschem2030026.
(57) Travnikova, E. Berger R.G. Flavours and Fragrances.
(58) Senyek, M. L. Isoprene Polymers. In *Encyclopedia of Polymer Science and Technology*; John Wiley C Sons, Ltd, 2008. https://doi.org/10.1002/0471440264.pst175.
(59) *Nitrogen-Containing Polymers Derived from Terpenes: Possibilities and Limitations - Scheelje - 2023 - Macromolecular Chemistryand Physics - Wiley Online Library*. https://onlinelibrary.wiley.com/doi/full/10.1002/macp.202200403 (accessed 2024-07-31).
(60) Winnacker, M.; Sag, J.; Tischner, A.; Rieger, B. Sustainable, Stereoregular, and Optically Active Polyamides via Cationic Polymerization of ε-Lactams Derived from the Terpene β- Pinene. *Macromol. Rapid Commun.* **2017**, *38* (9), 1600787. https://doi.org/10.1002/marc.201600787.
(61) Winnacker, M.; Neumeier, M.; Zhang, X.; Papadakis, C. M.; Rieger, B. Sustainable Chiral Polyamides with High Melting Temperature via Enhanced Anionic Polymerization of a Menthone-Derived Lactam. *Macromol. Rapid Commun.* **2016**, *37* (10), 851–857. https://doi.org/10.1002/marc.201600056.
(62) Stockmann, P. N.; Van Opdenbosch, D.; Poethig, A.; Pastoetter, D. L.; Hoehenberger, M.; Lessig, S.; Raab, J.; Woelbing, M.; Falcke, C.; Winnacker, M.; Zollfrank, C.; Strittmatter, H.; Sieber, V. Biobased Chiral Semi-Crystalline or Amorphous High-Performance Polyamides and Their Scalable Stereoselective Synthesis. *Nat Commun* **2020**, *11* (1), 509. https://doi.org/10.1038/s41467-020-14361-6.
(63) *Orange production worldwide 2023*. Statista. https://www.statista.com/statistics/577398/world-orange-production/ (accessed 2024-09-12).
(64) Nyamwihura, R. J.; Ogungbe, I. V. The Pinene Scaffold: Its Occurrence, Chemistry, Synthetic Utility, and Pharmacological Importance. *RSC Adv.* **2022**, *12* (18), 11346–11375. https://doi.org/10.1039/D2RA00423B.
(65) Monteiro, J. L. F.; Veloso, C. O. Catalytic Conversion of Terpenes into Fine Chemicals. *Topics in Catalysis* **2004**, *27* (1–4), 169–180. https://doi.org/10.1023/B:TOCA.0000013551.99872.8d.
(66) Harman-Ware, A. E. Conversion of Terpenes to Chemicals and Related Products. In *Chemical Catalysts for Biomass Upgrading*; John Wiley C Sons, Ltd, 2020; pp 529–568. https://doi.org/10.1002/9783527814794.ch13.
(67) Berg, A.; Guzmán, F. Wood Biorefineries. In *Springer Handbook of Wood Science and*

Technology; Niemz, P., Teischinger, A., Sandberg, D., Eds.; Springer International Publishing: Cham, 2023; pp 1713–1751. https://doi.org/10.1007/978-3-030-81315-4_32.

(68) Kumar, V.; Verma, P. Pulp-Paper Industry Sludge Waste Biorefinery for Sustainable Energy and Value-Added Products Development: A Systematic Valorization towards Waste Management. *Journal of Environmental Management* **2024**, *352*, 120052. https://doi.org/10.1016/j.jenvman.2024.120052.

(69) Klemm, D.; Heublein, B.; Fink, H.-P.; Bohn, A. Cellulose: Fascinatin Biopolymer and Sustainable Raw Material. *Angewandte Chemie International Edition* **2005**, *44* (22), 3358– 3393. https://doi.org/10.1002/anie.200460587.

(70) Polymers | Free Full-Text | A Critical Review on Wood-Based Polymer Composites: *Processing, Properties, and Prospects*. https://www.mdpi.com/2073-4360/14/3/589 (accessed 2024-09-17).

(71) Pandey, M. P.; Kim, C. S. Lignin Depolymerization and Conversion: A Review of Thermochemical Methods. *Chemical Engineering & Technology* **2011**, *34* (1), 29–41. https://doi.org/10.1002/ceat.201000270.

(72) Magalhães, S.; Fernandes, C.; Pedrosa, J. F. S.; Alves, L.; Medronho, B.; Ferreira, P. J. T.; Rasteiro, M. da G. Eco-Friendly Methods for Extraction and Modification of Cellulose: An Overview. *Polymers* **2023**, *15* (14), 3138. https://doi.org/10.3390/polym15143138.

(73) Jain, A.; Ong, S. P.; Hautier, G.; Chen, W.; Richards, W. D.; Dacek, S.; Cholia, S.; Gunter, D.; Skinner, D.; Ceder, G.; Persson, K. A. Commentary: The Materials Project: AMaterials Genome Approach to Accelerating Materials Innovation. *APL Materials* **2013**, *1* (1), 011002. https://doi.org/10.1063/1.4812323.

(74) Mazi, T. A.; Stanhope, K. L. Erythritol: An In-Depth Discussion of Its Potential to Be a Beneficial Dietary Component. *Nutrients* **2023**, *15* (1), 204. https://doi.org/10.3390/nu15010204.

(75) Delidovich, I.; Hausoul, P. J. C.; Deng, L.; Pfützenreuter, R.; Rose, M.; Palkovits, R. Alternative Monomers Based on Lignocellulose and Their Use for Polymer Production. *Chem. Rev.* **2016**, *11c* (3), 1540–1599. https://doi.org/10.1021/acs.chemrev.5b00354.

(76) Nakagawa, Y.; Kasumi, T.; Ogihara, J.; Tamura, M.; Arai, T.; Tomishige, K. Erythritol: Another C4 Platform Chemical in Biomass Refinery. *ACS Omega* **2020**, *5* (6), 2520–2530. https://doi.org/10.1021/acsomega.9b04046.

(77) Dannecker, P.-K.; Meier, M. A. R. Facile and Sustainable Synthesis of Erythritol Bis(Carbonate), a Valuable Monomer for Non-Isocyanate Polyurethanes (NIPUs). *Sci Rep* **201G**, *S* (1), 9858. https://doi.org/10.1038/s41598-019-46314-5.

(78) *Bio-Based Poly(hydroxy urethane)s for Efficient Organic High-Power Energy Storage | Journal of the American Chemical Society*. https://pubs.acs.org/doi/full/10.1021/jacs.2c12090 (accessed 2024-05-14).

(79) *Plastics – the fast Facts 2023 • Plastics Europe*. Plastics Europe. https://plasticseurope.org/knowledge-hub/plastics-the-fast-facts-2023/(accessed 2024-09-16).

(80) Janik, H.; Sienkiewicz, M.; Kucinska-Lipka, J. 9 - Polyurethanes. In *Handbookof Thermoset Plastics (Third Edition)*; Dodiuk, H., Goodman, S. H., Eds.; William Andrew Publishing: Boston, 2014; pp 253–295. https://doi.org/10.1016/B978-1-4557-3107-7.00009-9.

(81) Akindoyo, J. O.; Beg, M. D. H.; Ghazali, S.; Islam, M. R.; Jeyaratnam, N.; Yuvaraj, A. R. Polyurethane Types, Synthesis and Applications – a Review. *RSC Adv.* **2016**, *c* (115), 114453–114482. https://doi.org/10.1039/C6RA14525F.

(82) *Polyurethane Market Size, Share& Growth Report, 2030*. https://www.grandviewresearch.com/industry-analysis/polyurethane-pu-market (accessed 2024-11-06).

(83) Bayer, O. Das Di-Isocyanat-Polyadditionsverfahren (Polyurethane). *Angewandte Chemie***1G47**, *5S* (9), 257–272. https://doi.org/10.1002/ange.19470590901 .

(84) Das, A.; Mahanwar, P. A Brief Discussion on Advances in Polyurethane Applications. *Advanced*

Industrial and Engineering Polymer Research **2020**, *3* (3), 93–101. https://doi.org/10.1016/j.aiepr.2020.07.002.
(85) Zafar, F.; Sharmin, E. *Polyurethane*; BoD – Books on Demand, 2012.
(86) *Developments of polyurethane in biomedical applications: A review - ScienceDirect*. https://www.sciencedirect.com/science/article/pii/S2772443323000351 (accessed 2024-11-06).
(87) Adetunji, C. O.; Olaniyan, O. T.; Anani, O. A.; Inobeme, A.; Mathew, J. T. Environmental Impact of Polyurethane Chemistry. In *Polyurethane Chemistry: Renewable Polyols and Isocyanates*; ACS Symposium Series; American Chemical Society, 2021; Vol. 1380, pp 393–411. https://doi.org/10.1021/bk-2021-1380.ch014.
(88) Murphy, R. What Is Undermining Climate Change Mitigation? How Fossil-Fuelled Practices Challenge Low-Carbon Transitions. *Energy Research & Social Science* **2024**, *108*, 103390. https://doi.org/10.1016/j.erss.2023.103390.
(89) Ritchie, H.; Rosado, P.; Roser, M. Fossil Fuels. *Our World in Data* **2024**.
(90) Xie, Y.; Gao, S.; Zhang, D.; Wang, C.; Chu, F. Bio-Based Polymeric Materials Synthesized from Renewable Resources: A Mini-Review. *Resources Chemicals and Materials* **2023**, *2* (3), 223–230. https://doi.org/10.1016/j.recm.2023.05.001.
(91) Unverferth, M.; Meier, M. A. R. A Sustainable Tandem Catalysis Approach to Plant Oil-Based Polyols via Schenck-Ene Reaction and Epoxidation. *Eur. J. Lipid Sci. Technol.* **2018**, *120* (5), 1800015. https://doi.org/10.1002/ejlt.201800015.
(92) Zhang, C.; Madbouly, S. A.; Kessler, M. R. Biobased Polyurethanes Prepared from Different Vegetable Oils. *ACS Appl. Mater. Interfaces* **2015**, *7* (2), 1226–1233. https://doi.org/10.1021/am5071333.
(93) Hevus, I.; Webster, D. C. Short-Chain Polyols from Bio-Based Carboxylic Acids for High-Performance Polyurethane Coatings. *Prog. Org. Coat.* **2023**, *183*, 107825. https://doi.org/10.1016/j.porgcoat.2023.107825.
(94) Alagi, P.; Choi, Y. J.; Seog, J.; Hong, S. C. Efficient and Quantitative Chemical Transformation of Vegetable Oils to Polyols through a Thiol-Ene Reaction for Thermoplastic Polyurethanes. *Ind. Crops Prod.* **2016**, *87*, 78–88. https://doi.org/10.1016/j.indcrop.2016.04.027.
(95) Feng, Y.; Liang, H.; Yang, Z.; Yuan, T.; Luo, Y.; Li, P.; Yang, Z.; Zhang, C. A Solvent-Free and Scalable Method To Prepare Soybean-Oil-Based Polyols by Thiol–Ene Photo-Click Reaction and Biobased Polyurethanes Therefrom. *ACS Sustainable Chem. Eng.* **2017**, *5* (8), 7365–7373. https://doi.org/10.1021/acssuschemeng.7b01672.
(96) Sardon, H.; Mecerreyes, D.; Basterretxea, A.; Avérous, L.; Jehanno, C. From Lab to Market: Current Strategies for the Production of Biobased Polyols. *ACS Sustain. Chem. Eng.* **2021**, *9* (32), 10664–10677. https://doi.org/10.1021/acssuschemeng.1c02361.
(97) Lemouzy, S.; Delavarde, A.; Lamaty, F.; Bantreil, X.; Pinaud, J.; Caillol, S. Lignin-Based Bisguaiacol Diisocyanate: A Green Route for the Synthesis of Biobased Polyurethanes. *Green Chem.* **2023**, *25* (12), 4833–4839. https://doi.org/10.1039/d3gc00704a.
(98) Filippi, L.; Meier, M. A. R. Fully Renewable Non-Isocyanate Polyurethanes via the Lossen Rearrangement. *Macromolecular Rapid Communications* **2021**, *42* (3), 2000440. https://doi.org/10.1002/marc.202000440.
(99) *Emergency and Continuous Exposure Limits for Selected Airborne Contaminants: Volume 2 - PubMed*. https://pubmed.ncbi.nlm.nih.gov/25032441/ (accessed 2024-11-06).
(100) Niesiobędzka, J.; Datta, J. Challenges and Recent Advances in Bio-Based Isocyanate Production. *Green Chem.* 2023, *25* (7), 2482–2504. https://doi.org/10.1039/D2GC04644J.
(101) Hojabri, L.; Kong, X.; Narine, S. S. Fatty Acid-Derived Diisocyanate and Biobased Polyurethane Produced from Vegetable Oil: Synthesis, Polymerization, and Characterization. *Biomacromolecules* **2009**, *10* (4), 884–891. https://doi.org/10.1021/bm801411w.
(102) *Skin Exposure to Isocyanates: Reasons for Concern - PMC*.

https://pmc.ncbi.nlm.nih.gov/articles/PMC1849909/ (accessed 2024-11-06).
(103) Bello, D.; Herrick, C. A.; Smith, T. J.; Woskie, S. R.; Streicher, R. P.; Cullen, M. R.; Liu, Y.; Redlich, C. A. Skin Exposure to Isocyanates: Reasons for Concern. *Environmental Health Perspectives* **2007**, *115* (3), 328–335. https://doi.org/10.1289/ehp.9557.
(104) *Commission Regulation (EU) 2020/1149 of 3 August 2020 Amending Annex XVII to Regulation (EC) No 1907/2006 of the European Parliament and of the Council Concerning the Registration, Evaluation, Authorisation and Restriction of Chemicals (REACH) as Regards Diisocyanates (Text with EEA Relevance)*; 2020; Vol. 252. http://data.europa.eu/eli/reg/2020/1149/oj/eng (accessed 2024-09-18).
(105) *Commission Regulation (EU) 2016/2235 of 12 December 2016 Amending Annex XVII to Regulation (EC) No 1907/2006 of the European Parliament and of the Council Concerning the Registration, Evaluation, Authorisation and Restriction of Chemicals (REACH) as Regards Bisphenol A (Text with EEA Relevance)*; 2016; Vol. 337. http://data.europa.eu/eli/reg/2016/2235/oj/eng (accessed 2024-09-20).
(106) *Directive (EU) 2024/869 of the European Parliament and of the Council of 13 March 2024 Amending Directive 2004/37/EC of the European Parliament and of the Council and Council Directive 98/24/EC as Regards the Limit Values for Lead and Its Inorganic Compounds and for Diisocyanates*; 2024. http://data.europa.eu/eli/dir/2024/869/oj/eng (accessed 2024-09-18).
(107) *Emergency and Continuous Exposure Limits for Selected Airborne Contaminants: Volume 2 - PubMed*. https://pubmed.ncbi.nlm.nih.gov/25032441/ (accessed 2024-11-06).
(108) Gomez-Lopez, A.; Elizalde, F.; Calvo, I.; Sardon, H. Trends in Non-Isocyanate Polyurethane (NIPU) Development. *Chem. Commun.* **2021**, *57* (92), 12254–12265. https://doi.org/10.1039/D1CC05009E.
(109) Catalá, J.; Guerra, I.; García-Vargas, J. M.; Ramos, M. J.; García, M. T.; Rodríguez, J. F. Tailor-Made Bio-Based Non-Isocyanate Polyurethanes (NIPUs). *Polymers* **2023**, *15* (6), 1589. https://doi.org/10.3390/polym15061589.
(110) Maisonneuve, L.; Lamarzelle, O.; Rix, E.; Grau, E.; Cramail, H. Isocyanate-Free Routes to Polyurethanes and Poly(Hydroxy Urethane)s. *Chem. Rev.* **2015**, *115* (22), 12407–12439. https://doi.org/10.1021/acs.chemrev.5b00355.
(111) Wołosz, D. Non-Isocyanate Aliphatic-Aromatic Poly(Carbonate-Urethane)s-An Insight into Transurethanization Reactions and Structure-Property Relationships. *Int J Mol Sci* **2022**, *23* (19), 10999. https://doi.org/10.3390/ijms231910999.
(112) Cornille, A.; Auvergne, R.; Figovsky, O.; Boutevin, B.; Caillol, S. A Perspective Approach to Sustainable Routes for Non-Isocyanate Polyurethanes. *European Polymer Journal* **2017**, *87*, 535–552. https://doi.org/10.1016/j.eurpolymj.2016.11.027.
(113) Qiao, C.; Engel, P. D.; Ziegenhagen, L. A.; Rominger, F.; Schäfer, A.; Deglmann, P.; Rudolf, P.; Comba, P.; Hashmi, A. S. K.; Schaub, T. An Organocatalytic Route to Endo-Vinylene Carbonates from Carbon Dioxide-Based Exo-Vinylene Carbonates. *Advanced Synthesis & Catalysis* **2024**, *366* (2), 291–298. https://doi.org/10.1002/adsc.202301374.
(114) Mishra, V.; Peter, S. C. A Comprehensive Overview of the Catalytic Pathway for CO2 Utilization with Epoxide to Cyclic Carbonate. *Chem Catalysis* **2024**, *4* (1), 100796. https://doi.org/10.1016/j.checat.2023.100796.
(115) Tomita, H.; Sanda, F.; Endo, T. Polyaddition of Bis(Seven-Membered Cyclic Carbonate) with Diamines: A Novel and Efficient Synthetic Method for Polyhydroxyurethanes. *Journal of Polymer Science Part A: Polymer Chemistry* **2001**, *39* (23), 4091–4100. https://doi.org/10.1002/pola.10058.
(116) Habets, T.; Siragusa, F.; Grignard, B.; Detrembleur, C. Advancing the Synthesis of Isocyanate-Free Poly(Oxazolidones)s: Scope and Limitations. *Macromolecules* **2020**, *53* (15), 6396–6408. https://doi.org/10.1021/acs.macromol.0c01231.

(117) Hejna, A.; Kosmela, P.; Formela, K.; Piszczyk, Ł.; Haponiuk, J. T. Potential Applications of Crude Glycerol in Polymer Technology–Current State and Perspectives. *Renewable and Sustainable Energy Reviews* **2016**, *66*, 449–475. https://doi.org/10.1016/j.rser.2016.08.020.
(118) Bach, R. D.; Canepa, C.; Winter, J. E.; Blanchette, P. E. Mechanism of Acid-Catalyzed Epoxidation of Alkenes with Peroxy Acids. *J. Org. Chem.* **1997**, *62* (15), 5191–5197. https://doi.org/10.1021/jo950930e.
(119) Monnier, J. R. The Direct Epoxidation of Higher Olefins Using Molecular Oxygen. *Applied Catalysis A: General* **2001**, *221* (1), 73–91. https://doi.org/10.1016/S0926-860X(01)00799-2.
(120) Shin, I.-S.; Park, N.-H.; Lee, J.-H.; Kim, K.-H.; Moon, C.; Kim, S.-H.; Her, S.-H.; Park, S.-C.; Kim, H.-Y. One-Generation Reproductive Toxicity Study of Epichlorohydrin in Sprague-Dawley Rats. *Drug and chemical toxicology* **2010**, *33*, 291–301. https://doi.org/10.3109/01480541003734030.
(121) Yalçın, E.; Uzun, A.; Çavuşoğlu, K. In Vivo Epiclorohidrine Toxicity: Cytogenetic, Biochemical, Physiological, and Anatomical Evidences. *Environ Sci Pollut Res* **2019**, *26* (22), 22400–22406. https://doi.org/10.1007/s11356-019-05518-y.
(122) *Epoxidation of Vegetable Oils, Unsaturated Fatty Acids and Fatty Acid Esters: A Review | Bentham Science*. https://www.eurekaselect.com/article/98316 (accessed 2024-11-09).
(123) Jaillet, F.; Darroman, E.; Boutevin, B.; Caillol, S. A Chemical Platform Approach on Cardanol Oil: From the Synthesis of Building Blocks to Polymer Synthesis. *OCL Oilseeds and fats crops and lipids* **2016**, *23* (5), 511–518. https://doi.org/10.1051/ocl/2016022.
(124) Fache, M.; Darroman, E.; Besse, V.; Auvergne, R.; Caillol, S.; Boutevin, B. Vanillin, a Promising Biobased Building-Block for Monomer Synthesis. *Green Chemistry* **2014**, *16* (4), 1987–1998. https://doi.org/10.1039/C3GC42613K.
(125) Meng, Y.; Taddeo, F.; Aguilera, A. F.; Cai, X.; Russo, V.; Tolvanen, P.; Leveneur, S. The Lord of the Chemical Rings: Catalytic Synthesis of Important Industrial Epoxide Compounds. *Catalysts* **2021**, *11* (7), 765. https://doi.org/10.3390/catal11070765.
(126) Mora, A.-S.; Decostanzi, M.; David, G.; Caillol, S. Cardanol-Based Epoxy Monomers for High Thermal Properties Thermosets. *European Journal of Lipid Science and Technology* **2019**, *121* (8), 1800421. https://doi.org/10.1002/ejlt.201800421.
(127) Aouf, C.; Lecomte, J.; Villeneuve, P.; Dubreucq, E.; Fulcrand, H. Chemo-Enzymatic Functionalization of Gallic and Vanillic Acids: Synthesis of Bio-Based Epoxy Resins Prepolymers. *Green Chemistry* **2012**, *14* (8), 2328–2336. https://doi.org/10.1039/C2GC35558B.
(128) Miloslavskiy, D.; Gotlib, E.; Figovsky, O.; Pashin, D. Cyclic Carbonates Based on Vegetable Oils. *International Letters of Chemistry, Physics and Astronomy* **2014**, *27*, 20–29. https://doi.org/10.18052/www.scipress.com/ILCPA.27.20.
(129) Maisonneuve, L.; More, A. S.; Foltran, S.; Alfos, C.; Robert, F.; Landais, Y.; Tassaing, T.; Grau, E.; Cramail, H. Novel Green Fatty Acid-Based Bis-Cyclic Carbonates for the Synthesis of Isocyanate-Free Poly(Hydroxyurethane Amide)s. *RSC Adv.* **2014**, *4* (49), 25795–25803. https://doi.org/10.1039/C4RA03675A.
(130) Cramail, H.; Maisonneuve, L.; Grau, E.; Alfos, C.; Wirotius, A. Fatty Acid-Based (Bis) 6-Membered Cyclic Carbonates as Efficient Isocyanate Free Poly(Hydroxyurethane) Precursors. *Polym. Chem.* **2014**, *5*. https://doi.org/10.1039/C4PY00922C.
(131) Froidevaux, V.; Negrell, C.; Caillol, S.; Pascault, J.-P.; Boutevin, B. Biobased Amines: From Synthesis to Polymers; Present and Future. *Chem. Rev.* **2016**, *116* (22), 14181–14224. https://doi.org/10.1021/acs.chemrev.6b00486.
(132) Ghasemlou, M.; Daver, F.; Ivanova, E. P.; Adhikari, B. Bio-Based Routes to Synthesize Cyclic Carbonates and Polyamines Precursors of Non-Isocyanate Polyurethanes: A Review. *European Polymer Journal* **2019**, *118*, 668–684. https://doi.org/10.1016/j.eurpolymj.2019.06.032.
(133) Diakoumakos, C. D.; Kotzev, D. L. Non-Isocyanate-Based Polyurethanes Derived upon the

Reaction of Amines with Cyclocarbonate Resins. *Macromolecular Symposia* **2004**, *216* (1), 37–46. https://doi.org/10.1002/masy.200451205.

(134) Blain, M.; Jean-Gérard, L.; Auvergne, R.; Benazet, D.; Caillol, S.; Andrioletti, B. Rational Investigations in the Ring Opening of Cyclic Carbonates by Amines. *Green Chem.* **2014**, *16* (9), 4286–4291. https://doi.org/10.1039/C4GC01032A.

(135) Quienne, B.; Poli, R.; Pinaud, J.; Caillol, S. Enhanced Aminolysis of Cyclic Carbonates by β-Hydroxylamines for the Production of Fully Biobased Polyhydroxyurethanes. *Green Chem.* **2021**, *23* (4), 1678–1690. https://doi.org/10.1039/D0GC04120C.

(136) Webster, D. C.; Crain, A. L. Synthesis and Applications of Cyclic Carbonate Functional Polymers in Thermosetting Coatings. *Progress in Organic Coatings* **2000**, *40* (1), 275–282. https://doi.org/10.1016/S0300-9440(00)00114-4.

(137) Zevallos Torres, L.; Woiciechowski, A.; Tanobe, V.; Karp, S.; Lorenci, L.; Faulds, C.; Soccol, C. Lignin as a Potential Source of High-Added Value Compounds: A Review. *Journal of Cleaner Production* **2020**, *263*, 121499. https://doi.org/10.1016/j.jclepro.2020.121499.

(138) *Priamine™| Dimer Diamine | Cargill*. https://www.cargill.com/bioindustrial/priamine (accessed 2025-05-08).

(139) Holfinger, M. S.; Conner, A. H.; Holm, D. R.; Hill, C. G. Jr. Synthesis of Difurfuryl Diamines by the Acidic Condensation of Furfurylamine with Aldehydes and Their Mechanism of Formation. *J. Org. Chem.* **1995**, *60* (6), 1595–1598. https://doi.org/10.1021/jo00111a017.

(140) Wybo, N.; Duval, A.; Avérous, L. Benign and Selective Amination of Lignins towards Aromatic Biobased Building Blocks with Primary Amines. *Angewandte Chemie International Edition n/a* (n/a), e202403806. https://doi.org/10.1002/anie.202403806.

(141) Chung, J.-Y.; Hwang, U.; Kim, J.; Kim, N.-Y.; Nam, J.; Jung, J.; Kim, S.-H.; Cho, J. K.; Lee, B.; Park, I.-K.; Suhr, J.; Nam, J.-D. Amine-Functionalized Lignin as an Eco-Friendly Antioxidant for Rubber Compounds. *ACS Sustainable Chem. Eng.* **2023**, *11* (6), 2303–2313. https://doi.org/10.1021/acssuschemeng.2c05878.

(142) Liu, Y.; Zhou, K.; Shu, H.; Liu, H.; Lou, J.; Guo, D.; Wei, Z.; Li, X. Switchable Synthesis of Furfurylamine and Tetrahydrofurfurylamine from Furfuryl Alcohol over RANEY® Nickel. *Catal. Sci. Technol.* **2017**, *7* (18), 4129–4135. https://doi.org/10.1039/C7CY00981J.

(143) Behloul, S.; Gayraud, O.; Frapper, G.; Guégan, F.; Upitak, K.; Thomas, C. M.; Yan, Z.; De Oliveira Vigier, K.; Jérôme, F. Acid-Catalyzed Activation and Condensation of the =C5H Bond of Furfural on Aldehydes, an Entry Point to Biobased Monomers. *ChemSusChem* **2024**, *17* (10), e202400289. https://doi.org/10.1002/cssc.202400289.

(144) Wei, Z.; Cheng, Y.; Huang, H.; Ma, Z.; Zhou, K.; Liu, Y. Reductive Amination of 5-Hydroxymethylfurfural to 2,5-Bis(Aminomethyl)Furan over Alumina-Supported Ni-Based Catalytic Systems. *ChemSusChem* **2022**, *15* (13), e202200233. https://doi.org/10.1002/cssc.202200233.

(145) Holfinger, M. S.; Conner, A. H.; Holm, D. R.; Hill, C. G. Jr. Synthesis of Difurfuryl Diamines by the Acidic Condensation of Furfurylamine with Aldehydes and Their Mechanism of Formation. *J. Org. Chem.* **1995**, *60* (6), 1595–1598. https://doi.org/10.1021/jo00111a017.

(146) Firdaus, M.; Meier, M. A. R. Renewable Polyamides and Polyurethanes Derived from Limonene. *Green Chem.* **2013**, *15* (2), 370–380. https://doi.org/10.1039/C2GC36557J.

(147) Stemmelen, M.; Lapinte, V.; Habas, J.-P.; Robin, J.-J. Plant Oil-Based Epoxy Resins from Fatty Diamines and Epoxidized Vegetable Oil. *European Polymer Journal* **2015**, *68*, 536–545. https://doi.org/10.1016/j.eurpolymj.2015.03.062.

(148) Omonov, T. S.; Kharraz, E.; Curtis, J. M. Ozonolysis of Canola Oil: A Study of Product Yields and Ozonolysis Kinetics in Different Solvent Systems. *J Am Oil Chem Soc* **2011**, *88* (5), 689–705. https://doi.org/10.1007/s11746-010-1717-4.

(149) Wang, Z.; Li, Y.; Zhu, T.; Xiong, L.; Liu, F.; Qi, H. Conversion of Renewable Vanillin into

High Performance Polyimides via an Asymmetric Aromatic Diamine Derivation. *Polymer Degradation and Stability* **2019**, *167*, 67–76. https://doi.org/10.1016/j.polymdegradstab.2019.06.002.

(150) Darroman, E.; Bonnot, L.; Auvergne, R.; Boutevin, B.; Caillol, S. New Aromatic Amine Based on Cardanol Giving New Biobased Epoxy Networks with Cardanol. *European Journal of Lipid Science and Technology* **2015**, *117* (2), 178–189. https://doi.org/10.1002/ejlt.201400248

(151) Savonnet, E.; Le Coz, C.; Grau, E.; Grelier, S.; Defoort, B.; Cramail, H. Divanillin-Based Aromatic Amines: Synthesis and Use as Curing Agents for Fully Vanillin-Based Epoxy Thermosets. *Frontiers in Chemistry* **2019**, *7*.

(152) Wu, X.; De bruyn, M.; Barta, K. A Diamine-Oriented Biorefinery Concept Using Ammonia and Raney Ni as a Multifaceted Catalyst. *Chemie Ingenieur Technik* **2022**, *94* (11), 1808–1817. https://doi.org/10.1002/cite.202200091.

(153) Marchildon, K. Polyamides – Still Strong After Seventy Years. Macromolecular Reaction Engineering 2011, 5 (1), 22–54. https://doi.org/10.1002/mren.201000017.

(154) Gomez-Lopez, A.; Elizalde, F.; Calvo, I.; Sardon, H. Trends in Non-Isocyanate Polyurethane (NIPU) Development. Chem. Commun. 2021, 57 (92), 12254–12265. https://doi.org/10.1039/D1CC05009E.

(155) Santana, J. S.; Cardoso, E. S.; Triboni, E. R.; Politi, M. J. Polyureas Versatile Polymers for New Academic and Technological Applications. Polymers 2021, 13 (24), 4393. https://doi.org/10.3390/polym13244393.

(156) Jin, F.-L.; Li, X.; Park, S.-J. Synthesis and Application of Epoxy Resins: A Review. Journal of Industrial and Engineering Chemistry 2015, 29, 1–11. https://doi.org/10.1016/j.jiec.2015.03.026.

(157) Gupta, N. K.; Reif, P.; Palenicek, P.; Rose, M. Toward Renewable Amines: Recent Advances in the Catalytic Amination of Biomass-Derived Oxygenates. ACS Catal. 2022, 12 (16), 10400–10440. https://doi.org/10.1021/acscatal.2c01717.

(158) Zhang, C.; Garrison, T. F.; Madbouly, S. A.; Kessler, M. R. Recent Advances in Vegetable Oil-Based Polymers and Their Composites. Progress in Polymer Science 2017, 71, 91–143. https://doi.org/10.1016/j.progpolymsci.2016.12.009.

(159) Epoxidation of Vegetable Oils, Unsaturated Fatty Acids and Fatty ...: Ingenta Connect. https://www.ingentaconnect.com/content/ben/mroc/2020/00000017/00000004/art00006 (accessed 2024-09-24).

(160) von Czapiewski, M.; Rhein, M.; Meier, M. A. R. Fatty Acid Derived Renewable Platform Chemicals via Selective Oxidation Processes. ACS Sustainable Chem. Eng. 2018, 6 (11), 15170–15179. https://doi.org/10.1021/acssuschemeng.8b03644.

(161) Türünç, O.; Firdaus, M.; Klein, G.; Meier, M. A. R. Fatty Acid Derived Renewable Polyamides via Thiol–Ene Additions. Green Chem. 2012, 14 (9), 2577. https://doi.org/10.1039/c2gc35982k.

(162) Winkler, M.; Meier, M. A. R. Highly Efficient Oxyfunctionalization of Unsaturated Fatty Acid Esters: An Attractive Route for the Synthesis of Polyamides from Renewable Resources. Green Chem. 2014, 16 (4), 1784–1788. https://doi.org/10.1039/C3GC41921E.

(163) Stemmelen, M.; Pessel, F.; Lapinte, V.; Caillol, S.; Habas, J.-P.; Robin, J.-J. A Fully Biobased Epoxy Resin from Vegetable Oils: From the Synthesis of the Precursors by Thiol-Ene Reaction to the Study of the Final Material: A Fully Biobased Epoxy Resin. J. Polym. Sci. A Polym. Chem. 2011, 49 (11), 2434–2444. https://doi.org/10.1002/pola.24674.

(164) Echeverri, D. A.; Inciarte, H. C.; Cortés, N.; Estenoz, D. A.; Polo, M. L.; Rios, L. A. Synthesis of a Renewable Polyamine from Canola Oil by Photocatalyzed Thiol-Ene Addition of Cysteamine under Green Conditions. Journal of Applied Polymer Science 2023, 140 (28), e54036. https://doi.org/10.1002/app.54036.

(165) Gomna, A.; N'tsoukpoe, K. E.; Le Pierrès, N.; Coulibaly, Y. Review of Vegetable Oils Behaviour at High Temperature for Solar Plants: Stability, Properties and Current Applications.

Solar Energy Materials and Solar Cells 2019, 200, 109956-. https://doi.org/10.1016/j.solmat.2019.109956.
(166) Synthesis of a renewable polyamine from canola oil by photocatalyzed thiol-ene addition of cysteamine under green conditions - Echeverri - 2023 - Journal of Applied Polymer Science - Wiley Online Library. https://onlinelibrary.wiley.com/doi/full/10.1002/app.54036 (accessed 2023-07-10).
(167) Katalytische Umsetzungen von Olefinen an Platinmetall-Verbindungen Das Consortium-Verfahren zur Herstellung von Acetaldehyd - Smidt - 1959 - Angewandte Chemie - Wiley Online Library. https://onlinelibrary.wiley.com/doi/epdf/10.1002/ange.19590710503 (accessed 2024-09-22).
(168) A. Fernandes, R.; K. Jha, A.; Kumar, P. Recent Advances in Wacker Oxidation: From Conventional to Modern Variants and Applications. Catalysis Science & Technology 2020, 10 (22), 7448–7470. https://doi.org/10.1039/D0CY01820A.
(169) Baiju, T. V.; Gravel, E.; Doris, E.; Namboothiri, I. N. N. Recent Developments in Tsuji-Wacker Oxidation. Tetrahedron Letters 2016, 57 (36), 3993–4000. https://doi.org/10.1016/j.tetlet.2016.07.081.
(170) Rajeshwaran, P.; Trouvé, J.; Youssef, K.; Gramage-Doria, R. Sustainable Wacker-Type Oxidations. Angewandte Chemie International Edition 2022, 61 (50), e202211016. https://doi.org/10.1002/anie.202211016.
(171) Tsuji, J.; Shimizu, I.; Yamamoto, K. Convenient General Synthetic Method for 1,4- and 1,5-Diketones by Palladium Catalyzed Oxidation of α-Allyl and α-3-Butenyl Ketones. Tetrahedron Letters 1976, 17 (34), 2975–2976. https://doi.org/10.1016/S0040-4039(01)85504-0.
(172) Fernandes, R. A.; Jha, A. K.; Kumar, P. Recent Advances in Wacker Oxidation: From Conventional to Modern Variants and Applications. Catal. Sci. Technol. 2020, 10 (22), 7448–7470. https://doi.org/10.1039/D0CY01820A.
(173) Dong, J. J.; Browne, W. R.; Feringa, B. L. Palladium-Catalyzed Anti-Markovnikov Oxidation of Terminal Alkenes. Angewandte Chemie International Edition 2015, 54 (3), 734–744. https://doi.org/10.1002/anie.201404856.
(174) Keith, J. A.; Nielsen, R. J.; Oxgaard, J.; Goddard, W. A. Unraveling the Wacker Oxidation Mechanisms. J. Am. Chem. Soc. 2007, 129 (41), 12342–12343. https://doi.org/10.1021/ja072400t.
(175) Keith, J. A.; Henry, P. M. The Mechanism of the Wacker Reaction: A Tale of Two Hydroxypalladations. Angewandte Chemie International Edition 2009, 48 (48), 9038–9049. https://doi.org/10.1002/anie.200902194.
(176) Imandi, V.; Puri, P.; Korde, V. The Nature of Catalytic Species in the Wacker Oxidation Process-A Review. J. Phys.: Conf. Ser. 2021, 1913 (1), 012083. https://doi.org/10.1088/1742-6596/1913/1/012083.
(177) Kočovský, P.; Bäckvall, J.-E. The Syn/Anti-Dichotomy in the Palladium-Catalyzed Addition of Nucleophiles to Alkenes. Chemistry – A European Journal 2015, 21 (1), 36–56. https://doi.org/10.1002/chem.201404070.
(178) Oxidation of olefins by palladium(II). VIII. Kinetics of the oxidation of ethylene by palladium(II) chloride in methanol. https://cdnsciencepub.com/doi/10.1139/v76-246 (accessed 2024-09-22).
(179) Stangl, H.; Jira, R. Die Durch Palladium(II)Chlorid Und Kupfer(II)Chlorid Katalysierte Oxychlorierung von Äthylen Zu Äthylenchlorhydrin. Tetrahedron Letters 1970, 11 (41), 3589–3592. https://doi.org/10.1016/S0040-4039(01)98535-1.
(180) Trouvé, J.; Youssef, K.; Kasemthaveechok, S.; Gramage-Doria, R. Catalyst Complexity in a Highly Active and Selective Wacker-Type Markovnikov Oxidation of Olefins with a Bioinspired Iron Complex. ACS Catal. 2023, 13 (7), 4421–4432. https://doi.org/10.1021/acscatal.3c00593.

(181) Puls, F.; Linke, P.; Kataeva, O.; Knölker, H. Iron-Catalyzed Wacker-type Oxidation of Olefins at Room Temperature with 1,3-Diketones or Neocuproine as Ligands**. Angew. Chem. Int. Ed. 2021, 60 (25), 14083–14090. https://doi.org/10.1002/anie.202103222.
(182) Mitsudome, T.; Umetani, T.; Nosaka, N.; Mori, K.; Mizugaki, T.; Ebitani, K.; Kaneda, K. Convenient and Efficient Pd-Catalyzed Regioselective Oxyfunctionalization of Terminal Olefins by Using Molecular Oxygen as Sole Reoxidant. Angew. Chem. Int. Ed. 2006, 45 (3), 481–485. https://doi.org/10.1002/anie.200502886.
(183) Chaudhari, D. A.; Fernandes, R. A. Hypervalent Iodine as a Terminal Oxidant in Wacker-Type Oxidation of Terminal Olefins to Methyl Ketones. J. Org. Chem. 2016, 81 (5), 2113–2121. https://doi.org/10.1021/acs.joc.6b00137.
(184) Synthesis of methyl ketones from terminal olefins using PdCl2/CrO3 system mimicking the Wacker process - ScienceDirect. https://www.sciencedirect.com/science/article/pii/S0040402014006942?casa_token=-xOgOEXxpJwAAAAA:yX1y8L1Aka3G1I4BaQpwGpxsptKW0qMFezHxcZRTQzJZ8qKQGJRD0gGEzQGnv7CXWVFrjhNHvQ (accessed 2024-10-10).
(185) Phatake, R. S.; Ramana, C. V. Oxone–Acetone Mediated Wacker-Type Oxidation of Benzo-Fused Olefins. Tetrahedron Letters 2015, 56 (25), 3868–3871. https://doi.org/10.1016/j.tetlet.2015.04.102.
(186) Fernandes, C. I.; Vaz, P. D.; Nunes, T. G.; Nunes, C. D. Zinc Biomimetic Catalysts for Epoxidation of Olefins with H2O2. Applied Clay Science 2020, 190, 105562. https://doi.org/10.1016/j.clay.2020.105562.
(187) Ubiquitous Benzoquinones, Multitalented Compounds for Palladium-Catalyzed Oxidative Reactions - Vasseur - 2015 - European Journal of Organic Chemistry - Wiley Online Library. https://chemistry-europe.onlinelibrary.wiley.com/doi/abs/10.1002/ejoc.201500080 (accessed 2024-10-10).
(188) Regioselective Wacker-Type Oxidation of Internal Olefins in tBuOH Using Oxygen as the Sole Oxidant and tBuONO as the Organic Redox Cocatalyst | Organic Letters. https://pubs.acs.org/doi/10.1021/acs.orglett.9b04503 (accessed 2024-10-10).
(189) Zhao, J.; Liu, L.; Xiang, S.; Liu, Q.; Chen, H. Direct Conversion of Allyl Arenes to Aryl Ethylketones via a TBHP-Mediated Palladium-Catalyzed Tandem Isomerization–Wacker Oxidation of Terminal Alkenes. Org. Biomol. Chem. 2015, 13 (20), 5613–5616. https://doi.org/10.1039/C5OB00586H.
(190) Morandi, B.; Wickens, Z. K.; Grubbs, R. H. Practical and General Palladium-Catalyzed Synthesis of Ketones from Internal Olefins. Angew. Chem. Int. Ed. 2013, 52 (10), 2944–2948. https://doi.org/10.1002/anie.201209541.
(191) Hammer, S. C.; Kubik, G.; Watkins, E.; Huang, S.; Minges, H.; Arnold, F. H. Anti-Markovnikov Alkene Oxidation by Metal-Oxo–Mediated Enzyme Catalysis. Science 2017, 358 (6360), 215–218. https://doi.org/10.1126/science.aao1482.
(192) Chiappe, C.; Sanzone, A.; Dyson, P. J. Styrene Oxidation by Hydrogen Peroxide in Ionic Liquids: The Role of the Solvent on the Competition between Two Pd-Catalyzed Processes, Oxidation and Dimerization. Green Chem. 2011, 13 (6), 1437–1441. https://doi.org/10.1039/C0GC00945H.
(193) Wang, X.; Venkataramanan, N. S.; Kawanami, H.; Ikushima, Y. Selective Oxidation of Styrene to Acetophenone over Supported Au–Pd Catalyst with Hydrogen Peroxide in Supercritical Carbon Dioxide. Green Chem. 2007, 9 (12), 1352–1355. https://doi.org/10.1039/B703458J.
(194) Liu, B.; Hu, P.; Xu, F.; Cheng, L.; Tan, M.; Han, W. Nickel-Catalyzed Remote and Proximal Wacker-Type Oxidation. Commun Chem 2019, 2 (1), 5. https://doi.org/10.1038/s42004-018-0107-y.
(195) Islam, M.; Hossain, D.; Mondal, P.; Roy, A. S.; Mondal, S.; Mobarak, M. Selective Oxidation of

Olefins Catalyzed by Polymer-Anchored Nickel(II) Complex in Water Medium. Bulletin of the Korean Chemical Society 2010, 31 (12), 3765–3770. https://doi.org/10.5012/BKCS.2010.31.12.3765.

(196) Seetharamsingh, B.; Khairnar, P. V.; Reddy, D. S. First Total Synthesis of Gliomasolide C and Formal Total Synthesis of Sch-725674. J. Org. Chem. 2016, 81 (1), 290–296. https://doi.org/10.1021/acs.joc.5b02318.

(197) Mitsudome, T.; Mizumoto, K.; Mizugaki, T.; Jitsukawa, K.; Kaneda, K. Wacker-Type Oxidation of Internal Olefins Using a PdCl2/N,N-Dimethylacetamide Catalyst System under Copper-Free Reaction Conditions. Angewandte Chemie International Edition 2009, 49 (7), 1238–1240. https://doi.org/10.1002/anie.200905184.

(198) Improved Procedures for Converting Higher α-Olefins to Methyl Ketones with Palladium Chloride | The Journal of Organic Chemistry. https://pubs.acs.org/doi/10.1021/jo01024a517 (accessed 2024-09-22).

(199) Vela, P.; Vázquez-Tato, M. P.; Seijas, J. A.; Sainz, M. J.; Mansilla, J. P.; Feás, X.; Salinero, C. NMR Analysis of the Triglyceride Composition of Cold Pressed Oil from Camellia Reticulata and Camellia Japonica. In Proceedings of The 15th International Electronic Conference on Synthetic Organic Chemistry; MDPI: Sciforum.net, 2011; p 754. https://doi.org/10.3390/ecsoc-15-00754.

(200) Farnetti, E. Homogeneous and Heterogeneous Catalysis. INORGANIC CHEMISTRY.

(201) Evnin, A. Heterogeneously Catalyzed Vapor-Phase Oxidation of Ethylene to Acetaldehyde. Journal of Catalysis 1973, 30 (1), 109–117. https://doi.org/10.1016/0021-9517(73)90057-2.

(202) Barthos, R.; Hegyessy, A.; Novodárszki, G.; Pászti, Z.; Valyon, J. Structure and Activity of Pd/V2O5/TiO2 Catalysts in Wacker Oxidation of Ethylene. Applied Catalysis A: General 2017, 531, 96–105. https://doi.org/10.1016/j.apcata.2016.10.024.

(203) Vafaeezadeh, M.; Saynisch, R.; Lösch, A.; Kleist, W.; Thiel, W. R. Fast and Selective Aqueous-Phase Oxidation of Styrene to Acetophenone Using a Mesoporous Janus-Type Palladium Catalyst. Molecules 2021, 26 (21), 6450. https://doi.org/10.3390/molecules26216450.

(204) Neyyathala, A.; Flecken, F.; Hanf, S. A Supported Palladium Phosphide Catalyst for the Wacker-Tsuji-Oxidation of Styrene. ChemPlusChem 2023, 88 (2), e202200431. https://doi.org/10.1002/cplu.202200431.

(205) Xia, X.; Gao, X.; Xu, J.; Hu, C.; Peng, X. Selective Oxidation of Styrene Derivatives to Ketones over Palladium(0)/Carbon with Hydrogen Peroxide as the Sole Oxidant. Synlett 2016, 28. https://doi.org/10.1055/s-0036-1588656.

(206) Huang, G.; Wang, L.; Luo, H.; Shang, S.; Chen, B.; Gao, S.; An, Y. Isopropanol as a Hydrogen Source for Single Atom Cobalt-Catalyzed Wacker-Type Oxidation. Catal. Sci. Technol. 2020, 10 (9), 2769–2773. https://doi.org/10.1039/D0CY00409J.

(207) Barthos, R.; Drotár, E.; Szegedi, Á.; Valyon, J. Wacker Oxidation of Ethylene over Vanadia Nanotube Supported Pd Catalysts. Materials Research Bulletin 2012, 47 (12), 4452–4456. https://doi.org/10.1016/j.materresbull.2012.09.052.

(208) Neyyathala, A.; Flecken, F.; Hanf, S. A Supported Palladium Phosphide Catalyst for the Wacker-Tsuji-Oxidation of Styrene. ChemPlusChem 2023, 88 (2), e202200431. https://doi.org/10.1002/cplu.202200431.

(209) Yang, X.-F.; Wang, A.; Qiao, B.; Li, J.; Liu, J.; Zhang, T. Single-Atom Catalysts: A New Frontier in Heterogeneous Catalysis. Acc. Chem. Res. 2013, 46 (8), 1740–1748. https://doi.org/10.1021/ar300361m.

(210) Belykh, L. B.; Skripov, N. I.; Sterenchuk, T. P.; Akimov, V. V.; Tauson, V. L.; Schmidt, F. K. Influence of Phosphorus Concentration on the State of the Surface Layer of Pd–P Hydrogenation Catalysts. Russ J Gen Chem 2016, 86 (9), 2022–2032. https://doi.org/10.1134/S1070363216090073.

(211) Alvarado Rupflin, L.; Boscagli, C.; Schunk, S. A. Platinum Group Metal Phosphides as Efficient Catalysts in Hydroprocessing and Syngas-Related Catalysis. Catalysts 2018, 8 (3), 122. https://doi.org/10.3390/catal8030122.
(212) Belykh, L. B.; Skripov, N. I.; Akimov, V. V.; Tauson, V. L.; Stepanova, T. P.; Schmidt, F. K. The State of Palladium in the Nanosized Hydrogenation Catalysts Modified with Elemental Phosphorus. Russ J Gen Chem 2013, 83 (12), 2260–2268. https://doi.org/10.1134/S1070363213120062.
(213) von Czapiewski, M.; Meier, M. A. R. Synthesis of Dimer Fatty Acid Methyl Esters by Catalytic Oxidation and Reductive Amination: An Efficient Route to Branched Polyamides. Eur. J. Lipid Sci. Technol. 2018, 120 (1), 1700350. https://doi.org/10.1002/ejlt.201700350.
(214) Song, S.; Wang, Y.; Yan, N. A Remarkable Solvent Effect on Reductive Amination of Ketones. Molecular Catalysis 2018, 454, 87–93. https://doi.org/10.1016/j.mcat.2018.05.017.
(215) Yang, Z.; Huang, Y.-B.; Guo, Q.-X.; Fu, Y. RANEY® Ni Catalyzed Transfer Hydrogenation of Levulinate Esters to γ-Valerolactone at Room Temperature. Chem. Commun. 2013, 49 (46), 5328. https://doi.org/10.1039/c3cc40980e.
(216) Tsurugi, J.; Nakao, R.; Fukumoto, T. ..Gamma.-Induced Reduction with Trichlorosilane. Dialkyl Ether from Alkyl Aliphatic Carboxylate. J. Am. Chem. Soc. 1969, 91 (16), 4587–4588. https://doi.org/10.1021/ja01044a067.
(217) Mao, Z.; Gregg, B. T.; Cutler, A. R. Catalytic Hydrosilylation of Organic Esters Using Manganese Carbonyl Acetyl Complexes. J. Am. Chem. Soc. 1995, 117 (40), 10139–10140. https://doi.org/10.1021/ja00145a036.
(218) N, S.; T, M.; T, K. An Efficient One-Pot Synthesis of Unsymmetrical Ethers: A Directly Reductive Deoxygenation of Esters Using an InBr3/Et3SiH Catalytic System. The Journal of organic chemistry 2007, 72 (15). https://doi.org/10.1021/jo070814z.
(219) Biermann, U.; Metzger, J. O. Synthesis of Ethers by GaBr3-Catalyzed Reduction of Carboxylic Acid Esters and Lactones by Siloxanes. ChemSusChem 2014, 7 (2), 644–649. https://doi.org/10.1002/cssc.201300627.
(220) A Convenient Synthesis of Long-Chain 1-O-Alkyl Glyceryl Ethers. JAOCS, Journal of the American Oil Chemists' Society 1988, 65 (8), 1299–1302. https://doi.org/10.1007/bf02542409.
(221) Synthese und Eigenschaften gesättigter Trialkylglycerinäther - Müller - 1977 - Fette, Seifen, Anstrichmittel - Wiley Online Library. https://onlinelibrary.wiley.com/doi/abs/10.1002/lipi.19770790801 (accessed 2024-10-14).
(222) Biermann, U.; Metzger, J. O. Reduction of High Oleic Sunflower Oil to Glyceryl Trioleyl Ether. Eur. J. Lipid Sci. Technol. 2014, 116 (1), 74–79. https://doi.org/10.1002/ejlt.201300320.
(223) Dannecker, P.; Biermann, U.; von Czapiewski, M.; Metzger, J. O.; Meier, M. A. R. Renewable Polyethers via GaBr 3 -Catalyzed Reduction of Polyesters. Angew. Chem. Int. Ed. 2018, 57 (28), 8775–8779. https://doi.org/10.1002/anie.201804368.
(224) Rhein, M.; Zarbakhsh, S.; Meier, M. A. R. Further Insights into the Catalytic Reduction of Aliphatic Polyesters to Polyethers. Macromolecular Chemistry and Physics 2023, 224 (1), 2200289. https://doi.org/10.1002/macp.202200289.
(225) Gkizis, P. L.; Constantinou, C. T.; Kokotos, C. G. UVA-Light-Promoted Catalyst-Free Photochemical Aerobic Oxidation of Boronic Acids. Eur J Org Chem 2023, 26 (44), e202300898. https://doi.org/10.1002/ejoc.202300898.
(226) Kolb, H. C.; Finn, M. G.; Sharpless, K. B. Click Chemistry: Diverse Chemical Function from a Few Good Reactions. Angewandte Chemie International Edition 2001, 40 (11), 2004–2021. https://doi.org/10.1002/1521-3773(20010601)40:11<2004::AID-ANIE2004>3.0.CO;2-5.
(227) Recent developments in catalyst systems for selective oligomerization and polymerization of higher α-olefins - Polymer Chemistry (RSC Publishing). https://pubs.rsc.org/en/content/articlelanding/2023/py/d3py00028a (accessed 2024-11-07).

(228) Beiträge zur Kenntniss der ungesättigten Verbindungen. II. Ueber die Addition von Mercaptanen an ungesättigte Kohlenwasserstoffe - Posner - 1905 - Berichte der deutschen chemischen Gesellschaft - Wiley Online Library. https://chemistry-europe.onlinelibrary.wiley.com/doi/10.1002/cber.190503801106 (accessed 2024-11-07).
(229) Xiao, Q.; Zhang, H.; Li, J.-H.; Jian, J.-X.; Tong, Q.-X.; Zhong, J.-J. Directing-Group-Assisted Markovnikov-Selective Hydrothiolation of Styrenes with Thiols by Photoredox/Cobalt Catalysis. Org. Lett. 2021, 23 (9), 3604–3609. https://doi.org/10.1021/acs.orglett.1c00999.
(230) Wadhwa, P.; Kharbanda, A.; Sharma, A. Thia-Michael Addition: An Emerging Strategy in Organic Synthesis. *Asian Journal of Organic Chemistry* 2018, *7* (4), 634–661. https://doi.org/10.1002/ajoc.201700609.
(231) Chan, J. W.; Hoyle, C. E.; Lowe, A. B.; Bowman, M. The Nucleophile-Initiated Thiol-Michael Click Reaction: The Effect of Organocatalyst, Thiol, and Ene.
(232) Berne, D.; Ladmiral, V.; Leclerc, E.; Caillol, S. Thia-Michael Reaction: The Route to Promising Covalent Adaptable Networks. Polymers 2022, 14 (20), 4457. https://doi.org/10.3390/polym14204457.
(233) Initiation of Radical Chain Reactions of Thiol Compounds and Alkenes without any Added Initiator: Thiol-Catalyzed cis/trans Isomerization of Methyl Oleate - Biermann - 2012 - Chemistry – A European Journal - Wiley Online Library. https://chemistry-europe.onlinelibrary.wiley.com/doi/full/10.1002/chem.201103252 (accessed 2024-11-07).
(234) Reactivity and Reversibility in the Reaction of Thiyl Radicals with Olefins1 | Journal of the American Chemical Society. https://pubs.acs.org/doi/10.1021/ja01514a032 (accessed 2024-11-07).
(235) The thiol-ene (click) reaction for the synthesis of plant oil derived polymers - Türünç - 2013 - European Journal of Lipid Science and Technology - Wiley Online Library. https://onlinelibrary.wiley.com/doi/10.1002/ejlt.201200148 (accessed 2024-11-07).
(236) Chan, J. W.; Hoyle, C. E.; Lowe, A. B.; Bowman, M. Nucleophile-Initiated Thiol-Michael Reactions: Effect of Organocatalyst, Thiol, and Ene. Macromolecules 2010, 43 (15), 6381–6388. https://doi.org/10.1021/ma101069c.
(237) Hoyle, C. E.; Lee, T. Y.; Roper, T. Thiol-Enes: Chemistry of the Past with Promise for the Future. J. Polym. Sci. A Polym. Chem. 2004, 42 (21), 5301–5338. https://doi.org/10.1002/pola.20366.
(238) Campos, L. M.; Killops, K. L.; Sakai, R.; Paulusse, J. M. J.; Damiron, D.; Drockenmuller, E.; Messmore, B. W.; Hawker, C. J. Development of Thermal and Photochemical Strategies for Thiol−Ene Click Polymer Functionalization. Macromolecules 2008, 41 (19), 7063–7070. https://doi.org/10.1021/ma801630n.
(239) Uygun, M.; Tasdelen, M. A.; Yagci, Y. Influence of Type of Initiation on Thiol–Ene "Click" Chemistry. Macromolecular Chemistry and Physics 2010, 211 (1), 103–110. https://doi.org/10.1002/macp.200900442.
(240) Role of thiol oxidation by air in the mechanism of the self-initiated thermal thiol–ene polymerization - Polymer Chemistry (RSC Publishing). https://pubs.rsc.org/en/content/articlelanding/2021/py/d1py01301g (accessed 2024-11-07).
(241) Koenig, N. H.; Swern, D. Organic Sulfur Derivatives. I. Addition of Mercaptoacetic Acid to Long-Chain Monounsaturated Compounds. J. Am. Chem. Soc. 1957, 79 (2), 362–365. https://doi.org/10.1021/ja01559a033.
(242) Koenig, N. H.; Sasin, G. S.; Swern, D. Organic Sulfur Derivatives. V.2 Preparation and Properties of Some Long-Chain Mercapto Acids and Related Compounds3. J. Org. Chem. 1958, 23 (10), 1525–1530. https://doi.org/10.1021/jo01104a034.
(243) Schwab, A. W.; Gast, L. E.; Cowan, J. C. Free Radical Addition of Hydrogen Sulfide and Thiols to Linseed Oil and Methyl Oleate. J Am Oil Chem Soc 1968, 45 (6), 461–464.

https://doi.org/10.1007/BF02655509.
(244) Koenig, N. H.; Swern, D. Organic Sulfur Derivatives. I. Addition of Mercaptoacetic Acid to Long-Chain Monounsaturated Compounds. J. Am. Chem. Soc. 1957, 79 (2), 362–365. https://doi.org/10.1021/ja01559a033.
(245) Testa, A. C. Photosensitized Cis—Trans Isomerization of Methyl Oleate. J. Org. Chem. 1964, 29 (8), 2461–2462. https://doi.org/10.1021/jo01031a516.
(246) Ionescu, M.; Radojčić, D.; Wan, X.; Petrović, Z. S.; Upshaw, T. A. Functionalized Vegetable Oils as Precursors for Polymers by Thiol-Ene Reaction. European Polymer Journal 2015, 67, 439–448. https://doi.org/10.1016/j.eurpolymj.2014.12.037.
(247) Wang, M.; Jiang, X. Prospects and Challenges in Organosulfur Chemistry. ACS Sustainable Chem. Eng. 2022, 10 (2), 671–677. https://doi.org/10.1021/acssuschemeng.1c07636.
(248) Kaikade, D. S.; Sabnis, A. S. Polyurethane Foams from Vegetable Oil-Based Polyols: A Review. Polym. Bull. 2023, 80 (3), 2239–2261. https://doi.org/10.1007/s00289-022-04155-9.
(249) Maisonneuve, L.; Chollet, G.; Grau, E.; Cramail, H. Vegetable Oils: A Source of Polyols for Polyurethane Materials. OCL 2016, 23 (5), D508. https://doi.org/10.1051/ocl/2016031.
(250) Li, Y.; Luo, X.; Hu, S. Polyols and Polyurethanes from Vegetable Oils and Their Derivatives. In Bio-based Polyols and Polyurethanes; Li, Y., Luo, X., Hu, S., Eds.; Springer International Publishing: Cham, 2015; pp 15–43. https://doi.org/10.1007/978-3-319-21539-6_2.
(251) Desroches, M.; Caillol, S.; Lapinte, V.; Auvergne, R.; Boutevin, B. Synthesis of Biobased Polyols by Thiol−Ene Coupling from Vegetable Oils. Macromolecules 2011, 44 (8), 2489–2500. https://doi.org/10.1021/ma102884w.
(252) Liang, H.; Feng, Y.; Lu, J.; Liu, L.; Yang, Z.; Luo, Y.; Zhang, Y.; Zhang, C. Bio-Based Cationic Waterborne Polyurethanes Dispersions Prepared from Different Vegetable Oils. Industrial Crops and Products 2018, 122, 448–455. https://doi.org/10.1016/j.indcrop.2018.06.006.
(253) Shen, Y.; He, J.; Xie, Z.; Zhou, X.; Fang, C.; Zhang, C. Synthesis and Characterization of Vegetable Oil Based Polyurethanes with Tunable Thermomechanical Performance. Industrial Crops and Products 2019, 140, 111711. https://doi.org/10.1016/j.indcrop.2019.111711.
(254) Fridrihsone, A.; Romagnoli, F.; Kirsanovs, V.; Cabulis, U. Life Cycle Assessment of Vegetable Oil Based Polyols for Polyurethane Production. Journal of Cleaner Production 2020, 266, 121403. https://doi.org/10.1016/j.jclepro.2020.121403.
(255) Mattar, N.; Langlois, V.; Renard, E.; Rademacker, T.; Hübner, F.; Demleitner, M.; Altstädt, V.; Ruckdäschel, H.; Rios de Anda, A. Fully Bio-Based Epoxy-Amine Thermosets Reinforced with Recycled Carbon Fibers as a Low Carbon-Footprint Composite Alternative. ACS Appl. Polym. Mater. 2021, 3 (1), 426–435. https://doi.org/10.1021/acsapm.0c01187.
(256) Choe, E.; Min, D. B. Mechanisms and Factors for Edible Oil Oxidation. Comprehensive Reviews in Food Science and Food Safety 2006, 5 (4), 169–186. https://doi.org/10.1111/j.1541-4337.2006.00009.x.
(257) Van De Voort, F. R.; Ismail, A. A.; Sedman, J.; Emo, G. Monitoring the Oxidation of Edible Oils by Fourier Transform Infrared Spectroscopy. J Americ Oil Chem Soc 1994, 71 (3), 243–253. https://doi.org/10.1007/BF02638049.
(258) Rongxia, B.; Shiyong, L.; Wencai, X.; Ruiqiang, M.; Di, H.; Kelin, M.; Jiangwei, H.; Yong, X.; Caichang, L. CHARACTERIZATION OF THE UV - VISIBLE ABSORPTION SPECTRA OF COMMONLY USED PHOTOINITIATORS; 2017; pp 18–20. https://doi.org/10.26480/wsmce.01.2017.18.20.
(259) Darvas, F.; Dormán, G. 1 Fundamentals of Flow Chemistry. In Volume 1 Flow Chemistry – Fundamentals; Darvas, F., Dormán, G., Hessel, V., Ley, S. V., Eds.; De Gruyter, 2021; pp 1–50. https://doi.org/10.1515/9783110693676-001.
(260) Alvès, M.-H.; Sfeir, H.; Tranchant, J.-F.; Gombart, E.; Sagorin, G.; Caillol, S.; Billon, L.; Save, M. Terpene and Dextran Renewable Resources for the Synthesis of Amphiphilic Biopolymers.

Biomacromolecules 2014, 15 (1), 242–251. https://doi.org/10.1021/bm401521f.
(261) Stubbs, C. J.; Khalfa, A. L.; Chiaradia, V.; Worch, J. C.; Dove, A. P. Intrinsically Re-Curable Photopolymers Containing Dynamic Thiol-Michael Bonds. J. Am. Chem. Soc. 2022, 144 (26), 11729–11735. https://doi.org/10.1021/jacs.2c03525.
(262) Pyo, S.-H.; Persson, P.; Bornadel, A.; Sörensen, K.; Lundmark, S.; Hatti-Kaul, R. Cyclic Carbonates as Monomers for Phosgene- and Isocyanate-Free Polyurethanes and Polycarbonates. Pure and Applied Chemistry 2012, 84, 637–661. https://doi.org/10.1351/PAC-CON-11-06-14.
(263) Tomita, H.; Sanda, F.; Endo, T. Model Reaction for the Synthesis of Polyhydroxyurethanes from Cyclic Carbonates with Amines: Substituent Effect on the Reactivity and Selectivity of Ring-Opening Direction in the Reaction of Five-Membered Cyclic Carbonates with Amine. Journal of Polymer Science Part A: Polymer Chemistry 2001, 39 (21), 3678–3685. https://doi.org/10.1002/pola.10009.
(264) Venkataraman, S.; Ng, V. W. L.; Coady, D. J.; Horn, H. W.; Jones, G. O.; Fung, T. S.; Sardon, H.; Waymouth, R. M.; Hedrick, J. L.; Yang, Y. Y. A Simple and Facile Approach to Aliphatic N-Substituted Functional Eight-Membered Cyclic Carbonates and Their Organocatalytic Polymerization. J. Am. Chem. Soc. 2015, 137 (43), 13851–13860. https://doi.org/10.1021/jacs.5b06355.
(265) Lamarzelle, O.; Durand, P.-L.; Wirotius, A.-L.; Chollet, G.; Grau, E.; Cramail, H. Activated Lipidic Cyclic Carbonates for Non-Isocyanate Polyurethane Synthesis. Polymer Chemistry 2016, 7 (7), 1439–1451. https://doi.org/10.1039/C5PY01964H.
(266) Cornille, A.; Blain, M.; Auvergne, R.; Andrioletti, B.; Boutevin, B.; Caillol, S. A Study of Cyclic Carbonate Aminolysis at Room Temperature: Effect of Cyclic Carbonate Structures and Solvents on Polyhydroxyurethane Synthesis. Polymer Chemistry 2017, 8 (3), 592–604. https://doi.org/10.1039/C6PY01854H.
(267) O. Sonnati, M.; Amigoni, S.; Givenchy, E. P. T. de; Darmanin, T.; Choulet, O.; Guittard, F. Glycerol Carbonate as a Versatile Building Block for Tomorrow: Synthesis, Reactivity, Properties and Applications. Green Chemistry 2013, 15 (2), 283–306. https://doi.org/10.1039/C2GC36525A.
(268) Climent, M. J.; Corma, A.; Iborra, S.; Martínez-Silvestre, S.; Velty, A. Preparation of Glycerol Carbonate Esters by Using Hybrid Nafion–Silica Catalyst. ChemSusChem 2013, 6 (7), 1224–1234. https://doi.org/10.1002/cssc.201300146.
(269) Helbling, P.; Hermant, F.; Petit, M.; Tassaing, T.; Vidil, T.; Cramail, H. Unveiling the Reactivity of Epoxides in Carbonated Epoxidized Soybean Oil and Application in the Stepwise Synthesis of Hybrid Poly(Hydroxyurethane) Thermosets. Polym. Chem. 2023, 10.1039.D2PY01318E. https://doi.org/10.1039/D2PY01318E.
(270) Rix, E.; Grau, E.; Chollet, G.; Cramail, H. Synthesis of Fatty Acid-Based Non-Isocyanate Polyurethanes, NIPUs, in Bulk and Mini-Emulsion. European Polymer Journal 2016, 84, 863–872.
(271) Scheelje, F. C. M.; Meier, M. A. R. Non-Isocyanate Polyurethanes Synthesized from Terpenes Using Thiourea Organocatalysis and Thiol-Ene-Chemistry. Commun Chem 2023, 6 (1), 239. https://doi.org/10.1038/s42004-023-01041-x.
(272) Dr, K. J.; Dr, R. N.; Szillat, F.; Prof, D. R. H. Dental Composition. EP2813497A1, December 17, 2014.
(273) Qu, J.; Dai, J.; Wu, Z. Polycyclic Carbonate Resin, Normal-Pressures Rapid Preparation Method Thereof and Application of Resin. CN109824881A, May 31, 2019.
(274) Dai, J.; Wu, Z.; Tang, L.; Qu, J. Preparation of Five-Membered Bis(Cyclic Carbonate)s at Atmospheric Pressure for Polyhydroxyurethane Coatings. Journal of Applied Polymer Science 2019, 136 (37), 47957. https://doi.org/10.1002/app.47957.
(275) Nohra, B.; Candy, L.; Blanco, J.-F.; Raoul, Y.; Mouloungui, Z. Synthesis of Five and Six-

Membered Cyclic Glycerilic Carbonates Bearing Exocyclic Urethane Functions. European Journal of Lipid Science and Technology 2013, 115 (1), 111–122. https://doi.org/10.1002/ejlt.201200082.
(276) From the Synthesis of Biobased Cyclic Carbonate to Polyhydroxyurethanes: A Promising Route towards Renewable Non-Isocyanate Polyurethanes - Carré - 2019 - ChemSusChem - Wiley Online Library. https://chemistry-europe.onlinelibrary.wiley.com/doi/full/10.1002/cssc.201900737 (accessed 2024-09-16).
(277) Mundo, F.; Caillol, S.; Ladmiral, V.; Meier, M. A. R. On Sustainability Aspects of the Synthesis of Five-Membered Cyclic Carbonates. ACS Sustainable Chem. Eng. 2024, 12 (17), 6452–6466. https://doi.org/10.1021/acssuschemeng.4c01274.
(278) Scott, T. F.; Schneider, A. D.; Cook, W. D.; Bowman, C. N. Photoinduced Plasticity in Cross-Linked Polymers. Science 2005, 308 (5728), 1615–1617. https://doi.org/10.1126/science.1110505.
(279) Montarnal, D.; Capelot, M.; Tournilhac, F.; Leibler, L. Silica-Like Malleable Materials from Permanent Organic Networks. Science 2011, 334 (6058), 965–968. https://doi.org/10.1126/science.1212648.
(280) Denissen, W.; Winne, J. M.; Du Prez, F. E. Vitrimers: Permanent Organic Networks with Glass-like Fluidity. Chem Sci 2016, 7 (1), 30–38. https://doi.org/10.1039/c5sc02223a.
(281) Denissen, W.; Rivero, G.; Nicolaÿ, R.; Leibler, L.; Winne, J. M.; Du Prez, F. E. Vinylogous Urethane Vitrimers. Advanced Functional Materials 2015, 25 (16), 2451–2457. https://doi.org/10.1002/adfm.201404553.
(282) Kamarulzaman, S.; Png, Z. M.; Lim, E. Q.; Lim, I. Z. S.; Li, Z.; Goh, S. S. Covalent Adaptable Networks from Renewable Resources: Crosslinked Polymers for a Sustainable Future. Chem 2023, 9 (10), 2771–2816. https://doi.org/10.1016/j.chempr.2023.04.024.
(283) Zhao, X.-L.; Tian, P.-X.; Li, Y.-D.; Zeng, J.-B. Biobased Covalent Adaptable Networks: Towards Better Sustainability of Thermosets. Green Chem. 2022, 24 (11), 4363–4387. https://doi.org/10.1039/D2GC01325H.
(284) Lucherelli, M. A.; Duval, A.; Avérous, L. Biobased Vitrimers: Towards Sustainable and Adaptable Performing Polymer Materials. Progress in Polymer Science 2022, 127, 101515. https://doi.org/10.1016/j.progpolymsci.2022.101515.
(285) Scopus - Document search results. https://www.scopus.com/results/results.uri?sort=plf-f&src=s&st1=covalent+adaptable+networ&sid=b8b236c99067f8db8e07d7d5db3ee3ac&sot=b&sdt=b&sl=30&s=ALL%28covalent+AND+adaptable+AND+network%29&origin=searchbasic&editSaveSearch=&yearFrom=Before+1960&yearTo=Present&sessionSearchId=b8b236c99067f8db8e07d7d5db3ee3ac&limit=10 (accessed 2024-11-21).
(286) Denissen, W.; Winne, J. M.; Du Prez, F. E. Vitrimers: Permanent Organic Networks with Glass-like Fluidity. Chem Sci 2016, 7 (1), 30–38. https://doi.org/10.1039/c5sc02223a.
(287) Zhu, Y.; Gao, F.; Zhong, J.; Shen, L.; Lin, Y. Renewable Castor Oil and DL-Limonene Derived Fully Bio-Based Vinylogous Urethane Vitrimers. European Polymer Journal 2020, 135, 109865. https://doi.org/10.1016/j.eurpolymj.2020.109865.
(288) Sougrati, L.; Duval, A.; Avérous, L. From Lignins to Renewable Aromatic Vitrimers Based on Vinylogous Urethane. ChemSusChem 2023, 16 (23), e202300792. https://doi.org/10.1002/cssc.202300792.
(289) Hoyle, C. E.; Bowman, C. N. Thiol-Ene Click Chemistry. Angewandte Chemie International Edition 2010, 49 (9), 1540–1573. https://doi.org/10.1002/anie.200903924.
(290) Cornille, A.; Froidevaux, V.; Negrell, C.; Caillol, S.; Boutevin, B. Thiol-Ene Coupling: An Efficient Tool for the Synthesis of New Biobased Aliphatic Amines for Epoxy Curing. Polymer 2014, 55 (22), 5561–5570. https://doi.org/10.1016/j.polymer.2014.07.004.
(291) Nowacka, M.; Herc, A. S.; Kowalewska, A. Thiol-Ene Addition of Mercaptoalcohols to

Poly(Vinylsiloxanes) under Visible Light Photocatalysis – An Approach towards Cross-Linkable Hydrophilic Silicones. Polyhedron 2020, 185, 114588. https://doi.org/10.1016/j.poly.2020.114588.

(292) Hu, Y.; Tian, Y.; Cheng, J.; Zhang, J. Synthesis of Eugenol-Based Polyols via Thiol–Ene Click Reaction and High-Performance Thermosetting Polyurethane Therefrom. ACS Sustainable Chemistry & Engineering 2020, 10, 4158–4166. https://doi.org/10.1021/acssuschemeng.9b06867.

(293) Ma, Y.; Jiang, X.; Shi, Z.; Berrocal, J. A.; Weder, C. Closed-Loop Recycling of Vinylogous Urethane Vitrimers. Angewandte Chemie International Edition 2023, 62 (36), e202306188. https://doi.org/10.1002/anie.202306188.

(294) Shore Hardness for Plastics and Rubbers: Shore A and Shore D. Xometry Pro. https://xometry.pro/en-eu/articles/shore-hardness-for-plastics-and-rubbers/ (accessed 2024-11-27).

(295) Milisavljević, J.; Petrović, E.; Ćirić, I.; Mančić, M.; Marković, D.; Đorđević, M. TENSILE TESTING FOR DIFFERENT TYPES OF POLYMERS. 2012.

(296) Rao, J.; Lv, Z.; Chen, G.; Peng, F. Hemicellulose: Structure, Chemical Modification, and Application. Progress in Polymer Science 2023, 140, 101675. https://doi.org/10.1016/j.progpolymsci.2023.101675.

(297) Robert Ross. Wood Handbook/Wood as an Engineering Material; General Technical Report; General Technical Report FPL-GTR-282. Madison, WI: U.S. Department of Agriculture, Forest Service, Forest Products Laboratory., 2021.

(298) Chen, Q.; Gao, K.; Peng, C.; Xie, H.; Zhao, Z. K.; Bao, M. Preparation of Lignin/Glycerol-Based Bis(Cyclic Carbonate) for the Synthesis of Polyurethanes. Green Chem. 2015, 17 (9), 4546–4551. https://doi.org/10.1039/C5GC01340B.

(299) G.W. Critchlow; ,; D.M. Brewis. Review of Surface Pretreatments for Aluminium Alloys - ScienceDirect. International Journal of Adhesion and Adhesives 1996, 16 (4), 255–275.

(300) Landrock, A. H.; Ebnesajjad, S. Adhesives Technology Handbook, Third edition.; Elsevier/WA, William Andrew is an imprint of Elsevier: Amsterdam ; Boston, 2015.

(301) Liu, J.; Pich, A.; Bernaerts, K. V. Preparation of Lignin-Based Vinylogous Urethane Vitrimer Materials and Their Potential Use as on-Demand Removable Adhesives. Green Chem. 2024, 26 (3), 1414–1429. https://doi.org/10.1039/D3GC02799F.

(302) Cornille, A.; Michaud, G.; Simon, F.; Fouquay, S.; Auvergne, R.; Boutevin, B.; Caillol, S. Promising Mechanical and Adhesive Properties of Isocyanate-Free Poly(Hydroxyurethane). European Polymer Journal 2016, 84, 404–420. https://doi.org/10.1016/j.eurpolymj.2016.09.048.

(303) Delavarde, A.; Savin, G.; Derkenne, P.; Boursier, M.; Morales-Cerrada, R.; Nottelet, B.; Pinaud, J.; Caillol, S. Sustainable Polyurethanes: Toward New Cutting-Edge Opportunities. Progress in Polymer Science 2024, 151, 101805. https://doi.org/10.1016/j.progpolymsci.2024.101805.

(304) Cornille, A.; Dworakowska, S.; Bogdal, D.; Boutevin, B.; Caillol, S. A New Way of Creating Cellular Polyurethane Materials: NIPU Foams. European Polymer Journal 2015, 66, 129–138. https://doi.org/10.1016/j.eurpolymj.2015.01.034.

(305) Mhd. Haniffa, Mhd. Abd. C.; Munawar, K.; Ching, Y. C.; Illias, H. A.; Chuah, C. H. Bio-Based Poly(Hydroxy Urethane)s: Synthesis and Pre/Post-Functionalization. Chemistry – An Asian Journal 2021, 16 (11), 1281–1297. https://doi.org/10.1002/asia.202100226.

(306) Kotanen, S.; Poikelispää, M.; Efimov, A.; Harjunalanen, T.; Mills, C.; Laaksonen, T.; Sarlin, E. Hydrolytic Stability of Polyurethane/Polyhydroxyurethane Hybrid Adhesives. International Journal of Adhesion and Adhesives 2021, 110, 102950. https://doi.org/10.1016/j.ijadhadh.2021.102950.

(307) Leitsch, E. K.; Beniah, G.; Liu, K.; Lan, T.; Heath, W. H.; Scheidt, K. A.; Torkelson, J. M. Nonisocyanate Thermoplastic Polyhydroxyurethane Elastomers via Cyclic Carbonate

Aminolysis: Critical Role of Hydroxyl Groups in Controlling Nanophase Separation. ACS Macro Lett. 2016, 5 (4), 424–429. https://doi.org/10.1021/acsmacrolett.6b00102.
(308) Aminolysis Reaction of Glycerol Carbonate in Organic and Hydroorganic Medium. https://aocs.onlinelibrary.wiley.com/doi/epdf/10.1007/s11746-011-1995-5 (accessed 2024-11-14).
(309) Diakoumakos, C. D.; Kotzev, D. L. Non-Isocyanate-Based Polyurethanes Derived upon the Reaction of Amines with Cyclocarbonate Resins. Macromolecular Symposia 2004, 216 (1), 37–46. https://doi.org/10.1002/masy.200451205.
(310) Tomita, H.; Sanda, F.; Endo, T. Polyaddition Behavior of Bis(Five- and Six-Membered Cyclic Carbonate)s with Diamine. Journal of Polymer Science Part A: Polymer Chemistry 2001, 39 (6), 860–867. https://doi.org/10.1002/1099-0518(20010315)39:6<860::AID-POLA1059>3.0.CO;2-2.
(311) Zhang, X.; Zhao, B.; Fu, S.; Seruya, R. S.; Madey, J. F. I.; Bukhryakova, E.; Zhang, F. Rapid and Versatile Synthesis of Glutathione-Responsive Polycarbonates from Activated Cyclic Carbonates. Macromolecules 2024, 57 (6), 2858–2867. https://doi.org/10.1021/acs.macromol.3c02633.
(312) Siragusa, F.; Van Den Broeck, E.; Ocando, C.; Müller, A. J.; De Smet, G.; Maes, B. U. W.; De Winter, J.; Van Speybroeck, V.; Grignard, B.; Detrembleur, C. Access to Biorenewable and CO2-Based Polycarbonates from Exovinylene Cyclic Carbonates. ACS Sustainable Chem. Eng. 2021, 9 (4), 1714–1728. https://doi.org/10.1021/acssuschemeng.0c07683.
(313) Blain, M.; Cornille, A.; Boutevin, B.; Auvergne, R.; Benazet, D.; Andrioletti, B.; Caillol, S. Hydrogen Bonds Prevent Obtaining High Molar Mass PHUs. Journal of Applied Polymer Science 2017, 134. https://doi.org/10.1002/app.44958.
(314) Ecochard, Y.; Caillol, S. Hybrid Polyhydroxyurethanes: How to Overcome Limitations and Reach Cutting Edge Properties? European Polymer Journal 2020, 137, 109915. https://doi.org/10.1016/j.eurpolymj.2020.109915.
(315) Kotanen, S.; Poikelispää, M.; Efimov, A.; Harjunalanen, T.; Mills, C.; Laaksonen, T.; Sarlin, E. Hydrolytic Stability of Polyurethane/Polyhydroxyurethane Hybrid Adhesives. International Journal of Adhesion and Adhesives 2021, 110, 102950. https://doi.org/10.1016/j.ijadhadh.2021.102950.
(316) Lambeth, R. Progress in Hybrid Non-isocyanate Polyurethanes. Polymer International 2020, 70. https://doi.org/10.1002/pi.6078.
(317) Regnat, K.; Mach, R. L.; Mach-Aigner, A. R. Erythritol as Sweetener—Wherefrom and Whereto? Appl Microbiol Biotechnol 2018, 102 (2), 587–595. https://doi.org/10.1007/s00253-017-8654-1.
(318) Rzechonek, D. A.; Dobrowolski, A.; Rymowicz, W.; Mirończuk, A. M. Recent Advances in Biological Production of Erythritol. Critical Reviews in Biotechnology 2018, 38 (4), 620–633. https://doi.org/10.1080/07388551.2017.1380598.
(319) Lamarzelle, O. Design of Original Vegetable Oil-Based Cyclic Carbonates and Amines towards Poly(HydroxyUrethane)s.
(320) Rahman, Md. M.; Akhtarul Islam, M. Application of Epoxy Resins in Building Materials: Progress and Prospects. Polym. Bull. 2022, 79 (3), 1949–1975. https://doi.org/10.1007/s00289-021-03577-1.
(321) Assessment of the Quality of Epoxy Coating in the Automotive Industry. CT 2018, 11. https://doi.org/10.4467/2353737XCT.18.172.9428.
(322) Aradhana, R.; Mohanty, S.; Nayak, S. K. A Review on Epoxy-Based Electrically Conductive Adhesives. International Journal of Adhesion and Adhesives 2020, 99, 102596. https://doi.org/10.1016/j.ijadhadh.2020.102596.
(323) Verma, S.; Mohanty, S.; Nayak, S. K. A Review on Protective Polymeric Coatings for Marine Applications. J Coat Technol Res 2019, 16 (2), 307–338. https://doi.org/10.1007/s11998-018-

00174-2.
(324) Chen, Z.; Liu, X.; Chen, H.; Li, J.; Wang, X.; Zhu, J. Application of Epoxy Resin in Cultural Relics Protection. Chinese Chemical Letters 2024, 35 (4), 109194. https://doi.org/10.1016/j.cclet.2023.109194.
(325) Pappa, C.; Feghali, E.; Vanbroekhoven, K.; Triantafyllidis, K. S. Recent Advances in Epoxy Resins and Composites Derived from Lignin and Related Bio-Oils. Current Opinion in Green and Sustainable Chemistry 2022, 38, 100687. https://doi.org/10.1016/j.cogsc.2022.100687.
(326) Capricho, J. C.; Fox, B.; Hameed, N. Multifunctionality in Epoxy Resins. Polymer Reviews 2020, 60 (1), 1–41. https://doi.org/10.1080/15583724.2019.1650063.
(327) Prileschajew, N. Oxydation Ungesättigter Verbindungen Mittels Organischer Superoxyde. Berichte der deutschen chemischen Gesellschaft 1909, 42 (4), 4811–4815. https://doi.org/10.1002/cber.190904204100.
(328) Dodiuk, H. Handbook of Thermoset Plastics; William Andrew, 2021.
(329) Barton, O. A.; Littell, W. W. Epoxide Resin from Epichlorohydrin and a Mixture of Bisphenols. US3422063A, January 14, 1969. https://patents.google.com/patent/US3422063A/en (accessed 2024-09-20).
(330) Regulation (EC) No 1223/2009 of the European Parliament and of the Council of 30 November 2009 on Cosmetic Products (Recast) (Text with EEA Relevance) Text with EEA Relevance; 2023. http://data.europa.eu/eli/reg/2009/1223/2023-08-16/eng (accessed 2024-09-20).
(331) (Kadri, Z.; Mechnou, I.; Zyade, S. Migration of Bisphenol A from Epoxy Coating to Foodstuffs. Materials Today: Proceedings 2021, 45, 7584–7587. https://doi.org/10.1016/j.matpr.2021.02.581.
(332) Directive 2009/48/EC of the European Parliament and of the Council of 18 June 2009 on the Safety of Toys (Text with EEA Relevance) Text with EEA Relevance; 2022. http://data.europa.eu/eli/dir/2009/48/2022-12-05/eng (accessed 2024-09-20).
(333) den Braver-Sewradj, S. P.; van Spronsen, R.; Hessel, E. V. S. Substitution of Bisphenol A: A Review of the Carcinogenicity, Reproductive Toxicity, and Endocrine Disruption Potential of Alternative Substances. Critical Reviews in Toxicology 2020, 50 (2), 128–147. https://doi.org/10.1080/10408444.2019.1701986.
(334) Environmental Effects of BPA - PMC. https://www.ncbi.nlm.nih.gov/pmc/articles/PMC4674185/ (accessed 2024-09-25).
(335) Bisphenols - ECHA. https://echa.europa.eu/hot-topics/bisphenols (accessed 2024-09-20).
(336) Almeida, S.; Raposo, A.; Almeida-González, M.; Carrascosa, C. Bisphenol A: Food Exposure and Impact on Human Health. Comprehensive Reviews in Food Science and Food Safety 2018, 17 (6), 1503–1517. https://doi.org/10.1111/1541-4337.12388.
(337) Rudawska, A.; Sarna-Boś, K.; Rudawska, A.; Olewnik-Kruszkowska, E.; Frigione, M. Biological Effects and Toxicity of Compounds Based on Cured Epoxy Resins. Polymers 2022, 14 (22), 4915. https://doi.org/10.3390/polym14224915.
(338) Adamovsky, O.; Groh, K. J.; Białk-Bielińska, A.; Escher, B. I.; Beaudouin, R.; Mora Lagares, L.; Tollefsen, K. E.; Fenske, M.; Mulkiewicz, E.; Creusot, N.; Sosnowska, A.; Loureiro, S.; Beyer, J.; Repetto, G.; Štern, A.; Lopes, I.; Monteiro, M.; Zikova-Kloas, A.; Eleršek, T.; Vračko, M.; Zdybel, S.; Puzyn, T.; Koczur, W.; Ebsen Morthorst, J.; Holbech, H.; Carlsson, G.; Örn, S.; Herrero, Ó.; Siddique, A.; Liess, M.; Braun, G.; Srebny, V.; Žegura, B.; Hinfray, N.; Brion, F.; Knapen, D.; Vandeputte, E.; Stinckens, E.; Vergauwen, L.; Behrendt, L.; João Silva, M.; Blaha, L.; Kyriakopoulou, K. Exploring BPA Alternatives – Environmental Levels and Toxicity Review. Environment International 2024, 189, 108728. https://doi.org/10.1016/j.envint.2024.108728.
(339) den Braver-Sewradj, S. P.; van Spronsen, R.; Hessel, E. V. S. Substitution of Bisphenol A: A Review of the Carcinogenicity, Reproductive Toxicity, and Endocrine Disruption Potential of

Alternative Substances. Crit Rev Toxicol 2020, 50 (2), 128–147. https://doi.org/10.1080/10408444.2019.1701986.
(340) Xue, B.; Tang, R.; Xue, D.; Guan, Y.; Sun, Y.; Zhao, W.; Tan, J.; Li, X. Sustainable Alternative for Bisphenol A Epoxy Resin High-Performance and Recyclable Lignin-Based Epoxy Vitrimers. Industrial Crops and Products 2021, 168, 113583. https://doi.org/10.1016/j.indcrop.2021.113583.
(341) Łukaszczyk, J.; Janicki, B.; Kaczmarek, M. Synthesis and Properties of Isosorbide Based Epoxy Resin. European Polymer Journal 2011, 47 (8), 1601–1606. https://doi.org/10.1016/j.eurpolymj.2011.05.009.
(342) Li, Y.; Yang, L.; Zhang, H.; Tang, Z. Synthesis and Curing Performance of a Novel Bio-Based Epoxy Monomer from Soybean Oil. European Journal of Lipid Science and Technology 2017, 119 (8), 1600429. https://doi.org/10.1002/ejlt.201600429.
(343) Mattar, N.; De Anda, A. R.; Vahabi, H.; Renard, E.; Langlois, V. Resorcinol-Based Epoxy Resins Hardened with Limonene and Eugenol Derivatives: From the Synthesis of Renewable Diamines to the Mechanical Properties of Biobased Thermosets. ACS Sustainable Chem. Eng. 2020, 8 (34), 13064–13075. https://doi.org/10.1021/acssuschemeng.0c04780.
(344) Maiorana, A.; Subramaniam, B.; Centore, R.; Han, X.; Linhardt, R. J.; Gross, R. A. Synthesis and Characterization of an Adipic Acid–Derived Epoxy Resin. Journal of Polymer Science Part A: Polymer Chemistry 2016, 54 (16), 2625–2631. https://doi.org/10.1002/pola.28142.
(345) Chen, J.; De Liedekerke Beaufort, M.; Gyurik, L.; Dorresteijn, J.; Otte, M.; Klein Gebbink, R. J. M. Highly Efficient Epoxidation of Vegetable Oils Catalyzed by a Manganese Complex with Hydrogen Peroxide and Acetic Acid. Green Chem. 2019, 21 (9), 2436–2447. https://doi.org/10.1039/C8GC03857K.
(346) Derawi, D.; Salimon, J.; Abdo, W. Preparation of Epoxidized Palm Olein as Renewable Material by Using Peroxy Acids. Malaysian Journal of Analytical Sciences 2014, 18, 584–591.
(347) Warwel, S.; Rüsch gen. Klaas, M. Chemo-Enzymatic Epoxidation of Unsaturated Carboxylic Acids. Journal of Molecular Catalysis B: Enzymatic 1995, 1 (1), 29–35. https://doi.org/10.1016/1381-1177(95)00004-6.
(348) Aouf, C.; Lecomte, J.; Villeneuve, P.; Dubreucq, E.; Fulcrand, H. Chemo-Enzymatic Functionalization of Gallic and Vanillic Acids: Synthesis of Bio-Based Epoxy Resins Prepolymers. Green Chemistry 2012, 14 (8), 2328–2336. https://doi.org/10.1039/C2GC35558B.
(349) Shundo, A.; Yamamoto, S.; Tanaka, K. Network Formation and Physical Properties of Epoxy Resins for Future Practical Applications. JACS Au 2022, 2 (7), 1522–1542. https://doi.org/10.1021/jacsau.2c00120.
(350) Shundo, A.; Yamamoto, S.; Tanaka, K. Network Formation and Physical Properties of Epoxy Resins for Future Practical Applications. JACS Au 2022, 2, 1522–1542. https://doi.org/10.1021/jacsau.2c00120.
(351) Jubsilp, C.; Takeichi, T.; Rimdusit, S. Chapter 7 - Polymerization Kinetics. In Handbook of Benzoxazine Resins; Ishida, H., Agag, T., Eds.; Elsevier: Amsterdam, 2011; pp 157–174. https://doi.org/10.1016/B978-0-444-53790-4.00052-7.
(352) Stille, J. K. Step-Growth Polymerization. J. Chem. Educ. 1981, 58 (11), 862. https://doi.org/10.1021/ed058p862.
(353) Okay, O.; Bowman, C. N. Kinetic Modeling of Thiol-Ene Reactions with Both Step and Chain Growth Aspects. Macromolecular Theory and Simulations 2005, 14 (4), 267–277. https://doi.org/10.1002/mats.200500002.
(354) Law, R. M.; Maibach, H. I. Painters, Lacquerers, and Varnishers in Occupational Dermatology. In Kanerva's Occupational Dermatology; John, S. M., Johansen, J. D., Rustemeyer, T., Elsner, P., Maibach, H. I., Eds.; Springer International Publishing: Cham, 2020; pp 2173–2181. https://doi.org/10.1007/978-3-319-68617-2_178.

(355) Belin, L.; Wass, U.; Audunsson, G.; Mathiasson, L. Amines: Possible Causative Agents in the Development of Bronchial Hyperreactivity in Workers Manufacturing Polyurethanes from Isocyanates. Occupational and Environmental Medicine 1983, 40 (3), 251–257. https://doi.org/10.1136/oem.40.3.251.
(356) Schettgen, T.; Krichels, M.; Rossbach, B.; Kraus, T. 53 Human Bio-Monitoring of Epoxy Resins and Hardeners in the Production of Rotor: Blades. Occup Environ Med 2018, 75 (Suppl 2), A413–A413. https://doi.org/10.1136/oemed-2018-ICOHabstracts.1179.
(357) Krauklis, A. E.; Echtermeyer, A. T. Mechanism of Yellowing: Carbonyl Formation during Hygrothermal Aging in a Common Amine Epoxy. Polymers 2018, 10 (9), 1017. https://doi.org/10.3390/polym10091017.
(358) Wu, C.; Meng, B. C.; Tam, L.; He, L. Yellowing Mechanisms of Epoxy and Vinyl Ester Resins under Thermal, UV and Natural Aging Conditions and Protection Methods. Polymer Testing 2022, 114, 107708. https://doi.org/10.1016/j.polymertesting.2022.107708.
(359) Thomas, R.; Durix, S.; Sinturel, C.; Omonov, T.; Goossens, S.; Groeninckx, G.; Moldenaers, P.; Thomas, S. Cure Kinetics, Morphology and Miscibility of Modified DGEBA-Based Epoxy Resin – Effects of a Liquid Rubber Inclusion. Polymer 2007, 48 (6), 1695–1710. https://doi.org/10.1016/j.polymer.2007.01.018.
(360) Duemichen, E.; Javdanitehran, M.; Erdmann, M.; Trappe, V.; Sturm, H.; Braun, U.; Ziegmann, G. Analyzing the Network Formation and Curing Kinetics of Epoxy Resins by in Situ Near-Infrared Measurements with Variable Heating Rates. Thermochimica Acta 2015, 616, 49–60. https://doi.org/10.1016/j.tca.2015.08.008.
(361) González Garcia, F.; Leyva, M. E.; Oliveira, M. G.; De Queiroz, A. A. A.; Simões, A. Z. Influence of Chemical Structure of Hardener on Mechanical and Adhesive Properties of Epoxy Polymers. Journal of Applied Polymer Science 2010, 117 (4), 2213–2219. https://doi.org/10.1002/app.31892.
(362) Gioia, C.; Colonna, M.; Tagami, A.; Medina, L.; Sevastyanova, O.; Berglund, L. A.; Lawoko, M. Lignin-Based Epoxy Resins: Unravelling the Relationship between Structure and Material Properties. Biomacromolecules 2020, 21 (5), 1920–1928. https://doi.org/10.1021/acs.biomac.0c00057.
(363) Savonnet, E.; Le Coz, C.; Grau, E.; Grelier, S.; Defoort, B.; Cramail, H. Divanillin-Based Aromatic Amines: Synthesis and Use as Curing Agents for Fully Vanillin-Based Epoxy Thermosets. Frontiers in Chemistry 2019, 7.
(364) Lei, Y.-F.; Wang, X.-L.; Liu, B.-W.; Ding, X.-M.; Chen, L.; Wang, Y.-Z. Fully Bio-Based Pressure-Sensitive Adhesives with High Adhesivity Derived from Epoxidized Soybean Oil and Rosin Acid. ACS Sustainable Chem. Eng. 2020, 8 (35), 13261–13270. https://doi.org/10.1021/acssuschemeng.0c03451.
(365) Mattar, N.; Langlois, V.; Renard, E.; Rademacker, T.; Hübner, F.; Demleitner, M.; Altstädt, V.; Ruckdäschel, H.; Rios de Anda, A. Fully Bio-Based Epoxy-Amine Thermosets Reinforced with Recycled Carbon Fibers as a Low Carbon-Footprint Composite Alternative. ACS Appl. Polym. Mater. 2021, 3 (1), 426–435. https://doi.org/10.1021/acsapm.0c01187.
(366) PriamineTM| Dimer Diamine | Cargill | Cargill. https://www.cargill.com/bioindustrial/priamine (accessed 2024-09-24).
(367) Evonik launches first renewable isophorone-based products - Evonik Industries. https://crosslinkers.evonik.com/en/-169696.html (accessed 2024-09-24).
(368) Tabanelli, T.; Soccio, M.; Quattrosoldi, S.; Siracusa, V.; Fiorini, M.; Lotti, N. Priamine 1075 and Catechol Carbonate, a Perfect Match for Ecofriendly Production of a New Renewable Polyurea for Sustainable Flexible Food Packaging. Polymer 2023, 267, 125641. https://doi.org/10.1016/j.polymer.2022.125641.
(369) Zhang, X.; Zan, X.; Yin, J.; Wang, J. Non-Isocyanate Urethane Acrylate Derived from

Isophorone Diamine: Synthesis, Characterization and Its Application in 3D Printing. Molecules 2024, 29 (11), 2639. https://doi.org/10.3390/molecules29112639.

(370) Abe, I.; Shibata, M. Bio-Based Self-Healing Epoxy Vitrimers with Dynamic Imine and Disulfide Bonds Derived from Vanillin, Cystamine, and Dimer Diamine. Molecules 2024, 29 (20), 4839. https://doi.org/10.3390/molecules29204839.

(371) Baroncini, E. A.; Kumar Yadav, S.; Palmese, G. R.; Stanzione III, J. F. Recent Advances in Bio-Based Epoxy Resins and Bio-Based Epoxy Curing Agents. Journal of Applied Polymer Science 2016, 133 (45). https://doi.org/10.1002/app.44103.

8 APPENDIX

8.1 LIST OF FIGURES

8.2 FOUNDINGS

I would like to thank the financial support provided by the NIPU-EJD project; this project has received funding from the European Union's Horizon 2020 research and innovation programme under the Marie Skłodowska-Curie grant agreement No 955700.